DETECTION FOR NON-CAVITATED FISSURE CARIES WITH OPTICAL COHERENCE TOMOGRAPHY

ERUM ZAIN

FACULTY OF DENTISTRY
UNIVERSITY OF MALAYA
KUALA LUMPUR

2017

DETECTION FOR NON-CAVITATED FISSURE CARIES WITH OPTICAL COHERENCE TOMOGRAPHY

ERUM ZAIN

THESIS SUBMITTED IN FULFILMENT OF THE REQUIREMENTS FOR THE DEGREE OF DOCTOR OF PHILOSOPHY

FACULTY OF DENTISTRY
UNIVERSITY OF MALAYA
KUALA LUMPUR

2017

UNIVERSITY OF MALAYA

ORIGINAL LITERARY WORK DECLARATION

Name of Candidate: **ERUM ZAIN**

Registration/Matric No: **DHA140008**

Name of Degree: **DOCTOR OF PHILOSOPHY**

Title of Thesis: **Detection for Non-cavitated Fissure Caries with Optical Coherence Tomography**

Field of Study: **Restorative Dentistry**

I do solemnly and sincerely declare that:

(1) I am the sole author/writer of this Work;
(2) This Work is original;
(3) Any use of any work in which copyright exists was done by way of fair dealing and for permitted purposes and any excerpt or extract from, or reference to or reproduction of any copyright work has been disclosed expressly and sufficiently and the title of the Work and its authorship have been acknowledged in this Work;
(4) I do not have any actual knowledge nor do I ought reasonably to know that the making of this work constitutes an infringement of any copyright work;
(5) I hereby assign all and every rights in the copyright to this Work to the University of Malaya ("UM"), who henceforth shall be owner of the copyright in this Work and that any reproduction or use in any form or by any means whatsoever is prohibited without the written consent of UM having been first had and obtained;
(6) I am fully aware that if in the course of making this Work I have infringed any copyright whether intentionally or otherwise, I may be subject to legal action or any other action as may be determined by UM.

Candidate's Signature Date:

Subscribed and solemnly declared before,

Witness's Signature Date:

Name:

Designation:

DETECTION FOR NON-CAVITATED FISSURE CARIES WITH OPTICAL COHERENCE TOMOGRAPHY

ABSTRACT

Introduction: Early detection and preventive management of non-cavitated fissure caries (NCFC) are the standard of care today. The aim of this study was to explore the potential of an optical method, Optical Coherence Tomography (OCT), in detection of NCFC and discriminating its stages of severity on the occlusal surface. **Objective:** Firstly, to evaluate the accuracy of OCT in detecting sound fissure and NCFC using qualitative OCT analysis and to determine the lesion dimension agreement between OCT and PLM. Secondly, to optically characterize Ekstrand (Ek) histological codes 0, 1 and 2 and to identify OCT outcome measures that can differentiate between Ek codes. Thirdly, to validate the identified OCT outcome measures. Finally, compare the diagnostic accuracy of OCT outcome measures and ICDAS-II criteria. **Methods:** Premolars with sound and naturally occurring NCFC were scan bucco-lingually on the occlusal surface using Swept Source OCT (SS-OCT) and validated using Polarized Light Microscopy (PLM) and Micro-computed tomography (Micro-CT). Bespoke software developed with MATLAB (Mathworks Inc) was used for OCT data extraction and processing. **Results:** OCT qualitative assessment can detect NCFC with high sensitivity (SN) 0.98 and specificity (SP) 0.95. Agreement between OCT and PLM was observed for width of wall and height of slope lesion. Characterisation of OCT signals based on Ekstrand histological classification showed difference in rate of attenuation between Ek codes. Mean depth-resolved intensity attenuated in two phases, in phase I, Ek code 0 had bimodal pattern, where a sudden drop was seen at 30 µm, however, at 40 µm slow attenuation (1.43E+06 a.u./µm) was observed. Ek code 2 exhibited the fastest rate of attenuation (6.43E+06 a.u./µm). Thereafter, in phase II, relatively slower attenuation was observed for all three Ek codes. Area under the curve, partial (AUC_P) and total (AUC_T) were the

outcome measures to detect sound fissure from NCFC and differentiated stages of NCFC respectively. AUC_P at cut-off 3.038E+10 (a.u.) showed 0.86 SN and >0.99 SP with 0.95 area under receiver operating characteristic (AUROC) curves. AUC_T at a cut-off value of 7.031E+10 (a.u.) was limited to SN 0.61 and SP 0.73 with 0.66 AUROC. Validation of AUC_P showed no significant difference in detecting sound and NCFC when groove-fossa system was assessed overall compared to groove where both had accurate SN (> 0.99) and good SP (0.79). For differentiation, AUC_T showed similar SN at different anatomical locations (0.80), however, SP (0.75) was highest at the occlusal fissure. Quantitative OCT analysis when compared to visual criteria ICDAS-II showed similar SN (> 0.99) for detection of NCFC, whereas higher SP (> 0.99) was observed for OCT. OCT was able to accurately delineate ICDAS-Radiological (R)–code 2 versus ICDAS-R-code 1 with high SN (> 0.99) and good SP (0.83) as compared to ICDAS-II criteria. **Conclusion:** The attenuation characteristics of backscattered intensity and the derived outcome measures AUC_P and AUC_T can significantly detect sound fissure from NCFC and differentiate stages of severity respectively and can be used for predicting Ek codes 0, 1 and 2 with good accuracy.

Keywords: Non-cavitated fissure caries, occlusal caries, optical coherence tomography, sensitivity and specificity.

DETECTION FOR NON-CAVITATED FISSURE CARIES WITH OPTICAL COHERENCE TOMOGRAPHY

ABSTRAK

Pengenalan: Pengesanan awal dan pengurusan pencegahan karies tanpa kaviti adalah standard penjagaan hari ini. Tujuan utama kajian ini adalah untuk meneroka potensi kaedah optik, 'Optical Coherence Tomography' (OCT), dalam mengesan karies tanpa kaviti (NCFC) dan membezakan tahap keparahannya di permukaan oklusal. **Objektif**: Pertama, untuk mengesan gigi yang sihat dan NCFC apabila fisur pada bahagian oklusal dinilai secara keseluruhan dan di lokasi anatomi yang berbeza dalam satu fisur oklusal; dan untuk menentukan persetujuan antara OCT dan 'polarisasi cahaya Microscopy PLM bagi mengukur dimensi lesi pada NCFC di bahagian yang berbeza pada suatu bahagian fisur oklusi. Kedua, untuk mencirikan Ekstrand (Ek) Kod histologi 0, 1 dan 2 secara optikal, dan untuk meneroka dan mengenal pasti 'outcome measure' bagi OCT yang boleh membezakan antara ketiga-tiga kod Ek. Ketiga, untuk mengesahkan 'outcome measure' bagi OCT yang telah dikenalpasti bagi gigi yang sihat (Ek code 0) dan NCFC (kod Ek 1 dan 2), dan perbezaan antara peringkat NCFC. Akhir sekali, untuk membandingkan ketepatan diagnostik 'outcome measure' bagi OCT dan kriteria ICDAS-II untuk pengesanan dan pembezaan NCFC. **Kaedah:** Gigi geraham kecil yang sihat dan secara semula jadi terdapatnya NCFC, diimbas pada arah 'bucco-lingual' di permukaan oklusal menggunakan 'Swept Source OCT' (SS-OCT) dan disahkan menggunakan 'Polarized Light Microscopy' (PLM) dan 'Micro-computed tomography' (Micro-CT). Perisian Bespoke yang dibangunkan dengan MATLAB (Mathworks Inc) telah digunakan untuk pengekstrakan dan pemprosesan data OCT. **Keputusan:** Penilaian visual OCT secara kualitatif boleh mengesan NCFC, secara keseluruhannya pada fisur oklusal dengan nilai SN yang tinggi (0.98) dan SP (0.95). Lesi pada dinding

mempunyai nilai SN (0.94) yang lebih kurang sama tetapi nilai SP (0.95) yang lebih tinggi berbanding dengan lesi yang terletak pada bahagian cerun. Persamaan antara OCT dan PLM dapat diperhatikan untuk nilai wWL dan hSL. Pencirian isyarat OCT berdasarkan klasifikasi histologi Ekstrand menunjukkan perbezaan dalam kadar pengecilan antara Kod Ek 0, 1 dan 2. Nilai purata intensiti penyelesaian kedalaman dilemahkan dalam dua fasa di mana ia dilemahkan lebih cepat dalam yang fasa pertama berbanding dengan yang kedua. Dalam fasa pertama, kod Ek 0 mempunyai corak bimodal, di mana terdapat penurunan mendadak dilihat pada 30 mikron, walau bagaimanapun, pada kedalaman fizikal 40 mikron, kadar pengecilan adalah perlahan dan beransur-ansur (1.43E + 06 a.u./ mikron) dapat diperhatikan. Kod Ek 2 menunjukkan kadar pengecilan terpantas (6.43E + 06 a.u./ mikron) diikuti dengan kod Ek 1 (4.46E + 06 a.u./ mikron). Selepas itu, pada fasa II, diperhatikan kadar pengecilan adalah agak perlahan dan linear bagi ketiga-tiga kod Ek sehingga kadar mendatar dicapai pada 220 mikron. AUC_P da n AUC_T merupakan dua 'outcome measures' yang dapat mengesan bunyi dari NCFC dan membezakan antara peringkat (kod Ek 1 berbanding kod Ek 2) NCFC masing-masing. AUC_P pada 3.038E + 10 (a.u.) menunjukkan 0.86 SN dan > 0.99 SP dengan 0. 95 AUROC untuk mengesan bunyi (kod Ek 0) dan NCFC (kod Ek 1 dan 2). AUC_T pada nilai 7.031E + 10 (au) adalah terhad kepada sensitiviti 0.61 dan sederhana rendah SP 0.73 dengan 0.66 AUROC dalam menggariskan kod Ek 1 dan kod Ek 2. Pengesahan 'outcome measures' AUC_P bagi OCT menunjukkan tiada perbezaan signifikan dalam mengesan gigi yang sihat dan NCFC apabila sistem alur-lekuk dinilai secara keseluruhan berbanding alur aklusal di mana kedua-dua lokasi anatomi mempunyai sensitiviti tepat (> 0.99) dan kekhususan yang baik (0,79). Untuk pembezaan, 'outcome measures' AUC_T bagi OCT menunjukkan sensitiviti yang sama di lokasi anatomi yang berbeza (0.80), namun begitu, kekhususan (0.75) adalah paling tinggi di fisur oklusal. Analisa OCT secara kuantitatif jika

dibandingkan dengan kriteria visual ICDAS-II menunjukkan sensitiviti yang sama (> 0.99) bagi mengesan NCFC, manakala kekhususan tinggi (> 0.99) diperhatikan bagi OCT pada permukaan oklusal. OCT didapati dapat menggambarkan dengan tepat ICDAS-Radiologi (R) -code 2 berbanding dengan ICDAS-R-kod 1 dengan nilai kepekaan yang tinggi dan kekhususan yang baik (0.83) berbanding dengan kriteria ICDAS-II. **Kesimpulan:** Ciri-ciri pengecilan OCT 'backscattered intensity' dan 'outcome measure' AUC_P dan AUC_T yang terhasil, dengan siknifikannya dapat mengesan dan membezakan gigi yang sihat dari NCFC, dan peringkat keparahan di permukaan oklusal. Ianya juga boleh digunakan untuk meramalkan Kod Ek 0, 1 dan 2 dengan lebih tepat.

ACKNOWLEDGEMENTS

In the name of God, the Gracious, the merciful. All praise and thanks is due to Allah (SWT), the lord of mankind. Foremost, I would like to express my sincere gratitude to my supervisor Dr Chew Hooi Pin for her continuous support, patience and motivation. Her knowledge and guidance has immensely helped me personally and professionally. Her systematic approach in conducting research has been truly inspirational for me. I would like to take this opportunity to thank Dr. Christian Zakian for his dedication and efforts, spending hours of discussions in designing and refining the methods involved in this research project. He has also played a key role as a mentor and advisor. I especially thank him for his constant support. My sincere thanks to Prof Dr Alex Fok and the support team for his scientific guidance. I would like to thank the University Malaya for offering the High Impact research grants from the Ministry of Education to conduct this research. Special thanks to my colleague Saad for his time, unlimited discussions and keeping me motivated. He has been instrumental in designing the methodology for this research project. Ali for his immense support and understanding. Thanks to my wonderful colleagues, OCT research team, science officers and wonderful friends who made this journey memorable. These past several years have not been an easy ride, both personally and professionally. Most importantly I would like to thank my family for their unconditional support. My husband, Zain for believing in me and standing by me throughout this journey. Special thanks to my parents and siblings who have been my inspiration. My love and appreciation to Hyatt, Zeest and Safia for patiently bearing with me and allowing me to pursue my dreams. God is kind and helped me sail through with his blessings in the form of immense support from my supervisors, colleagues and friends who gave this journey countless unforgettable moments of lifetime. This

doctorate would not have been possible without you all. I dedicate this thesis to my lovely daughters.

TABLE OF CONTENTS

LIST OF FIGURES

LIST OF TABLES

LIST OF ABBREVIATIONS

NCFC: Non-cavitated fissure caries

PLM: Polarized light microscopy

OCT: Optical coherence tomography

DEJ: Dentin enamel junction

R.I: refractive index

ICDAS: International Caries Detection and Assessment System

Ek : Ekstrand

E: Entrance

L: Whole lesion

SL: Slope lesion

WL: Wall lesion

hSL: Height of slope lesion

wWL: Width of wall lesion

hWL: Height of wall lesion

3D: 3 dimensional

SN: Sensitivity

SP: Specificity

PPV: Positive predictive values

NPV: Negative predictive values

ICC: Intra-class coefficient

I: Mean depth-resolved intensity

AR: Attenuation rate

R: Attenuation ratio

AUC_P: Partial area under the curve

AUC_T: Total area under the curve

FWHM: Full width half maximum

Z: Distance between the physical depth points

GUI: Graphic Unit interface

Y.I: Youden's index

Micro-CT: Micro-computed tomography

MDRCBB: Minnesota Dental Research for Biomaterials and Biomechanics

ICDAS-R- code: ICDAS-Radiological code

MD: Mineral density

HA: Hydroxyapatite

ISA: Interlobal structural angle

ROC: Receiver operating characteristics

db: Decibel

µm: Micrometer

mm: Millimeter

µA: Microampere

kV: Kilovolt

gm/cm^{-3}: Gram per cubic centimeter

CHAPTER 1: INTRODUCTION

Oral disease continues to be a major public health burden (Jin et al., 2016) and approximately 3.9 billion people are affected by oral conditions worldwide. Almost 10% of the global population is affected with dental caries amongst which, untreated dental caries in permanent teeth has the highest prevalence (Marcenes et al., 2013). Dental caries, when in enamel results in sub clinical changes when microbes within the biofilm metabolize fermentable carbohydrate producing lactic acid. The acid diffuses into the porous subsurface enamel via plaque resulting in loss of minerals (Featherstone, 2000; Featherstone & Rodgers, 1981; Kidd & Fejerskov, 2004). Progression of such demineralization can lead to cavitation of the tooth structure. The early lesions have a macroscopically intact surface with no visual evidence of cavitation and are termed as non-cavitated caries lesions (Gomez, 2015; Longbottom, Huysmans, Pitts, & Fontana, 2009). Early caries lesion when present on the occlusal surface can be termed as non-cavitated fissure caries (NCFC). NCFC progress slower compared to cavitated lesions (Baelum, Heidmann, & Nyvad, 2006) providing an opportunity to apply preventive regimens to reverse or arrest the disease earlier in its course (Gomez, 2015). NCFC are reversed (Kidd, 1996) or arrested by preventive, non-surgical strategies such as topical fluoride therapy (Lam & Chu, 2012), anti-bacterial therapy and/or dietary changes (Bradshaw & Lynch, 2013) and risk adjusted clinical decision making (Ismail et al., 2015; Mejare et al., 2014).

Failure to detect NCFC at the reversible stage and leaving it untreated until cavitation can lead to serious health issues and may influence individuals and communities in terms of general health, impaired function and decreased overall health related quality (Pitts et al., 2011). It increases the morbidity that is associated with

cavitation and its surgical treatment, the number of dental visits and eventually the overall cost of treatment (Hayes, Azarpazhooh, Dempster, Ravaghi, & Quinonez, 2013; Jin et al., 2016). It has a negative impact on the quality of life and patient's well-being with issues such as lack of eating, chewing, smiling and communicating due to an unpleasant appearance, damaged or lost teeth. The annual cost for oral care in European countries is approximately 79 billion Euros, and if the current trend of managing dental caries based on a restorative plan continues, then it is expected that by the year 2020 the expenditure may hit 93 billion Euros (http://www.oralhealthplatform.eu/wp-content/uploads/2015/09/Report-the-State-of-Oral-Health-in-Europe.pdf) (Patel, 2012). NCFC when undetected early in its course enters the invasive repeated restorative cycle that eventually decreases the longevity of the tooth in the dental arch. A restorative patient's care plays a vital role in caries management; however, it cannot solely assist in controlling the disease (Ismail et al., 2015). Other impacts observed in school going children and adults are low attendance, limited performance and decreased social interactions at school and work (Petersen, Bourgeois, Ogawa, Estupinan-Day, & Ndiaye, 2005). A national survey of the Canadian population reported an annual loss of over 40 million hours due to dental problems with over $1 billion dollars loss of productivity (Hayes et al., 2013).

Caries diagnosis is a step by step procedure which implies summation and analysis of all the available information (Pitts & Stamm, 2004) including detection of lesion, assessment of lesion severity, lesion activity (Ekstrand, Ricketts, & Kidd, 2001) and future risk (Reich, Lussi, & Newbrun, 1999) to formulate a comprehensive patient care management plan (Ismail et al., 2015; Ismail et al., 2013). These plans differ from the traditional recommendation of clinical restorative procedures where the clinician only focuses on the high quality of restorations without taking into account the control and prevention of the disease (Ismail et al., 2015). In the light of current evidence-based

understanding, the caries management pathway focuses on oral health promotion and preservation of the tooth structure as much as possible, and only restore when it is obligatory (Ismail et al., 2013).

Detection of NCFC is the first step towards minimal invasive dentistry (Nyvad, 2004), however, the complex anatomy of the occlusal surface makes the early detection more difficult (Jablonski-Momeni, Stachniss, Ricketts, Heinzel-Gutenbrunner, & Pieper, 2008). Detection without its assessment of severity has minimal clinical significance as it only represents part of the diagnostic process and cannot fully assist in achieving the goals of the caries management pathway (Banting et al., 2005). Severity assessment helps in understanding and recording the classical stages from a reversible non-cavitated stage to an irreversible cavitated stage. In the ORCA symposium proceedings, it was concluded that there is an urgent need for methods that can determine whether the lesion is stable or progressing (Pine & ten Bosch, 1996). Staging of NCFC can be useful in monitoring the progress of the lesion, arrest or regression over time (Banting et al., 2005). To achieve these goals clinically, objective tools are needed that can be used reliably by one or more operators to yield identical results.

In a systematic review, the performance of current caries detection methods for non-cavitated lesion was reported to be poor when compared with Electrical conductance (EC) that was rated fair (Gomez, Tellez, Pretty, Ellwood, & Ismail, 2013). Currently, visual inspection and radiography are the most common and ubiquitous methods used clinically to detect healthy tissue from NCFC (Bader, Shugars, Rozier, et al., 2001; Ismail, 2004). The current visual caries detection methods lack accuracy due to the qualitative assessment of features such as color, texture and roughness which results in wide variation in reproducibility between and among the examiners (Gomez, Tellez, et al., 2013; Ismail, 2004). Recently, the scientifically validated International

Caries Detection and Assessment System (ICDAS) has revealed moderate to high levels of accuracy and reproducibility using visual-tactile examination to detect healthy tissue from NCFC and differentiating its stages of severity (Diniz, Rodrigues, Hug, Cordeiro Rde, & Lussi, 2009; Jablonski-Momeni et al., 2008). However, it requires extensive training and calibration with a reference examiner (Diniz et al., 2009; Jablonski-Momeni et al., 2008; Shimada et al., 2010) and can be time-consuming (Braga, Oliveira, Bonini, Bonecker, & Mendes, 2009). Nevertheless, this visual examination also depends on the clinician's ability to qualitatively identify subtle alterations on the enamel surface. Radiographic 2D images due to its low resolution have limited usage in detecting enamel caries lesions. The NCFC is only detected on the radiograph, once it has reached the middle third of dentin and hence, beyond the scope of preventive care (Ricketts, Kidd, Smith, & Wilson, 1995; Wenzel, Larsen, & Fejerskov, 1991).

Caries detection tools using increase (Electronic Caries Monitor) or decrease (Caries Scan Pro) in the electrical conductivity or resistance respectively (Longbottom & Huysmans, 2004; Ricketts, Kidd, & Wilson, 1997) have also shown limited use on the occlusal surface (Gomez, Tellez, et al., 2013; Mortensen, Dannemand, Twetman, & Keller, 2014). Techniques using the fluorescence phenomenon utilize the change of fluorescence due to the presence of porphyrins, and metalloporphyrins to differentiate sound from carious lesions (Konig, Flemming, & Hibst, 1998). Laser Induced Fluorescence (LIFE), commercially available as DIAGNOdent® (Lussi, Hibst, & Paulus, 2004; Lussi, Imwinkelried, Pitts, Longbottom, & Reich, 1999; Lussi, Megert, Longbottom, Reich, & Francescut, 2001), Light Induced Fluorescence Evaluator for Diagnosis & Treatment (LIFEDT) (Terrer et al., 2009) and Quantitative Light-induced Fluorescence (QLF) (Gomez, Tellez, et al., 2013) either lacks sensitivity (SN) or specificity (SP) to detect NCFC on the occlusal surface. Another new technology, the Canary system based on photo thermal radiometry and modulated luminescence

(PTR/LUM) technology is limited to preliminary results and is not ready to be used in clinical settings (Gomez, 2015; Jallad, Zero, Eckert, & Ferreira Zandona, 2015). All these techniques may help the clinician in early detection and staging of NCFC with wide variation of accuracy and reproducibility. Factors like stain, plaque and calculus hamper the performance of the fluorescence-based systems (Lussi et al., 1999; Lussi et al., 2001). On the other hand, degree of hydration, thickness of enamel and inconsistent probe contact with the tooth surface, influence the outcome of electrical-based methods (Huysmans, Kuhnisch, & ten Bosch, 2005; Longbottom & Huysmans, 2004). Currently, such modalities have limited use for the detection and differentiation of NCFC on the occlusal surface (Gomez, 2015; Gomez, Tellez, et al., 2013). Therefore, an accurate and quantitative method is needed for this challenging decision in clinical practice.

Optical coherence tomography (OCT) is a non-invasive imaging technique that uses the broadband light source to obtain high resolution, cross-sectional images up to several millimeters in depth from a specimen by measuring the backscattered intensity profile. OCT is much akin to ultrasound imaging as both can create cross-sectional images except that ultra sound imaging utilizes sound waves instead of light waves with later technique requires coupling medium to transmit its signals (Huang et al., 1991). However, the resolution of OCT is 10-100 times higher than clinical ultrasound (Fujimoto, Pitris, Boppart, & Brezinski, 2000). OCT is highly sensitive to early changes in optical scattering and refractive index from non-cavitated lesions (Fried et al., 2002; Holtzman et al., 2015), as early as 5% mineral loss can produce 20 times increase in light scattering (Louie et al., 2010). In a non-cavitated lesion loss of mineral can reach up to 50% with an overlying intact surface layer enabling early detection (Silverstone, 1973).

NCFC on the occlusal surface has been detected with OCT, qualitative methods using visual assessment (Gomez, Zakian, et al., 2013; Nakajima et al., 2014; Shimada et al., 2010) and by quantification methods using intensity profile of back scattered light from the OCT A-scans (depth versus reflectivity) (Holtzman et al., 2014; Holtzman et al., 2015; Ngaotheppitak, Darling, Fried, Bush, & Bell, 2006). These studies involve the use of swept-source (SS-) and polarization sensitive (PS-) OCT systems both showed increase in the light back scatter due to increased porosities from the early demineralized enamel compared to adjacent sound enamel (Gomez, Zakian, et al., 2013; Holtzman et al., 2014; Louie et al., 2010; Nakajima et al., 2014; Ngaotheppitak et al., 2006; Shimada et al., 2010). Several studies have also demonstrated strong correlation between increased intensity and mineral loss (Darling, Huynh, & Fried, 2006; Ngaotheppitak et al., 2006). However, the diagnostic accuracy of the above mentioned OCT studies were calculated in the spectrum of various cavitated lesions where detecting a cavity from sound enamel or NCFC is not a challenge. Therefore, it would not be appropriate to extrapolate the OCT findings from a cavitated cohort to non-cavitated sample population.

Various studies of OCT have looked into quantifying the severity of the lesion by using integrated reflectivity on the occlusal surface. Jones et al, demonstrated an increase in the mean reflectivity from artificially induced early caries lesion on the occlusal surface when the specimens were exposed to 14 days pH cycle (Jones, Staninec, & Fried, 2004). In another study, Jones et al. found a strong correlation between the integrated reflectivity and mineral loss caused by artificially induced early enamel caries on the occlusal surface (Jones, Darling, Featherstone, & Fried, 2006). There are few studies that have explored the potential of OCT in quantifying lesion severity with naturally occurring early demineralization on the occlusal surface and

reported a strong correlation between mineral loss and increase in the integrated reflectivity (Louie et al., 2010; Ngaotheppitak et al., 2006).

To date, no study has quantitatively differentiated between the stages of NCFC in relation to Ek histological criteria. Therefore, there is a need for a clinical method that provides accurate detection of NCFC and differentiates its stages on the convoluted occlusal surface to achieve the goals of the current management pathway. This research focuses on optical detection and differentiation of stages of naturally occurring NCFC from each other on the occlusal surface.

1.1 Research motivation

The study aims to accurately detect and differentiate between naturally occurring stages of NCFC on the occlusal surface using OCT. The findings from this research can potentially be used as a reliable and objective method for early caries detection and assessment of the lesion (characterize and monitor) which can assist clinicians to formulate a value-based decision to manage dental caries a disease and not a lesion.

1.2 Research significance and scope

The current evidenced-based understanding of dental caries has made early detection, assessment of the lesion (severity and activity), future risk assessment and minimal invasive management the standard of care today (Berg & Swift, 2010). Current available caries detection technologies have limited abilities to clinically quantify, detect and differentiate sound fissures from naturally occurring NCFC on the occlusal surface which is a vital step in caries diagnosis (Gomez, Tellez, et al., 2013). The use of current modalities together with conventional methods increases the cumulative

efficiency clinically, however, variations in the accuracy and reproducibility decreases the diagnostic accuracy of these methods (Gomez, 2015).

Evidence shows that there is still a growing need for accurate methods of detection of NCFC (Gomez, Tellez, et al., 2013) and managing the disease at an individual as well as population level that focuses on the promotion of the oral health (Ismail et al., 2015). Therefore, the purpose of the current research is to provide an objective diagnostic tool to assist dentists in clinical decision-making to design a comprehensive patient care plan.

1.3 Aim

The aim of this study was to assess the potential of OCT to qualitatively and quantitatively detect sound fissures and NCFC and to identify OCT outcome measures which can differentiate between stages of NCFC on the occlusal surface.

The objectives of this study are:

1.3.1 Research Objective 1: To evaluate the accuracy of OCT in detecting sound fissures and naturally occurring NCFC qualitatively by visual assessment of OCT B-scan.

This objective looks into:

i) Detection accuracy of visual assessment of OCT B-scan for sound fissures and NCFC compared to Polarized light microscopy (PLM), when occlusal fissures are assessed as a whole lesion,

ii) Detection accuracy of visual assessment OCT B-scan for sound fissures and NCFC compared to PLM when the occlusal fissure is assessed at its different anatomical locations,

iii) Agreement between OCT and PLM for measuring the dimensions of naturally occurring NCFC at different anatomical locations of an occlusal fissure.

The Null Hypotheses are:

i) Visual assessment of OCT B-scan cannot detect sound fissures and NCFC when an occlusal fissure is assessed as a whole,

ii) Visual assessment of OCT B-scan cannot detect sound fissures and NCFC when the fissure is assessed at its different anatomical locations,

iii) There is no agreement between OCT and PLM in the measuring of lesion dimensions at different anatomical locations of an occlusal fissure.

1.3.2 Research Objective 2: To identify quantitative OCT outcome measures derived from depth-resolved intensity profile (A-scans) to detect sound fissures from naturally occurring NCFC and differentiate the stages of NCFC as described by the Ekstrand (Ek) histological classification.

This objective looks into:

i) Characterization of the depth-resolved intensity profile (A-scan) of sound fissures (Ek code 0) and NCFC (Ek codes 1 and 2),

ii) Exploration and identification of quantitative OCT outcome measures derived from A-scans which can detect sound fissure (Ek code 0) and NCFC (Ek codes 1 and 2),

iii) Exploration and identification of quantitative OCT outcome measures derived from A-scans which can differentiate Ek code 1 and Ek code 2,

iv) Determination of a threshold value for the identified OCT outcome measures that detect sound fissure (Ek code 0) and NCFC (Ek codes 1-2),

v) Determination of a threshold value for the identified OCT outcome measure that differentiate between the stages of NCFC (Ek code 1 and Ek code 2).

The Null Hypotheses are:

i) OCT outcome measures derived from A-scans cannot detect sound fissures (Ek code 0) and NCFC (Ek codes 1-2),

ii) OCT outcome measures derived from A-scans cannot differentiate the stages of NCFC (Ek code 1 and Ek code 2),

1.3.3 Research Objective 3: Validation of the OCT outcome measures identified in Research Objective 2 on sound enamel and NCFC characterized by Micro-CT

This objective looks into:

i) Diagnostic accuracy of the OCT outcome measure identified in Research Objective 2 to detect sound (ICDAS-Radiological (R) code 0) and NCFC (ICDAS-R codes 1-2) within the groove-fossa system and when divided as a fissure and groove,

ii) Diagnostic accuracy of OCT outcome measure to differentiate ICDAS-R code 1 and ICDAS-R code 2 within the groove-fossa system and when divided as a fissure and groove.

1.3.4 Research Objective 4: Comparison of diagnostic accuracy of OCT outcome measures and ICDAS II criteria for the detection of sound fissures (ICDAS-R code 0) and NCFC (ICDAS-R codes 1-2) and differentiation of stages of NCFC (ICDAS-R code 1 and code 2) using Micro-CT.

1.4 Research framework

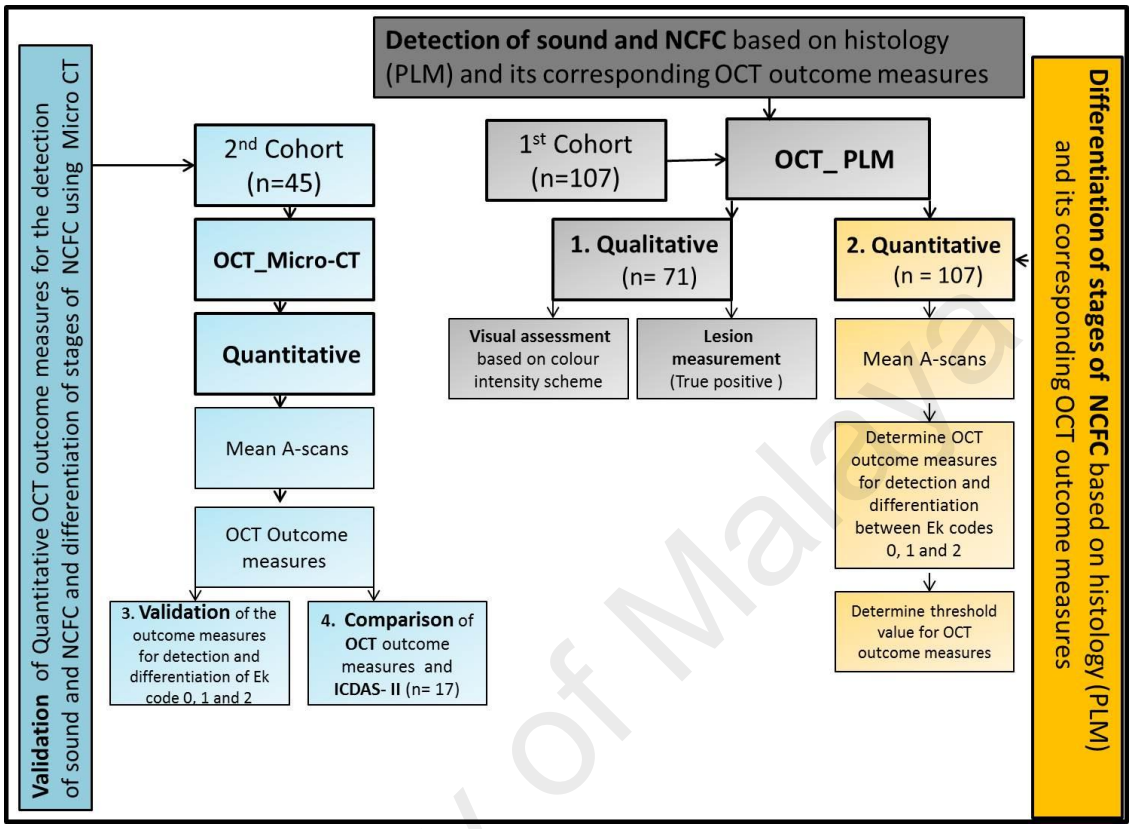

Figure 1.1: Detection and differentiation of NCFC using OCT and its comparative methods

CHAPTER 2: LITERATURE REVIEW

Detailed electronic search using MEDLINE/PubMed (National Library of Medicine, Bethesda, MD), Web of Science, The Cochrane Database of Systemic Review (CDSR) and Google Scholar databases were performed from 1961 up to 2017 using various Boolean terms.

2.1 Ultrastructure of enamel

Human dental enamel is a specialized acellular tissue that is comprised of carbonated calcium hydroxyapatite crystals (80-90%), water (2-3%) and organic material (7-18%) by volume (Robinson et al., 2000). The stoichiometric structure of hydroxyapatite crystals consist of a central hydroxyl column surrounded by a triangle of calcium ions (calcium II) which are enclosed by phosphate ions arranged in another triangle and rotated out of phase at 60 degrees. Both these triangles are further enclosed by calcium ions (calcium I) forming a hexagon, that is stacked one on top of another, each rotated at 60 degrees with respect to its adjacent neighbor (Figure 2.1) (Ichijo, Yamashita, & Terashima, 1992).

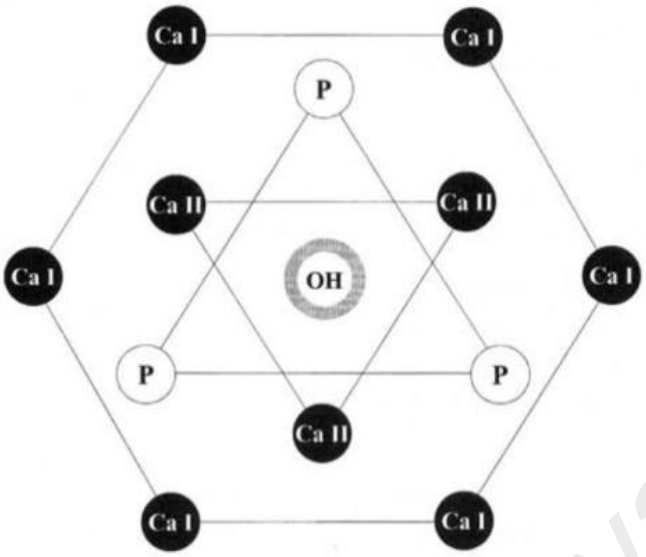

Figure 2.1: Crystal structure of hydroxyapatite. Adapted from (Robinson et al., 2000) with permission from SAGE journals.

The hydroxyapatite crystals are approximately 1mm long, 25 nm thick and 50 nm in width. Each crystal is organized in bundles of approximately 1000 crystals referred as enamel prisms that may extend the full thickness of the enamel from the enamel surface and end at the dentin-enamel junction (DEJ) (Johansen, 1965). From the cross-sectional view, the prism appears to be circular to a keyhole-shape with its head interlocking the tail (Boyde, 1989). The long axis of the crystal is arranged parallel within the head of the keyhole whereas in the tail it is perpendicular to the long axis of the prisms. There is deviation observed at the periphery of each prism which produces an interface resulting in increased inter crystalline space which is approximately 0.1 µm thick and facilitates diffusion of the materials within the tissue (Arends & Tencate, 1981; Zelander, 1973). There are a number of variations seen in the apatite crystal like missing calcium and hydroxyl ions. The density of crystals is not uniform within the enamel and is dependent on the morphology of the specific tooth (Robinson, Weatherell, & Hallsworth, 1971). The mineral content decreases while the organic material, fluid and protein content increases as it travels from the surface towards the

interior (dentin). However, at some locations like fissure enamel, the protein content is higher and the mineral content is rather low resulting in porous structures due to poor inter prismatic packing (Robinson, Weatherell, & Hallsworth, 1983).

Extraneous ions like fluoride, carbonate, magnesium along with some minor quantities of sodium, chloride and lead are also found in the mature enamel (Robinson et al., 2000). The hydroxyl group in the c-axis is less stable and can be replaced by fluoride ions during amelogenesis if the oral cavity is exposed to systematic or topical fluoride during or after the eruption of the immature enamel. The resultant fluorapatite (FAP) or fluor hydroxy apatite crystal (FHAP), depending upon the partial or complete substitution of the fluoride ion has a closer fit within the Ca II triangle. The formation of this new configuration decreases inter crystalline stress and strain by lowering the lattice energy which decreases the susceptibility to acid attack and stabilizes the crystal (Kay, Young, & Posner, 1964; Young, 1975). The concentration of the fluoride is not uniform throughout the enamel (Weatherell, Robinson, & Hallsworth, 1972). The accumulation of fluoride ions from the tissue fluid during the pre and post- eruptive phases is one of the sources for high fluoride concentrations on the enamel surface. After the formation of stable fluoridated apatite crystals on the surface, further passage of fluoride ions is restricted. This explains the highest concentration of fluoride observed on the enamel surface as compared to the inner enamel tissue (Robinson et al., 1983; Weatherell et al., 1972).

The incorporation of carbonate ions occurs during the development phase with approximately 2% concentrated at the enamel surface and 4-6% near the dentin (Weatherell, Robinson, & Hiller, 1968). The hydroxyl or phosphate/acid phosphate can be replaced by carbonate ions. There is a steep drop reported in the carbonate concentration as the ameloblasts secrete the enamel matrix (Robinson, Kirkham,

Brookes, Bonass, & Shore, 1995). The substitution of carbonate for phosphate may also involve the exchange of sodium for calcium which reflects the carbonate concentration in the crystal structure. Unlike fluoride, the carbonate has a poor fit in the lattice and less ordered crystalline structure that result in a destabilized crystal and acid soluble apatite phase (Robinson et al., 1995; Robinson et al., 2000).

The distribution of magnesium ions takes place during enamel formation similar to carbonate ions, with increased concentration from 0.2% at the surface to approximately 0.5% in the deeper layers of the enamel. Pockets of high concentration of magnesium have been observed in areas rich in protein concentrations for example areas near dentin (Robinson, Weatherell, & Hallsworth, 1981). Magnesium can be replaced by calcium, although this replacement is as minimal as 0.3% (Featherstone, Mayer, Driessens, Verbeeck, & Heijligers, 1983). Similar to carbonate, magnesium has increased charge density, hence the apatite lattice is less stable resulting in increased susceptibility for demineralization. Moreover, the carbonate and magnesium have a positive synergistic effect together which increase the solubility of the crystal mineral (LeGeros, 1984). The presence of insoluble protein is also reported with the highest amount present near the areas with less dense crystal packing and near the dentin (Weatherell, Weidmann, & Eyre, 1968).

2.2 Morphometric analysis of occlusal groove-fossa system

The caries process on the occlusal groove-fossa system starts soon after the tooth has been erupted into the oral cavity, (Ekstrand, Kuzmina, Kuzmina, & Christiansen, 2000; Ferreira Zandona et al., 2012). Therefore, it is important to have an understanding of the groove-fossa system of the occlusal surface. A system that connects each and every groove and fossa on the occlusal surface is termed as groove-fossa system. A

“fossa” is an area or depression where two or more grooves unite on the occlusal surface. An “interlobal groove” is a groove present between two or more lobes. A “lobe” is an independent, constant and stable fundamental unit which forms part of the crown. An “inter lobal groove” is a groove located between two lobe segments. All these anatomical sites together constitute the groove-fossa system (Ekstrand & Bjorndal, 1997; Ekstrand, Carlsen, & Thylstrup, 1991).

Ekstrand et al (Ekstrand et al., 1991) reported the morphometric analysis of groove fossa system in third molar teeth based on the fundamental macro morphology introduced by Carlsen in 1987 (Walsh & Brostek, 2013). Carlsen’s research was based on systematic approach in which he reported that groove-fossa system is considered as a fundamental and general structural entity in all human molar teeth (Walsh & Brostek, 2013). Therefore, the observations from groove fossa system of third molar can be extrapolated to other occlusal surfaces of the human molar teeth.

The groove-fossa system of molars mainly consists of fossa centralis which is a prominent depression approximately in the middle of the occlusal surface. There are three interlobal grooves present on the occlusal surface: the mesial, the distal and the lingual. The mesial, distal and lingual interlobal grooves are oriented mesially, distally and lingually respectively. The mesial interlobal groove ends corresponding to the fossa mesialis. However, in the absence of actual mesial marginal ridge it runs into the mesial surface. Similarly, distal interlobal groove ends corresponding to the fossa distalis or runs directly into the distal surface if the actual distal marginal ridge is absent.

Fejerskov et al (1973) reported that the morphology of the occlusal surface of the premolars varies among different teeth as well as among the same teeth within an indiviual. In 1973, he conducted a study to describe the morphology of the occlusal fissures in the premolar teeth and concluded low or no correlation between the

parameters like width of the fissure, depth of the fissure and thickness of adjecent enamel. However, occlusal angle and depth of the fissure showed a correlation (Fejerskov, Melsen, & Karring, 1973). The above findings indicated that fissures of human teeth cannot be categorized on the basis of morphological features as previously reported by Nagano, who classified occlusal fissures into five types based on morphology (Nagano, 1961).

Later, in 1991, Ekstrand and his collegues reported the quantitative characterization of the occlusal groove-fossa system based on groove depth and the structural angle in human mandibular third molars and found that interlobal groove depth varied between 0.13 and 0.55 and the structural angle varied between 2 degrees and 170 degress. He further concluded that the structure angle equal to or less than 25° were classified as a fissure, whereas the structural angle more than or equal to 25 degrees was classifed as a groove (Ekstrand et al., 1991).

2.3 Enamel caries process

Dental caries is a dynamic, ubiquitous natural process resulting in episodes of demineralization and remineralization. It is not a singular event, but an accumulation of stages and events, a continuum of increasing severity of tooth disease and destruction (Featherstone, 2004). The process of dental caries is multifactorial and reliant upon the protective and the harmful biological factors in saliva and plaque, the equilibrium between cariogenic and non-cariogenic microorganisms in the dental biofilm and the susceptibility of the dental hard tissue structures during the acidic challenge (Hicks, Garcia-Godoy, & Flaitz, 2003).

During an early demineralization process, there is a selective attack on the enamel structure. Darling (1961) reported that in a non-cavitated caries lesion, the surface zone of the enamel remains undisturbed while the subsurface or the underlying enamel is affected first. He further demonstrated that the changes in the surface zone occur at a relatively later stage and is much slower compared to the deeper enamel. The very initial path of attack starts from the enamel surface zone through striae of Retzius. However, in an established lesion where the lesion has spread deeply into the enamel, the progression of caries attack follows striae of Retzius which are incremental growth lines that runs obliquely across the prisms to approach the enamel surface. From here, the caries further spreads to the overlying enamel via inter prismatic substance to the cross-striations and reaches the core of the prism. The prism cortex remains relatively unaffected (Darling, 1961). The caries process is initiated between the biofilm and the tooth surface when fermentable carbohydrate (glucose, sucrose or fructose) is metabolized by the acidogenic and aciduric bacteria, resulting in production of organic acids including lactic, formic, acetic and propionic as a by-product of this metabolism (Featherstone, 2000). The acid diffuses via plaque, dissociating to produce hydrogen ions which dissolve the mineral crystal, setting free calcium and phosphate that diffuses out of the tooth (LeGeros, 1991). Interestingly, the lactic acid disassociates more readily resulting in the production of hydrogen ions, decreasing the plaque pH dramatically. However, this situation can be reversed by bringing back calcium, phosphate and the fluoride ions into the tooth by the process of remineralization resulting in the deposition of a new layer on the crystal in non-cavitated caries lesion. This process occurs multiple times daily in the oral cavity, depending upon the pH that favors the reverse, repair, arrest or demineralization of the tooth (Featherstone, 2000).

2.4 Etiological factors of dental caries

It is established that dental caries is multifactorial in origin and is caused by an 'imbalance' between pathological factors and protective factors (Featherstone, 2006). The biological factors play a prime role in the process of dental caries. Numerous factors like saliva, buffering capacity, oral clearance, anti-microbial properties, the concentration of acid producing microorganisms and binding of calcium phosphate to the proteins dictate the process of demineralization, reverse or arrest. When these factors create an imbalance it results in the initiation of the demineralization process (Hicks et al., 2003). Some of the factors are discussed in the following section.

2.4.1 Saliva

Saliva plays a vital role in oral health maintenance (Mandel & Wotman, 1976) . The oral cavity is bathed in oral fluids mainly secreted from major and minor salivary glands (Lenander-Lumikari & Loimaranta, 2000). It helps in the digestive process, lubrication, humidification, buffering, defense mechanism, immune surveillance, oral clearance, anti-microbial activity and maintaining calcium, phosphate rich environment in the oral cavity (Stookey, 2008).

The development and process of dental caries is dependent on the composition and concentration of salivary secretions. The composition of the saliva changes from mucoid to serous, when the salivary gland is stimulated. It assists in increased oral clearance of the ingested food particles from the oral cavity. However, conditions such as xerostomia, advanced age, female gender, oral contraceptive and certain medicines example antipsychotics, antidepressants, antihistamines and diuretics are associated with decrease salivary flow leaving the patient at an increased risk of developing caries (Hicks et al., 2003; Scully, 1986).

The buffering capacity of the saliva involves bicarbonate, phosphate and protein buffer systems (Lenander-Lumikari & Loimaranta, 2000). High concentration of sodium, protein, chloride and bicarbonate are achieved by increasing the salivary flow and helps decrease the magnesium and phosphorus concentration in the saliva. Diffusion of the bicarbonates into the plaque helps to neutralize acid which eventually increases the plaque pH and favors remineralization of the hard tissues (Dawes, 2004).

Saliva is also supersaturated with calcium and phosphate ions in relation to hydroxyapatite. The calcium, phosphate and fluoride favor the reprecipitation of the mineral on the tooth surface thus, limiting the demineralization. The first clinical evidence of the saliva to remineralize enamel was reported by Backers Dirks (1966). He included 90 children aged 7 and examined them annually for demineralization until they reached age 15. Interestingly, at age 8 he observed 72 white spot lesions on the buccal surface of the maxillary first molar. At the end of 8 years, 26 (36%) lesions were arrested and 37 (51%) had been remineralize and were no longer detectable clinically (Dirks, 1966).

The resting pH (normal pH) levels of saliva are useful predictors of the caries experience and buffering capability. Individuals that have a resting pH of saliva similar to the critical pH 5.5 are at a high risk of developing caries whereas those having a resting pH of approximately 7 are at low or no risk. The pH values between 5.5 and 7 results in less intense caries activity. However, when an individual is exposed to a refined carbohydrate diet, the presence of low resting salivary pH maintains the decrease in pH for a longer duration before returning back to the base levels which could be a serious threat to the teeth. The recovery rate of the plaque pH to its resting level is markedly increased by stimulation of the salivary flow after carbohydrates exposure (Hicks et al., 2003).

2.4.2 Dental plaque

Dental plaque is extremely complex and dynamic in nature (Thomas & Nakaishi, 2006). There are three hypotheses proposed in relation to plaque and dental caries (Loesche, 1976; Marsh, 2003; Theilade, 1986). The specific plaque hypothesis suggested that out of the diverse microorganisms present in the oral cavity within the dental plaque, only a few organisms are actively involved in the process of dental caries (Loesche, 1976). While the non-specific plaque hypothesis debates on the overall activity of the total plaque micro flora which is responsible for this dynamic process (Theilade, 1986). However, Marsh reconciled the previous findings and suggested the ecological plaque hypothesis which states the changes in the local environment due to frequent intake of fermentable carbohydrates causes a rise in the acidogenic and aciduric microorganisms, lowering the plaque pH and shifting the balance towards demineralization. The process of dental caries is better explained under ecological perspective where both diet and biofilm are the main contributing factors of dental caries, thus a more holistic approach should be taken during treatment planning (Marsh, 2003).

Several studies have shown that caries related microorganisms have a natural tendency to attach to a clean tooth surface in order to survive, colonize and grow (Thomas & Nakaishi, 2006). When the naked tooth surface is exposed to saliva, within minutes to hours it is covered by an acellular proteinaceous layer called a salivary pellicle. This tenacious coating measures 0.1–1 μm in thickness and is semi-permeable in nature restricting the transport of ions in and out of the tooth. It protects the tooth from abrasion, grinding forces during mastication and reduces friction between the oral mucosa and the teeth. The salivary contents that are rich in protein stimulates the secretion of calcium and phosphate ions within the fluid phase resulting in the super saturation of these ions decreasing the process of demineralization (Hicks et al., 2003).

Once the pellicle is formed, there is single bacterial cell colonization within 0-4 hours which becomes accumulated with the microbes. It is of utmost importance that only 2 % of the initial streptococci are mutans. The bacteria attach themselves firmly to the pellicle by electrostatic, hydrophobic ions and van der Waals forces. Within 24 hours, the bacteria grow and form micro-colonies. After 14 days the micro-colonies become more diverse and in 2 weeks, the plaque is mature and complex, in regards to its composition at different sites. Once matured, bacteria detach from the plaque biofilm and colonize to other sites (Kidd, 2005).

2.4.3 Microbiome within the dental plaque

Dental caries is an endogenous disease which occurs due to a shift in the microbial ecosystem from the mutualistic symbiosis to parasitic symbiosis. According to this hypothesis, the full range of acidogenic and aciduric bacterial species have some contribution in the process of dental caries (Takahashi & Nyvad, 2011). The oral cavity is a non-homogeneous environment for bacterial colonization. There are 700 species of microorganisms identified in the mouth (Aas, Paster, Stokes, Olsen, & Dewhirst, 2005) out of which 100- 200 species may be present in the healthy oral cavity (Kolenbrander, Palmer, Periasamy, & Jakubovics, 2010). Recently molecular studies have isolated more diverse micro flora from clinically sound and carious surfaces with hundreds of species being predominant in nature, out of which only 50% could be identified and cultured using culture media to date. Perhaps, these advanced molecular studies suggest that microbiota of dental caries is more complex and diverse than expected (Aas et al., 2005). Mutans streptococci (MS) levels identified in caries related biofilms are reported as low. The use of next-generation-sequencing and metagenomics techniques have revealed that Streptococcus mutans account for only 0.1% in dental biofilm and 0.7-

1.6% in carious lesions (Simon-Soro, Belda-Ferre, Cabrera-Rubio, Alcaraz, & Mira, 2013; Simon-Soro, Guillen-Navarro, & Mira, 2014; van Ruyven, Lingstrom, van Houte, & Kent, 2000). In another study designed to identify the metabolically active bacterial composition of different stages of caries it was concluded that out of the total bacterial community, 40% Streptococci were found in relation to enamel caries out of which only 0.02-0.73% were Streptococcus mutans (Simon-Soro et al., 2014). In fact, the microbes isolated in the formation of early lesions are non-mutans acidogenic and aciduric including lactobacilli and bifidobacterium with the most common microbes involved in the initiation of dental caries being non-mutans streptococci and Actinomyces (van Ruyven et al., 2000). It has also been reported that in the absence of MS and lactobacilli, the dissolution of enamel can occur with the presence of exclusively early micro flora only (Boyar, Thylstrup, Holmen, & Bowden, 1989).

When the fermentable carbohydrates are supplied frequently in the oral cavity, environmental acidification increases frequently. This stimulates the acidogenic and aciduric strains of non-mutans bacteria selectively, destabilizing the plaque homeostasis, thus tipping the net mineral gain to net mineral loss and favoring the process of caries initiation (acidogenic stage). Under acidic circumstances, more acid producing bacteria become dominant (aciduric stage). Perhaps, after the acidic environment is established in the oral cavity, MS, Actinomyces and other aciduric strains of non-mutans streptococci multiply in number and promotes the lesion from a non-cavitated to a cavitated stage (Takahashi & Nyvad, 2011). In conclusion, metatranscriptomics, metaproteomics and metabolomics analysis may assist in better understanding the mechanism of pathogenesis at a molecular level which initiates and progresses dental caries (Nyvad, Crielaard, Mira, Takahashi, & Beighton, 2013).

2.4.4 Dietary sugars

The fermentable carbohydrates are often referred to as free sugars, glucose polymers, fermentable oligosaccharides and refined starches. Free sugars are commonly used in reference to mono and disaccharides which are used by food manufacturers in the form of corn syrups, honey, fruit juices and other concentrates. Within these dietary sugars, sucrose in the form of processed food or monosaccharide form is considered as the most cariogenic sugar. It is readily fermented by the oral bacteria and serves as a substrate for the synthesis of extracellular polysaccharides in dental plaque (Ccahuana-Vasquez et al., 2007; Zero, van Houte, & Russo, 1986).

Oral health is dynamically related with sugar and other fermentable carbohydrates. It impacts the composition, quantity, concentration, pH of the saliva and plaque which has a local effect on oral health and integrity of the teeth. Diet related cariogenic risk depends upon numerous factors such as the type of food consumed, frequency of intake and time of retention of food in the oral cavity (Touger-Decker & van Loveren, 2003). The relationship between the quantity and frequency of free sugar intake has been well documented in the literature (Moynihan & Petersen, 2004). The frequency of sucrose exposure plays a vital role in lowering the pH to a critical level. However, calcium reserved in the dental plaque acts as a saturation buffer. In a study, Gao et al. successfully restricted the dissolution of enamel at a critically low pH (2.5) after a introducing massive amount of calcium and phosphate into the demineralization solution (Gao, Elliott, & Anderson, 1991). It is very interesting to note that during pH challenge after the free sugar diet is consumed, the reserved calcium is released into the plaque fluid to neutralize its effect. However, repeated exposure to free sugar and fermentable carbohydrate eventually results in depletion of the calcium reservoir leading to a net loss in minerals and initiation of the caries process (Pearce, 1998).

In countries with high consumption of free sugar, it has been recommended by national health authorities and decision makers to limit the amount to not more than 10% of energy intake. However, for countries with low intake levels of free sugar, the consumption should not exceed 6-10% of energy intake to achieve a decline in dental caries (Moynihan & Petersen, 2004). A quantitative analysis between sucrose and monosaccharide intake showed the log-linear dose-response relationship and its association with progressive lifetime development of dental caries (Sheiham & James, 2015).

2.4.5 Other etiological factors

There have been a significant amount of studies in the literature that has investigated the etiology of caries and the probable role of genetics as a risk predictor. There are several other traits such as tooth morphology, immune response, saliva and preference to diets that support the genetic determination of dental caries (Wright, 2010).

2.5 Non-cavitated fissure caries

Non-cavitated caries lesion is defined as a lesion with a surface that appears macroscopically intact with no visual evidence of cavitation. These lesions are also termed as incipient lesions, early lesions, and white spot lesions (Young, Fontana, & Wolff, 2010). The above mentioned terminologies encompass the clinical appearances of early caries lesion that has not yet reached the cavitation stage according to commonly used caries detection criteria in cariology. Early caries lesion when present on the occlusal surface can be termed as non-cavitated fissure caries (NCFC).

2.6 Epidemiology of NCFC

The World Health Organization (WHO) published a review in 2003 on oral health issues and concluded that despite a general drop in the oral health conditions in several countries, global oral health issues still persist (Petersen, 2003). Dental caries and periodontal disease are the bulk of oral health burdens today (Petersen et al., 2005). Dental caries is the most prevalent oral disease in most Asian and Latin American countries affecting 60-90% of children and adults (Petersen, 2005).

In a report published in 1992, the most frequent carious lesion in children of Montreal, Quebec, Canada were NCFC mainly found on the pits and fissures of the occlusal or gingival margin of smooth surfaces (Ismail et al., 1992). Another study conducted in Istanbul also reported high prevalence of active and inactive non-cavitated caries lesion in a 5 year old Turkish children (Kuvvetli, Cildir, Ergeneli, & Sandalli, 2008) . Furthermore, the inclusion of non-cavitated caries lesions in 1-5 year old children showed a significant decrease in the caries prevalence and severity with a significant reduction ($p < 0.05$) in the individual caries experience from 1996 to 2006 in Brazilian children (Carvalho, Figueiredo, Vieira, & Mestrinho, 2009). Hence, detection at a cavitation stage is no longer in accordance with the standard of care and current concepts in cariology (Carvalho & Mestrinho, 2014). Therefore, it has been suggested that extensive efforts should be made to limit the initiation of new caries lesions and to reverse or arrest existing non-cavitated caries lesions so that by 2026 every child that is born will be cavity free throughout their life (www.allianceforacavityfreefuture.eu) (Kuhnisch et al., 2016).

The World Health Organization Global Oral Health Programme (WHO GOHP) has put forward health agenda worldwide for the progression of a healthier world (Petersen, 2010). Over the past 20 years, a decrease in the caries has been observed in

most industrialized countries due to use of systemic and topical fluorides, changing life styles, diet alterations and improved oral health education (Bagramian, Garcia-Godoy, & Volpe, 2009). The prevention of dental caries does not involve detection of cavities but the earliest signs of demineralization (Ismail, 1997). The diagnosis of NCFC in epidemiological studies engaging preschool children, school children and young adults has been increasing over the last decade (Carvalho & Mestrinho, 2014). Recording of NCFC in children has been frequent in many industrialized countries (Kuhnisch, Senkel, & Heinrich-Weltzien, 2003) with pits and fissures of the first permanent molar mostly affected (Kuhnisch J, 2001).

2.7 Rationale of detection of NCFC

Detecting a lesion early in its course can increase the longevity of the tooth in the dental arch by preserving the tooth structure as much as possible. It increases the quality of life that is associated with health related problems like low nutritional intake, eating problems, growth and developmental issues which in turn elevates the efficiency and social interaction of the individual at work and school (Bagramian et al., 2009). It also decreases the number of dental visits which eventually decreases the overall cost of treatment (Pitts et al., 2011).

Studies have shown that the oral cavity is among the most expensive body parts when oral treatment is considered in some countries like Japan, Australia and Germany. In many industrialized countries, oral dental care contributes as a significant economic burden with approximately €79 billion spent on oral treatment and if the current trend continues the figure could increase to €93 billion. In the report "The State of Oral Health in Europe" in 2012 commissioned by the Platform for Better Oral Health in Europe, it was concluded that in high-income countries significant financial burdens to

the individual and society are due to dental caries and its complications. However, this disease is preventable through early detection and non-surgical, preventive regimes and other cost–effective measures like the use of fluoride (Patel, 2012).

2.8 Rationale of detection of NCFC on the occlusal surface

Dental caries is typically located on the occlusal and proximal surfaces of the permanent molars (Mejare, Kallestal, Stenlund, & Johansson, 1998; Mejare, Stenlund, & Zelezny-Holmlund, 2004). Although occlusal surfaces represent only 13 percent of total surfaces of the permanent dentition (Ripa, 1973), 88% of caries experienced by schoolchildren in the United States has been found to be pit and fissure lesions (Brunelle, 1989). Furthermore, pit and fissures contributes for majority of the caries increment observed in both fluoridated and non-fluoridated communities (Garcia, 1989). The occlusal surface provides anatomical and ecological shelter in comparison to the smooth surfaces. Hence, the prevalence of new caries lesions is highest on these anatomical sites (Hannigan, O'Mullane, Barry, Schafer, & Roberts, 2000; Mejare et al., 1998).

The presence of thick plaque on the groove-fossa system and the tooth erupting stage both are prime contributing biological determinants for caries initiation, development and arrest (Carvalho, 2014). Nevertheless, current literature does not support that during the eruption stage the early onset of dental caries on the occlusal surface is due to its incomplete post eruptive maturation (Carvalho, 2014). The enamel of the erupting teeth is more porous compared to the fully erupted teeth which are more resistant and have increased fluoride concentration limited to the surface. During the eruption period, there is constant demineralization and remineralization within the oral environment, and under favorable circumstances, the fluoro-hydroxyapatite mixed

crystal is formed in the outermost part of the enamel, limiting its role in caries reduction (Aoba & Fejerskov, 2002; ten Cate, 2013). The fluorotic and non-fluorotic opacities are not caries prone (Carvalho, Silva, Gomes, Fonseca, & Mestrinho, 2011). However, hypoplasia may be associated with increased caries risk. A large population based study conducted in 2012, demonstrated 8.7% prevalence of molar–incisor hypomineralization in the permanent teeth at the child level and 5.4% at the tooth level (Elfrink et al., 2012) explaining that the increased prevalence and initial attack on the occlusal surface is not because of erupting teeth being immature but due to the stage of tooth eruption favoring the occlusal plaque formation (Carvalho, 2014).

Stages of teeth eruption play an important role in plaque accumulation. In 1989, a clinical study carried out recording visual plaque and detailed mapping on partly and fully erupted first permanent molar and reported reduced accumulation of thick plaque and decrease in active lesions in fully erupted teeth. It further indicated that erupting teeth encourages plaque deposition due to unfavorable conditions such as lack of mechanical oral function and difficulty in accessing and cleaning these sites with a toothbrush (Carvalho, Ekstrand, & Thylstrup, 1989). It is worth noting that during the period of eruption, the tooth is most susceptible to plaque accumulation due to a decrease in the mechanical oral function (Carvalho, 2014; Carvalho et al., 1989). It may take 12 -18 months for a molar to fully erupt into a dental arch (Ekstrand et al., 2001). The stage of tooth eruption is one of the important risk determinants for caries development. Another clinical study conducted over a period of three years demonstrated a decline in the plaque scores in the groove-fossa system in fully erupted teeth on the basis of rigorous patient education and professional cleaning of the teeth (Carvalho, Thylstrup, & Ekstrand, 1992). Hence, if the nonsurgical strategies are maintained right from the beginning until the tooth is fully occluded, it can prevent the events of caries attack (Carvalho, 2014).

2.9 Susceptibility of occlusal surface

Susceptibility of the occlusal surface and its relation to fissure morphology has been proposed to play a vital role in caries initiation and progression (Konig, 1963; Nagano, 1961). Numerous studies have been carried out to identify caries resistant teeth and concluded that such relative resistance of enamel structure to caries attack does not exist. However, incorporation of fluoride into the apatite crystal of the enamel surface interferes with the carious process and has a cariostatic effect (Weathereel JA, Robinson C, & Haeesworth AS, 1983). The susceptibility of caries varies on individual tooth surfaces depending on the time period, with the shortest survival time (time from start of trial until surface is carious) reported for occlusal surfaces of first molar (Hannigan et al., 2000).

Pits and fissures of the occlusal surface of the permanent first molar followed by second molar are the most susceptible site for early decay (Carvalho, Van Nieuwenhuysen, & D'Hoore, 2001; Weintraub & Burt, 1987). Conventionally, the above claim was explained due to the morphology of the groove-fossa system that favors caries initiation, however, more recent data does not support this concept (Carvalho, 2014; Carvalho et al., 1989). Dental caries is a process resulting from imbalance of the metabolic activity in the biofilm leaving behind subsequent changes in dental hard tissues (Nyvad et al., 2013). This process is not surface bound and may take place where ever dental biofilm is undisturbed and left to accumulate and grow over time (Thylstrup & Qvist, 1987). In low cariogenic challenges, the acid produced by the bacteria may be neutralized by the saliva compensating the episodes of demineralization and remineralization. However, with an increased consumption of fermentable carbohydrates, there is an increase in acid production that decreases the pH in the mouth for prolonged periods favoring net loss in the mineral from teeth (Takahashi & Nyvad, 2011). Therefore, increased susceptibility of occlusal fissures should be re-evaluated as

more recent data suggests that if good oral hygiene and plaque removal is maintained, these sites are not easily prone to caries (Carvalho, 2014; Carvalho et al., 1992).

2.10 Shape of NCFC

Enamel caries on the occlusal surface is a localized phenomenon and mainly depends upon the site where the plaque has been accumulated and left undisturbed on the groove-fossa system. These sites are the deepest part of the groove-fossa system which are well protected from functional wear and daily cleaning by tooth brush bristles. It is interesting to note that the development of caries is three dimensional and is often seen first at the site of a fossa (Ekstrand et al., 2001). The progression of the enamel caries follows the direction of the enamel prism (Black, 1908; Ekstrand, Ricketts, & Kidd, 1998). Histologically, the prism in the pits and fissure is arranged divergently in an occlusal-apical direction, hence the shape of the NCFC on the occlusal surface assumes a cone with its apex towards the occlusal surface and the base pointing towards the DEJ (Thylstrup & Fejerskov, 1994).

2.11 Histology of the non-cavitated caries lesion

In 1961, Darling had described four porosity related zones of the non-cavitated caries lesion travelling from the sound enamel to the enamel surface and are discussed below (Darling, 1956, 1961):

2.11.1 Translucent zone

The earliest lesion consists of only a translucent zone at the advancing edge of the lesion and is a zone of demineralized enamel. However, this zone is not always present. It consists of approximately 1-2 % of spaces, some minutely that are accessible to water molecules and the rest are large enough to accept molecules such as quinolone. There are no intermediate spaces between these extreme ranges. It is interesting to note that these large spaces do not further increase in size. Since the formation of this zone is very early, the large spaces can only be visible when filled with air (R.I = 1.0) without evidence of demineralization. However, this zone is completely translucent when immersed in media of a similar refractive index as enamel (e.g. quinolone RI 1.62) with no form of birefringence. This phenomenon could be explained due to difference in the refractive index (RI) between enamel and the medium. The characteristic appearance of this zone is the absence of structural markings in any medium which is visible in normal enamel. The early loss of organic molecules results in the removal of large fragments from the enamel structure compared to small inorganic molecules that resist the initial attack. Furthermore, a loss of about 1% of mineral loss is also reported.

2.11.2 Dark zone

The succeeding dark zone is a zone of remineralization with a pore volume of 5-10% when immersed in non-aqueous media (e.g. quinolone) and produces birefringence. However, with a similar refractive index (aqueous media) it disappears. Further detailed investigation revealed that the appearance of the dark zone from aqueous to non-aqueous media is due to the molecular size of the medium and not related to the type of medium used. This zone comprises of a series of mixed spaces including the largest to intermediate to the smaller size. The small spaces continue to

grow to various sizes until they are big enough to admit molecules of quinolone. The small and the growing spaces are the characteristics of the dark zone. In this zone the larger pores are derived from the translucent zone and the smallest pores could possibly be formed due to removal of small minerals showing evidence of demineralization. Another possible explanation for the formation of smaller pores could be due to the blockage of larger pores in the initial translucent zone representing natural repair and some form of remineralization or due to accumulation of some exogenous proteins.

Darling further reported that when the specimen was dried and imbibed with quinolone (R.I = 1.62) having a larger molecular size, it penetrated only to larger spaces leaving behind the smaller spaces filled with air resulting in the birefringence due to the difference in the refractive index between air and enamel. When the same specimen was immersed with Thoulet's solution (R.I = 1.62) having a small molecular size, the molecules penetrated all over the spaces and no birefringence and no dark zone was produced. Hence, the dark zone was regarded as a molecular sieve.

2.11.3 Body of lesion

This is the zone of demineralization which predominantly consists of fully grown large spaces up to 25–50 %, filling these spaces with molecules of all media used, and highlighting further demineralization. The smaller spaces from the dark zone grow in size and result in the formation of larger spaces of the body of the lesion. These fully grown spaces are distinctive features of the body of the lesion. This zone is situated 15 to 30 μm below the intact enamel surface.

2.11.4 Surface zone

The intact surface zone was seen shortly after the initial caries attack, the translucent zone was formed. This zone was negatively birefringent due to the presence of pore volume less than 5%. When viewed under polarized light microscopy under water imbibition, the adjacent sound enamel has a pore volume of 0.1% with negative birefringence. This zone remains unaffected and subsequent demineralization occurred subsurface. The porosity of this zone accounted for 1-2 %, very similar to the sound enamel. The process of demineralization in this zone was protected and delayed in relation to the immediate subjacent tissues proving the relatively resistant nature of this zone or due to reformation and redeposition of the mineral dissolved from the deeper layers during the caries process.

2.12 Clinical appearance of NCFC

The clinical manifestation of NCFC is the white spot lesion. These lesions are opaque and have decreased fluorescence in comparison to sound enamel. The opaque appearance of the NCFC is due to an optical phenomenon that changes the refractive index (RI) and increases the light scattering due to loss of minerals (Gorelick, Geiger, & Gwinnett, 1982). The key aspect in understanding the clinical presentation of NCFC is that the demineralized enamel is more porous than the healthy, sound enamel. Once there is loss of minerals the micro pores fill with saliva. However, early demineralization is only visible after thorough air drying that displaces water from the micro porosities and leaves behind air. The difference in the refractive index between enamel (1.62) and water (1.33) is less compared to enamel and air (1.0), therefore, less porous lesions that are early in its course can be detected as an obvious white spot (Ekstrand et al., 2001).

2.13 Caries diagnosis

The art of identification of a disease based on its signs and symptoms is regarded as Caries diagnosis (Nyvad, 2004). The aim of caries diagnosis is to accuretly detect the lesion, assess its severity, characterize the caries activity of lesions and its risk assesment inorder to assist clinicians in the evidence-based decision making process (Ekstrand et al., 2001). Diagnosis is the art of balancing and a mental resting place (Baelum V, 2003) where the clinician implies summation of all the available data for therapeutic decisions (Pitts & Stamm, 2004). It involves recognition of the disease pattern, probability of the disease and hypothetico-deductive thinking to select the best possible treatment for the patient (Wulff HR & PC, 2000). Diagnosis gives the foundation to formulate the informed treatment decisions based on present and future occurrence of disease. Perhaps, if there was no act of diagnosing probability of a disease, we can never have the evidence-based approach to non-surgical treatments and clinicians may fix the problems based on the previous clinical experience of similar findings. The process of diagnosis has an inherent complexity which is why the clinician should take action when treatment is needed and must not make a decision when it is not warranted (Nyvad, 2004). This research will discuss and look into the detection and severity assessment of NCFC on the occlusal surface.

2.13.1 Detection of NCFC and its clinical significance

Detection is an objective way of determination of the presence or absence of a disease (Pitts & Stamm, 2004). Detection of non-cavitated caries lesion is essential for managing disease at the surface level (Kuhnisch et al., 2016). The current evidence-based understanding of dental caries focuses on the detection, severity assessment,

lesion assessment of non-cavitated caries lesion and its management based on preventive regimes and non-invasive procedures (Gomez, 2015).

The technical foundation of a restorative dentistry was established by Dr G.V. Black, who was well aware of the limitation of restorative approach in managing dental caries and recognized the importance of enamel caries. Prevention until 20th century was mechanical in nature and based on the principle of "extension for prevention" along with some alteration in the oral hygiene status of the patient (Black, 1880, 1910; Black & Black, 1924). This mindset of the dentist was challenged with the development of fluoride and the understanding of its caries preventive mechanism of action, enhancing the process of remineralization and inhibition of bacterial activity within the dental plaque on the non-cavitated caries lesion (Anderson, Bales, & Omnell, 1993; Featherstone, 1999; ten Cate & Featherstone, 1991). Later in 1996, Pine and Ten Bosch, asserted that detection of non-cavitated caries lesion and finding new methods and technologies to detect these early lesions is important but is only part of the existing problem and researchers should look into whether the use of such new methods will facilitate treatment decisions or not (Pine & ten Bosch, 1996).

The importance of detection of non-cavitated caries lesion have been recognized since early 1900, however, dental caries is still diagnosed at the cavitation stage and managed using a restorative approach (Gomez, 2015). Unfortunately, managing dental caries exclusively based on a biological model (Featherstone, 1999) has not helped by far in significantly changing the caries societal burden, dental education system, patient care management as well as reimbursement and incentive systems that reward the operator based on the number of restorations and complex procedures performed (Ismail et al., 2013). In general practice, the operative patient care for caries management has always been in the limelight which has a negative impact on clinical outcomes and the

quality of life of the patient (Gomez, 2015). Evidence suggests that the quality of patient care should be evaluated by promotion of oral health, prevention of early and advanced lesions, preservation of the tooth structure as much as possible and behavioral alterations to achieve health outcomes and not by the quality of restorations (Ismail et al., 2013).

The systematic review of literature on the clinical caries detection system and other sources reported discrepancies in measuring the process of dental caries (Ekstrand, Ricketts, & Kidd, 1997; Fyffe, Deery, Nugent, Nuttall, & Pitts, 2000; Ismail, 2004). There were inconsistencies observed between the European and American caries detection systems. In Europe the research community recorded and measured the process of demineralization of non-cavitated caries lesion, whereas in USA it was acknowledged at the cavitation stage. Comparison of data among different countries would only be possible and beneficial if the caries detection system is universally accepted by epidemiologists, scientific researchers and dental practitioners (Banting et al., 2005). Therefore, the development of an integrated system for research, education and clinical practice was much needed (Banting et al., 2005). In 2003, International Caries Detection and Assessment System ICDAS was established that incorporated the research conducted by Ekstrand et al (Ekstrand, Kuzmina, Bjørndal, & Thylstrup, 1995; Ekstrand et al., 1997) and other systems described by Ismail in a systematic review (Ismail, 2004).

The current caries detection methods offer challenges clinically, primarily due to the lack of accuracy to detect and differentiate early changes, let alone monitor their progression over time (Gomez, Tellez, et al., 2013; Ismail, 2004). The main short falls are in terms of precision and wide variation in inter-examiner and intra-examiner reproducibility due to subjectivity of these detection methods. A commonly used

practice by the dentist is use of color, consistency and texture to detect and differentiate NCFC. These parameters lack the objectivity in detecting early lesions and designing comprehensive patient care (Ismail, 2004; Ismail et al., 2015).

2.13.2 Severity assessment of NCFC and its clinical significance

Detection and severity assessment of NCFC are important and initial steps which together can help the clinicians to strategize and plan non-invasive management for caries control (Gomez, 2015). In the literature there have been many systems availabe for visually grading the severity of dental caries that includes NCFC (Banting et al., 2005; Ekstrand et al., 1997; Kuhnisch et al., 2009; Nyvad, Machiulskiene, & Baelum, 1999; Pitts, 2004; Pitts & Stamm, 2004). However, the ICDAS system provides a global platform and an integrated international system for caries detection in the cariology community (Banting et al., 2005). ICDAS measures the sequential stages of the carious process rather than a single decayed stage (Ismail et al., 2007). ICDAS caries detection criteria emphasized, on clinically recording early non-cavitated caries lesion separately as the first visual change in enamel after prolonged air drying of > 5 seconds (Code 1) from distinct visual changes in enamel visible on the wet surface without air drying (Code 2) (Ekstrand et al., 1997).

Detection of NCFC is a part of the act of diagnosis, hence assessing its severity is part of the diagnostic process (Banting et al., 2005). From a clinical perspective it is very important to understand the relationship between stages of NCFC and the corresponding changes that take place at a histological level as the lesion progresses. The cariogenic plaque present on the occlusal surface results in the dissolution of the crystal periphery (Holmen, Thylstrup, Ogaard, & Kragh, 1985; Thylstrup & Fejerskov, 1994). During an acidic challenge the dissolution of the crystal continues favoring the

enlargement of inter crystalline spaces confined to the outer 50% of the enamel (Figure 2.2b) (Thylstrup & Fejerskov, 1994). This advancement of the lesion gives rise to the optical properties of the white spot which is only visible after air drying (Ek code 1). It is worth noting that at this stage the underlying dentin is sound and not affected at all. This is a critical stage and detection of NCFC at this early stage is important as the lesion can be reversed or arrested by caries preventive measures (Ekstrand et al., 1997, 1998).

Differentiating stages of NCFC is indispensible because after this stage (Ek code 2) the reversal of the lesion is not possible (Figure 2.2c,d). When the NCFC reaches more than the inner 50% of enamel, a defense reaction within the dentinal tubules starts. The odontoblast process starts to lay down calcific deposits within the tubules, plugging it then with mineral deposits and decreasing the acid diffusion and providing some protection to the pulp, corresponding to the extent of the enamel lesion only (Figure 2.2c) (Bjorndal & Thylstrup, 1995; Thylstrup & Fejerskov, 1994). Nevertheless, when the lesion further progresses to the DEJ and enters the outer one third of the dentin, the dentin caries is still within or equal to the width of the overlying enamel lesion with no undermining of the adjacent enamel (Ek code 2) (Figure 2.2d). The dentin at this stage is stained and demineralized but remains hard and is non-infected (Ekstrand et al., 1998). Therefore, detection and assessment of lesion severity and activity at this stage is crucial because after this point micro cavitation occurs, hence, it is beyond the scope of preventive dentistry alone to manage it. After this stage the lesion has progressed to the middle third of the dentin (Ek code 3) (Ekstrand et al., 1997). This is an irreversible stage where the occlusal enamel has been undermined along with the lateral spread of the caries from DEJ (Figure 2.2e, f). At this stage dentin is infected and the texture has changed from hard to soft (Ekstrand et al., 1998). Therefore, this new lesion cannot be

reversed but should be treated with minimal invasive and preventive treatment according to the patient's risk level.

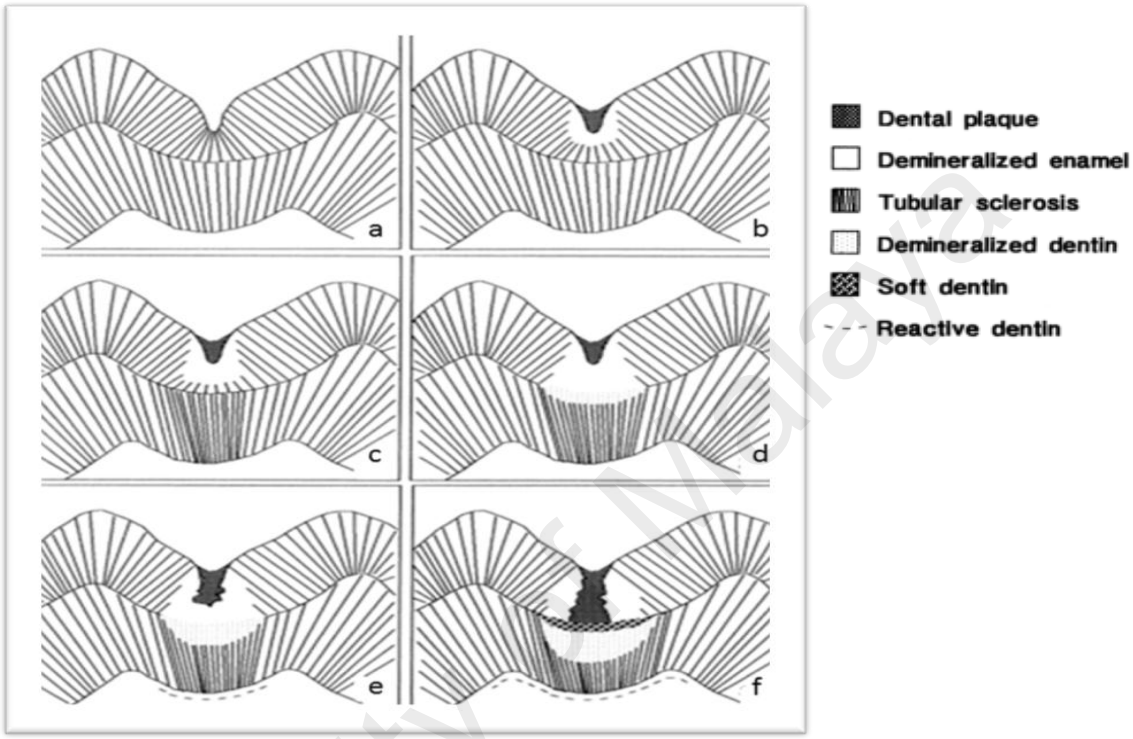

Figure 2.2: The relationship between progressive stages of occlusal caries and the corresponding histological changes. Adapted from (Ekstrand et al., 1998), with permission from Springer Link.

2.14 Detection methods of NCFC

In the 21st century, dental practitioners and researchers have multiple tools, devices and methods for the detection of NCFC. Apart from the traditional methods such as visual, visuo-tactile and radiography, there are non-optical and optical based methods available (Jablonski-Momeni et al., 2008). However, non-invasive medical

imaging techniques have received immense attention recently and a lot of research and development has been conducted to replace the traditional invasive methods by optical methods like scanning laser microscopy, fluorescence microscopy and more recently optical coherence tomography.

2.14.1 Conventional methods

2.14.1.1 Visual tactile detection

Visual inspection is the global clinical detection system and is based on qualitative assessment of features like color, texture and roughness (Maupome & Pretty, 2004). Based on current literature these parameters suffer from subjectivity. Until 2001, early lesions were recorded at cavitation level by the WHO standard (organization). In a systematic review, detection of early occlusal caries with visual examination recorded at the cavitation level by the WHO standard was reported to be weak with low SN (0.66) and SP (0.69) (Bader, Shugars, & Bonito, 2001). In another systematic review, Ismail concluded that there is a vast variation among the new caries detection methods and how the caries process was being quantified. In 2001, a systematic review, regarding the "diagnosis and management of dental caries throughout life" was presented at the National Institute of Health (NIH) conference and concluded that the available evidence of reliability and reproducibility of currently diagnostic methods were weak (Bader, Shugars, & Bonito, 2001). Nevertheless, there is a need for defining one international system for visual and visuo-tactile examination of the caries based on scientific evidence (Ismail, 2004). In a systematic review, Gomez et al. critically appraised the performance of different detection methods for non-cavitated caries lesion and observed extensive variations in the SN (0.20-0.96) and the SP (0.5-1.0) using visual examination. Furthermore, the strength of the evidence for visual examination was rated

poor (Gomez, Tellez, et al., 2013). In a proceeding in Cape town, Gomez concluded that based on previous systematic reviews, additional caries detection methods should be used in combination with visual methods as an adjunct to comprehensive patient care (Gomez, 2015). The following section briefly describes the commonly used visual tactile caries detection and classification systems.

(a) Ekstrand (Ek) visual criteria

In 1995, Ekstrand et al for the first time reported the relationship between eight obvious macroscopic changes on the occlusal surface with the histological depth of the lesion (K. Ekstrand et al., 1995). Later, in 1997, Ekstrand et al proposed the modified version of 5 point visual ranked scoring system and the corresponding histological changes (Table 2.1) (Ekstrand et al., 1997). It has shown good correlation ranging between 0.87-0.93 when compared to the histology. The system has shown promising results, however it is time consuming and requires time to learn by new examiners (Ekstrand et al., 1997).

Table 2.1:Ekstrand criteria for visual examination and its corresponding histology.

Code	Visual Criteria	Histology
0	No or slight change in enamel translucency after prolonged air drying (> 5 seconds)	No enamel demineralization or a narrow surface zone of opacity (edge phenomenon).
1	Opacity or discoloration hardly visible on the wet surface, but distantly visible after air drying	Enamel demineralization limited to the outer 50% of the enamel layer.
2	Opacity or discoloration distinctly visible without air drying	Demineralization involving between 50% of the enamel and outer third of the dentin.
3	Localized enamel breakdown in opaque or discolored enamel and/or greyish discoloration from the underlying dentin	Demineralization involving the middle third of the dentin.
4	Cavitation in opaque or discolored enamel exposing the dentin	Demineralization involving the inner third of the dentin.

(Ekstrand et al., 1997)

*(b) **Nyvad visual system***

Another system devised by Nyvad et al aims at caries detection and activity assessment of both non-cavitated and cavitated caries lesions in permanent teeth (Nyvad et al., 1999). Later in 2009, this system was also used to evaluate the detection of occlusal lesions in primary teeth and showed good SN of 0.89 at D1 threshold (caries limited to the outer half of the enamel) (Braga, Mendes, Martignon, Ricketts, & Ekstrand, 2009). This scoring system was based on ten diagnostic codes (Table 2.2) and has shown good inter-examiner and intra examiner reliability in the range of 0.78-0.80 and 0.74-0.85 respectively (Nyvad et al., 1999). It has also proven to have good validity for severity scoring with caries activity assessment (Nyvad, Machiulskiene, & Baelum, 2003).

Table 2.2: Nyvad Diagnostic criteria for active and inactive lesions.

Score	Category	Criteria
0	Sound	Normal enamel translucency and texture (slight staining allowed in otherwise sound fissure).
1	Active caries (intact surface)	Surface of enamel is whitish/yellowish opaque with loss of luster; feels rough when the tip of the probe is moved gently across the surface; generally covered with plaque. No clinically detectable loss of substance. Smooth surface: Caries lesion typically located close to gingival margin. Fissure/pit: Intact fissure morphology; lesion extending along the walls of the fissure.
2	Active caries (surface discontinuity)	Same criteria as score 1. Localized surface defect (microcavity) in enamel only. No undermined enamel or softened floor detectable with the explorer.
3	Active caries (cavity)	Enamel/dentin cavity easily visible with the naked eye; surface of cavity feels soft or leathery on gentle probing. There may or may not be pulpal involvement.
4	Inactive caries (intact surface)	Surface of enamel is whitish, brownish or black. Enamel may be shiny and feels hard and smooth when the tip of the probe is moved gently across the surface. No clinically detectable loss of substance. Smooth surface: Caries lesion typically located at some distance from gingival margin. Fissure/pit: Intact fissure morphology; lesion extending along the walls of the fissure.
5	Inactive caries (surface discontinuity)	Same criteria as score 4. Localized surface defect (microcavity) in enamel only. No undermined enamel or softened floor detectable with the explorer.
6	Inactive caries (cavity)	Enamel/dentin cavity easily visible with the naked eye; surface of cavity may be shiny and feels hard on probing with gentle pressure. No pulpal involvement.

Table 2.2. Continued.

7	Filling (sound surface)	
8	Filling + active caries	Caries lesion may be cavitated or non-cavitated.
9	Filling + inactive caries	Caries lesion may be cavitated or non-cavitated.

(Nyvad et al., 1999)

(c) ***Universal visual scoring system (UniViSS)***

Universal visual scoring system (UniViSS) aims at systematizing the clinical appearance of caries lesions for occlusal and smooth surfaces that can be used for the primary and permanent dentitions (Kuhnisch et al., 2009). It is a 5 point visual ranked scoring system (Figure 2.3) based on detection of the lesion and its severity assessment, followed by discoloration assessment and lastly activity assessment. The clinical index has shown encouraging results, however, there is not strong evidence reported in literature and further research is required (Kuhnisch et al., 2011; Kuhnisch et al., 2009).

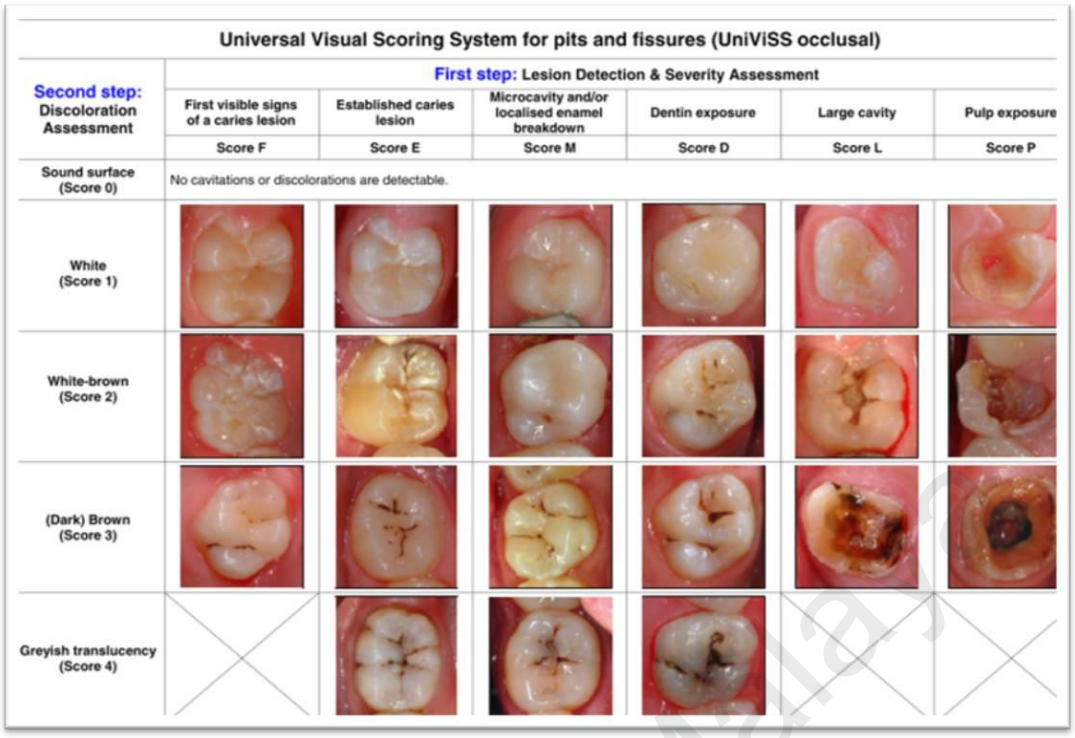

Figure 2.3: Criteria for the universal visual scoring system for pits and fissures. Adapted from 2009 Kuhnisch (Kuhnisch et al., 2009) with permission from MDPI.

(d) ***International caries detection and assessment system (ICDAS)***

ICDAS provides a new paradigm for measuring dental caries in modern dentistry. In 2002, the international group of researchers created International Caries Detection and Assessment System (ICDAS), established on the systematic review of clinical, epidemiological, and research for caries detection. As a result of discussions, a new visual ranked clinical index ICDAS-I was devised in 2003 that incorporated the concepts from Ekstrand et al research (K. Ekstrand et al., 1995; Ekstrand et al., 1997) and other systems reported in the systematic review by Ismail (Ismail, 2004). Later in 2005, in Baltimore, USA, 70 participants including researchers and cariologists from all over the world came together at the ICDAS II workshop and based on their feedback ICDAS-I was modified as ICDAS II switching code 3 (localized enamel breakdown with no visible dentin) with code 4 (underlying dentin shadow with or without localized

enamel breakdown) based on ordinal sequence of histology (Banting et al., 2005). ICDAS primarily focuses that the examination surface should be clean and plaque free prior to visual assessment. Furthermore, to detect NCFC, the surface of the teeth should be carefully air dried for 5 seconds before visual examination (Ismail et al., 2007). Nevertheless, visual-tactile examination is no more an acceptable standard for the assessment of NCFC today and ICDAS has replaced the use of sharp explorers and the probes with a ball ended periodontal probe when necessary to check the roughness, discontinuity of surface and extension of the lesion. This could be explained because probing NCFC can traumatize the potentially remineralizable, subsurface lesion into cavitated lesions which is irreversible and more vulnerable to caries progression (Ekstrand, Qvist, & Thylstrup, 1987). Additionally, probing the fissures can also transfer the cariogenic bacteria from one site to another (Lussi, 1991).

A scanning electron microscopic evaluation of probing sound and early caries lesions on the occlusal surface reported 20- 120 µm wide marks and distinct enamel breakdown up to approximately 500 µm. Therefore, dental probing is considered a harmful and damaging procedure while detecting NCFC and should be replaced by sharp eyes and careful examination (Kuhnisch, Dietz, Stosser, Hickel, & Heinrich-Weltzien, 2007). Another review reported 29 different criteria used for detection of caries, each having individual methodology and evaluation (Ismail, 2004). Out of all, approximately 50 % of the criteria suggested cleaning of the surface and drying it prior to visual examination which could adversely affect the detection of NCFC, hence risk of missing a lesion was higher where the cleaning and air drying was not advised (Ekstrand, 2004; Ismail, 2004).

ICDAS II has proven to have good validity and accuracy for the detection of occlusal caries at different severity stages (Diniz et al., 2009; Jablonski-Momeni et al.,

2008) . It has also shown significant correlation with histology in relation to lesion depth (Ekstrand, Kuzmina, Bjorndal, & Thylstrup, 1995). Although ICDAS is a novel system for caries diagnosis internationally, yet the subjectivity of this visual method affects its outcome. ICDAS II has presented lower kappa values of 0.51 and 0.59 respectively for inter and intra examiners reproducibility that did not have previous experience of using ICDAS II but were given short introduction to ICDAS II. However, the dentists involved in the above study were experienced and had been involved in various research in cariology and exposed to a variety of other systems of non-cavitated occlusal caries detection (Diniz et al., 2009). Similar lower kappa values were reported in another in-vitro study, when no training was given to the examiners (Rodrigues, Hug, Diniz, & Lussi, 2008). Nevertheless, it has generated disagreements between the examiners while differentiating NCFC from sound surfaces, decreasing the inter-examiner reproducibility (Braga, Oliveira, et al., 2009). Braga et al compared the use of ICDAS II and WHO criteria in epidemiological surveys and concluded that ICDAS II took twice as long time as taken by WHO criteria, hence it is time consuming (Braga, Oliveira, et al., 2009), and requires baseline training and calibration sessions from the reference examiner prior to ICDAS II examination (Nelson et al., 2011). Hence, the need and research of development of new technology for the detection of NCFC is still ongoing (Diniz et al., 2009; Shimada et al., 2010). In this research ICDAS II criteria and its corresponding Ek histological classification have been used for NCFC detection, severity assessment and validation purposes.

2.14.1.2 Radiographic detection

Radiography has been one of the detection tools in clinical settings for nearly 100 years. It has proven to be useful in detecting occlusal dentin lesions (Bader,

Shugars, & Bonito, 2002; Gomez, 2015). However, the validity of detecting occlusal enamel lesions is low on the occlusal surface (Gomez, Zakian, et al., 2013; Ricketts et al., 1995; Wenzel et al., 1991).

2.14.2 Non-optical caries detection method

2.14.2.1 Electrical conductance (EC)

Detection tools using electrical conductance measurements (EC) utilize the increase in the electrical conductivity to differentiate sound from non-cavitated caries lesions. The increase in the electrical conductance occurs due to porosities formed during demineralization that are filled with saliva to form conductive pathways (Ie & Verdonschot, 1994; Longbottom & Huysmans, 2004; Ricketts et al., 1997). Conversely, The Electrical Impedance Spectroscopy, commercially available as Caries Scan Pro, measures the decrease in the electrical resistance or impedance due to demineralization to detect sound and non-cavitated caries lesion (Longbottom & Huysmans, 2004). An Electronic caries monitor (ECM) measures the bulk resistance of the tooth and works on a single fixed- frequency alternating current. However, Caries Pro uses electrical impedance spectroscopy and has an advantage over ECM, taking into account the different electrical responses at different frequencies (Longbottom & Huysmans, 2004). There is limited data available in literature for the use of Caries Pro for the detection of NCFC on the occlusal surface.

In a systematic review conducted by Gomez et al. the SN score for the detection of NCFC on occlusal surfaces of permanent teeth ranged from 0.61-0.92 and the SP scores ranged from 0.73-1.0 (Gomez, Tellez, et al., 2013). Perhaps, on the occlusal surface, EC methods may provide higher SN but at a cost of lower SP (Bader, Shugars, & Bonito, 2001). There are several factors such as porosity, surface area, enamel

thickness, hydration, temperature and the concentration of ions within the saliva that can immensely impact the EC measurement (Longbottom & Huysmans, 2004).

In a systematic review, Bader et al. calculated the strength of evidence of the performance of various diagnostic methods used for caries detection based on clear and explicit assessment of the validity for a method to identify particular lesion on the particular surface. This judgment was based on 11 elements such as sample size, setting of the experiment, lesion prevalence, criteria used to detect and score the lesion, teeth and surface type, examiners reliability and number, validation method and criteria used (Bader et al., 2002). In another systematic review using the same criteria, Gomez and colleagues rated the strength of evidence for ECM as fair (Gomez, Tellez, et al., 2013). It is advisable that ECM should be used as a supplementary device along with visual examination and radiography for monitoring the disease over a period of time. However, it needs further research to use these methods in detection of NCFC on a routine basis (Gomez, 2015).

2.14.2.2 Canary system

The Canary System, developed by Quantum Dental Technologies in Toronto, Canada, is based on photo thermal radiometry and modulated luminescence (PTR/LUM) technology. The alteration in temperature (PTR) and decrease in the glow (LUM) due to the caries process can assist clinicians to detect early lesions on the occlusal surface. When the pulsating laser beam is exposed to the tooth surface, the optical energy is absorbed and converted to thermal energy (PTR) and the radiating energy (LUM), resulting in the alteration of the temperature of the tooth structure (Hellen, Mandelis, Finer, & Amaechi, 2011; Jeon, Han, Mandelis, Sanchez, & Abrams, 2004).

Jeon and colleagues in 2004 concluded that the combination of PTR and LUM technique has a lot of potential to detect the NCFC on the occlusal surface and can provide information as deep as 5mm (Jeon et al., 2004). Later in 2015, the performance of a commercially available system, The Canary system was evaluated for the detection of NCFC on permanent teeth and was reported that further assessment is needed to identify suitable thresholds in order to make treatment decisions. Currently, the literature is limited to the use of canary system clinically (Gomez, 2015; Jallad et al., 2015).

2.14.3 Optical caries detection methods

2.14.3.1 Principles of optical caries detection methods

An optical method utilizes the observation of interaction of energy in the form of a wave in the electromagnetic spectrum that is applied to or emitted from the tooth. When the energy wave is applied to the tooth it may interact with the tooth by scattering, reflection, absorption or fluorescence (Hall & Girkin, 2004).

(a) ***Scattering***

When light interacts with a small particle or an object within a non-homogeneous material, it results in change in the direction of the wave at single or multiple occasions with or without loss of energy. There is deviation of the incident light observed when the light interacts with small objects within the medium. Depending on the wavelength of the light, in relation to the size of the feature within the sample, the scattered light can transmit from a sample or be backscattered towards the source. The direction and the quantity of light scattering depends upon the size of the

object and the wavelength to which it is exposed. It is highly sensitive to wavelength with shorter wavelengths scattering higher than the longer wavelength (Hall & Girkin, 2004).

(b) ***Reflection***

Reflection is based on a single interaction with a large object resulting in the alteration of the direction of the wave in an opposite direction without altering the wavelength or energy of light (Hall & Girkin, 2004).

(c) ***Absorption or fluorescence***

Absorption is regarded as a material property in which the wave is stopped and taken in by an object and converted into various forms. Nevertheless, an object can stop wave energy and change it to another wave energy which has less energy than the previous wave with a longer wavelength. This emission of the longer wavelength light can be released through the process of fluorescence (Hall & Girkin, 2004). Demineralization of the teeth results in loss or change of fluorescence which can be detected and quantified using new caries detection methods by differentiating the fluorescence between sound and carious enamel (Borisova, Uzunov, & Avramov, 2006). The caries detection method described in this thesis uses near-infrared (NIR) light of 1310 nm and utilizes the former property of backscattering to detect and quantify NCFC from the sound enamel.

2.14.3.2 Fiber optic trans illumination (FOTI) and digital imaging fiber optic trans illumination (DIFOTI)

Fiber Optic Trans illumination (FOTI) and Digital Imaging Fiber Optic Trans illumination (DIFOTI) are easy, portable and affordable methods and accepted by the dental professional as a supplementary method for the detection of NCFC during clinical examination (Cortes, Ellwood, & Ekstrand, 2003).

Light is applied from the side of the tooth and the transmission is visualized from the occlusal surface or the opposite side, when tested with premolars and molars. FOTI device increases the contrast between the healthy and the diseased enamel by scattering and absorption of light photons which enable the operator to differentiate sound from the carious enamel. It is also worth noting that the carious enamel scatters more light compared to the sound enamel, therefore demineralized enamel appears dark whereas sound enamel appears transparent. Besides, dentin appears orange, brown to grey in color underneath the enamel. This distinct color contrast can assist in discriminating the enamel from dentin lesions (Gomez, 2015; Neuhaus, Longbottom, Ellwood, & Lussi, 2009).

It is primarily used in the detection of proximal caries and has also been explored for enamel occlusal caries detection aiding enhanced visual examination. The performance of FOTI for enamel caries detection on the occlusal surface was reported to be similar to visual examination (Cortes et al., 2003) and greater when compared with radiography (Cortes, Ekstrand, Elias-Boneta, & Ellwood, 2000). The strength of evidence reported by Bader et al. and Gomez et al. in a systematic review for FOTI and DIFOTI was poor when detecting non-cavitated caries lesion due to limited studies available and the average quality score (Bader et al., 2002; Gomez, Tellez, et al., 2013).

Since the method is not quantitative and diagnostic decisions are based on subjective outcomes using the naked eye, low reliability scores are expected due to variability between inter-examiner and intra-examiner agreement (Neuhaus et al., 2009). Furthermore, this device has a limitation in longitudinal monitoring of the caries activity as the technique does not provide any information regarding the mineral loss or gain (Choo-Smith, Dong, Cleghorn, & Hewko, 2009). To overcome the variability and the monitoring problem, Digital Imaging Fiber Optic Trans illumination (DIFOTI) has replaced the human eye with a CCD sensor. Images are saved and displayed on a computer at repeat visits. However, the software cannot quantify the images and the analysis is still subjective (Manton, 2013). In the light of current literature, the diagnostic performance of FOTI and DIFOTI to non-cavitated caries lesion is still limited (Bader, Shugars, & Bonito, 2001; Manton, 2013; Schneiderman et al., 1997).

2.14.3.3 Laser induced fluorescence (LF)

Diagnodent® is used commercially for the detection and quantification of caries (Lussi et al., 2004). The optic fiber emits red laser light (λ = 655nm) to the demineralized lesion via a probe on a suspected tooth surface, the light interacts with certain organic molecules present in the porosities and emits back in the NIR region as invisible fluorescence. The basis of the NIR fluorescence is protoporphyrin IX and related metabolic products of the bacteria resulting in the absorption of red light. The emitted light is displayed digitally on the screen via hand piece to the detector. The increase in the number represents higher fluorescence and extensive lesion (Gostanian, Shey, Kasinathan, Caceda, & Janal, 2006).

There is variation reported in literature for the detection of NCFC on occlusal surface of permanent teeth with SN score ranged from 0.46-0.96 (Lussi et al., 2001; Shi,

Welander, & Angmar-Mansson, 2000) and the SP ranged from 0.69-1 (de Paula, Campos, Diniz, Hebling, & Rodrigues, 2011; Lussi & Hellwig, 2006). Another study conducted by Achilleos and colleagues, reported moderate SN 0.66-0.75 with low SP 0.5 when detecting NCFC on the occlusal surface of posterior teeth (Achilleos, Rahiotis, Kakaboura, & Vougiouklakis, 2013). In 2013, a systematic review rated the quality of evidence for the detection of non-cavitated occlusal caries as poor (Gomez, Tellez, et al., 2013). Perhaps, in the non-cavitated caries lesion, the presence of bacterial metabolites is low compared to dentinal lesions (Kidd, Banerjee, Ferrier, Longbottom, & Nugent, 2003) which may hamper the performance of Diagnodent® by producing an insignificant increase in fluorescence compared to sound surfaces (Gomez, 2015; Lussi et al., 2001). The early lesion goes undetected by clinicians and if detected, the phenomenon is confounded by stain, plaque and calculus commonly present on the occlusal surface resulting in false positive findings (Lussi et al., 2004; Lussi et al., 1999; Lussi et al., 2001; Shi et al., 2000). It was also observed that Diagnodent® works best on occlusal and accessible smooth surfaces but is not recommended at D1 diagnostic threshold (enamel) when identifying NCFC (Lussi et al., 2004). Since the fundamental basis of Diagnodent® is registering the change in the physical characteristics of demineralized tooth structure in relation to the surrounding healthy hard tissue, higher false positive readings and poor correlation with the mineral content are expected due to the above mentioned limitations (Gomez, Tellez, et al., 2013; Shi et al., 2000). A systematic review on Diagnodent® concluded to use this tool with caution and limit its implementation as a principal diagnostic tool (Bader & Shugars, 2004).

2.14.3.4 Quantitative laser fluorescence (QLF)

Quantitative light-induced fluorescence (QLF) is a commercially available device capable of detection, quantification and monitoring the non-cavitated caries

lesion. The QLF is based on auto fluorescence and objectively measures loss of flourescence that apperas as a dark spot on a green fluorescence background, when distigushing non-cavitated caries lesion from adjecent healthy enamel that is assumed to have 100% fluorescence. Although this technique is promising in detecting and monitoring early enamel lesions on the proximal surface, studies reported on the occlusal surface are less with weak evidence (Gomez, Tellez, et al., 2013; Karlsson, 2010). De Josselin de Jong and his colleagues developed a technique taking advantage of this optical property (de Josselin de Jong et al., 1995). In a non-cavitated caries lesion the increased porosities scatter light as the fluorescence is emitted, resulting in the loss in the natural fluorescence. This alteration of fluorescence can be detected and quantified from a camera hand piece, when the tooth is eradiated by violet blue light (λ= 290 – 450nm). The image is then captured using a camera with a yellow 520 nm high pass filter. This change in fluorescence can be monitored over time to assess the lesion progression (Karlsson, 2010; van der Veen & de Josselin de Jong, 2000).

The SN and SP for detecting NCFC on the occlusal surface is reported to be 0.68 and 0.70 respectively (Pretty, 2006). In another study, QLF showed moderate SN (0.62-0.72) and high SP (0.91-0.94) while detecting occlusal caries (Gomez, Zakian, et al., 2013). In a systematic review, Gomez reported poor strength of evidence for detection of NCFC using QLF (Gomez, Tellez, et al., 2013).

There are numerous confounders reported while using the QLF device. The presence of fluorosis is one of the confounders, as the device can detect demineralization but may not be able to differentiate between caries and fluorosis. Furthermore, hydration of the lesion and inadequate reconstruction of sound fluorescence values may also confound the findings, decreasing the SP (Angmar-Mansson & ten Bosch, 2001). The current evidence for QLF as whether the method is

helpful in detection of NCFC in everyday practice is yet to be established. Further research is also needed to implement QLF as a monitoring tool. Perhaps, it is recommended to use it as a supplementary tool with the visual assessment and radiography for monitoring the lesion progression (Gomez, 2015; Pretty, 2006).

Table 2.3: Summary of performance of detection systems used for the detection of NCFC (sound versus non-cavitated lesions) on occlusal surface (Gomez, Tellez, et al., 2013)

Diagnostic method	Number of studies	Range Sensitivity	Range Specificity	Range AUROC	Strength of evidence
Visual	9	0.44-0.83	0.46-0.90	0.73	Poor
Diagnodent	0	-	-	-	-
Radiography	5	0.14-0.38	0.59-0.90	NA	Poor
FOTI	0	-	-	-	-
EC	1	0.63	0.87	NA	-
QLF	0	-	-	-	-

Fiber Optic Trans illumination (FOTI); Electrical Conductance (EC); Quantitative Laser Fluorescence (QLF)

2.14.3.5 Optical coherence tomography (OCT)

(a) ***OCT background***

Two decades and a half ago, Huang's group (Huang et al., 1991) reported Optical coherence tomography (OCT) for the first time for in-vitro imaging of the human eye. Later, in 1995, Fujimoto's group (Fujimoto et al., 1995) pioneered in vivo imaging of the human eye and since then due to its numerous advantages, the method has matured into a novel imaging modality. The use of OCT has been highlighted in

various disciplines including ophthalmology (Huang et al., 1991), dermatology (Pierce, Strasswimmer, Park, Cense, & de Boer, 2004) and dentistry (Baumgartner et al., 2000).

(b) ***Principles of OCT***

OCT is an interferometer-based system that utilizes a low coherence broadband light source to obtain a high quality cross-sectional image. The laser light is emitted from the fiber optic source and is divided by a fiber optic beam splitter into the sample and the reference arms (mirror) within a Michelson or Mach-Zehnder interferometer. The reflected signals from the reference mirror and the backscattered signals from the sample are combined together and detected by a photodetector (Figure 2.4) (Otis, Colston, Everett, & Nathel, 2000). It is important to note that the interferometric signals can only be detected when there is a constructive interference produced by matching the distance of the reference and sample arm reflections within the coherence length of the light source (Hsieh et al., 2013).

The OCT system transversely scans the incident light beam and performs numerous axial measurements of echo time delay (A-scans) at a constant velocity to obtain a two dimensional data (B- scans). Signal amplitudes are displayed using grey scale or false color value and axial signals are serially projected to form an OCT image. A cross-sectional OCT image signifies the optical reflections of a tissue. The OCT B-scans can be saved digitally and viewed in real time (Otis et al., 2000). It measures the magnitude from its depth-resolved intensity curves (A-scans) and echo time delay of backscattered light and uses broadband NIR light operating at 1310-nm to obtain cross-sectional images. The imaging depth of OCT is dependent on the structure being imaged, moreover, attenuation from the tissue scattering and absorption. The imaging depth of 2–3 mm has been attained in most cases (Fujimoto et al., 2000; Shimada, Sadr,

Sumi, & Tagami, 2015). Nevertheless, optical scattering from an image determines the magnitude of the reflective signals, thus, the contrast of the image is determined by the optical properties of the specimen being investigated (Otis et al., 2000). OCT uses low-coherence interferometry that selectively removes the backscattered signal that has undergone multiple scattering yielding high quality images that can be useful to produce both qualitative and quantitative data from morphological cross-sectional images and by quantifying change in the back scattered intensity from the tissue respectively (Hsieh et al., 2013; Otis et al., 2000).

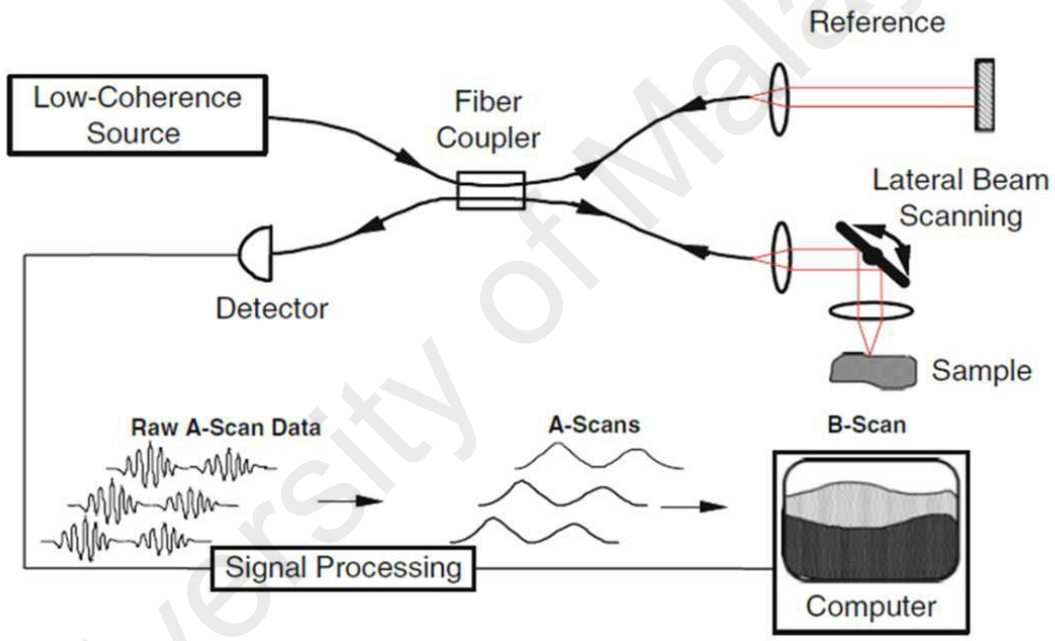

Figure 2.4: Illustration of generic OCT system

(c) ***Swept source OCT system***

Since the beginning, conventional OCT systems have always faced group delay from the reference arm which coherently channels the back scattered signals from different depth points in a given specimen. As an alternate to decrease the scanning delay, spectral discrimination (SD) approach was developed (Choma, Sarunic, Yang, & Izatt, 2003; Fercher, Hitzenberger, Kamp, & Elzaiat, 1995). Swept-source OCT (SS-

OCT) is an implementation of the spectral discrimination (SD) OCT of which time translates spectral information by sweeping a linear narrow based laser through a broad optical bandwidth that illuminates the interferometer which is detected by a photodetector. It constructs the depth profile (A-scans) of the sample by measuring both the magnitude and the time delay of the light reflected from the sample being imaged (Choma et al., 2003).

The SS-OCT system takes advantage of the Fourier-domain (FD) technology that enables a distinct increase in the SN of 20 – 30 dB compared to the traditional time-domain OCT (TD- OCT) system (Choma et al., 2003; Leitgeb, Hitzenberger, & Fercher, 2003). The first medical application of the Fourier-domain (FD) OCT was reported by Fercher et al (Fercher et al., 1995). The application of SS-OCT has found its trail into clinical diagnostics due to quick and fast image acquisition that enables real-time video rate imaging speed by improving the signal to noise ratio of the images captured. The 5-6 mm coherence length of the laser allows imaging up to a depth of approximately 3 mm without compromising the detection SN (Choma et al., 2003; Leitgeb et al., 2003). The focused light beam is projected from an objective, onto the selected location to scan a maximum range of 15mm vertically and horizontally (x and y axis) obtaining a depth-reflectivity profile and constructing a cross-sectional image. The distance between the objective and the sample is more than 25mm to ensure ease of handling of the samples (Ozawa, Sumi, Shimozato, Chong, & Kurabayashi, 2009).

(d) ***OCT and NCFC***

Dental enamel is nearly transparent in the NIR used for imaging dental hard tissue and exhibits better imaging depth compared to visible light (Jones, Huynh, Jones, & Fried, 2003). Visible light range from 400-700 nm scatters light intensely in sound

enamel limiting its transmission through the tissue being investigated. However, the optical behavior of NIR spectrum from 780 to 1550 nm is prevailed by scattering properties due to weak absorption of light by enamel. The latter property of NIR spectrum was due to partial dissolution of mineral crystals during dental caries process forming micropores of different sizes, the principal scatterers in enamel (Fried, Glena, Featherstone, & Seka, 1995; Huynh, Darling, & Fried, 2004).

NCFC on the occlusal surface has been assessed by several modalities of OCT such as swept-source (SS-) and polarization sensitive (PS-) OCT (Gomez, Zakian, et al., 2013; Holtzman et al., 2014; Louie et al., 2010; Nakajima et al., 2014; Ngaotheppitak et al., 2006; Shimada et al., 2010). Several lines of evidence indicated that OCT can distinguish sound enamel from the demineralized enamel based on increased scattering and depolarization of the incident light from demineralized enamel. However, PS-OCT or cross-polarization is necessary for the latter phenomenon of OCT (Jones et al., 2006; Jones et al., 2004; Louie et al., 2010; Shimada et al., 2015). Some of these studies used qualitative visual assessment of OCT B-scans (longitudinal images) to assess the increased intensity and the continuity of the enamel surface for the detection of NCFC (Gomez, Zakian, et al., 2013; Holtzman et al., 2010; Nakajima et al., 2014; Shimada et al., 2010), much akin to the assessment of increased radiolucency of caries lesions in radiographs. While others chose to detect and quantify non-cavitated occlusal caries (Holtzman et al., 2014; Holtzman et al., 2015) and its severity by using intensity profiles of the backscattered light obtained from the OCT A-scans (depth versus reflectivity curve) (Jones et al., 2006; Louie et al., 2010; Ngaotheppitak, Darling, & Fried, 2005).

The qualitative detection of NCFC on the occlusal surface using OCT visual assessment has been evaluated by a couple of research groups by determining the presence of increased intensity but the results are inconsistent with moderate to high

range of SN (0.89-1.00) and low to high range of SP (0.39-0.93) (Gomez, Zakian, et al., 2013; Holtzman et al., 2010; Nakajima et al., 2014; Shimada et al., 2010). Within the methodology of the above mentioned studies, the inclusion of various stages of caries (non-cavitated enamel caries, cavitated enamel caries and cavitated dentin caries), the heterogeneity of the diagnostic thresholds and the scoring of single OCT B- scan, may have resulted in over estimation of the reported results (Gomez, Zakian, et al., 2013; Holtzman et al., 2010; Nakajima et al., 2014; Shimada et al., 2010). Interestingly, in the process of detecting sound and NCFC, the diagnostic threshold in the above studies was not reported at a non-cavitated threshold (Sound versus non- cavitated caries only). Perhaps, this could result in the reporting of enhanced detection performance for NCFC. It is therefore required to understand whether OCT can assist in this challenging decision in practice while detecting NCFC from sound tissue.

It has been proven in the literature that initiation of NCFC does not involve the whole length of the groove-fossa system simultaneously. In fact, the signs of NCFC can be independent from one another at different anatomical locations which may coalesce in future (Juhl, 1983; Konig, 1963). Hence, the distance of the area above the entrance of the fissure (slope) and the wall of the fissure, relative to source of the OCT light is substantially different. The penetration depth of the OCT varies with the topography of the tooth surface to which the laser is exposed. Furthermore, the intensity of OCT signals may vary, when OCT laser is oriented to an asymmetrical geometry of slopes due to a variation in the inclination and steepness of the buccal and lingual cuspal slope of the groove-fossa system (Nakajima et al., 2012). Therefore, the true ability of OCT in NCFC detection and lesion measurement, when a groove-fossa system is assessed in totality (whole fissure) and at different anatomical locations separately requires further investigation. To the best of our knowledge, none of the studies reported earlier have

evaluated the influence of the loci of NCFC on its detection and lesion measurement with OCT.

Detection and accessing the severity for NCFC is challenging for dental practitioners due to qualitative assessment of the clinical index to date (Gomez, Tellez, et al., 2013). Therefore, quantitative analysis is the way forward to provide an easy, quick, effective and accurate detection and severity assessment of NCFC. Quantifying the changes in the optical scattering properties and refractive index detected by OCT due to early demineralization are well documented in the literature (Fried et al., 2002; Holtzman et al., 2015; Louie et al., 2010). Few studies have looked into objective methods to detect NCFC from sound enamel on the occlusal surfaces by using a log of back scattered light intensity (Holtzman et al., 2014; Holtzman et al., 2015). However, the detection threshold was set including cavitated lesions. Nevertheless, various researchers have also quantified severity by integrating the reflectivity of the orthogonal polarization (perpendicular-axis) or cross polarization of PS-OCT image (Jones et al., 2006; Jones et al., 2004; Louie et al., 2010; Ngaotheppitak et al., 2006). Louie et al, have demonstrated a strong correlation between integrated mineral loss and increase integrated light reflectivity on occlusal surface of early naturally demineralized enamel (Darling et al., 2006; Jones et al., 2006). Interestingly, non-cavitated caries lesion has shown marked increased in the light scattering compared to severe caries where only a minimal increase in scattering was observed (Darling et al., 2006). Hence, to the best of our knowledge, no study has looked into the diagnostic accuracy of OCT at non-cavitated threshold detection and quantified the severity of NCFC using Ek histological classification.

2.15 Management of NCFC

Management of dental caries based only on its biological process has not shown any promising results globally in patient management and dental education systems (Ismail et al., 2013). Hence, a caries pathway is a sequential and systematic way of patient caries management based upon personal and clinical data collection to comprehend management strategies for the patient according to individuals need. These systematic step by step protocols differ from the traditional treatment that only focused on listing the restorative procedures needed at that time for the patient (Ismail et al., 2015). Furthermore, detection of disease does not automatically justify restoring the tooth. In fact, any management method should be able to defend why a restoration is preferred over non-surgical management (Ismail et al., 2013).

In California, a questionnaire survey was conducted in 2013 to evaluate the treatment strategies in dental practice and reported that 42.6% of recently graduated dentists (20 years or less) would immediately restore a non-cavitated caries lesion that is still confined to the enamel and 49% would wait and monitor the lesion and will only restore if the lesion has reached the outer-third of the dentin (Rechmann, Domejean, Rechmann, Kinsel, & Featherstone, 2016). This clearly shows that to date, most dental practitioners are opting for restorations earlier than the scientific evidence would recommend. The clinical evidence shows that NCFC in enamel and dentin can be treated with preventive strategies without the need of restorations (Baelum, Machiulskiene, Nyvad, Richards, & Vaeth, 2003; Sbaraini & Evans, 2008). Hence, it is important to detect a NCFC and have deep understanding of the lesion severity, activity and risk factors enabling the dentist to tailor non-invasive strategies for the patient.

There are multiple systems available in literature for caries management (Ismail et al., 2013; Jenson et al., 2007; Young, Kutsch, & Whitehouse, 2009), however, the

International Caries Classification and Management System (ICCMS™) is a well-developed and thoroughly documented protocol that is based on widely and internationally used ICDAS and the policy set by FDI Word Dental Federation in 2013 (Federation, 2013; Ismail et al., 2015; Ismail et al., 2013). It addresses all diagnostic, preventive and restorative assessments obligatory to save the structure of the tooth and intervene restoratively only when it is necessary (Ismail et al., 2013). It is a comprehensive system that emphasized on patient management founded on 5 integral steps (Figure 2.4). It includes stages of the caries process, caries risk assessment, classification, ICCMS decision matrices, ICCMS comprehensive patient management plan and finally the outcome of caries management using ICCMS. ICCMS considers dental caries as a disease and not a lesion based on current evidence from literature to preserve the tooth structure as much as possible (Loe, 1995).

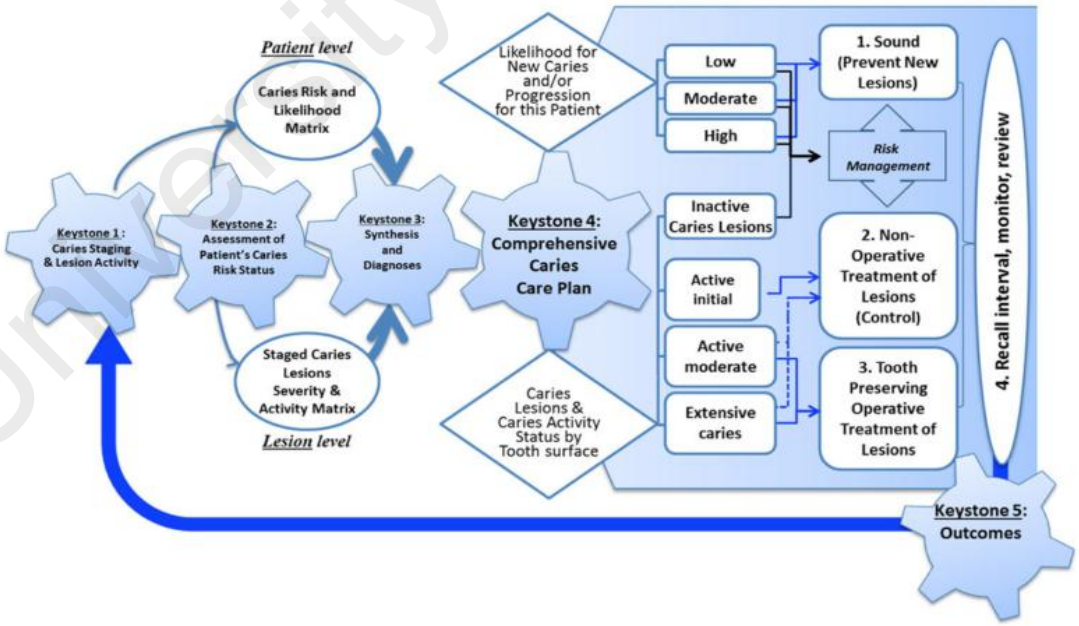

Figure 2.5: Keystones of ICCMS. Adapted from (Ismail et al., 2015), with permission from Springer Link.

CHAPTER 3: MATERIALS AND METHODS

3.1 Introduction

Human extracted premolar teeth with sound fissure and naturally occurring NCFC were used in this study. Convenient sampling was done but we assured that the number of samples included in this study was higher than reported in literature in similar studies (Gomez, Zakian, et al., 2013; Shimada et al., 2010). Pilot studies were attempted prior to deciding on the final design of this research. Special emphasis was given on techniques on sample preparation, mounting and cutting of the specimen to ensure that the early caries lesion was preserved to its maximum during histology. Furthermore, for OCT quantitative analysis (Research Objective 2,3,4), several pilots were conducted to identify the optimum number of A-scans for the selection of region of interest on the OCT-B-scans to achieve the maximum depth-resolved intensity (*I*) profile of NCFC.

3.1.1 Pilot studies for sample mounting, sectioning and polishing protocol

The aim of this pilot was to identify a minimally traumatic method that can yield 180 ± 10 μm thick specimens without damaging the early lesion for PLM imaging. Enamel is very brittle and difficult to cut into thin sections without fracture. Therefore, two methods were explored for mounting the samples to avoid fracture of the thin sections. Four premolar teeth were taken and investigation sites were identified and marked on each tooth. A reference line approximately 3 mm buccal to the investigation site was marked with a rotary diamond disc (Figure 3.1a). Two teeth were embedded in resin approximately 2 mm below the marginal ridge, exposing the occlusal portion of

the crown (Figure 3.1a) and the other two were completely submerged with resin covering the entire occlusal surface (Figure 3.1b).

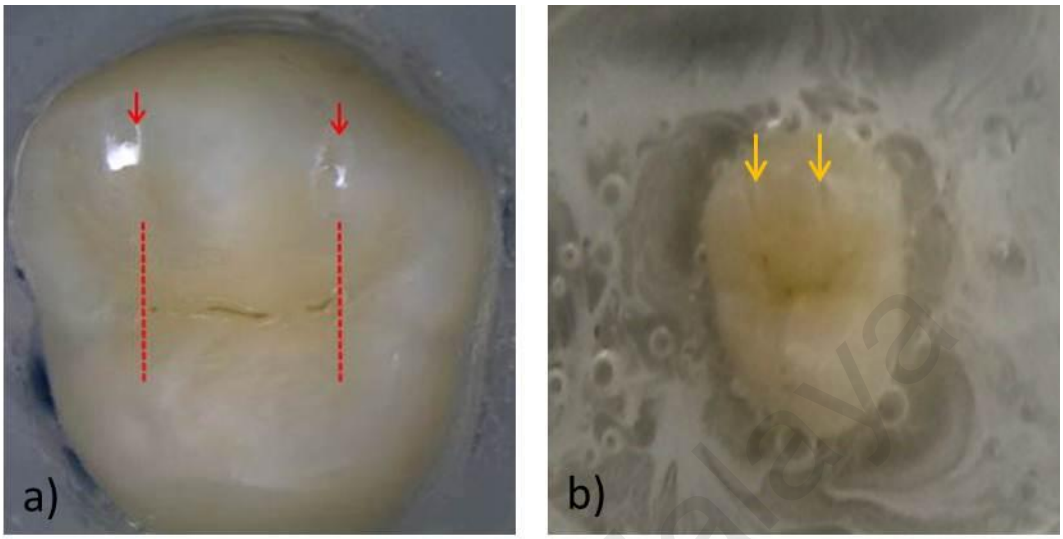

Figure 3.1: Occlusal surface of the crown showing marked investigation sites. (a) clear and distinctly marked investigation sites (red arrows) on the occlusal surface of the crown with resin poured 2 mm below the marginal ridge, (b) the investigation sites (yellow arrows) were not clear and distinctly visible from the resin surface after embedding the entire occlusal surface of the crown with resin.

The investigation sites were clearly visible on the teeth that were not embedded completely with resin and easy to section (Figure 3.1a). However, the visibility of investigation sites on the teeth embedded completely in resin were low (Figure 3.1b). Entrapment of the air bubbles on the occlusal surface during pouring further decreased the visibility of the marked investigation sites from the resin surface. For the teeth fully embedded in resin, the investigation sites were carefully transferred on the resin surface and marked with the permanent marker as a reference for PLM sectioning. The slide block, sandwich block, sectioning of the teeth and sonication of the samples were conducted according to the details mentioned in Section 3.2.5.1 up to 3.2.5.4. The

obtained sections from both procedures were approximately ≤ 200 µm. No additional grinding or polishing was done on the samples with exposed occlusal crowns. However, samples that were embedded completely with resin were subjected to polishing using Exakt polishing machine with 1200-grit polishing paper, 3 turns per sample initially. The procedure was continued until the lesion was visible for viewing under PLM. Polishing was carried out due to inaccurate positioning of the investigation site corresponding to the cutting blade that mostly resulted in sectioning before the marked investigation sites. The obtained samples after polishing were 120 ± 10 µm.

Sections were then imbibed in water, examined under a 4X-magnification microscope (Nikon Eclipse 55i, Nikon, Japan) equipped with an Analyzer Slide (Nikon C-AS Nikon, Japan) and Polarizer (Nikon C-TP Nikon, Japan) for first order red compensation, and imaged using an integrated digital camera (Nikon DSFI2, Nikon, Japan) for PLM imaging.

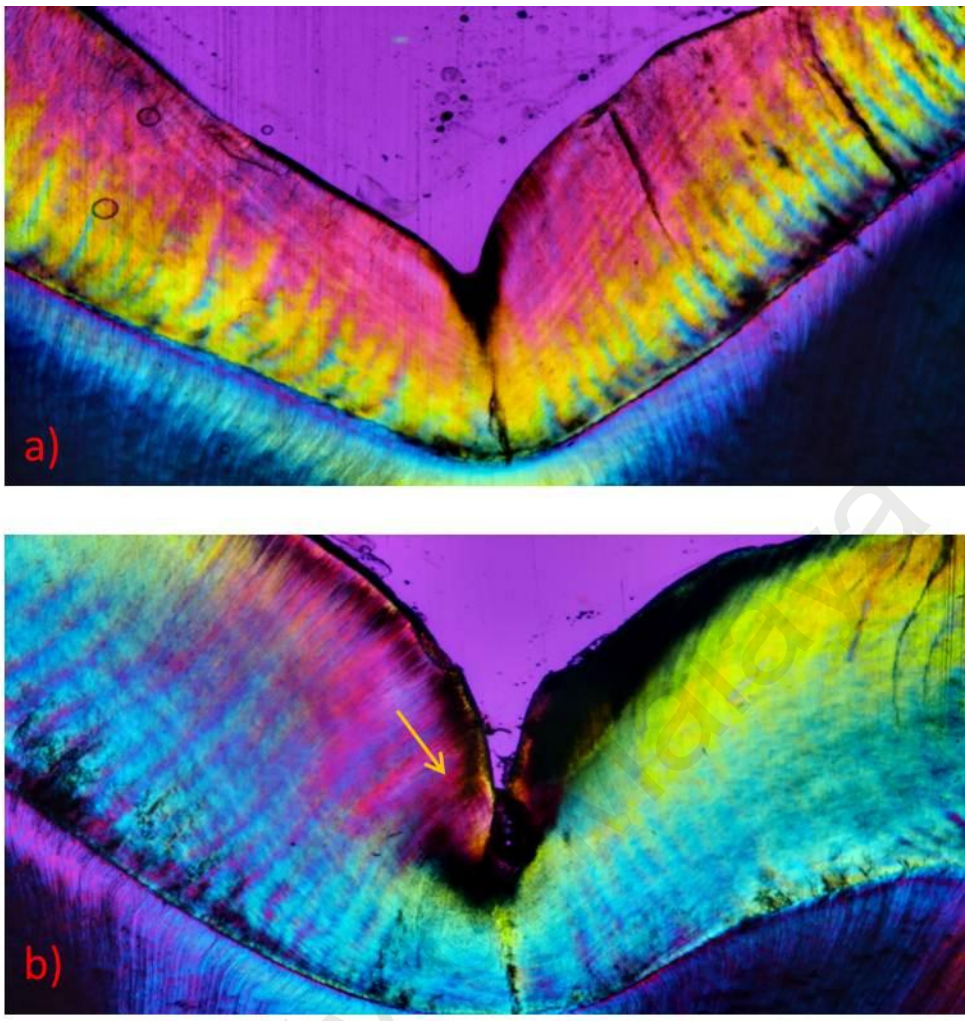

Figure 3.2: PLM images of bucco-lingual sections of occlusal fissure. (a) section without polishing shows presence of caries without any damage or loss to the early lesion (b) partial loss of caries (yellow arrow) at one side of the wall of the fissure after polishing.

None of the two methods resulted in the fracture of the sections. Four sections were obtained from each method. Teeth with exposed occlusal surfaces had intact early lesions with no damage (Figure 3.2a). However, 3 sections of early lesions out of 4 sections that were fully embedded in the resin were partially lost during polishing (Figure 3.2b). It was concluded that mounting of the samples with resin 2 mm below the

marginal ridge helped to position the investigation sites accurately with the cutting blade to obtain desired sections without loss of early lesions.

3.1.2 OCT data processing and analysis

This pilot study was conducted for Research Objective 2, 3 and 4. The aim of this pilot was to identify optimum number of A-scans for the selection of the region of interest to achieve maximum depth-resolved intensity (*I*) that can be used to quantify the differentiation of stages of NCFC (Ek code 1 versus Ek code 2) using OCT outcome measure total area under the curve (AUC_T). A bespoke 2D OCT software was developed in Matlab (Tha Math works, USA) for the OCT caries research under HIR UM.C / 625 / 1 / HIR / MOHE /_Dent_/1 for OCT data processing with a Graphic Unit interface (GUI). The best selected OCT B-scan was loaded from the 3D OCT volume data as .frg file format.

Five groups were made based on the number of the A-scans (Figure 3.3) and are shown below:

i) Group 1 = 50 A-scans

ii) Group 2 = 80 A-scans

iii) Group 3 = 150 A-scans

iv) Group 4 = 200 A-scans

v) Group 5 = selection of region of interest based on the extension of the lesion on the corresponding PLM image irrespective of number of A-scans.

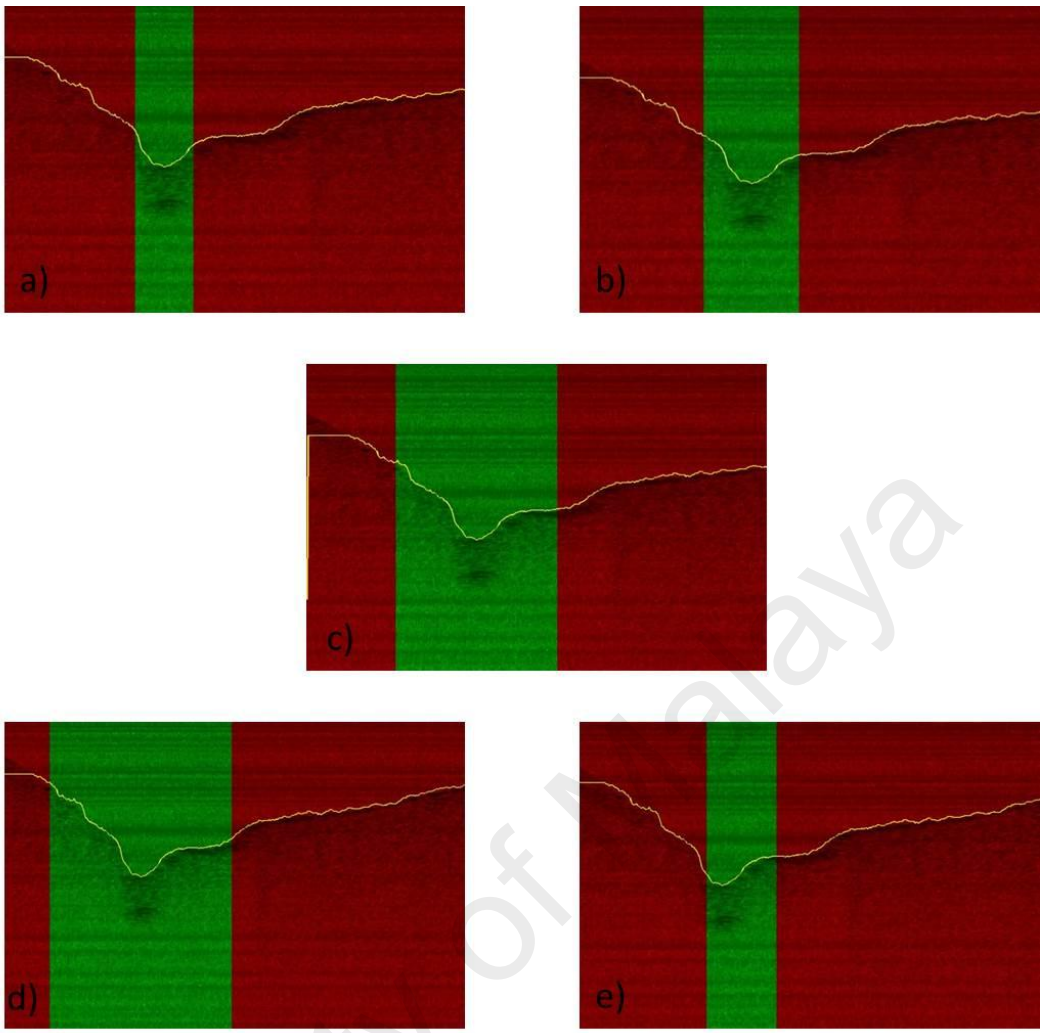

Figure 3.3: 2D OCT B-scans showing selection of different numbers of A-scans (green area). (a) 50 A-scans, (b) 80 A-scans (c) 150 A-scans (d) 200 A-scans (e) multiple A-scans highlighting the entire lesion.

The depth-resolved intensity (*I*) from Ek code 1 (n=30) and Ek code 2 (n=60) were collated to produce mean depth-resolved intensity (*I*) profile of 200 µm for all 5 groups of Ek codes 1 and 2 lesion respectively (Figure 3.4 and 3.5). The outcome measure AUC_T was calculated for Ek code 1 and Ek code 2 starting from 0 µm up to 150 µm physical depths for all five groups (Table 3.1). The summary of the AUC_T is shown in Table 3.1.

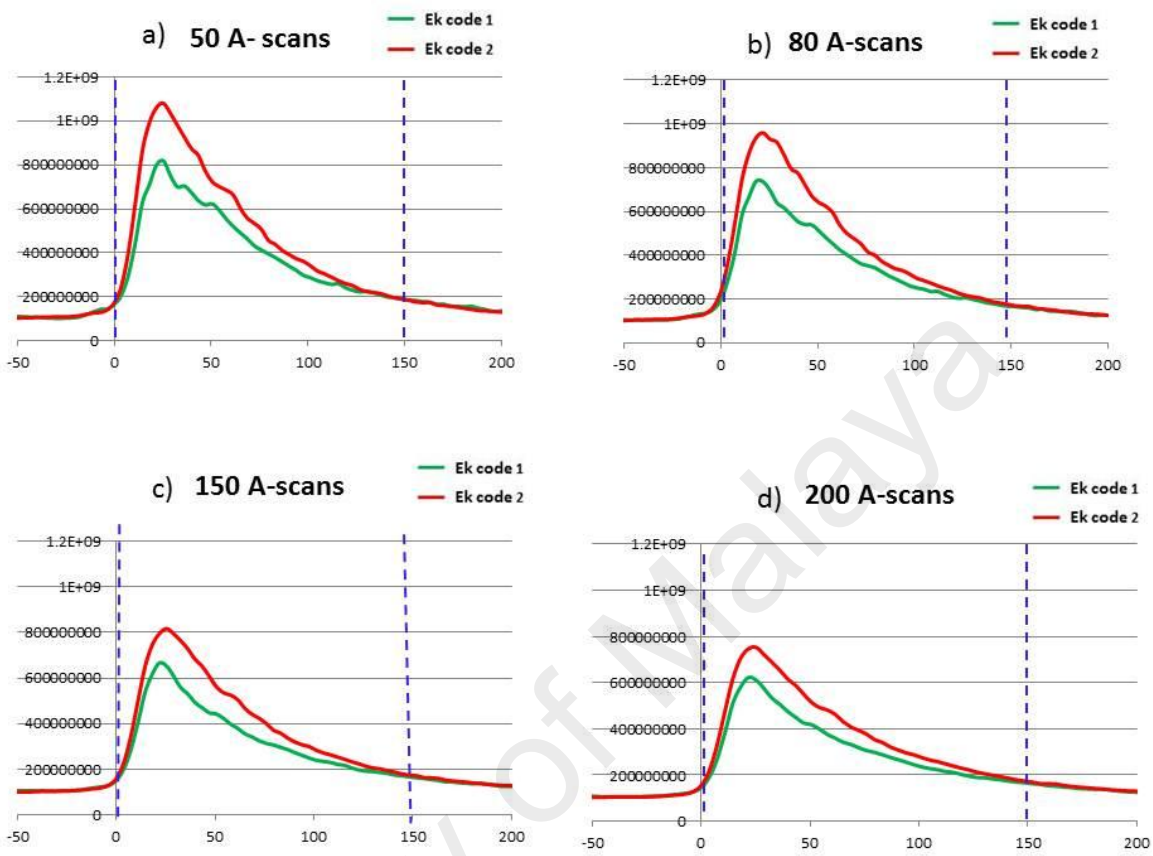

Figure 3.4: Mean depth-resolved intensity (*I*) profile of 200 µm physical depth from different numbers of A-scans of Ek codes 1 and 2. (a) 50 A-scans (b) 80 A-scans (c) 150 A-scans and (d) 200 A-scans from Ek codes 1 and 2 and the selected physical depth points starting from 0 µm up to 150 µm for AUC_T (blue dotted lines).

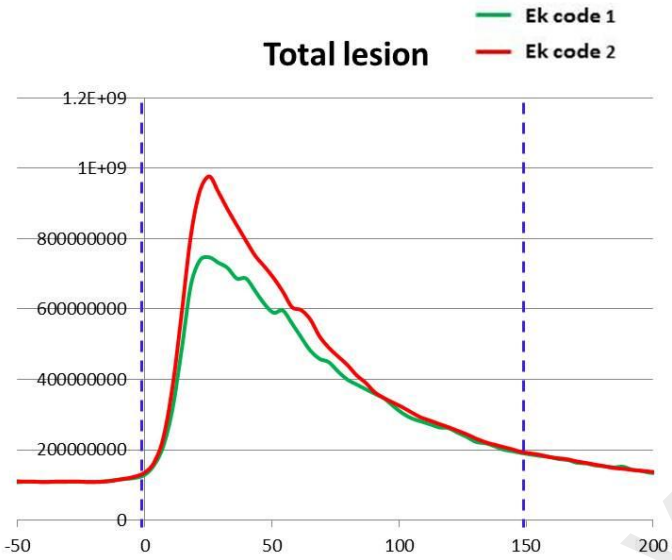

Figure 3.5: Mean depth-resolved intensity (*I*) profile from Ek codes 1 and 2 after the selection of entire lesion and the selected physical depth points starting from 0 µm up to 150 µm for AUC_T (blue dotted lines).

Table 3.1: Mean AUC_T between Ek code 1 and code 2 using different number of A-scans

Number of A-scans	**Ek code 1**		**Ek code 2**	
	Mean AUC_T	Mean ±SD	Mean AUC_T	Mean ±SD
50	6.35E+10	1.98E+08	7.92E+10	2.94E+08
80	5.71E+10	1.76E+08	7.22E+10	2.63E+08
150	5.07E+10	1.49E+08	6.32E+10	2.15E+08
200	4.87E+10	1.38E+08	5.94E+10	1.91E+08
Total lesion	6.23E+10	1.87E+08	7.00E+10	2.46E+08

Total area under the curve (AUC_T)

The mean AUC_T calculated from 50 A-scans showed maximum difference between the Ek code 1 and Ek code 2. It was concluded that 50 A-scans were the optimum number of A-scans for the selection of region of interest to achieve maximum

depth-resolved intensity (I) profile and that can be used to differentiate stages of NCFC (Ek code 1 versus Ek code 2) using OCT outcome measure AUC_T.

3.2 Research Objective 1: Evaluating the accuracy of OCT in detecting sound fissure and naturally occurring NCFC by visual assessment of OCT B-scan

3.2.1 Preliminary selection of teeth

Fifty four human extracted premolars with sound fissure and naturally occurring NCFC on the occlusal surface were used in this study. The teeth were collected from orthodontic clinic that were schedule for extraction and approved by the Dental Faculty University of Malaya Ethics and Research Committee for usage. The teeth were stored in 1% chloramine solution for 2 weeks to inhibit bacterial growth and in normal saline thereafter to ensure hydration throughout the study.

The inclusion criteria used in this study were:

i) Upper and lower premolar teeth.
ii) Sound premolar teeth with no signs of early demineralization on occlusal surface.
iii) Early occlusal caries lesion without cavitation.
iv) Teeth without sealants.
v) Teeth without restorations.

The exclusion criteria used in this study were:

i) Teeth with fluorosis or any other white discoloration on the occlusal surface other than due to early caries.
ii) Early caries lesion with micro cavitation (ICDAS II code 3).

iii) Heavily stained occlusal fissure.

iv) Teeth with attrition and abrasion on the occlusal surface.

3.2.2 Sample preparation

Prior to visual scoring, scaling was carried out away from the occlusal fissure to remove calculus using ultrasonic scaler (Cavitron; Dentsply Professional, York, PA, USA). Special care was taken during scaling to avoid any potential damage to the early lesions. The occlusal fissures were then cleaned with slurry of pumice with polishing tips with a low speed hand piece and rinsed with water for 10 seconds to ensure removal of residual pumice.

The roots were sectioned 2 mm below the cemento-enamel junction (CEJ) using slow speed microtome cutting machine (Micracut 125, Metkon Ins., Bursa, Turkey) with medium concentration diamond disc under copious water irrigation. The roots were sectioned as flat as possible to ensure upright positioning of the occlusal crown during mounting. Careful attention was paid to glue each sectioned crown upright with the long axis of the tooth parallel to the z-axis, inside separate plastic moulds (5x5x2 mm) using fixation adhesives (Technovit 7230 VLC, Exact). Epoxy resin was prepared, mixed and poured 2 mm below the marginal ridge exposing the crown portion and was left for 24 hours to set. After the resin was set, the mould was placed in hot water to gently separate the sample embedded in resin from the mould.

Each tooth was given a sample identification number (ID) which was also carved on the resin using a high speed hand piece (Micracut 176, Metkon Ins., Bursa, Turkey). For orientation purposes, the occlusal surfaces were photographed at 1.2X magnification using a 2048 x 1536 resolution stereomicroscope (Nikon Eclipse 55i, Nikon, Japan) with an integrated digital camera (Nikon DSFI2, Nikon, Japan).

Furthermore, investigation sites were identified and marked with a reference line approximately 3 mm buccal to the investigation site with a rotary diamond disc as shown in Figure 3.6.

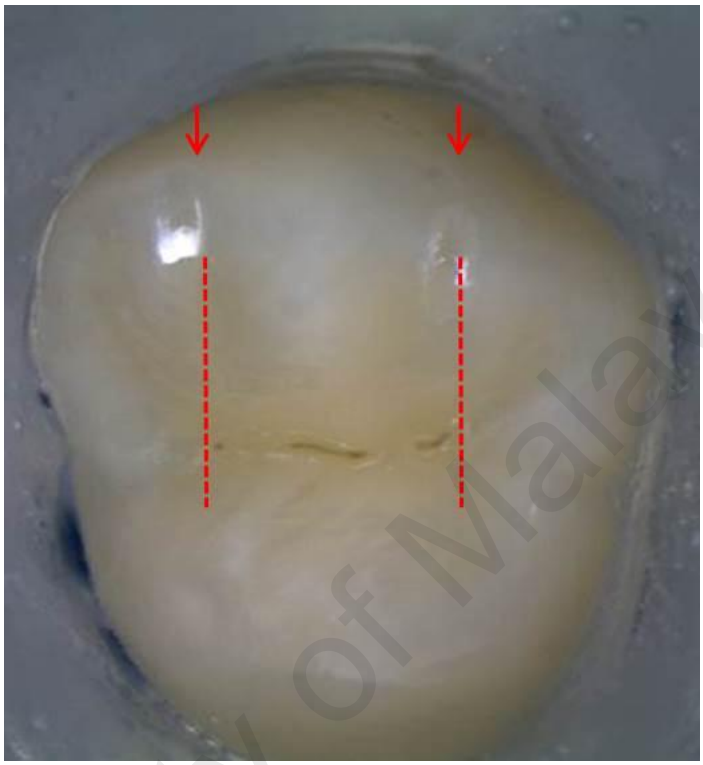

Figure 3.6: Stereomicroscope image (1.2X) of a premolar crown with reference lines (red arrows) marked approximately 3 mm buccal to the investigation site (red dotted line).

3.2.3 Visual examination of the occlusal fissure

Prior to visual examination, both the examiners (first examiner was the researcher of this study and the second examiner was a research assistant and a clinician) took a 90 minute-e-learning programme (http://www.icdas.org/) to familiarize and train them in use of ICDAS II coding system. Later, approximately 10 extracted

teeth that were not included in the main study were examined and scored (code 0-2) followed by discussion.

To select sound fissure and NCFC of different stages, 121 investigation sites were coded using International Caries Detection and Assessment System (ICDAS II) protocol (Pitts, 2004) by two trained and calibrated examiners. Consensus was sought when discrepancies of code was observed between the examiners. The focus of this study was sound fissure and NCFC, therefore the ICDAS II codes used were as follows (Figure 3.7):

i) Code 0 = sound tooth surface: no evidence of caries after prolonged air drying (> 5 seconds),

ii) Code 1 = first visual change in enamel: opacity or discoloration (white or brown) is visible at the entrance to the pit or fissure after prolonged air drying, which is not or hardly seen on a wet surface.

iii) Code 2= distinct visual change in enamel: opacity or discoloration distinctly visible at the entrance to the pit and fissure when wet, lesion must still be visible when dry.

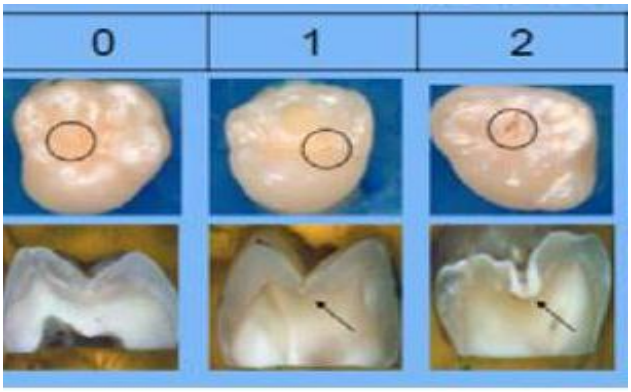

Figure 3.7: ICDAS II codes and the corresponding histological depth of caries. Adapted from (http://www.dimensionsofdentalhygiene.com).

3.2.4 OCT scanning

A Swept Source OCT Imaging System (OCS1300SS, Thorlabs Ltd., USA) with emission wavelength centered at 1325 nm, axial and transverse resolution of 9 μm and 11 μm in air respectively, was used to scan the investigation sites. The Thorlab OCT software was used to configure the scan settings, view real-time B-scans and capture the scans. Each tooth was removed from its container at the time of imaging, air dried for 10 seconds under moderate pressure with a three-in-one syringe. Three- dimensional (3D) scans of 1024 x 104 x 512 pixels in the x-y-z directions were obtained from each investigation site. The scanning beam was positioned in the center and set perpendicular to the investigation site to cover a scanned surface of 3 mm x 3 mm in the x-y direction with an optical depth of 3 mm in air, corresponding to 1.8 mm of physical depth when the refractive index of enamel ($\eta = 1.62$) was used. A total of 104 cross-sectional OCT B-scans were generated, approximately 30 μm distance between each scan. The B-scans were captured in a linear scale with a brightness and contrast configured to cover an intensity signal level range of -40 dB to -10 dB.

3.2.5 Polarized light microscopy

After being scanned with OCT, the samples were prepared for histology. The tooth was cut into two halves (mesial and distal). The bulbous portion from each half of the crown was removed mesially and distally using low speed cutting machine (Metkon 125, Instrument ltd, Bursa, Turkey) with a medium concentration diamond disc under copious water irrigation to make the surface parallel to the long axis of the tooth. The following steps were performed to obtain 180 ± 10 μm thick specimens for PLM imaging.

3.2.5.1 Preparation of slide block (SL_B)

The flat portion of the crown was mounted on a clean slide using adhesive. The adhesive was carefully prepared by mixing 2 portions of Syrup 1 (S1) (Technovit 400) and 1 portion of Syrup 2 (S2) (Technovit 400) to produce a homogeneous S1/S2 mixture according to manufacturer's instructions. Later, 5-6 portions of Technovit 400 powder was mixed with 1 portion of S1/S2 mixture to obtain a homogeneously mixed adhesive. The crown was then glued to the clean slide mesially or distally using freshly prepared adhesive (Figure 3.8 a). The prepared slide block (SL_B) was placed in the Exakt vacuum press (Exakt, Germany) with adhesive placed on the lower plate of the vacuum press for 15 minutes to allow hardening of the adhesive (Figure 3.8b). After drying, the thickness of slide block was measured with a micrometer and recorded (Figure 3.8c).

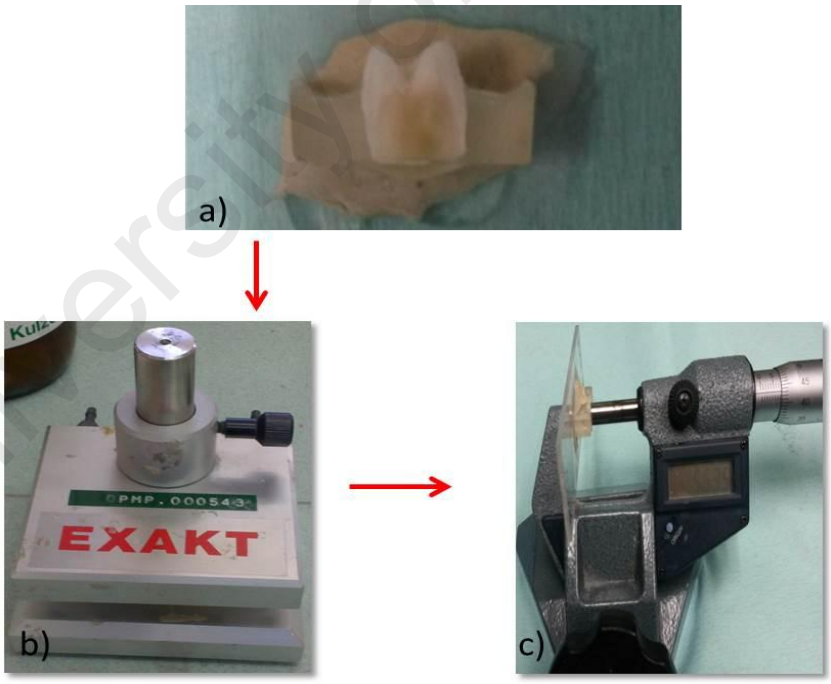

Figure 3.8: Preparation of a slide block. (a) bucco-lingual section of the crown of a premolar glued mesially to the glass slide, (b) the slide block was kept in Exakt vacuum press (Exakt, Germany) for 15 minutes to allow hardening of the adhesive, (c) measuring the thickness of the slide block using a micrometer.

3.2.5.2 Preparation of sandwich slide block (SW_B)

A clean new slide (N_S) (Exakt 25x 75 x 1.5mm) was measured and recorded using a micrometer (Figure 3.9a). The prepared slide block was trimmed as close as possible to the marked investigation site using Exakt 300CP Band system under copious water irrigation. The light cured adhesive (Technovit VLC 7210) was evenly spread on the slide block to avoid entrapment of air bubbles (Figure 3.9b). The clean new slide was glued to the slide block (Figure 3.9c) and was placed in Exakt Precision-Adhesive Press (Exakt, Germany) for 30 minutes for curing (Figure 3.9d). The prepared sandwich block (SW_B) was then measured with a micrometer and the thickness was recorded.

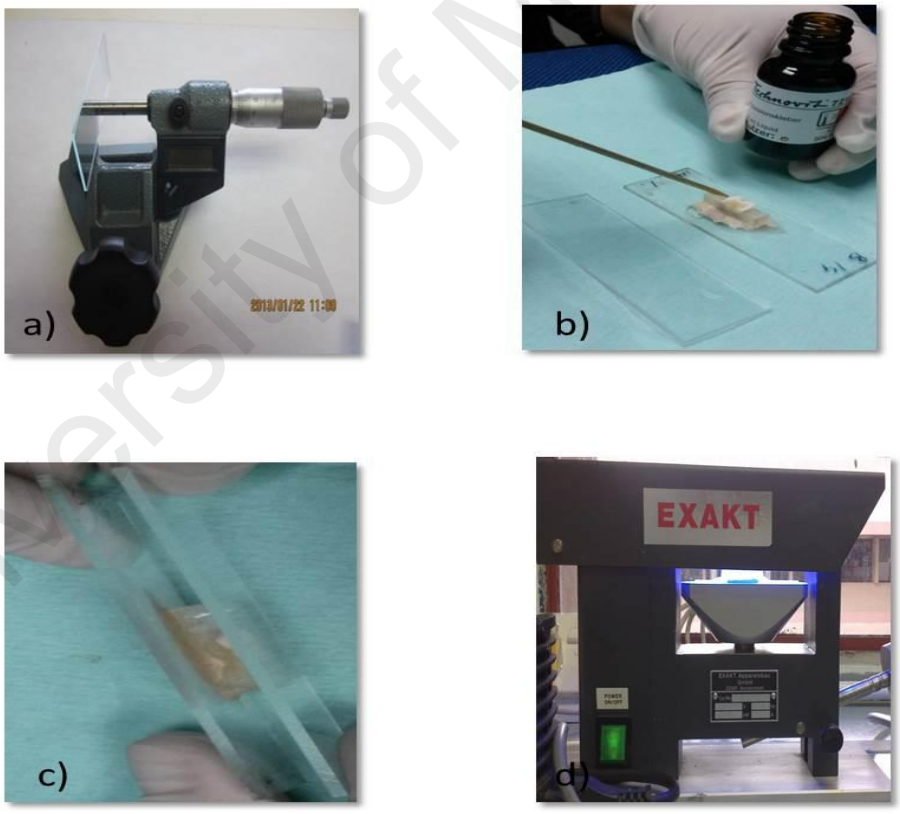

Figure 3.9: Preparation of a sandwich block. (a) measuring the new slide with micro meter, (b) applying thin layer of adhesive on the slide block (c) gluing the new slide with the slide block (d) placing the sandwich block in Exakt Precision-Adhesive Press (Exakt, Germany) for 30 minutes for curing.

3.2.5.3 Sectioning of teeth

The sectioning of the sample was carried out using the Exakt 300CP Band system (Exakt, Germany) (Figure 3.10a). A suitable slide holder was selected based on the size of the sample. The slide holder and sandwich block were cleaned prior to sectioning procedure. The sandwich block was attached to the slide holder using a vacuum. The entire setup was advanced towards the edge of cutting band that was 200 µm thick with grade D diamonds (Figure 3.10b) using a micrometer until the inner surface of the slide contacted the blade. Exakt 300CP Band system was turned on with copious water irrigation to test the friction between cutting band and the inner surface of the sandwich block. The point where the sandwich block was free of friction was recorded as point zero and the position was locked. The thickness of the specimen to be sectioned was set using automated micrometer to 220 µm. The sections were cut in the bucco-lingual direction perpendicular to the fissure. Two 180 ± 10 µm thick-serial sections, 200 ± 10 µm apart, were obtained from each investigation site. No further polishing and finishing was performed after sectioning to avoid damage to the early lesions. The new section was measured using a micrometer and recorded. The summary of calculation for thickness of the new section ($\mathbf{S_N}$) and the adhesive (A) is shown in Table 3.2.

Figure 3.10: Set up for sectioning the PLM samples (a) the Exakt 300CP Band system (Exakt, Germany) (b) the cutting band having 200 µm thickness with grade D diamonds used for sample sectioning.

Table 3.2: Calculation for thickness of the section

Thickness of Adhesive (A)	$\mathbf{A = SW_B - SL_B - N_S}$ Where SW_B, SL_B and N_S are the thickness of sandwich block, slide block and the new slide.
Thickness of new section ($\mathbf{S_N}$)	$\mathbf{S_N = N_S - A}$

3.2.5.4 Sonication of slide samples

Sections were sonicated for 10 minutes in a stainless steel basket filled with distal water at a frequency of 20 kHz with the acoustic energy and power in Ultrasonic sonicator (ELMA, Transonic T 460/H, Germany) (Figure 3.11).

Figure 3.11: Ultrasonic sonicator (ELMA, Transonic T 460/H, Germany) used for sample sonication.

3.2.6 Imaging under PLM

242 sections were obtained from 121 investigation sites. Sections were imbibed in water, examined under a 4X-magnification microscope (Nikon Eclipse 55i, Nikon, Japan) equipped with an Analyzer Slide (Nikon C-AS Nikon, Japan) and Polarizer (Nikon C-TP Nikon, Japan) for first order red compensation, and imaged using an integrated digital camera (Nikon DSFI2, Nikon, Japan) (Figure 3.12). The section with the demineralized area nearest to the dentin-enamel-junction was selected of the two and used for final analysis.

Figure 3.12: Microscope (Nikon Eclipse 55i, Nikon, Japan) equipped with an Analyzer Slide (Nikon C-AS Nikon, Japan) and Polarizer (Nikon C-TP Nikon, Japan) for first order red compensation for section imaging.

3.2.7 Final cohort

A final cohort of 71 investigation sites from the 121 preliminary investigation sites were selected by two examiners based on Ek histology criteria shown in Table 3.3 (Ekstrand et al., 1997) with a final distribution of Ek codes 0 (n=21), 1 (n= 25) and 2 (n= 25). Samples were then grouped as sound (Ek code 0) and NCFC (Ek codes 1 and 2) for final analysis.

Table 3.3: Ek histology classification

Code 0	No enamel demineralization or a narrow surface zone of opacity (edge phenomenon).
Code 1	Enamel demineralization limited to the outer 50% of the enamel layer.
Code 2	Demineralization involving between 50% of the enamel and outer third of the dentin.

(Ekstrand et al., 1997)

3.2.8 Matching of OCT B-scans to PLM images

From a 104 B-scans obtained from each investigation site (Figure 3.13), the best matching scan to the PLM section (Figure 3.14a) was identified based on fissure anatomy and cuspal slopes by two examiners on grey scale OCT B-scans (Figure 3.14b). The selected best grey scale B-scan was then converted to colored scale B-scan (large DR3 map) and used for final lesion scoring and measurement (Figure 3.14c).

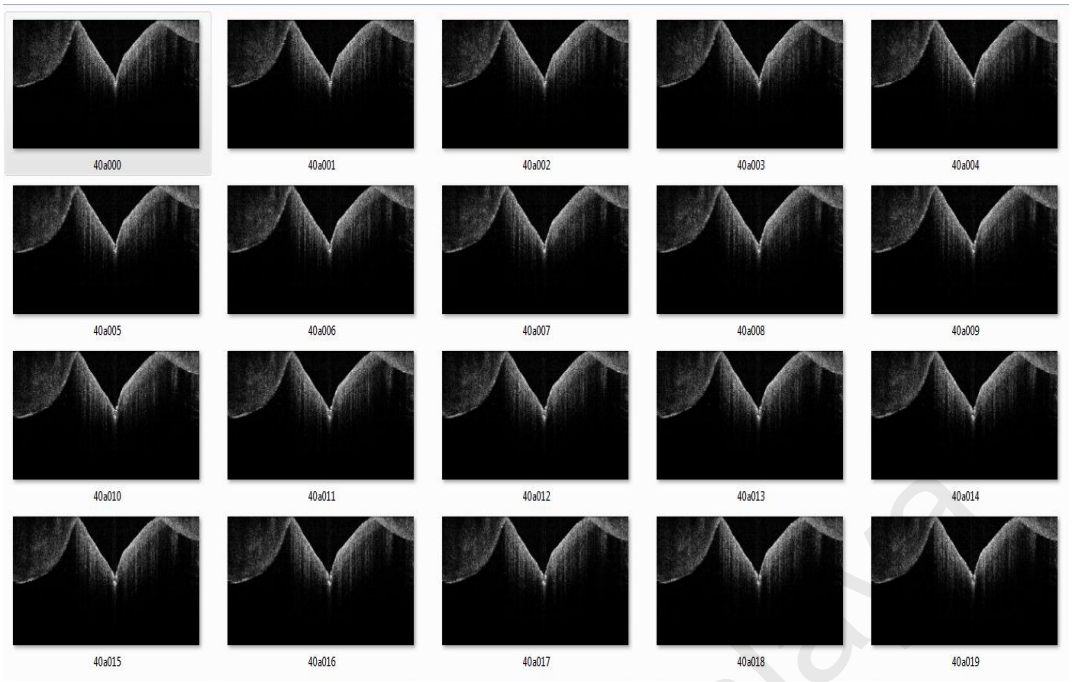

Figure 3.13: Multiple cross-sectional OCT-B-scans generated in grey scale for the selection of best possible OCT B-scan.

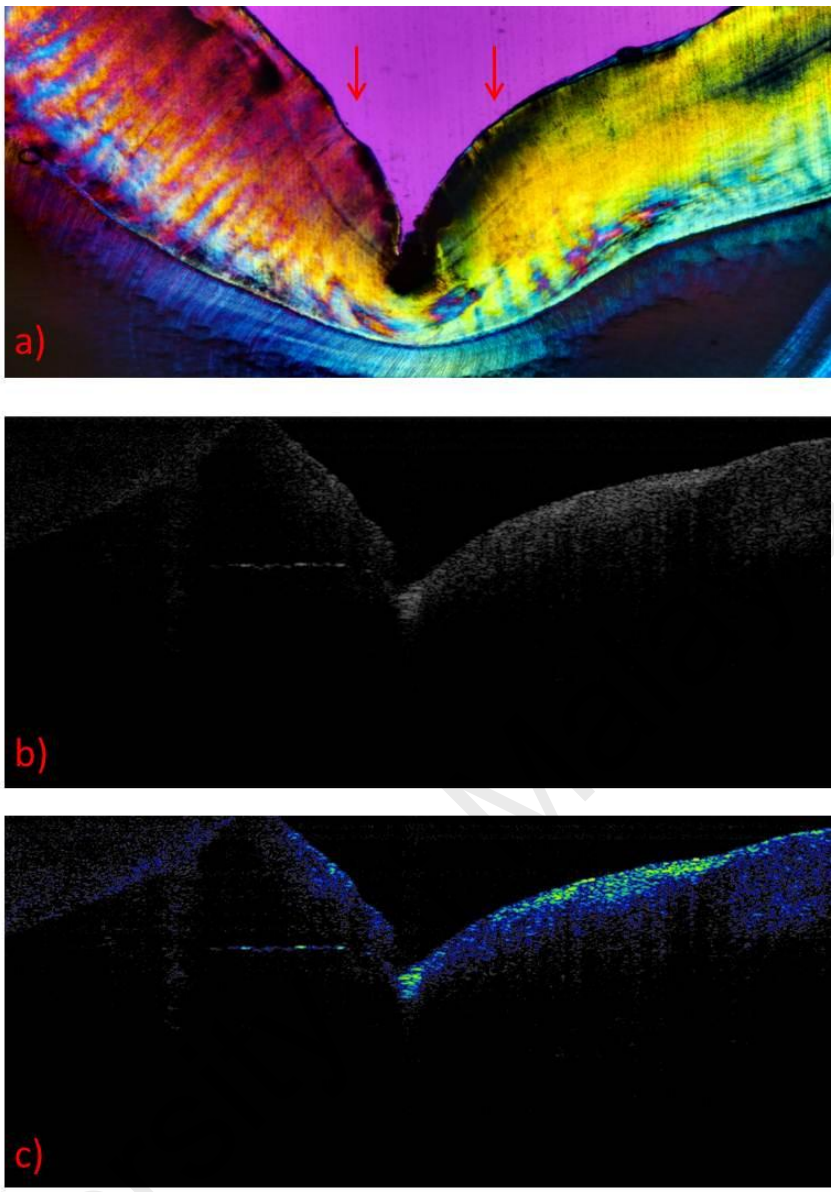

Figure 3.14: Corresponding PLM image and OCT B-scans. (a) a PLM image showing the anatomy of the occlusal fissure and the slope of the cusp (red arrows shows the beginning of the slope) used as reference to match the best OCT B-scan out of multiple OCT B-scans (b) the identified corresponding grey scale OCT B-scan and (c) the same identified OCT B-scan shown in (b) but in a color scale, used for scoring the investigation site for the presence or absence of NCFC and for dimension measurements of NCFC.

3.2.9 Detection of sound fissure and NCFC with qualitative assessment of OCT B-scans and PLM images

The investigation site was sub-divided into two distinct anatomical sites at the entrance of the fissure (E). The entrance of fissure was defined as the point where its width was 200 µm, as previously described by Juhl et.al (Juhl, 1983). The area of the fissure above the entrance was termed as slopes (S) and the lesion observed at this site was termed as slope lesion (SL). The area of the fissure below the entrance was termed as walls of the fissure and the lesion present here was termed as wall lesion (WL). The whole lesion was defined as presence of both wall or slope lesion or either one at the investigation site (SL and/or WL) (Figure 3.15).

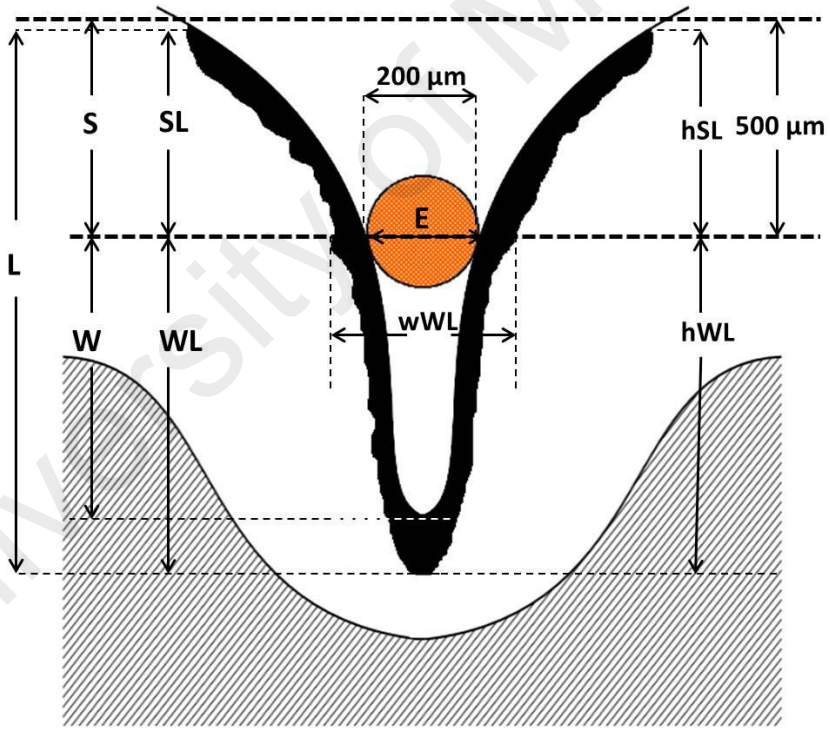

Figure 3.15: An illustration of a fissure showing the entrance of the fissure (E) and a whole lesion (L) with its sub-divisions; slope lesion (SL), wall lesion (WL). The limits of the sub-division of the lesion are labeled as the height of slope lesion (hSL), width of wall lesion (wWL) and height of wall lesion (hWL).

The absence (Figures 3.16 and 3.17) or presence (Figures 3.18) of a whole lesion (L= SL and/or WL) was determined with OCT using the criteria described in Table 3.4 and validated against PLM. In addition to this, for investigation sites with true positive lesions, the location of the lesion was also determined as SL and/or WL with OCT and validated against PLM. Table 3.4 shows the summary of the criteria used for scoring the absence or presence of the NCFC.

Table 3.4: Criteria for detection of sound fissure and NCFC with PLM and OCT

	PLM	**OCT**
Absence of caries	Absence of dark brown to black areas at the region of interest (Figure 3.16a, 3.17a)	i) Presence of a distinct surface border commonly limited to only one to two pixels thick in the green/yellow range (20dB to-10 dB) (Specular reflection) (Figure 3.16b) **and/or** ii. Absence of subsurface regions of diffused elevated backscattered intensity appearing in the yellow/green range (-20 dB to -10 dB) of the chosen color map (Figure 3.17 b).
Presence of caries	Presence of dark brown to black areas at the region of interest (Figure 3.18a).	Presence of subsurface regions of diffused elevated backscattered intensity appearing in the yellow/green range (-20 dB to -10 dB) of the chosen color map (Figure 3.18b).

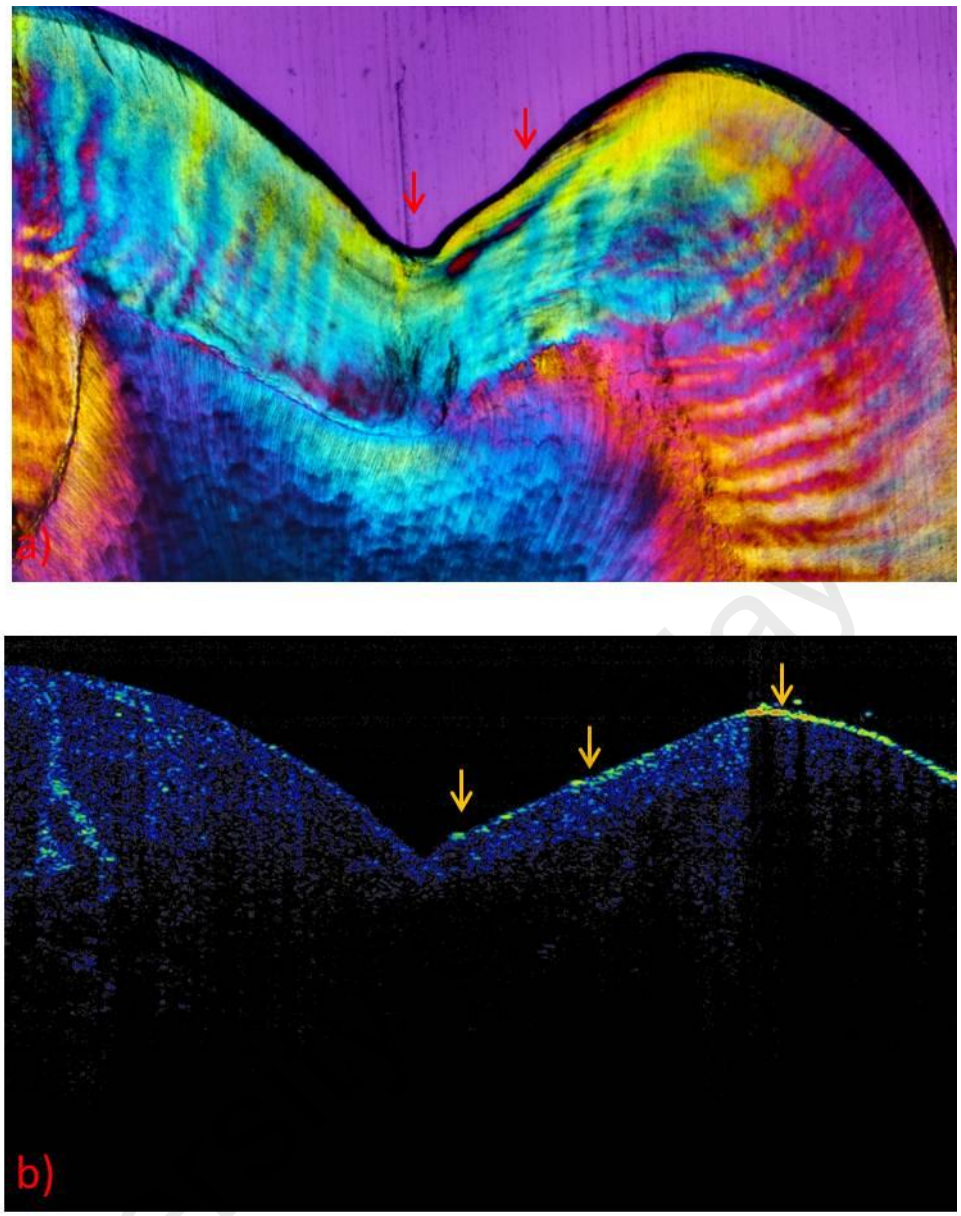

Figure 3.16: Sound fissure showing absence of caries. (a) a PLM image with absence of dark brown to black areas (red arrows) at the region of interest (b) OCT B-scan showing a distinct surface border limited to only one to two pixels thick in the green/yellow range on the slope and cusp of the fissure (yellow arrows), indicating specular reflection. This was distinguished from caries and scored as a sound fissure.

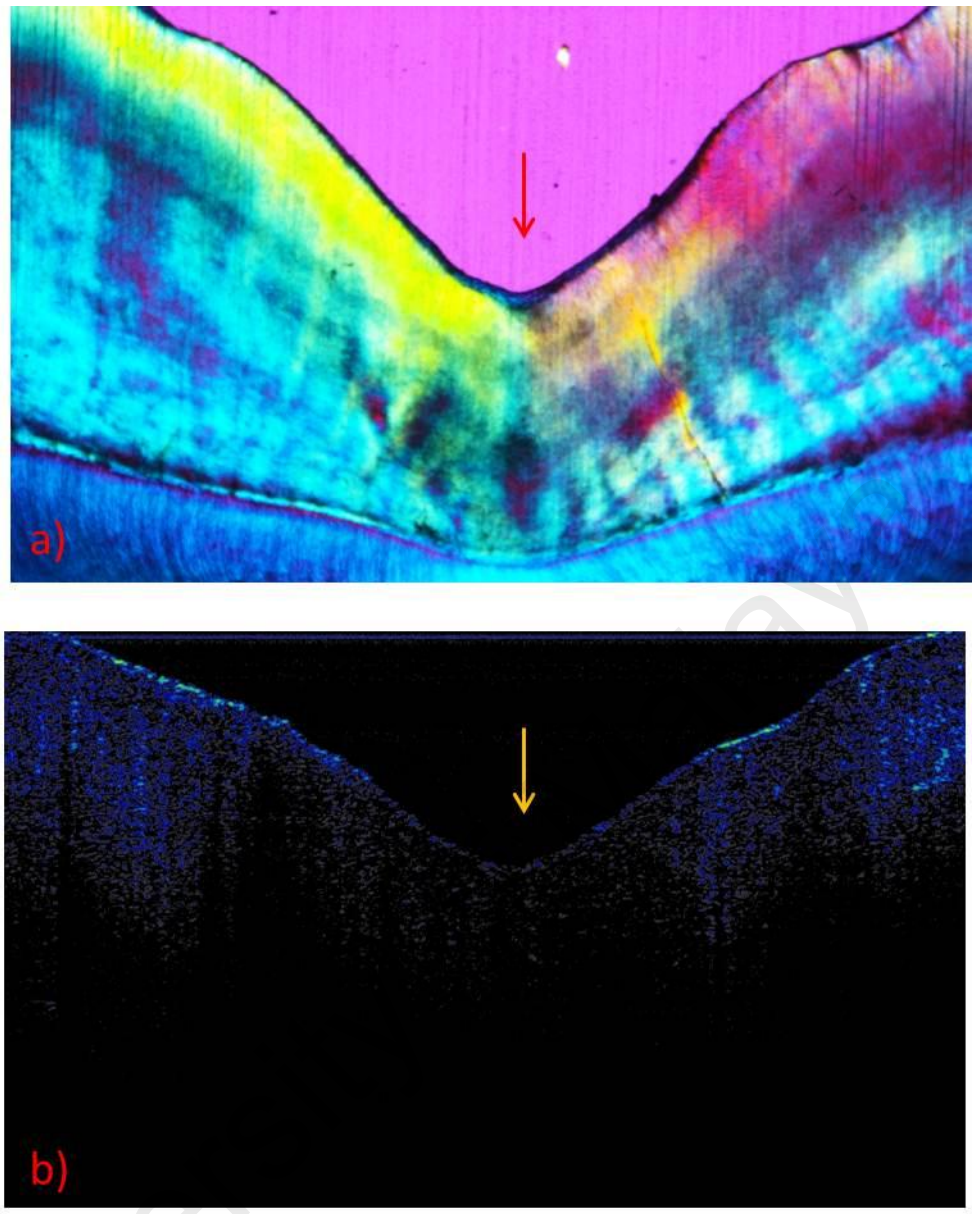

Figure 3.17: Absence of caries on PLM and OCT B-scan. (a) a PLM image with absence of dark brown to black areas (red arrows) at the region of interest and (b) an OCT B-scan showing absence of subsurface regions of diffused elevated backscattered intensity appearing in the yellow/green range (yellow arrows) and was regarded as sound.

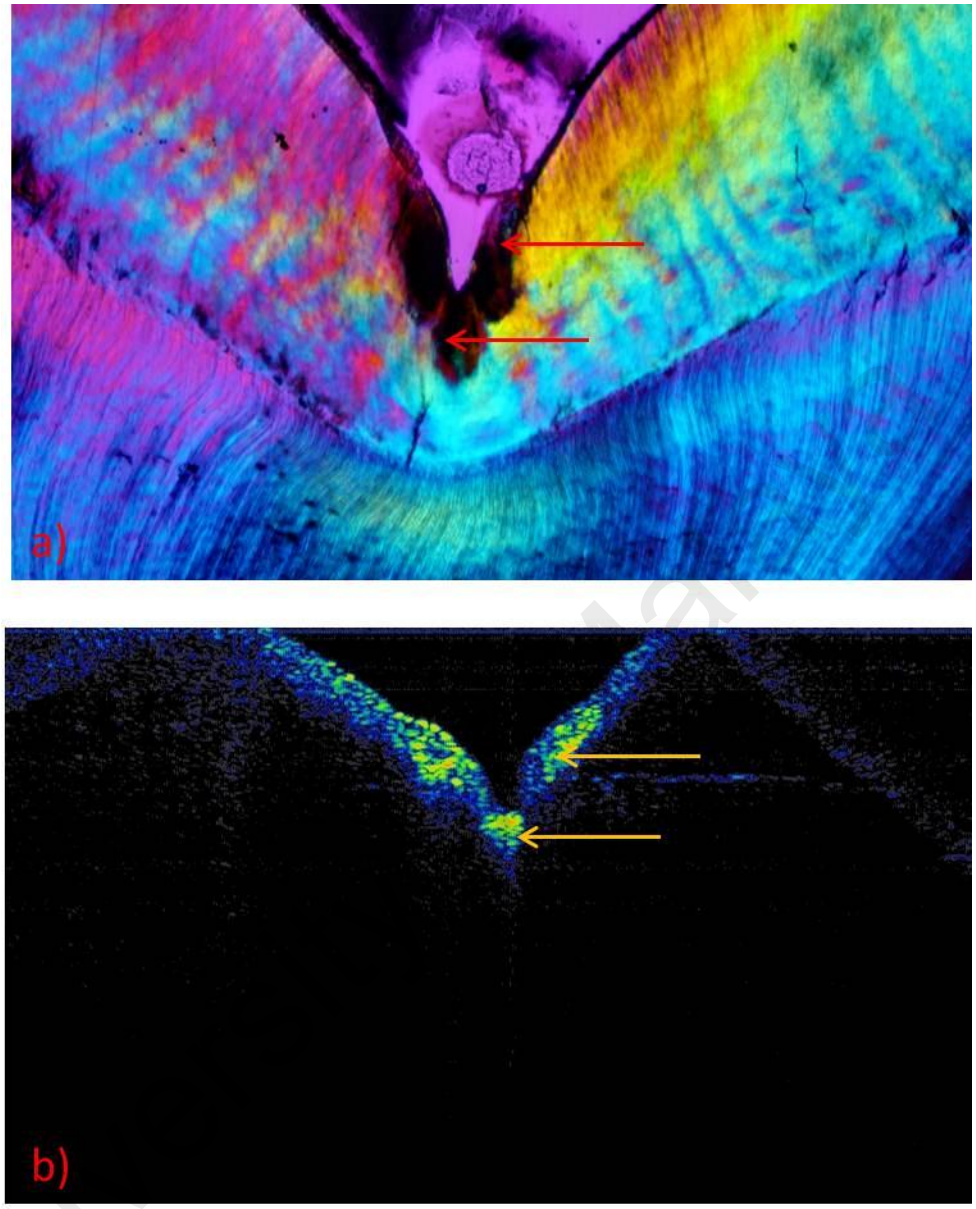

Figure 3.18: Presence of caries on PLM and OCT B-scan. (a) a PLM image with presence of dark brown to black areas (red arrows) at the region of interest (b) OCT B-scan showing presence of subsurface regions of diffused elevated backscattered intensity appearing in the yellow/green range (yellow arrows) and was regarded as caries.

3.2.10 Measurements of the lesion

The following dimensions of the lesions were obtained from the positive lesions (Figure 3.15):

i) **Height of slope lesion (hSL):** The vertical extent of the slope lesion, within 500 µm from the entrance of the fissure.

ii) **Width of wall lesion (wWL):** The horizontal extent of the wall lesion.

iii) **Height of wall lesion (hWL):** The vertical extent of the wall lesion.

The measurements were done on the selected OCT B-scans and the corresponding PLM images using the Thorlabs OCT software (Swept Source OCT Imaging System Version 2.3.1, Thorlabs, USA) and the Nikon software (NIS- Elements AR 3.2 Nikon Japan), respectively.

Scoring and measurements were done by two trained and calibrated examiners separately on two different occasions. The inter-examiner agreement was calculated. For the analysis of SN and SP, a consensus score was sought in the event of a discrepancy between examiners.

3.2.11 Statistical analysis

Statistical analysis was performed using SPSS (SPSS version 22, IBM, USA) on the final cohort of 71 investigation sites. Inter-examiner agreement for the detection of lesions was calculated using Cohen's un-weighted kappa. Inter-examiner agreement for measurement of lesion dimension was calculated using single measure intra-class coefficient (ICC), with a 2-way mixed effect model and consistency type.

NCFC detection SN and SP for OCT, at and within the investigation site were calculated. The lesion dimension agreement between OCT and PLM was evaluated using the Bland-Altman test.

3.3 Research Objective 2: Identifying the quantitative OCT outcome measures derived from depth-resolved intensity profile to detect sound fissure and NCFC and distinguish stages of NCFC

3.3.1 Selection of teeth and sample preparation

Premolar teeth with sound fissure and naturally occurring NCFC used for this section were same cohort as those used in Section 3.2.1. The protocol for sample preparation was same as described in Section 3.2.2.

3.3.2 Visual examination of occlusal fissure

The same criteria as mentioned in Section 3.2.3 was used to select sound fissure and NCFC for this study.

3.3.3 OCT scanning

The same protocol of OCT scanning was used as described in Section 3.2.4.

3.3.4 Polarized light microscopy

The same protocol for mounting, sectioning, sonication and imaging of PLM sections were used as described in Section 3.2.5 and 3.2.6.

3.3.5 Final cohort of samples based on Ek histological criteria

From 121 samples, 10 samples from Ek code 2 with base of the fissures deeper than two-third of the enamel thickness and four samples that had caries in the outer one third of the dentin were removed from this study.

A final cohort of 107 investigation sites were selected by two examiners based on Ek histology criteria (Ekstrand et al., 1997) (Table 3.3) with a final distribution of Ek code 0 (n=17), Ek code 1 (n= 30) and Ek code 2 (n= 60).

3.3.6 Matching OCT B-scans with PLM images

Same protocol for matching OCT B-scans with PLM images were used as described in Section 3.2.8.

3.3.7 OCT data processing with bespoke software

A bespoke software with a Graphic Unit interface (GUI) was developed in Matlab (Tha Math works, USA) for OCT data processing. The best selected OCT B-scan was loaded from the 3D OCT volume data as .frg file format. The region of interest within the investigation site was identified using the corresponding PLM image for each sample (Figure 3.19).

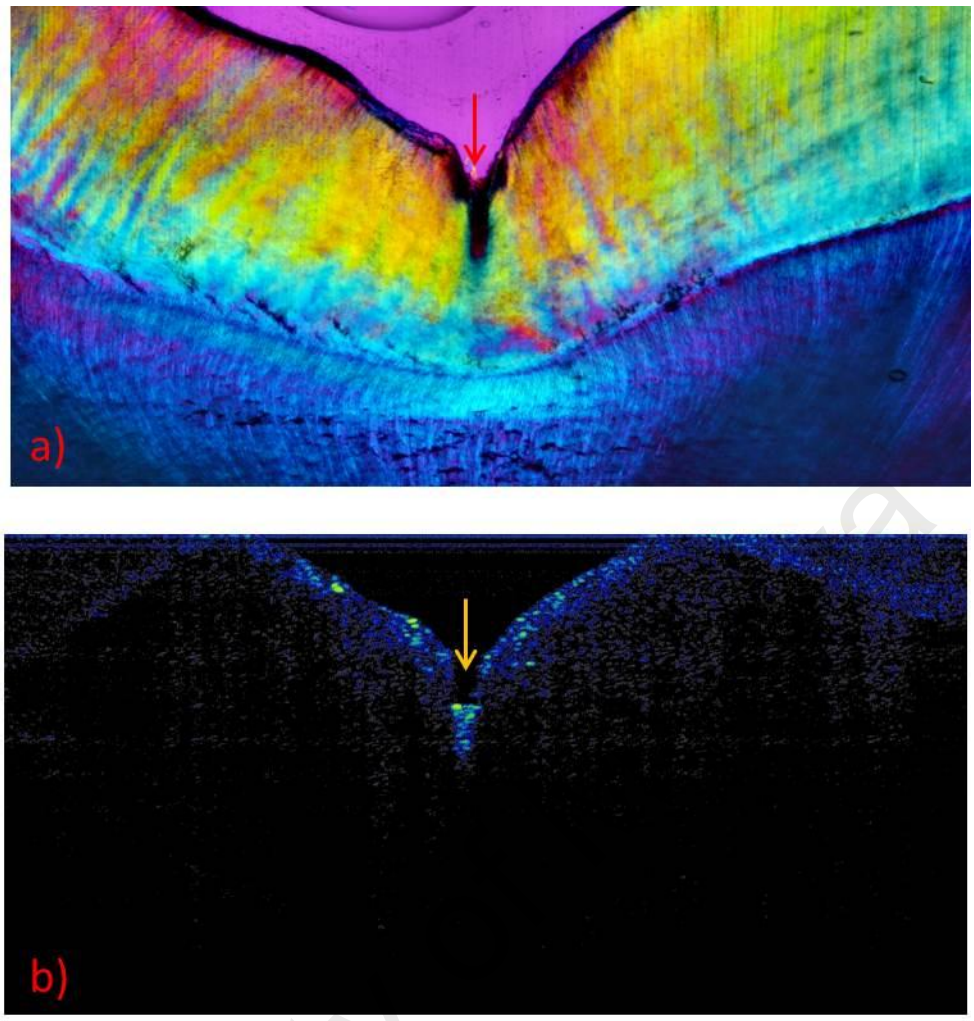

Figure 3.19: PLM image and OCT B-scan showing the region of interest. (a) location of region of interest within the investigation site on the PLM image (red arrow) (b) region of interest was identified on the corresponding OCT B-scans (yellow arrow) for OCT data analysis.

This region of interest consisted of 50 A-scans and was approximately 146 µm wide (Figure 3.20). The regions of interest was selected by keeping 25 A-scans on either side from the center of the fissure (Figure 3.20 a). The refractive index was set to 1.62 corresponding to enamel. Surface determination was automated by the software (Figure 3.20 a) and fine-tuned manually. After surface determination was completed, the

curvature of the occlusal surface was aligned into a straight line (Figure 3.20 b) The depth-resolved intensity (*I*) profile for each of the 107 samples was generated in the linear scale and exported into Microsoft Office Excel® 2010 for further analysis.

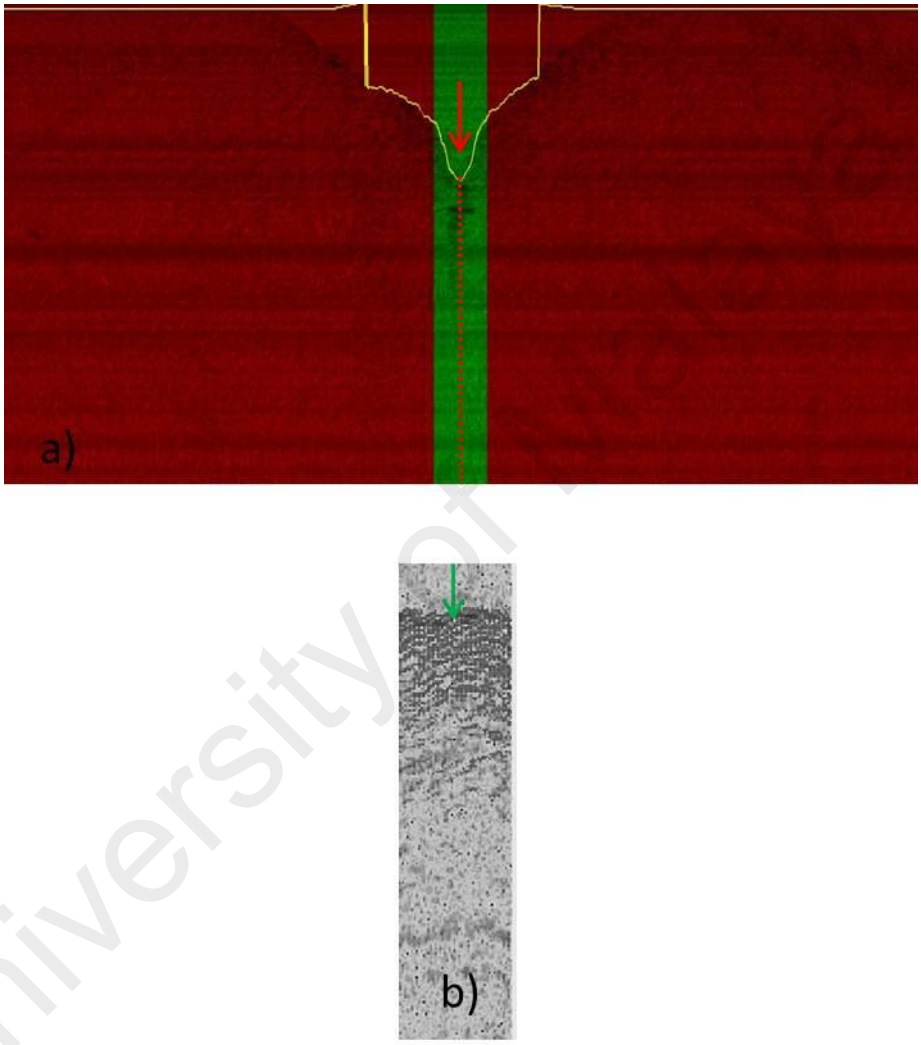

Figure 3.20: OCT B-scan of shows with selected region of interest. (a) the selection of 50 A-scans (green area) by keeping the occlusal fissure in the center (red arrow and dotted line) and the well fitted line (yellow line) outlining the surface of the occlusal fissure within the region of interest (green area) (b) the surface of selected region of interest (green area) shown in (a) was aligned as straight as possible (green arrow) using bespoke 2D OCT software.

3.3.8 OCT data analysis

In order to study the characteristics of the near infra-red light passing through sound (Ek code 0) and NCFC (Ek codes 1 and 2), the depth-resolved intensity (*I*) from each of the 107 samples were collated to produce a mean depth-resolved intensity (*I*) profile of 800 µm. It was observed from the mean *I* profile (mean A-scan) that the physical depth of first 250 µm was useful to study the characteristic of the mean A-scan after which the back scattered intensity light had reached a plateau and was not affected by early demineralization.

Characteristic of the A-scans such as the maximum intensity (I_{max}) and pattern of attenuation through first 300 µm were observed and compared between Ek histological codes 0, 1 and 2 using Microsoft Office Excel® 2010.

3.3.8.1 OCT outcome measures derived from the mean depth-resolved intensity profile

Five outcome measures derived from the mean depth-resolved intensity (*I*) were explored to detect sound (Ek code 0) and NCFC (Ek codes 1 and 2), and to differentiate stages of NCFC (Ek code 1 and Ek code 2). With the refractive index of enamel being 1.62, the chosen physical depth points for this study were 0 µm (z_0) at tooth-air interface, 40 µm (z_1) and 150 µm (z_2) below the tooth-air interface (Figure 3.21). The summary of the outcome measures is shown in Table 3.5.

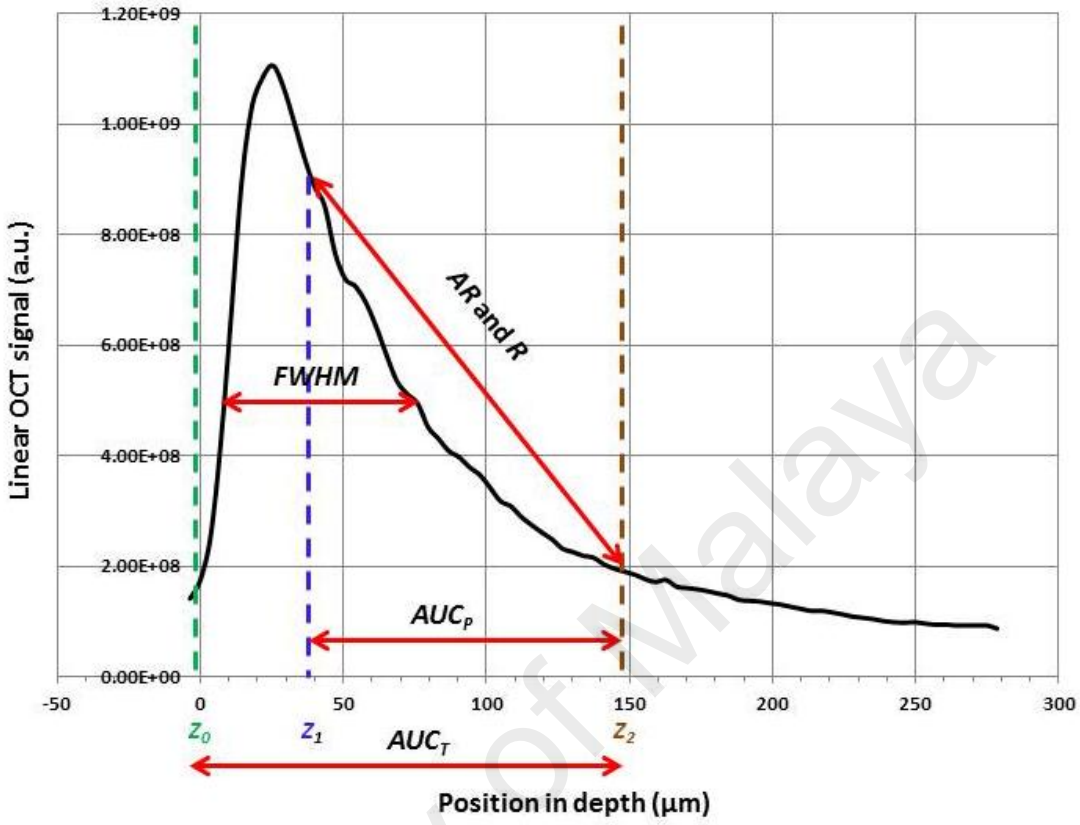

Figure 3.21: Mean depth-resolved intensity (*I*) profile of the first 300 µm of Ek code 2 and the exploration of OCT outcome measures attenuation rate (*AR*), attenuation ratio (*R*), partial area under the curve (AUC_P), total area under the curve (AUC_T) and full width half maximum (*FWHM*) to identify the best OCT outcome measure for the detection of sound (Ek code 0) and NCFC (Ek codes 1 and 2), and for the differentiation of stages of NCFC (Ek code 1 and Ek code 2). Z_0 (green dotted line) is the tooth-air interface; Z_1 (blue dotted line) and Z_2 (brown dotted line) are the physical depth points at 40 and 150 µm respectively.

Table 3.5: OCT outcome measures for differentiating Ek histological codes 0 , 1 and 2.

Outcome measures	**Description**
Attenuation Rate **(*AR*)**	$AR = I_{z2} - I_{z1} \,/\, Z_2 - Z_1$ With I_{z1} and I_{z2} being the intensity at the physical depth point of Z_1 and Z_2
Intensity Ratio **(*R*)**	$R = I_{z2} / I_{z1}$
Partial Area under the curve **(AUC_P)**	$AUC_P = (\sum I_{z1} : I_{z2}) \times Z$ With Z being the distance between the physical depth points
Total Area under the curve **(AUC_T)**	$AUC_T = (\sum I_{z0} : I_{z2}) \times Z$ With I_{z0} being the intensity at the physical depth point of Z_0
Full Width Half Maximum **(*FWHM*)**	The distance between two intensity ponits on the curve at which I_{max} reaches half of its maximum value ($I_{max}/2$)

3.3.9 Statistical analysis

Statistical software version 22 (SPSS, IBM, USA) was used for analysis. The data was analyzed to verify the assumption of normality using Shapiro-Wilk test. Non-parametric Kruskal Wallis H-test was performed to assess the difference between Ek codes 0, 1 and 2 and the OCT outcome measures. A Post-hoc analysis was further conducted for pair-wise comparisons between each EK codes (0, 1 and 2) and the

outcome measures *AR, R, AUC_P, and AUC_T* using Dunnet's T3 analysis. Receiver operating characteristic (ROC) curve analysis was performed to find the best outcome measure and its cut-off point by determining the highest *AUC* and the Youden's index (sensitivity + specificity) -1 respectively.

3.4 Research Objective 3: Validation of OCT outcome measures identified in Research Objective 2

3.4.1 Selection of teeth, sample preparation and visual scoring

Twenty one extracted human premolars with sound enamel and NCFC on the occlusal surface were used in this study. The inclusion criteria, sample preparation protocol and visual scoring of the occlusal fissure remained the same as discussed in Sections 3.2.1, 3.2.2 and 3.2.3. In this study the investigation area was identified on the occlusal surface instead of multiple investigation sites. The occlusal surface was then scored based on highest severity ICDAS II code for initial sampling. The investigation area was marked on the power point slides (Figure 3.26) for reference.

3.4.2 Transportation for radiographic imaging (Micro-CT)

The Micro-CT imaging of samples was scheduled to take place in Minnesota Dental Research for Biomaterials and Biomechanics (MDRCBB) School of Dentistry, University of Minnesota. Before the transportation of teeth for Micro-CT scanning a careful protocol was followed to avoid damage to the samples during transportation. Each tooth were taken out from its individual container and wrapped with moist cotton gauze to ensure humidity and avoid dehydration. Each wrapped tooth was then carefully placed in a small aluminium packet and sample number was written with a permanent

marker on top of the packet. Twenty one packets were prepared and then placed in one big aluminium bag which was vacum-sealed and placed in a thermocol box to avoid any damage to the samples. The box was couriered to reach MDRCBB School of Dentistry, University of Minnesota for Micro-CT scan within four days. All teeth were unpacked when it reached MDRCBB School of Dentistry, University of Minnesota and kept in container with distilled water during the scanning. Post-scanning, all 21 teeth were packed and couriered back to the Biomaterial laboratory, Faculty of Dentistry, University of Malaya (Figure 3.22).

Figure 3.22: Packaging of teeth samples for Micro-CT imaging. (a) teeth samples were taken out of their respective container (b) moist cotton gauze was wrapped around each teeth sample to ensure humidity (c) each sample was packed in a small aluminum bag and sample number was written on top of each packet (d, e) all samples were prepared and then placed in one big aluminum bag which was air vacuumed and sealed (f, g) and placed in a thermocol box and sealed to avoid any damage to the samples.

3.4.3 Micro-CT scanning and image processing

The crown portion 2 mm below the cemento-enamel junction embedded in resin block exposing the crown of the tooth was placed vertically and scanned with Micro-CT system (Model XTH 255, X-tek system, Nikon Metrology, Brighton, MI, USA). Scanning was performed using X-rays produced with tube voltage of 90 kV and tube current of 90 µA. A total of 720 projections and 4 frames per projection were taken at each scan. Hydroxyapatite phantom disks with known mineral density (MD) were scanned before and during the scanning of teeth to ensure the calibration of the Micro-CT system. The reconstruction of volume data was achieved by using the software CT Pro 3D (Nikon, Metrology, Brighton, MI, USA). The reconstructed volume data were exported as a DICOM image stack for further image analysis. The reconstruction of volume data determined the distance between each frame. The Micro-CT scan yielded images at approximately 10 µm/frame distance. Eleven pre-constructed Hydroxyapatite (HA) tablets with known MD ranged from 0.099 to 1.54 gm/cm^{-3} with standard dimensions were used as phantoms for calibration purposes. The eleven HA tablets were vertically stacked using an acrylic holder and were position next to the scanned tooth each time.

3.4.4 Micro-CT data extraction

3.4.4.1 Surface determination and orientation of the tooth

DICOM image format was used to reconstruct the Micro-CT data into a 3D format by using VG Studio Max (Version 2.1, 64 bit, Volume Graphics, Charlotte, NC, USA). Subsequently the 3D image stack or the volume data of each tooth were used for visualization and quantitative measurements. Once the volume data were constructed in

3D, the surface determination was manually adjusted to determine the surface of the tooth (Figure 3.23).

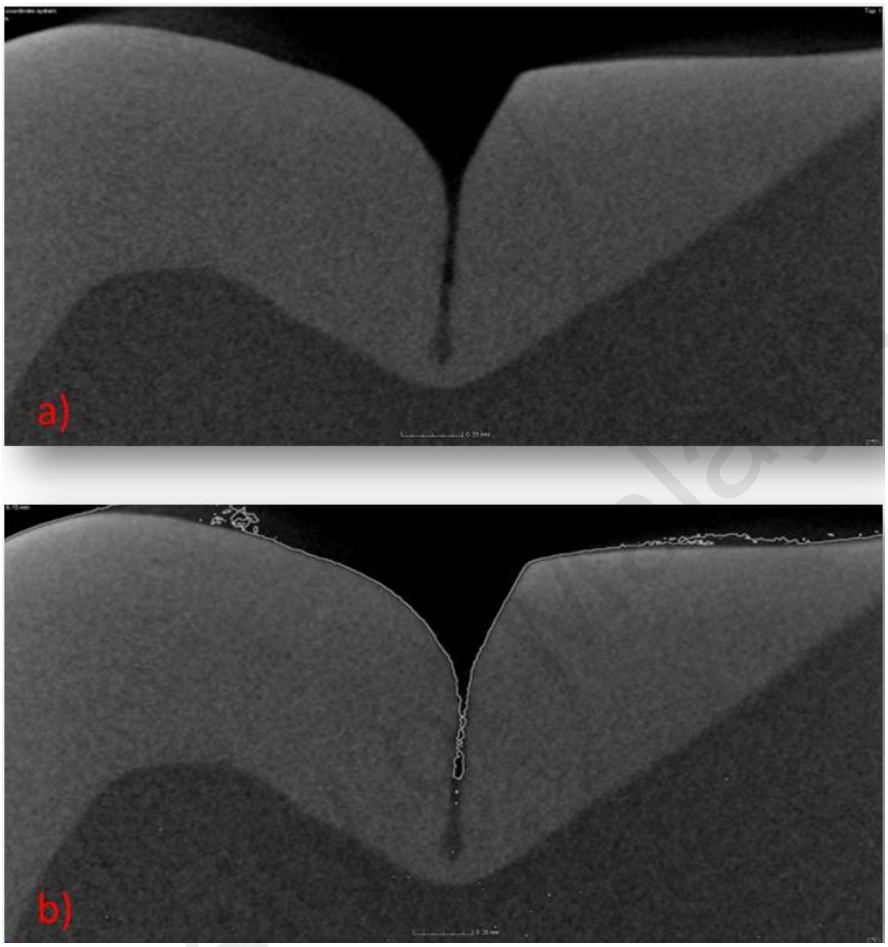

Figure 3.23: Occlusal fissure before and after surface determination. (a) occlusal surface of the fissure before surface determination, (b) white line outlining the surface of the occlusal fissure representing determined surface.

The surface determination histograms represented two bars in the form of a histogram, each demonstrating the background and the enamel (Figure 3.24). The x-axis shows the grey values of the material while the y-axis represents the count of grey values. The iso-surface determination cut-off was set between the background and the enamel. Opacity rendering option was used to adjust the contrast of the samples where sound enamel and early caries were not clearly distinguishable (Figure 3.24).

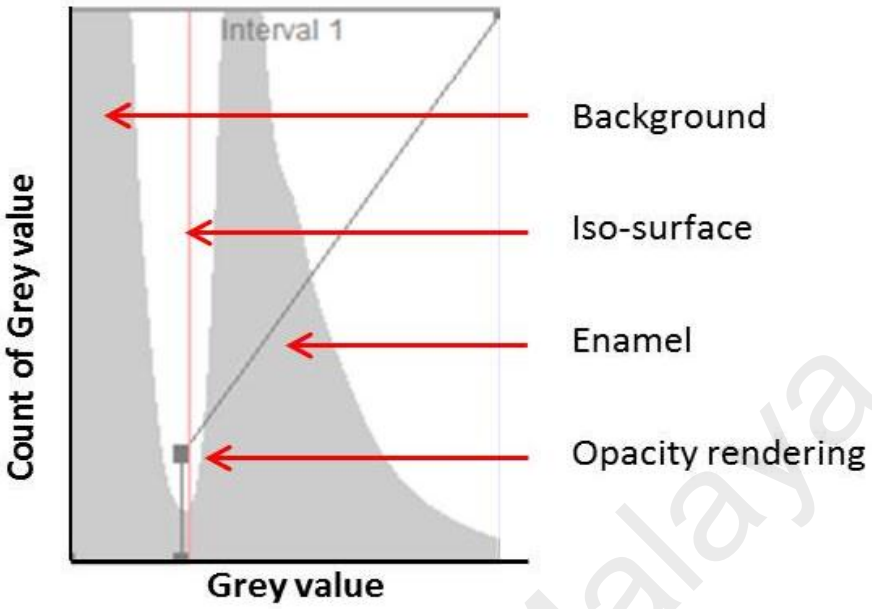

Figure 3.24: Histogram showing surface determination of the tooth. The red line represents the set iso-surface which is between the background and the enamel. The grey line on the histogram shows the *opacity rendering function* use to adjust the contrast between the sound enamel and demineralized enamel.

Amongst the four viewing panes within the tripod coordinate system, the 3D preview window indicates the orientation of the tooth (Figure 3.25d). Using the *3D rendering* tool, the orientation of the crown was locked with the long axis of the tooth parallel to the z-axis, occlusal table oriented on the x-y plane and the y-z plane set perpendicular to the central groove (Figure 3.25).

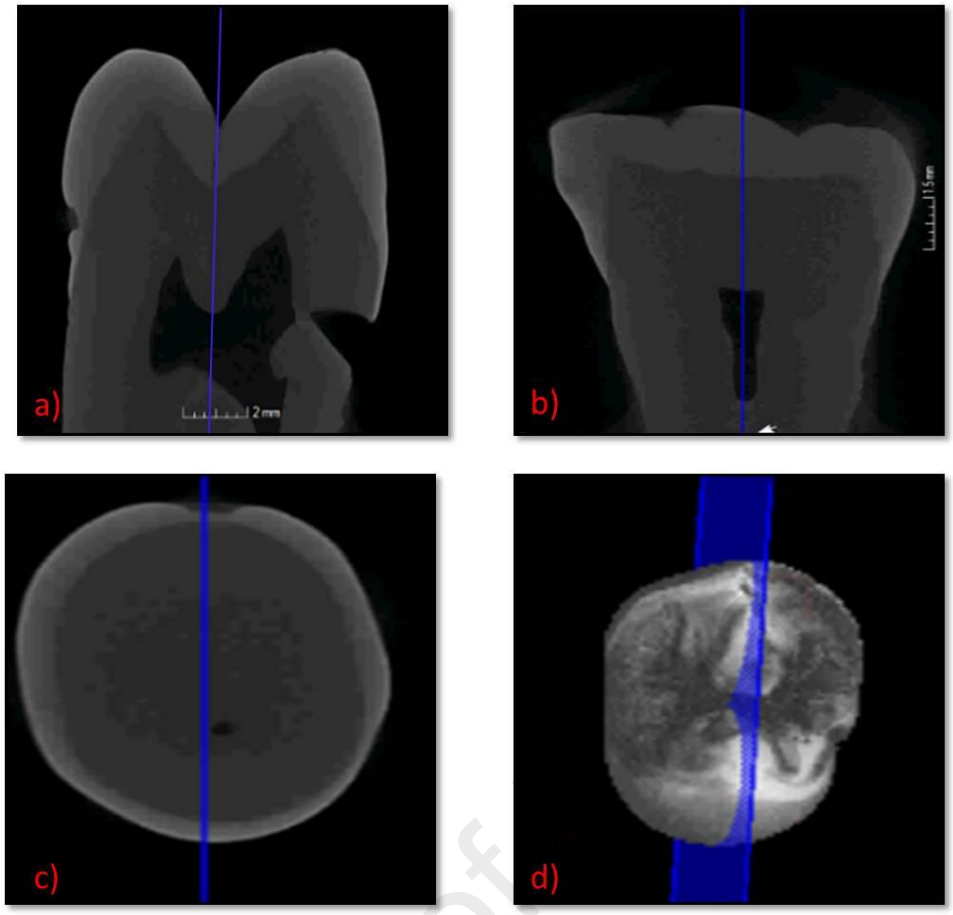

Figure 3.25: Images of tripod in the coordinate system. (a) bucco-lingual direction along the y-z plane set perpendicular to the central groove, (b) mesio-distal direction along the x-z plane, (c) occluso-pulpal direction, (d) live *3D rendering* window of the tooth. The blue line shows the orientation of the crow with long axis of the tooth parallel to the z-axis.

3.4.4.2 Thresholding of the 3D volume data

The investigation area marked on the stereomicroscope image (Figure 3.26a) was identified on the corresponding Micro-CT image on the *3D rendering* view (Figure 3.26b).

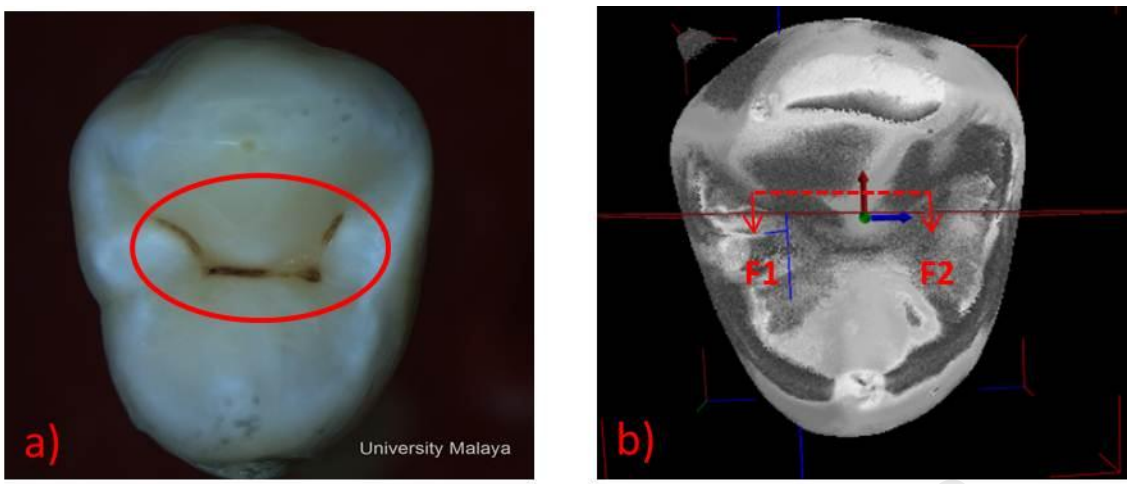

Figure 3.26: Investigation area on the stereomicroscope and Micro-CT image. (a) a stereomicroscope image used as reference to identify the investigation site (red circle) on the 3D rendering view (b) corresponding Micro-CT *3D rendering* view with identified investigation area in red dotted line. F1and F2 is the first and last frame of the investigation area shown in red arrows respectively.

The total distance between the first and last frame of the investigation area was calculated and a frame from every one third of the distance was extracted to calculate the mean range of grey values for sound enamel and air. The mean range of grey value for demineralized enamel for each tooth was then taken as between the mean maximum of air and the mean minimum of sound enamel. This mean range of demineralized enamel was input into the *Threshold function* and the voxels with the gray value in the range were highlighted in amber and outlined in green color (Figure 3.27). After the area of demineralized enamel had been outlined with the threshold function, the frame with the demineralized area nearest to the dentin-enamel junction was selected from the entire volume data as the representative frame to be visually scored for severity.

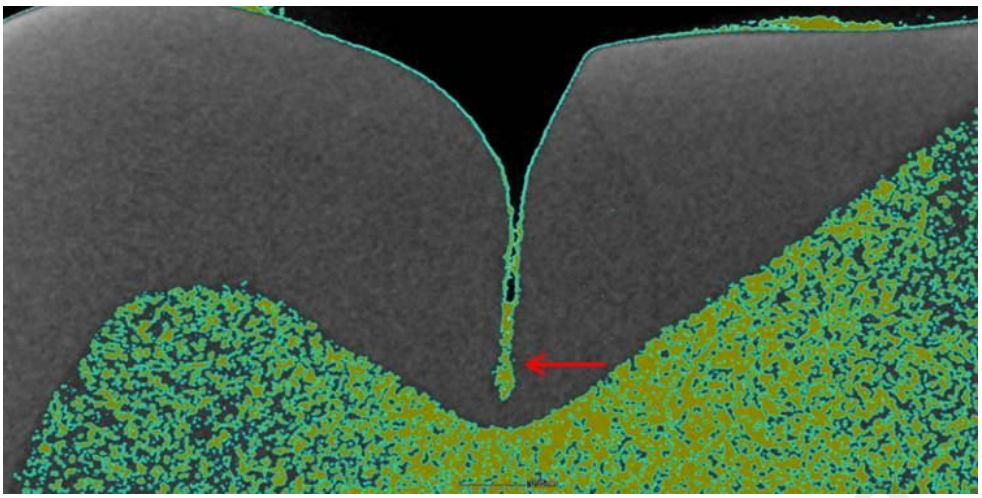

Figure 3.27: The occlusal fissure with the threshold demineralized enamel in amber and outlined in green color (red arrow).

3.4.4.3 Micro-CT scoring

Two images from each investigation site, one with surface determination and the other with image thresholding was standardized in size (height 3”and width 6”) and brightness and displayed simultaneously on the computer screen for scoring the presence or absence of caries (Figure 3.28).

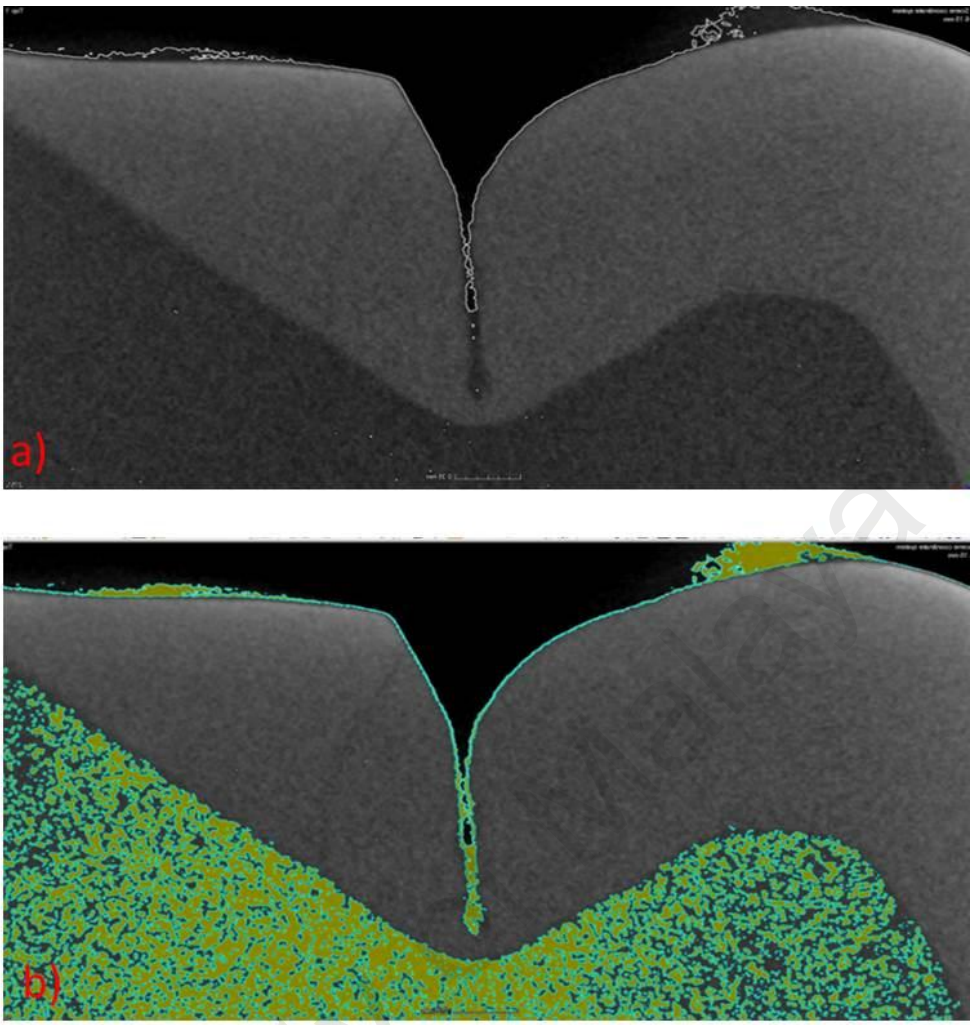

Figure 3.28: Investigation area after surface determination and image thresholding. (a) image of an occlusal fissure with surface determination (b) threshold image highlighting the demineralized enamel (yellow and green) for scoring of absence or presence of caries.

(a) ***Identification of base of the fissure***

Figure 3.29a and 3.29b shows Micro-CT images of two samples before surface determination was performed. The first and crucial step of determining presence or absence of caries was the determination of the tooth-air interface which hereon will be referred to as the surface. The surface was determined using the manual *Surface*

Determination function of the *VG Studio Max 2.1* software and it was elucidated by the software as a white line (Figure 3.29c and 3.29d).

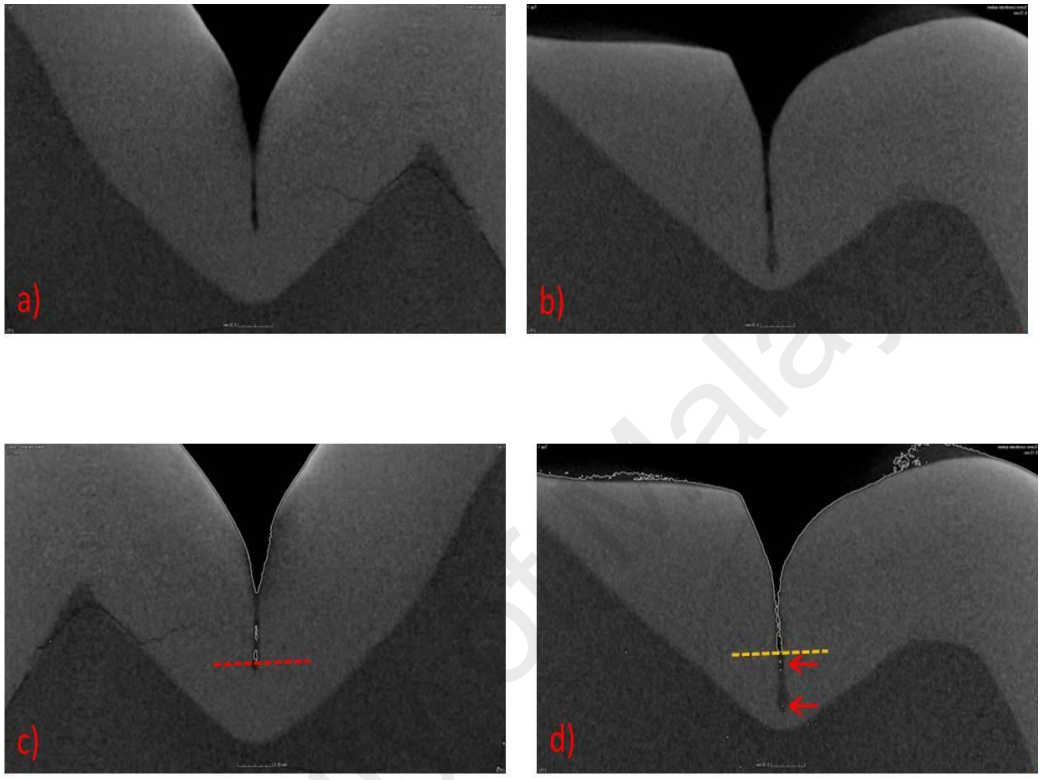

Figure 3.29: Micro-CT images showing base of the fissure before and after surface determination. (a) and (b) shows the Micro-CT images of occlusal fissures before surface determination, (c) shows the contour of the tooth surface and the base of the fissure outlined with white line (red dotted line) after surface determination and, (d) shows white lines outlining the contour of the tooth surface after surface determination that also continues as white dots (red arrows) below the base of the fissure (yellow dotted lines) that were not considered as an extension of the base of the fissure.

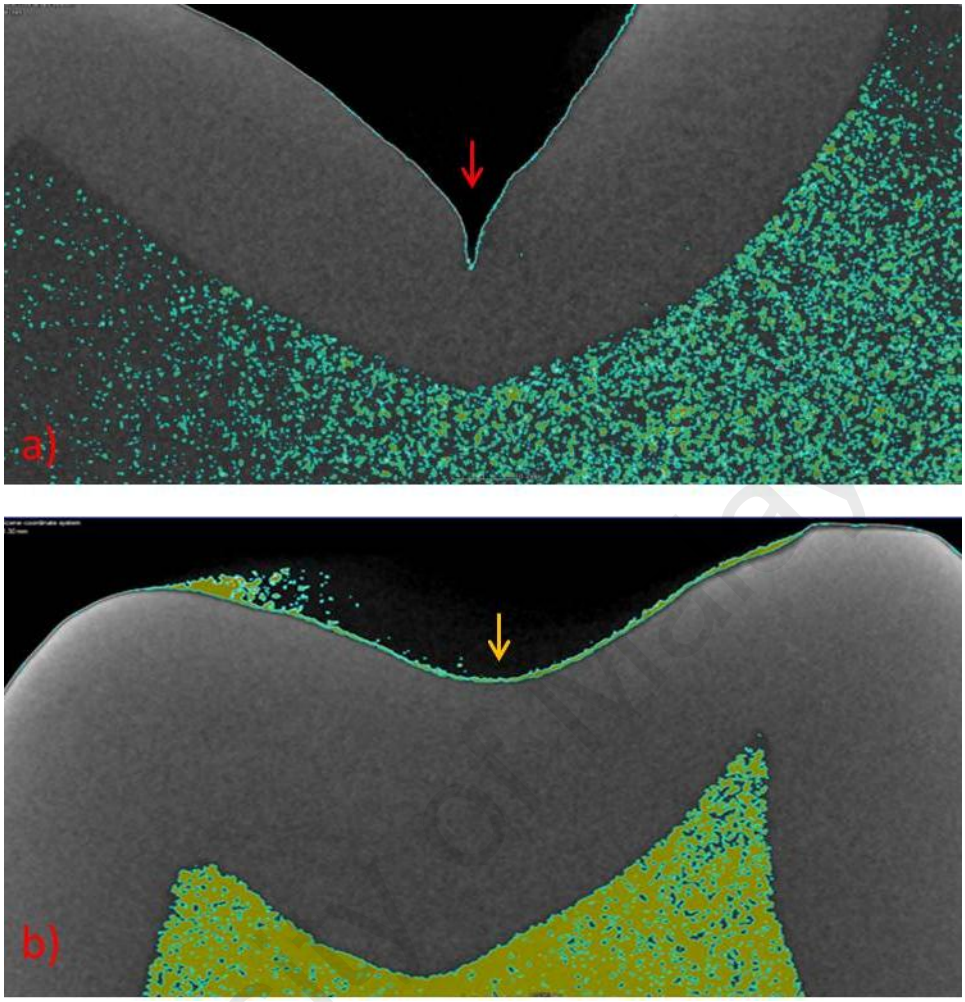

Figure 3.30: Threshold Micro-CT image of the occlusal surface. (a) threshold Micro-CT image of the sound occlusal fissure with absence of sub-surface areas with voxels highlighted in amber and outlined in green color (red arrow) (b) sound occlusal surface with voxels highlighted in amber and/or green color present above the surface after image thresholding (yellow arrow). For both the situations the images were scored as sound.

The base of the fissure was identified as the lowest point where the white line (mentioned above) encloses an area and an example of this is pointed out by a red

dotted line in Figure 3.29c and by a yellow dotted line in Figure 3.29d. White lines that appear as dots within the fissure area, as pointed out by red arrows in Figure 3.29d, were not considered as extension of the base of the fissure (yellow dotted line).

(b) ***Absence of caries***

Regions of interest, i.e. the fissure area was scored as absence of caries if the following criteria were fulfilled:

i) In images that had been subjected to the thresholding process mentioned in Section 3.4.4.2, there is an absence of sub-surface areas with voxels highlighted in amber and outlined in green (Figure 3.30a).
ii) The presence of voxels highlighted in amber and/or green above the surface (Figure 3.30b) was not regarded as caries.

(c) ***Presence of caries***

Images that had been subjected to the thresholding process mentioned in Section 3.4.4.2, presence of sub-surface areas with voxels highlighted in amber and outlined in green were regarded as caries (Figure 3.31).

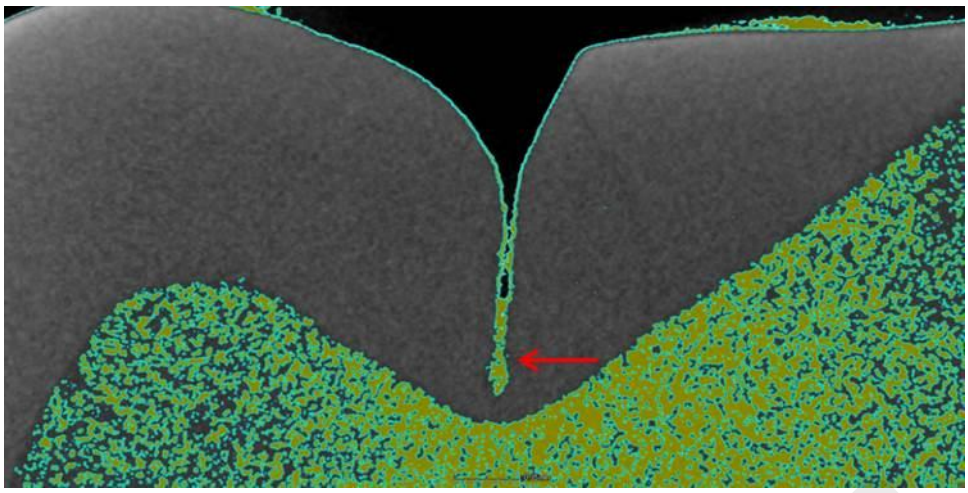

Figure 3.31: Threshold Micro-CT image of NCFC of occlusal fissure representing presence of NCFC highlighted in amber and outlined in green color after image thresholding (red arrow).

Table 3.6: ICDAS radiological criteria.

ICDAS-R-Codes	**Description**
Code 0	No radiolucency
Code 1	Radiolucency in outer ½ of the enamel
Code 2	Radiolucency in inner ½ of the enamel ± EDJ

(d) ***Scoring of stages of NCFC***

The NCFC on the threshold image was further categorized based on severity into code 1 and 2, using the ICDAS Radiological Criteria (ICDAS-R) (Table 3.6) (http://www.icdas.org/). Enamel at the base of the fissure up to DEJ was divided into outer and inner halves using the non-threshold image after surface determination (Figure 3.32).

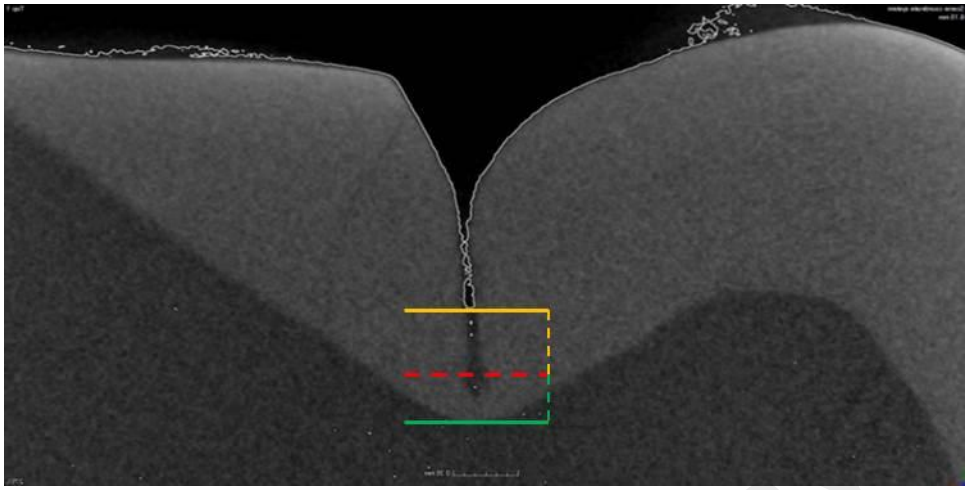

Figure 3.32: Bucco-lingual section of occlusal fissure showing enamel halves. Enamel from base of the occlusal fissure (yellow solid line) up to DEJ (green solid line) was divided (red dotted line) into outer (yellow dotted line) and inner (green dotted line) 50% enamel.

Once the demarcation between the outer and inner 50% of enamel had been identified (Figure 3.33a and 3.34a), the region of interest was scored for severity of NCFC using threshold image (Figure 3.33b and 3.34b). The presence of sub-surface areas with voxels highlighted in amber and outlined in green within the outer 50% of the enamel were scored as ICDAS-R-code 1 (Figure 3.33b). Whereas, if these sub-surface areas with voxels highlighted in amber and green color were present in the inner 50% of the enamel ± DEJ, the region of interest was scored ICDAS-R-code 2 (Figure 3.34b).

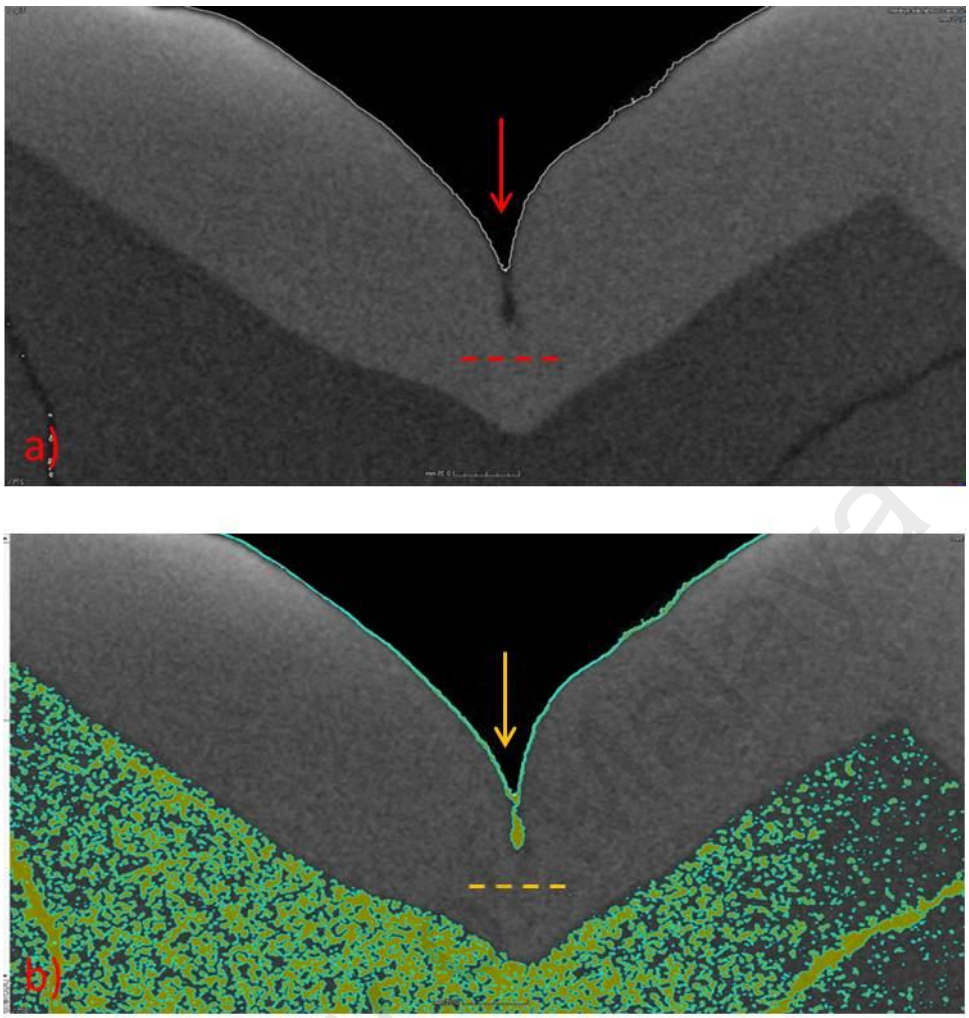

Figure 3.33: ICDAS-R-code 1. (a) non-threshold Micro-CT image with demarcated 50% enamel area (red dotted line) within the region of interest (red arrow) dividing into outer and inner halves (b) a Micro-CT image after thresholding of the region of interest (yellow arrow) with marked 50% enamel area (yellow dotted line) and the extension of demineralization limited to outer 50% of the enamel (yellow and green color voxels) scored as ICDAS-R-code1.

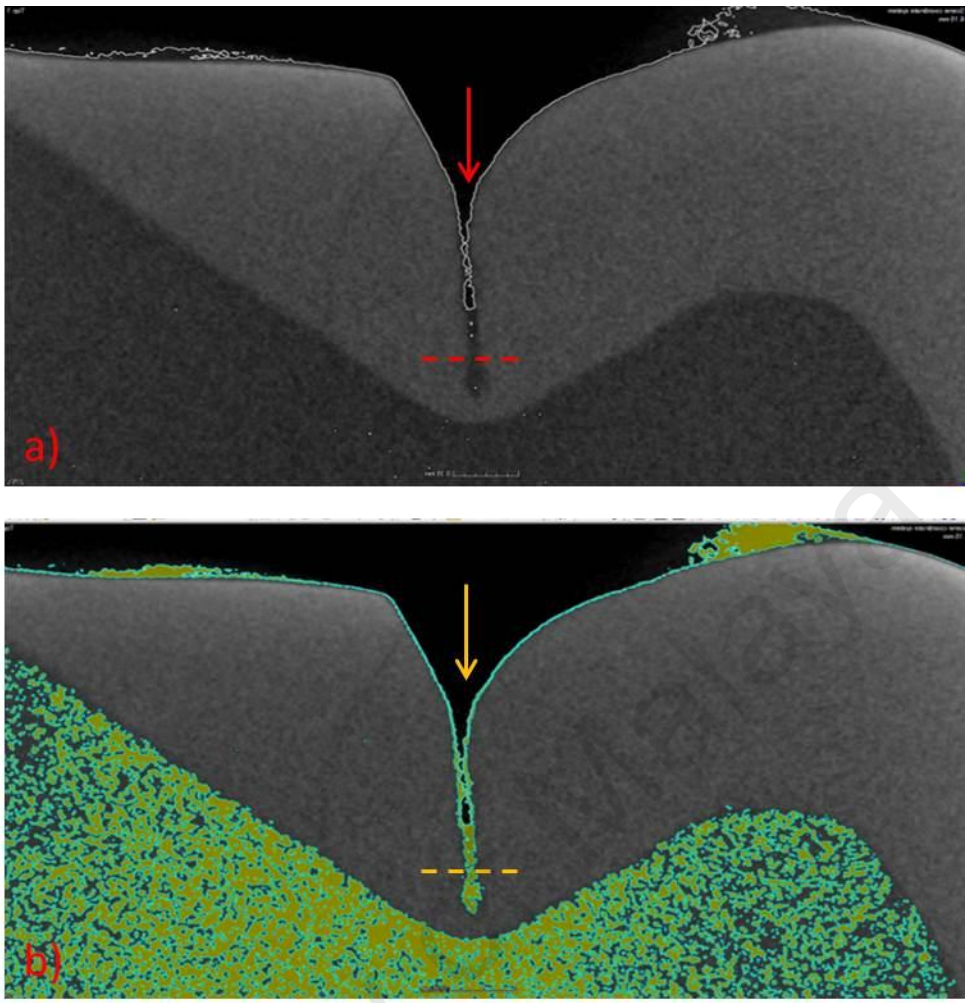

Figure 3.34: ICDAS-R-code 2. (a) non-threshold Micro-CT image dividing the enamel (red dotted line) within the region of interest (red arrow) into outer and inner halves (b) threshold Micro-CT image of the region of interest (yellow arrow) with marked 50% enamel area (yellow dotted line) showing the extension of the demineralization in inner 50% of the enamel (yellow and green color voxels) score as ICDAS-R-code2.

3.4.5 Morphometric analysis

The samples were quantitatively characterized as fissure or groove based on the criteria used by Ekstrand (Ekstrand et al., 1991). The interlobal groove (groove located between two or more lobes) was classified as “fissure” if the structural angle (an angle between two positive neighboring structures) was less than or equal to 25 degrees, and

if the angle was more than 25 degrees, the interlobal groove was classified as ‘’groove’’.

The interlobal structural angle (ISA) was measured, as previously described by Ekstrand (Ekstrand et al., 1991) using image J 1.41 (USA). The most occlusal parts of the two adjacent positive structures were identified and marked on the image as A (lingual) and B (buccal). Deepest part of the interlobal groove was labeled as point C. The three points were joined together as AC and BC line segments. These segments were than divided into thirds and the point closest to the interlobal groove on both line segments AC and BC were marked as D and E respectively. A right angle was drawn and raised, corresponding to point D and E and the new points were designated as D1 and E1 respectively. The angle between the D1, C and E1 was measured as ISA (Figure 3.35).

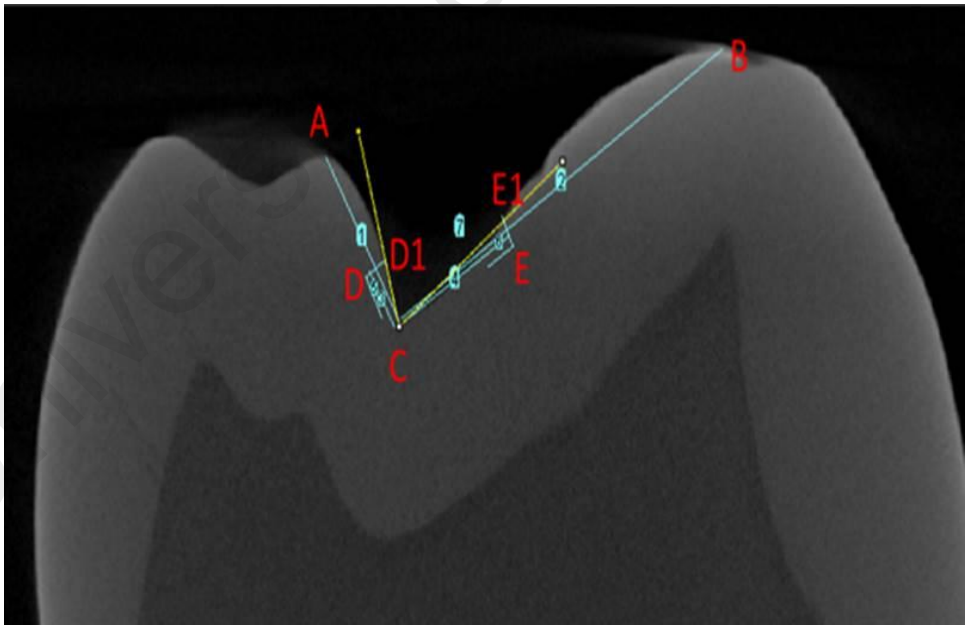

Figure 3.35: Bucco-lingual section through crown of premolar teeth with marked structural angle D1-C-E1 (yellow line).

In some cases, it was not possible to identify one of the positive structures adjacent to interlobal groove. Therefore, an adjusted ISA (ISAa) was drawn by identifying point F, point with the largest perpendicular distance from CE1. The angle between D1, C and F was than measured as ISAa (Figure 3.36).

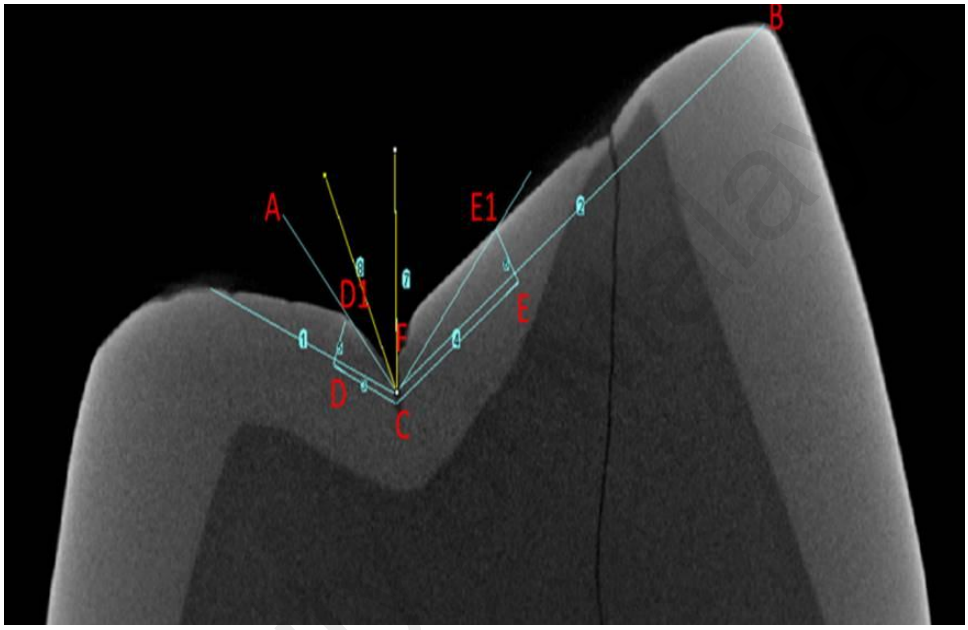

Figure 3.36: Bucco-lingual section through crown of premolar teeth with marked adjusted structural angle D1-C-F (yellow line).

3.4.6 Final cohort

One tooth was excluded from the study due to the presence of a clear fissure sealant on the occlusal fissure. A final cohort of 45 investigation sites were selected by one examiner based on ICDAS-R criteria (Table 3.6) (http://www.icdas.org/) with a final distribution of Ek's code 0 (n=14), 1 (n=21) and 2 (n=10).

3.4.7 OCT scanning

A Swept Source OCT Imaging System (OCS1300SS, Thorlabs Ltd., USA) with emission wavelength centered at 1325 nm and axial and transverse resolution of 9 µm and 11 µm in air, respectively, was used to scan the investigation sites. Figure 3.37a shows the live 3D rendering view and the stereomicroscope image with marked investigation sites used as reference for OCT scanning (Figure 3.37b).

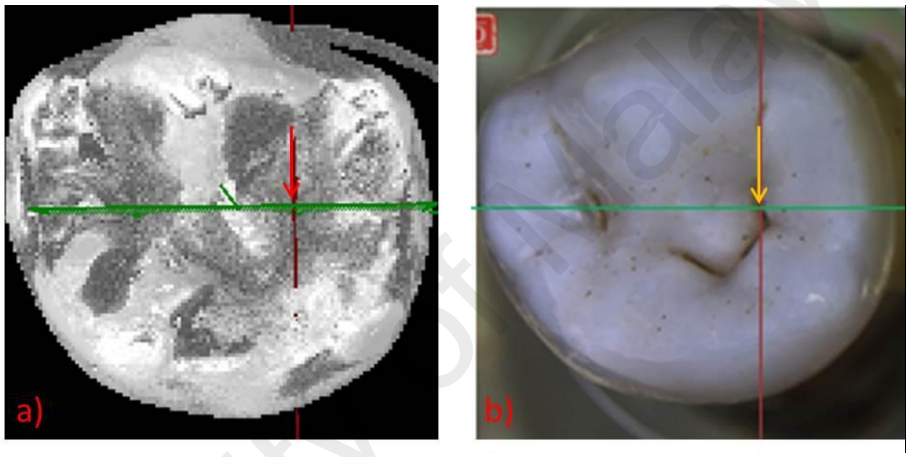

Figure 3.37: Investigation site for OCT scanning. (a) 3D rendering view with selected region of interest (red arrow), (b) region of interest (yellow arrow) has been transferred to stereomicroscope image on the power point slide to serve as reference for OCT scanning.

Each tooth was removed from its container at the time of imaging, air dried for 5 seconds under moderate pressure with a three-in-one syringe. Three-dimensional (3D) scans of 1712 x 504 x 512 in the x-y-z directions were obtained from each investigation site. The scanning beam was oriented perpendicular to the occlusal fissure to cover a scanned surface of 5mm x 1.5 mm in the x-y direction and a depth of 3mm in air, corresponding to 1.85 mm in enamel (refractive index = 1.62). A total of 504 OCT

cross-sectional scans (B-scans) were generated, approximately 3 µm apart, for each investigation site in order to facilitate the identification of a best matching OCT B-scan with the Micro-CT image. The OCT B-scans were captured in a linear scale and saved in the grey scale of the image capturing software. The brightness and contrast were configured to cover an intensity range between -40 dB and -10 dB.

3.4.8 Matching OCT B-scans with Micro-CT

The same protocol for matching OCT scans with Micro-CT was used as described in Section 3.3.6.

3.4.9 OCT data processing with bespoke software

The same protocol of OCT processing was used as described in Section 3.3.7.

3.4.10 OCT data analysis

The depth-resolved intensity (*I*) was collated to produce a mean depth-resolved intensity (*I*) profile from each of the 45 samples. To quantify detection of sound (ICDAS-R code 0) and NCFC (ICDAS-R codes 1 and 2), previously identified OCT outcome measure AUC_P was calculated for each sample as discussed in Section 3.3.8.1. Furthermore, true positive NCFC detected on both OCT and Micro-CT were further categorized based on severity into OCT code 1 and 2 by calculating the AUC_T as discussed in Section 3.3.8.1.

3.4.11 Statistical analysis

Statistical analysis was performed using SPSS (SPSS version 22, IBM, USA) on the final cohort of 45 investigation sites. The cut off points 3.038E+10 (a.u.) (AUC_P) and 7.031E+10 (a.u.) (AUC_T) were used to detect sound (OCT code 0) from NCFC (OCT code 1 and 2) and to differentiate stages of severity of NCFC (OCT code 1 versus OCT code 2) respectively. Samples having cut-off less than or equal to 3.038E+10 (a.u.) were scored sound (OCT code 0) and samples above this cut-off were identified as caries (OCT code 1 and 2). For differentiation between stages of NCFC, true positive samples below or equal to 7.031E+10 (a.u.) were scored OCT code 1 and samples above this cut-off point were scored OCT code 2.

The SN, SP, PPV and NPV for detection and differentiation of ICDAS-R code 0, 1 and 2 for overall the groove fossa system, within the fissure and groove were calculated. At sound level threshold detection, ICDAS-R 1 and code 2 were classified as caries. At non-cavitated level threshold detection, ICDAS-R code 2 was classified as caries. The ROC analysis was also performed and AUROC curves were calculated at both the above mentioned thresholds.

3.5 Research Objective 4: Comparison of the diagnostic accuracy of OCT outcome measures and ICDAS II criteria

3.5.1 Selection of teeth

21 human extracted premolars with sound fissures and naturally occurring NCFC on the occlusal surface were used in this study. The sound fissures and NCFC for this research was same cohort as those used in Section 3.4.1. The inclusion criteria were same as discussed in Section 3.2.1.

3.5.2 Sample preparation

The same protocol was used as mentioned in Section 3.2.2 for sample preparation.

3.5.3 Visual examination of occlusal fissure

Stereomicroscope images of the occlusal surface were taken under 1.25X magnification. Investigation area was identified on the tooth and marked on the hard copy of the stereomicroscope image using a marker. The investigation area was scored by bench mark using ICDAS II protocol without magnification (Pitts, 2004) aided by WHO probe, air syringe and artificial light using conventional dental equipment, as discussed in Section 3.2.3. The highest ICDAS II code was given to the investigation area. Later the marked investigation area was transferred on the power point presentation as reference for Micro-CT data extraction and OCT scanning (Figure 3.38).

Figure 3.38: Stereomicroscope image with the marked investigation area (red circle) with 1.25X magnification.

3.5.4 Transportation for radiographic imaging (Micro-CT), scanning, image processing and Micro-CT data extraction

The same protocol and methods of transportation of samples, Micro-CT scanning, image processing, data extraction and Micro-CT image scoring were used as Section 3.4.2 up to 3.4.4.

3.5.5 Final cohort

The final cohort of 17 samples was included in this study. 4 samples were removed after Micro-CT scanning because the exported data were reconstructed in .vgl format and not as DICOM image stack which may affect the image thresholding procedure. The frame with the demineralized area nearest to the DEJ was selected from

the entire volume data as the representative frame to be visually scored for severity and for comparison between benchmark ICDAS II codes.

3.5.6 OCT scanning

The same protocol was used as mentioned in Section 3.4.7 for OCT scanning.

3.5.7 Matching OCT B-scans with PLM images

The same protocol was used as mentioned in Section 3.4.8.

3.5.8 OCT Data processing and data analysis

The same protocol was used as mentioned in Section 3.4.9 and 3.4.10.

3.5.9 Statistical analysis

Statistical analysis was performed using SPSS (SPSS version 22, IBM, USA) on the final cohort of 17 samples. The cut off points 3.038E+10 (a.u.) (AUC_P) and 7.031E+10 (a.u.) (AUC_T) were used to detect sound (OCT code 0) from NCFC (OCT code 1 and 2) and differentiation between stages of NCFC (OCT code 1 versus OCT code 2) respectively. The SN, SP, PPV, NPV and AUROC curve were calculated at sound and non-cavitated detection threshold as previously described in Section 3.4.11.

CHAPTER 4: RESULTS

4.1 Research Objective 1: Evaluating the accuracy of OCT in detecting sound fissure and naturally occurring NCFC by visual assessment of OCT B-scan

4.1.1 Detection accuracy of qualitative visual assessment of OCT increased back scattered intensity for the detection of sound fissure and NCFC as whole lesion and within different anatomical locations of the fissure

The analysis was performed on the final cohort of the 71 investigation sites.

4.1.1.1 Inter-observer agreement for presence or absence of NCFC using OCT B-scans and PLM image assessment

In the present study, the inter-observer agreement was used to assess the reliability of the qualitative visual criteria used to detect lesions with OCT and PLM. Substantial inter-examiner agreement for the detection of NCFC, at and within the investigation site, with both OCT and PLM were found (0.85-0.87) (0.82- > 0.99) with $p < 0.001$ respectively, as shown in Table 4.1 and 4.2. 84% of the NCFC were found to have both SL and WL. Distribution of SL and WL of samples with NCFC are as shown in Table 4.3. In cases of disagreement, a consensus was taken and the consensual scores were used for SN and SP calculations.

Table 4.1: Inter observer agreement for presence or absence of lesion using OCT.

Lesion	Agreement (%)	Kappa agreement	Sig.
Whole lesion (L)	94	0.87	<0.001*
Slope lesion (SL)	93	0.85	<0.001*
Wall lesion (WL)	94	0.87	<0.001*

P <0.05*

Table 4.2: Inter observer agreement for presence or absence of lesion using PLM.

Lesion	Agreement (%)	Kappa agreement	Sig.
Whole lesion (L)	>99	>0.99	<0.001*
Slope lesion (SL)	92	0.82	<0.001*
Wall lesion (WL)	>99	>0.99	<0.001*

P <0.05*

Table 4.3: Distribution of SL and WL of samples with NCFC.

Lesion	Ek code 1	Ek code 2	Total
WL only	7	1	8
WL and 1 SL	2	3	5
WL and 2 SL	16	21	37

wall lesion (WL), slope lesion (SL)

4.1.1.2 Diagnostic accuracy of OCT qualitative visual assessment for detection of sound fissure and NCFC

Table 4.4 shows the sensitivities, specificities, positive and negative predictive values (PPV and NPV) of NCFC detection with OCT as a whole lesion and for both individual anatomical sites. The detection of the lesion as a whole had the highest SN and NPV when compared to detection of slope or wall lesions separately. On the other

hand, detection of the lesion as a whole had similar SP and PPV to the detection of the wall lesion.

Table 4.4: SN, SP, PPV and NPV for detection of NCFC using OCT.

Lesion	SN	SP	PPV (%)	NPV (%)
Whole lesion (L)	0.98	0.95	98	95
Slopes lesion (SL)	0.95	0.90	93	93
Wall lesion (WL)	0.94	0.95	98	87

Sensitivity (SN), Specificity (SP), Positive predictive value (PPV), Negative predictive value (NPV).True positive values are 49, 40 and 47; False positive values are 1,3 and 1;True negative values are 20, 26 and 20 and False negative are 1, 2 and 3 for L, SL and WL respectively.

4.1.2 Measurement of the NCFC dimensions at different anatomical locations of occlusal fissures using qualitative visual assessment of OCT increased back scattered intensity

4.1.2.1 Inter-observer agreement of the measurement of the lesions

Lesion measurements on OCT B-Scans were performed on true positive lesions detected by OCT and PLM. Good inter-observer agreement was found in the measurement of hSL, wWL and hWL, with an ICC ranging from 0.65-0.85 for OCT and 0.81-0.98 PLM respectively (Table 4.5 and 4.6).

Table 4.5: Inter-observer agreement for lesion dimension measurements of NCFC using OCT.

Lesion	ICC (Consistency)	Sig.	95% Confidence Interval	
			Lower bound	Upper bound
Height of slope lesion (hSL)	0.65	< 0.001*	0.501	0.767
Width of wall lesion (wWL)	0.82	< 0.001*	0.713	0.901
Height of wall lesion (hWL)	0.85	< 0.001*	0.746	0.914

P <0.05*

Table 4.6: Inter-observer agreement for lesion dimension measurements of NCFC using PLM.

Lesion	ICC (Consistency)	Sig.	95% Confidence Interval	
			Lower bound	Upper bound
Height of slope lesion (hSL)	0.92	< 0.001*	0.880	0.951
Width of wall lesion (wWL)	0.81	< 0.001*	0.686	0.891
Height of wall lesion (hWL)	0.98	< 0.001*	0.974	0.992

P <0.05*

4.1.2.2 Agreement of NCFC dimension between OCT and PLM

In order to study the level of dimension measurement agreement between techniques, measurements done with OCT, differing greater than 50% between the two examiners (absolute difference of the two measurements divided by the maximum of the two measurements) were revised and a consensual measurement was obtained. Otherwise, the measurements of the two examiners were averaged.

The mean differences of measurements between these two techniques were -0.084 mm (95% CI 0.16-0.33) for hSL; 0.025 mm (95% CI 0.27-0.22) for wWL and 0.570 mm (95% CI 1.3-0.15) for hWL. The levels of agreement of these measurements are shown with Bland Altman plots as shown in Figure 4.1, 4.2 and 4.3.

(a) ***Height of slope of lesion (hSL)***

For hSLs, the distribution of Δm (PLM measurement–OCT measurement) was almost random around the mean difference, with the majority falling within 2 standard deviations and only two below the lower confidence line (Figure 4.1). Interestingly, the Δm varies significantly from 0 (one-sample t test, $p < 0.05$), however the linear regression slope between the difference and average values showed no significant

difference (slope = 1.22, p > 0.05). This suggested an agreement between techniques although with a constant bias of 0.084 mm in the OCT measurement but no proportional bias. Hence, OCT measurements were overestimated and constantly higher compared to PLM measurements at the slope.

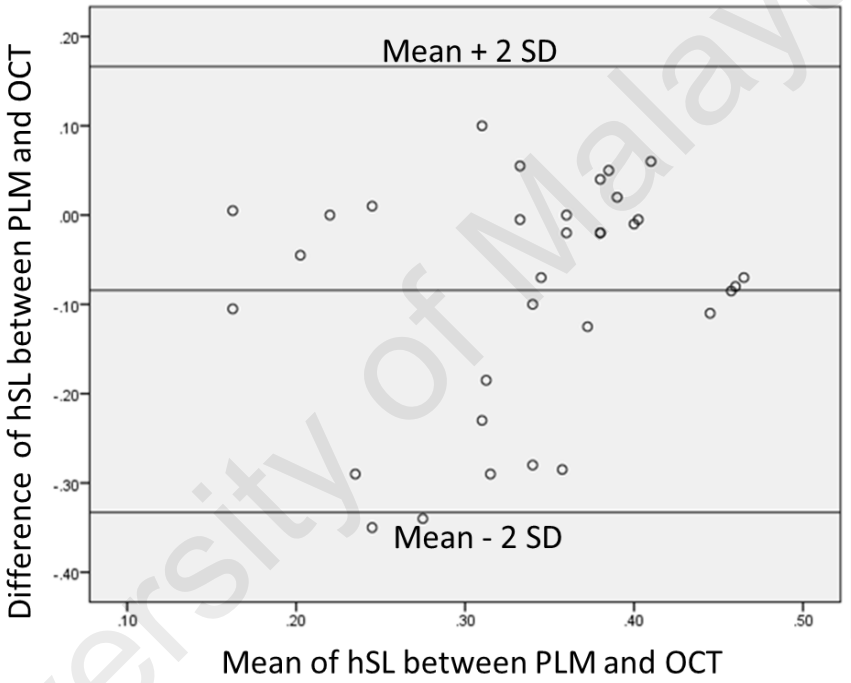

Figure 4.1: Bland Altman plot of hSL between OCT and PLM.

Figure 4.1 shows bland Altman plot of height of slope lesion (hSL) between OCT and PLM methods. The solid central line indicates the mean difference between the compared methods, the upper and the lower lines represents ±2 standard deviations from the mean difference. The linear regression slope between the difference and average values shows no significance (slope = 1.22, p > 0.05). This suggested an agreement between the two methods.

(b) ***Width of wall of lesion (wWL)***

Similar to hSL, an even spread of Δm in the wWL measurement around the mean difference was also found, with most values falling within 2 standard deviations except for two cases (Figure 4.2). The mean difference did not vary significantly from zero ($p > 0.05$) and the slope in the regression between the difference and average values also showed no significant difference (slope = 0.613, $p > 0.05$). This suggested that both methods were in agreement.

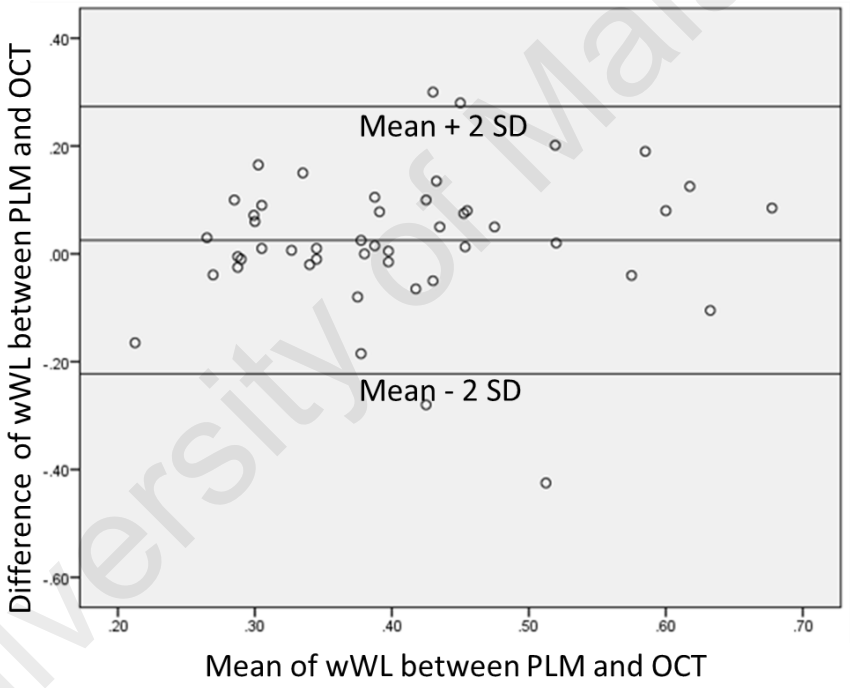

Figure 4.2: Bland Altman plot of wWL between OCT and PLM.

Figure 4.2 shows bland Altman plot of width of wall lesion (wWL) between OCT and PLM. The solid central line indicates the mean difference between the compared methods, the upper and the lower lines represents ±2 standard deviations from the mean difference. The mean difference does not vary significantly from zero (p

> 0.05) and the slope in the regression between the difference and average values also shows no significance (slope = 0.613, $p > 0.05$). This suggests that both methods are in agreement.

(c) ***Height of wall lesion (hWL)***

The spread of Δm in the hWL however, was narrow around the regression line between the difference and the average Δm and presented a significant slope (11.84, $p < 0.05$), suggesting a proportional bias in the data (Figure 4.3). Not surprisingly, one-sample T-test also revealed a significant constant bias ($p < 0.05$). In other words, OCT underestimated the distance measured for hWL. Therefore, there was no agreement between the measurements of PLM and OCT for hWL.

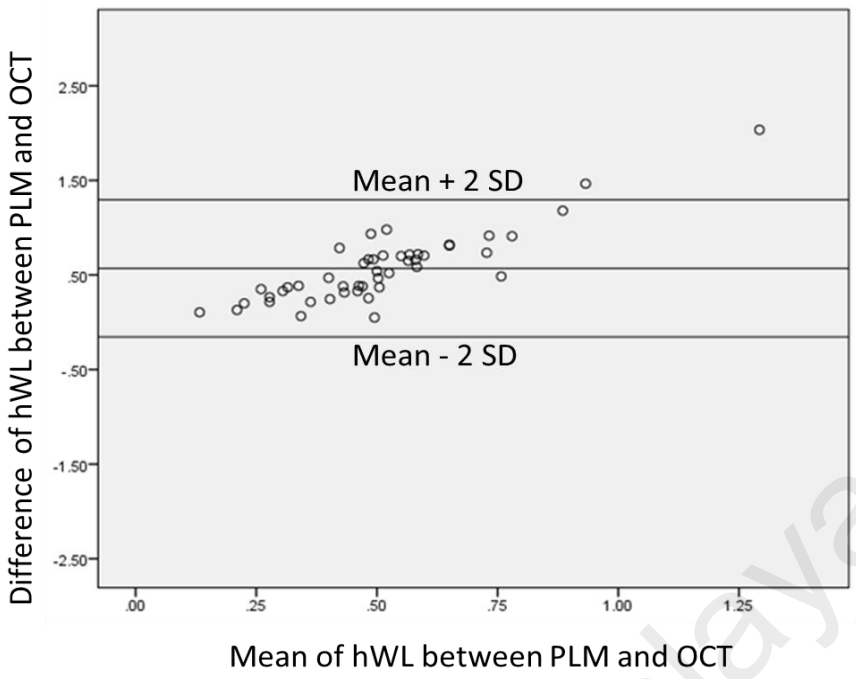

Figure 4.3: Bland Altman plot of hWL between OCT and PLM.

Figure 4.3 shows bland Altman plot of height of wall lesion (hWL) between OCT and PLM. The solid central line indicates the mean difference between the compared methods, the upper and the lower lines represents ±2 standard deviations from the mean difference. The spread of Δm in the hWL is narrow around the regression line between the difference and the average Δm and presented a significant slope (11.84, $p < 0.05$). Therefore, there is no agreement between the measurements of PLM and OCT for hWL.

4.2 Research Objective 2: Identify quantitative OCT outcome measures derived from depth-resolved intensity profile to detect sound fissure from NCFC and distinguish stages of NCFC

4.2.1 Characterizing depth-resolved intensity profile of OCT backscattered intensity through sound fissure (Ek code 0) and NCFC (Ek codes 1 and 2)

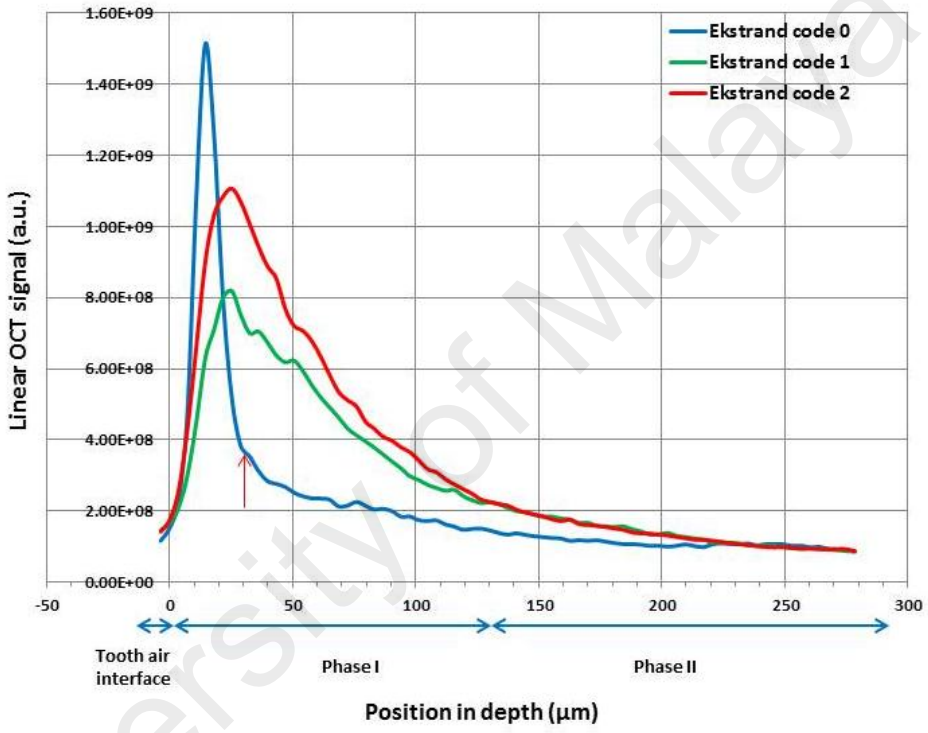

Figure 4.4: Mean depth-resolved intensity (*I*) profile of Ek codes 0, 1 and 2.

Figure 4.4 shows the mean depth-resolved intensity (*I*) profile of OCT A-scan plotting first 300 µm of sound (Ek code 0) and NCFC (Ek codes 1 and 2). At the beginning, an increase in the back scattered intensity from the level of background noise is seen at physical depth 0 µm. This occurrence is defined as tooth-air interface. Different attenuation rates and patterns were observed for all three Ek codes, therefore, *I* was divided into two phases. In phase I, the back scattered intensity continues to rise until it reaches a maximum (I_{max}). The highest I_{max} was observed for Ek code 0

(1.513E+09 ± 2.41E+09 a.u.) followed by Ek code 2 (1.11E+09 ± 9.12E+08 a.u) while Ek code 1 showed the lowest I_{max} (8.19E+08 ± 6.31E+08 a.u). Thereafter, as *I* travel through the enamel it attenuates. In phase I, two distinct rates of attenuation were observed for Ek code 0 starting from I_{max} up to 30 µm physical depth (red arrow) (Figure 4.4) and from 40 µm until 150 µm physical depth when observed visually. Initially there was a sudden and rapid drop seen from I_{max} up to 30 µm which was not observed in the Ek codes 1 and 2. The sound enamel attenuated faster compared to NCFC from I_{max} up to 30 µm physical depth. At 40 µm depth, slow and gradual attenuation was observed for Ek code 0 (1.43E+06 a.u./µm), however, Ek code 2 exhibited the fastest rate of attenuation (6.43E+06 a.u./µm) followed by Ek code 1 (4.46E+06 a.u./µm). Ek codes 1 and 2 maintained higher intensity than Ek code 0 after 40 µm depth. The juncture between phase I and phase II attenuations were seen at 130 µm for Ek code 1 and 2. Thereafter, in phase II, relatively slower and linear attenuations were observed for all three Ek codes until the plateau was reached at 220 µm. Distinct change in the patterns of light and rate of light attenuation of OCT signals at 1310 nm are observed in Figure 4.4 as the light travels to sound (Ek code 0) and NCFC (Ek code 1 and 2) on the occlusal surface. These unique characteristics can be used as a marker to quantify, detect and differentiate NCFC on the occlusal surface.

4.2.2 Outcome measures derived from the mean depth-resolved intensity profile (A-scan)

The characteristics of the attenuation of the OCT intensity was further explored by using outcome measures *AR*, *R*, AUC_P, AUC_T and *FWHM* previously described in Section 3.3.8.1 (Table 3.5). Table 4.7 shows the mean *AR*, *R*, AUC_P, AUC_T and *FWHM* for each depth point between Ek codes 0, 1 and 2.

Table 4.7: Mean *AR*, *R*, AUC_P, AUC_T and *FWHM* of Ek code 0, 1 and 2.

	$\boldsymbol{AR}$	$\boldsymbol{R}$	$\boldsymbol{AUC_P}$	$\boldsymbol{AUC_T}$	$\boldsymbol{FWHM}$
Ek code 0	1.43E+06	4.45E-01	2.19E+10	4.68E+10	36
Ek code 1	4.46E+06	2.73E-01	4.16E+10	6.35E+10	85
Ek code 2	6.40E+06	2.08E-01	4.86E+10	7.92E+10	74

Attenuation rate (*AR*), Attenuation ratio (*R*), Partial area under the curve (AUC_P), Total area under the curve (AUC_T) and Full width half maximum (*FWHM*)

4.2.3 Differentiation of Ek codes 0, 1 and 2 using outcome measures derived from the depth-resolved backscattered intensity (*I*) profile (A-scans)

A total of 107 investigation sites were included in this study based on histology (PLM), where Ek code 0 =17, Ek code 1 = 30 and Ek code 2 = 60. The Shapiro-Wilk test was used to confirm the assumption of normality and it was found the data were not normally distributed. Hence, Kruskal Wallis H-test analysis was performed to compare the outcome measures between Ek codes 0, 1 and 2.

Kruskal Wallis H-test analysis showed that OCT outcome measures were statistically different from at least one of the three Ek codes ($p < 0.001$), except outcome measure *FWHM* which was not significant ($p > 0.001$). The chi-square values were 27.4, 15.4, 39 and 21.6 for outcome measures *AR*, *Ar*, AUC_P and AUC_T respectively. This test did not discriminate which of the Ek codes were different from each other. Therefore, post hoc Dunnet's T3 test was performed.

4.2.4 Pair wise comparison of *AR* between Ek codes 0, 1 and 2

The post hoc Dunnet's T3 test further indicated that using *AR* the difference was only found between Ek code 0 versus Ek codes 1 and 2 with mean difference of -3.116E+06 and - 4.995E+06 ($p < 0.001$) respectively. The summary of the results is shown in Table 4.8.

Table 4.8: Post hoc Dunnet's T3 test, comparing *AR* for Ek codes 0, 1 and 2.

I	J	Mean Difference (I-J)	Standard Error	Sig.	95% Confidence Interval	
					Lower bound	Upper bound
Code 0	Code 1	-3.116E+06*	6.985E+05	.000	-4.863E+06	-1.370E+06
	Code 2	-4.995E+06*	7.020E+05	.000	-6.711E+06	-3.280E+06
Code 1	Code 0	3.116E+06*	6.985E+05	.000	1.370E+06	4.863E+06
	Code 2	-1.879E+07	9.339E+05	.135	-4.156E+06	3.979E+05
Code 2	Code 0	4.995E+06*	7.020E+05	.000	3.280E+06	6.711E+06
	Code 1	1.879E+06	9.339E+05	.135	-3.979E+05	4.156E+06

Attenuation rate (*AR*), * $p < 0.05$

4.2.5 Pair wise comparison of *R* between Ek codes 0, 1 and 2

The post hoc comparison using Dunnet's T3 test showed that only *R* of Ek code 0 and Ek code 2 were significantly different from one another with a mean difference of 2.131E-01 ($p < 0.001$). The summary of the results is shown in Table 4.9.

Table 4.9: Post hoc Dunnet's T3 test, comparing *R* for Ek codes 0, 1 and 2.

I	J	Mean Difference (I-J)	Standard Error	Sig.	95% Confidence Interval	
					Lower bound	Upper bound
Code 0	Code 1	1.329E-01	7.760E-02	.253	-5.975E-02	3.256E-01
	Code 2	2.131E-01*	6.243E-02	.006	5.478E-02	3.715E-01
Code 1	Code 0	-1.329E-01	7.760E-02	.253	-3.256E-01	5.975E-02
	Code 2	8.018E-02	6.354E-02	.508	-7.684E-02	2.372E-01
Code 2	Code 0	2.131E-01*	6.243E-02	.006	-3.715E-01	-5.478E-02
	Code 1	-8.018E-02	6.354E-02	.508	-2.372E-01	7.684E-02

Attenuation ratio (*R*), * $p < 0.05$

4.2.6 Pair wise comparison of AUC_P between Ek codes 0, 1 and 2

Similar to outcome measure *AR*, there was statistically significant difference found among Ek code 0 versus Ek codes 1 and 2 with a mean difference of -19.69E9 and -26.70E9 ($p < 0.001$) respectively. The summary of the results is shown in Table 4.10.

Table 4.10: Post hoc Dunnet's T3 test, comparing AUC_P for Ek codes 0, 1 and 2.

I	J	Mean Difference (I-J)	Standard Error	Sig.	95% Confidence Interval	
					Lower bound	Upper bound
Code 0	Code 1	-19.69E9*	3.432E9	.000	-28.25E9	-11.13E9
	Code 2	-26.70E9*	2.499E9	.000	-32.80E9	-20.60E9
Code 1	Code 0	19.69E9*	3.432E9	.000	11.13E9	28.25E9
	Code 2	-7.011E9	3.829E9	.200	-16.43E9	2.40E9
Code 2	Code 0	26.70E9*	2.499E9	.000	20.60E9	32.80E9
	Code 1	7.011E09	3.829E9	.200	-2.40E9	16.43E9

Partial area under the curve (AUC_P), * $p < 0.05$

4.2.7 Pair wise comparison of AUC_T between Ek codes 0, 1 and 2

AUC_T was significantly different for Ek code 1 and Ek code 2, when compared amongst each other for pair wise comparison. AUC_T was the only OCT outcome measure identified in this study that could statistically quantify the differentiation amongst stages of NCFC with a mean difference of -1.57E10 ($p < 0.05$) but cannot help in detection. The summary of the results is shown in Table 4.11.

Table 4.11: Post hoc Dunnet's T3 test, comparing AUC_T for Ek codes 0, 1 and 2.

I	J	Mean Difference (I-J)	Standard Error	Sig.	95% Confidence Interval	
					Lower bound	Upper bound
Code 0	Code 1	-1.67E10	8.30E9	.151	-37.70E9	4.353E9
	Code 2	-3.24E10*	8.24E9	.001	-53.23E9	-11.52E9
Code 1	Code 0	1.67E10	8.30E9	.151	-4.35E9	37.70E9
	Code 2	-1.57E10*	6.01E9	.032	-30.37E9	-1.04E9
Code 2	Code 0	3.24E10*	8.24E9	.001	11.52E9	53.23E9
	Code 1	1.57E10*	6.01E9	.032	1.039E9	30.37E9

Total area under the curve (AUC_T), * $p < 0.05$

4.2.8 Summary of outcome measures that are significantly different for Ek codes 0, 1 and 2

Out of all the outcomes measures tested, *AR* and AUC_P were significantly different between Ek code 0 versus Ek codes 1 and 2. There was no significant difference observed for *AR* and AUC_P to differentiate between Ek code 1 and Ek code 2. Outcome measure AUC_T was significantly different between Ek code 1 and Ek code 2. Therefore, *AR* and AUC_P both were suitable to quantify detection of sound fissure and naturally occurring NCFC whereas AUC_T can be used as an outcome measure to

differentiate between Ek code 1 and Ek code 2 on the occlusal surface. The summary of the outcome measures that are significantly different for Ek codes 0, 1 and 2 representing significant difference ($p > 0.05$) are shown in Table 4.12.

Table 4.12: Summary of outcome measures that are significantly different for Ek codes 0, 1 and 2.

	AR	***AUC_P***	***AUC_T***
Ek code 0 vs. Ek codes 1 and 2	√	√	
Ek code 1 vs. Ek code 2			√

Attenuation rate (*AR*), Partial area under the curve (AUC_P), Total area under the curve (AUC_T)

4.2.9 Identifying the best OCT outcome measure to quantify detection of sound fissure and NCFC and differentiation of stages of NCFC ROC curve analysis

To identify the best outcome measure for the detection of sound (Ek code 0) and NCFC (Ek codes 1 and 2) ROC curve analysis was performed (Figure 4.5 and 4.6). The curve illustrated a graphic representation by plotting true positive rate (SN) against the false positive rate (1- SP) for different possible cut points of a diagnostic test. The area under ROC (AUROC) curve for outcome measure AUC_P was calculated excellent, 0.95 (95% CI 0.916-0.99) with p value <0.001 (Figure 4.5) whereas good AUROC, 0.88 (95% CI 0.81-0.94) with p value <0.001 for outcome measure *AR* was reported (Figure 4.6). Based on highest AUROC curve, AUC_P was the better OCT outcome measure identified in this study to quantify detection of sound (Ek code 0) and NCFC (Ek codes 1 and 2) on the occlusal surface.

In this study, AUC_T was the only outcome measure identified that could statistically differentiate between Ek code 1 and Ek code 2. The AUROC curve for AUC_T was calculated to be 0.66 (95% CI 0.52 – 0.79) with p value < 0.05 (Figure 4.7). Therefore, outcome measure AUC_T was used for further analysis.

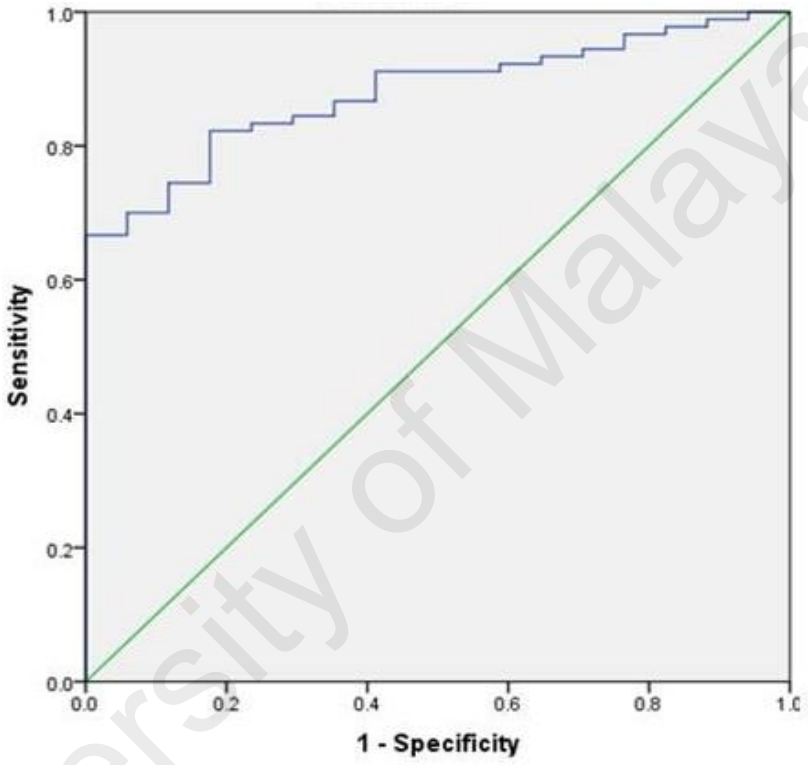

Figure 4.5: ROC curve plot of *AR*.

Figure 4.5 shows area under the ROC curve of outcome measure *AR* discriminating between Ek code 0 versus Ek codes 1 and 2 with AUROC = 0.88

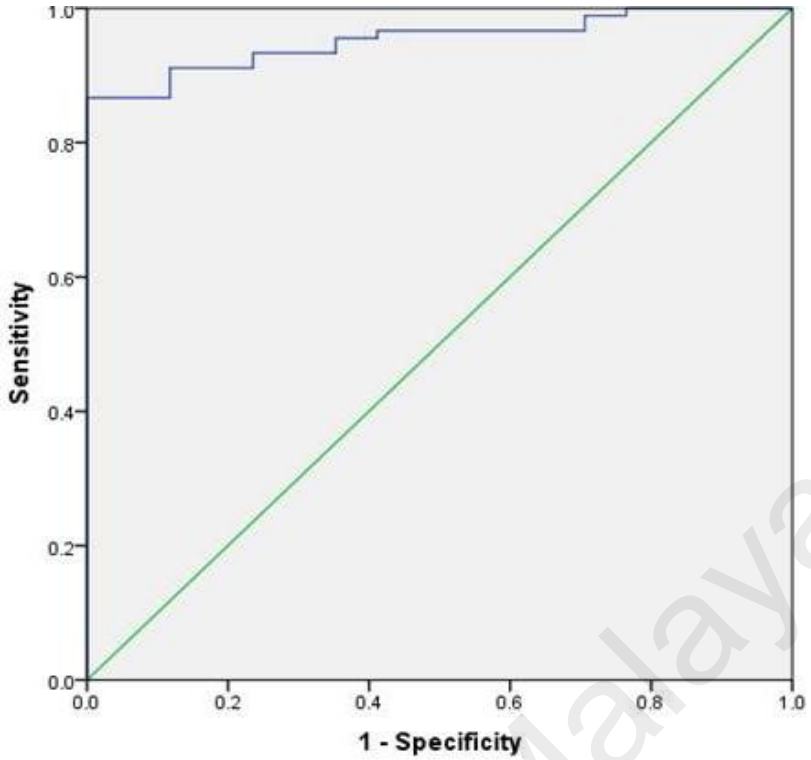

Figure 4.6: ROC curve plot of mean AUC_P

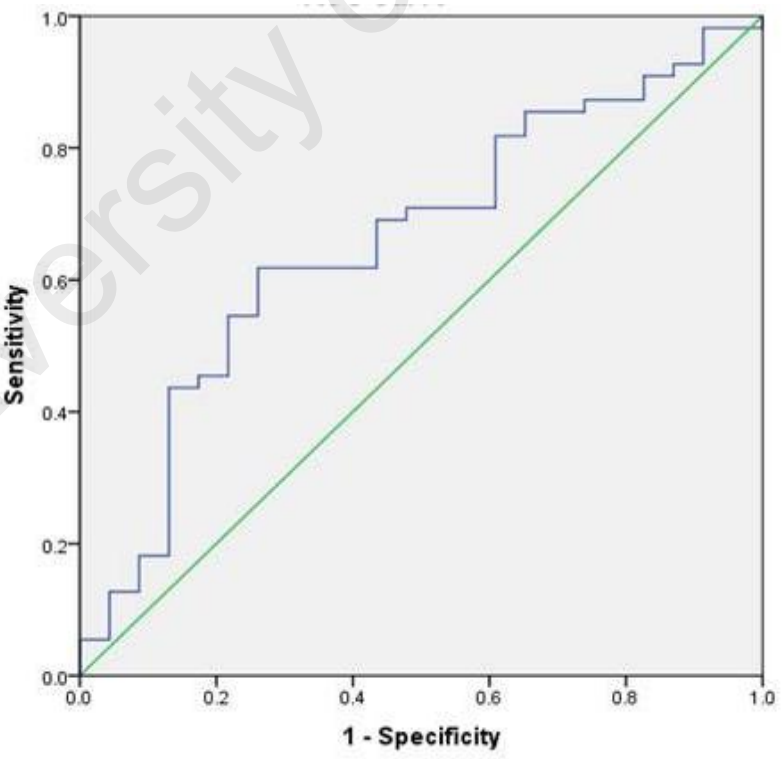

Figure 4.7: ROC curve plot of AUC_T

Figure 4.6 shows area under the ROC curve of outcome measure AUCP discriminating between Ek code 0 versus Ek codes 1 and 2 with AUROC =0.95 and Figure 4.7 shows area under the ROC curve of outcome measure AUC_T discriminating between Ek code 1 and Ek code 2 with AUROC =0.66

4.2.10 To identify cut-off values for detection of sound fissure and NCFC and differentiation of stages of NCFC using AUC_P and AUC_T threshold values

Amongst all the significantly contributing OCT outcome measures AUC_P was ranked the most significant outcome measure to detect sound (Ek code 0) and NCFC (Ek codes 1 and 2) and AUC_T to differentiate between the stages of NCFC (Ek code 1 and Ek code 2) showing the highest AUROC curve. The summary of the results is shown in table 4.13. ROC curve analysis was performed to find the best cut-off point by determining highest Youden's index (Y.I) (SN+SP)-1. The ROC curve was obtained by plotting AUC_P and AUC_T points as shown in Table 4.14 and 4.15 respectively.

At a cut-off value of 3.038E+10 (a.u.), AUC_P showed 0.86 SN and > 0.99 SP with 0.87 Y.I in detecting sound fissure and NCFC (Ek codes 1 and 2). However, AUC_T at a cut-off value of 7.031E+10 (a.u.) was limited to low SN 0.61 and 0.73 moderate SP with 0.36 Y.I for Ek code 1 and Ek code 2.

Table 4.13: Overall best outcome measure to detect sound fissure from NCFC and differentiate stages of NCFC and its AUROC curve, SN, SP and Y.I

Outcome measures	AUROC	SN	SP	Y.I
AUC_P	0.95	0.86	> 0.99	0.87
AUC_T	0.66	0.61	0.73	0.36

Partial area under the curve (AUC_P), Total area under the curve (AUC_T), Area under Receiver operating characteristics (AUROC), Sensitivity (SN), Specificity (SP), Youden index (Y.I)

Table 4.14: AUC_P values and its corresponding SN, SP and Y.I.

Positive if Greater Than or Equal To[a]	SN	1 - SP	SP	Youden's index
1.10E+10	1.000	1.000	0.000	0.000
1.21E+10	1.000	.941	0.059	0.059
1.41E+10	1.000	.882	0.118	0.118
1.65E+10	1.000	.824	0.176	0.176
1.89E+10	1.000	.765	0.235	0.235
2.01E+10	.989	.765	0.235	0.224
2.04E+10	.989	.706	0.294	0.283
2.06E+10	.978	.706	0.294	0.272
2.10E+10	.967	.706	0.294	0.261
2.13E+10	.967	.647	0.353	0.320
2.13E+10	.967	.588	0.412	0.378
2.15E+10	.967	.529	0.471	0.437
2.22E+10	.967	.471	0.529	0.496
2.31E+10	.967	.412	0.588	0.555
2.36E+10	.956	.412	0.588	0.544
2.41E+10	.956	.353	0.647	0.603
2.48E+10	.944	.353	0.647	0.592
2.51E+10	.933	.353	0.647	0.580
2.52E+10	.933	.294	0.706	0.639
2.53E+10	.933	.235	0.765	0.698
2.58E+10	.922	.235	0.765	0.687
2.64E+10	.911	.235	0.765	0.676
2.67E+10	.911	.176	0.824	0.735
2.73E+10	.911	.118	0.882	0.793
2.80E+10	.900	.118	0.882	0.782
2.86E+10	.889	.118	0.882	0.771
2.93E+10	.878	.118	0.882	0.760
2.98E+10	.867	.118	0.882	0.749
2.98E+10	.867	.059	0.941	0.808
3.04E+10	.867	0.000	1.000	0.867
3.10E+10	.856	0.000	1.000	0.856
3.13E+10	.844	0.000	1.000	0.844
3.19E+10	.833	0.000	1.000	0.833
3.22E+10	.822	0.000	1.000	0.822
3.24E+10	.811	0.000	1.000	0.811
3.27E+10	.800	0.000	1.000	0.800
3.31E+10	.789	0.000	1.000	0.789
3.34E+10	.778	0.000	1.000	0.778
3.37E+10	.767	0.000	1.000	0.767
3.40E+10	.756	0.000	1.000	0.756

Partial area under the curve (AUC_P), Sensitivity (SN), Specificity (SP), Youden index (Y.I)

Table 4.15: AUC_T values and its corresponding SN, SP and Y.I.

Positive if Greater Than or Equal To[a]	SN	1 - SP	SP	Youden's index
3.89E+10	1.000	1.000	0.000	0.000
3.99E+10	.982	1.000	0.000	-0.018
4.11E+10	.982	.957	0.043	0.025
4.32E+10	.982	.913	0.087	0.069
4.57E+10	.964	.913	0.087	0.051
4.62E+10	.945	.913	0.087	0.032
4.64E+10	.927	.913	0.087	0.014
4.67E+10	.927	.870	0.130	0.058
4.75E+10	.909	.870	0.130	0.040
4.86E+10	.909	.826	0.174	0.083
4.97E+10	.891	.826	0.174	0.065
5.05E+10	.873	.826	0.174	0.047
5.09E+10	.873	.783	0.217	0.090
5.16E+10	.873	.739	0.261	0.134
5.24E+10	.855	.739	0.261	0.115
5.38E+10	.855	.696	0.304	0.159
5.53E+10	.855	.652	0.348	0.202
5.72E+10	.836	.652	0.348	0.184
5.88E+10	.818	.652	0.348	0.166
5.92E+10	.818	.609	0.391	0.209
5.97E+10	.800	.609	0.391	0.191
6.08E+10	.782	.609	0.391	0.173
6.19E+10	.764	.609	0.391	0.155
6.26E+10	.745	.609	0.391	0.137
6.31E+10	.727	.609	0.391	0.119
6.36E+10	.709	.609	0.391	0.100
6.42E+10	.709	.565	0.435	0.144
6.45E+10	.709	.522	0.478	0.187
6.51E+10	.709	.478	0.522	0.231
6.58E+10	.691	.478	0.522	0.213
6.63E+10	.691	.435	0.565	0.256
6.67E+10	.673	.435	0.565	0.238
6.71E+10	.655	.435	0.565	0.220
6.75E+10	.636	.435	0.565	0.202
6.78E+10	.618	.435	0.565	0.183
6.86E+10	.618	.391	0.609	0.227
6.94E+10	.618	.348	0.652	0.270
6.97E+10	.618	.304	0.696	0.314
7.03E+10	.618	.261	0.739	0.367
7.09E+10	.600	.261	0.739	0.339
7.10E+10	.582	.261	0.739	0.321

Total area under the curve (AUC_T), Sensitivity (SN), Specificity (SP), Youden index (Y.I)

4.3 Research Objective 3: Validation of OCT outcome measures identified in Research Objective 2

4.3.1 Distribution of sound enamel and NCFC within the groove-fossa system overall and when divided as fissure and groove separately

45 occlusal investigation sites within the groove-fossa system were analyzed out of which ICDAS-radiological examination revealed that 14 investigation sites were sound, 21 showed radiolucency in the outer 50% of the enamel and 10 had radiolucency in the inner 50% of the enamel or had reached the DEJ. Furthermore, the investigation sites within the groove-fossa system were classified as fissure or groove separately. Out of 45 investigation sites, 13 were classified as fissures and 32 as grooves. Interestingly, none of the fissures were caries free, however, 14 grooves were classified as sound. A total of 13 fissures and 18 grooves showed NCFC with 8 fissures and 13 grooves having radiolucency in the outer 50% of the enamel. Similar grooves and fissures (n=5 each) had radiolucency in the inner 50% of the enamel. Table 4.16 summarizes the distribution of the sound investigation sites and NCFC within the groove-fossa system and at the fissure and grooves separately.

Table 4.16: Distribution of the sound enamel and NCFC within the investigation sites

Anatomical Location	ICDAS-R-code 0	ICDAS-R-code 1	ICDAS-R-code 2	Total (n)
Groove fossa system	14	21	10	45
Fissure	0	8	5	13
Groove	14	13	5	32

4.3.2 Diagnostic accuracy of the OCT outcome measure to detect sound (ICDAS-R code 0) and NCFC (ICDAS-R codes 1-2) within the groove-fossa system overall and when divided as fissure and groove separately

The disease prevalence was 69% and 56% for groove-fossa and groove sample cohorts respectively. The diagnostic accuracy was calculated at sound level threshold detection as described in Section 3.4.11. At sound level threshold detection (ICDAS–R-code 0 versus ICDAS–R-code 1 and 2) OCT presented similar SN (> 0.99) and SP (0.79) at both, overall groove-fossa system and within the occlusal groove. Since none of the investigation sites within the occlusal fissure in this study were caries free, calculation of diagnostic accuracy measures for fissures were not possible. Table 4.17 shows the SN, SP, PPV and NPV, and AUROC curve of OCT outcome measure AUC_P for the detection of sound enamel and NCFC corresponding to reference test Micro-CT.

Table 4.17: SN, SP, PPV, NPV and AUROC curve of OCT for the detection of sound enamel and NCFC using AUC_P.

Morphology	Cut-off points Sound level threshold detection (ICDAS –R-code 0 versus ICDAS–R-code 1 and 2)				
	SN	**SP**	**PPV (%)**	**NPV (%)**	**AUROC**
Groove fossa system	> 0.99	0.79	90	> 99	0.89
Fissure	-	-	-	-	-
Groove	> 0.99	0.79	86	> 99	0.89

Sensitivity (SN), Specificity (SP), Positive predictive value (PPV), Negative predictive value (NPV), Area under Receiver operating characteristics (AUROC),

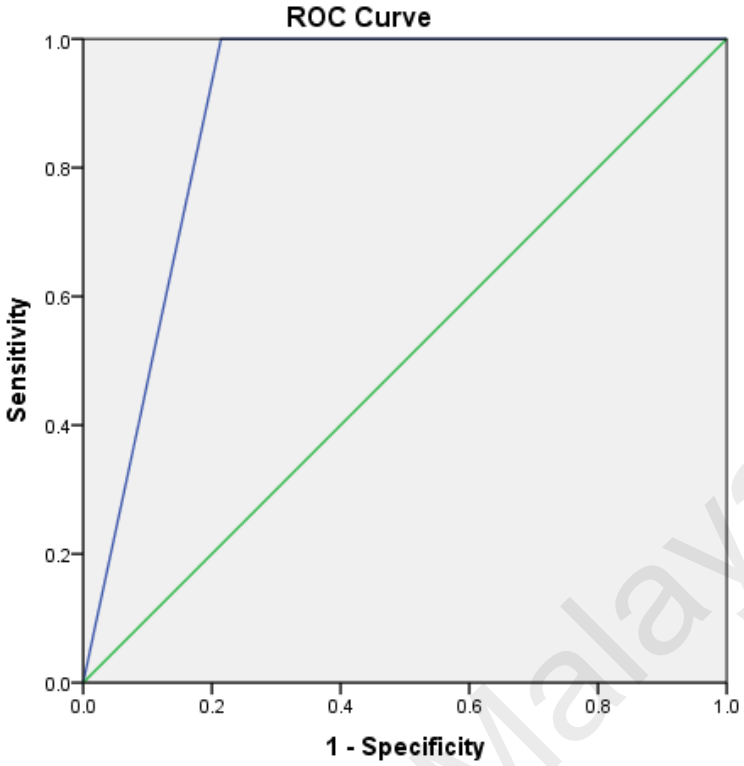

Figure 4.8: ROC curve of OCT detection at groove-fossa system using AUC_P.

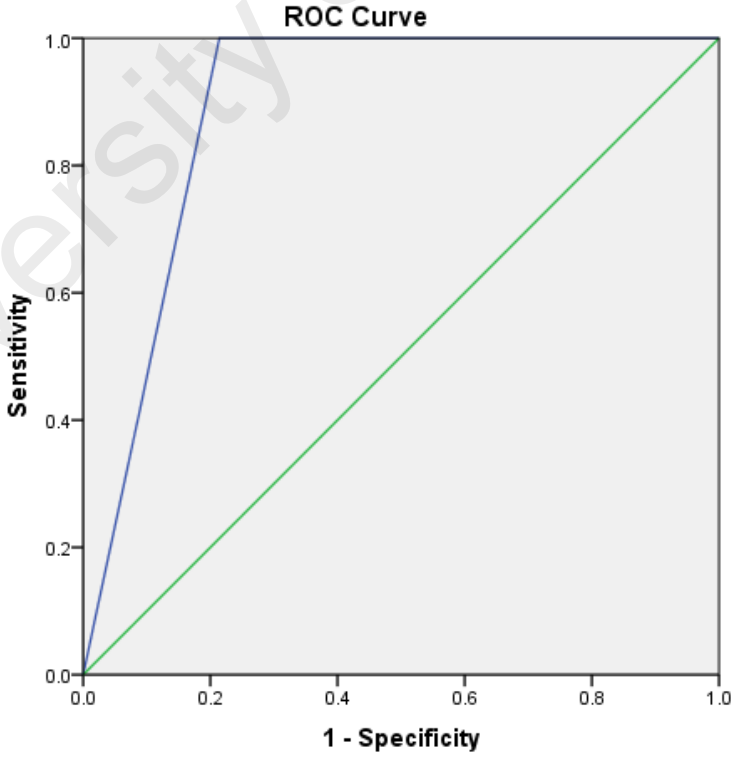

Figure 4.9: ROC curve of OCT detection at occlusal groove using AUC_P.

Figure 4.8 and 4.9 show AUROC curves for the detection of sound enamel and NCFC at groove-fossa system and occlusal groove using partial area under the curve (AUC_P) with similar AUROC = 0.89.

4.3.3 Diagnostic accuracy of OCT outcome measure to differentiate ICDAS-R code 1 and ICDAS-R code 2 within the groove-fossa system overall and when divided as fissure and groove separately

The disease prevalence was 32%, 39% and 28% for groove-fossa, fissure and groove sample cohorts respectively. Table 4.18 shows the SN, SP, PPV, NPV and AUROC of stages of NCFC within groove-fossa system and for both fissures and grooves separately. The ICDAS-R code 2 within the groove-fossa system and at the occlusal fissure and groove had similar SN (0.80) with slightly higher NPV at the occlusal grooves (88%). However, the SP (0.75) and the PPV (67%) for ICDAS-R-code 1 within the occlusal fissure were higher when compared to groove-fossa system SN (0.62) and PPV (50 %) or occlusal groove SN (0.54) and PPV (40%) separately.

Table 4.18: SN, SP, PPV, NPV and AUROC curve of OCT for the differentiation of stages of NCFC using AUC_T.

Morphology	Cut-off points Non- cavitated level threshold detection (ICDAS –R-code 1 versus ICDAS –R-code 2)				
	SN	**SP**	**PPV (%)**	**NPV (%)**	**AUROC**
Groove fossa system	0.80	0.62	50	87	0.71
Fissure	0.80	0.75	67	86	0.72
Groove	0.80	0.54	40	88	0.67

Sensitivity (SN), Specificity (SP), Positive predictive value (PPV), Negative predictive value (NPV), Area under Receiver operating characteristics (AUROC),

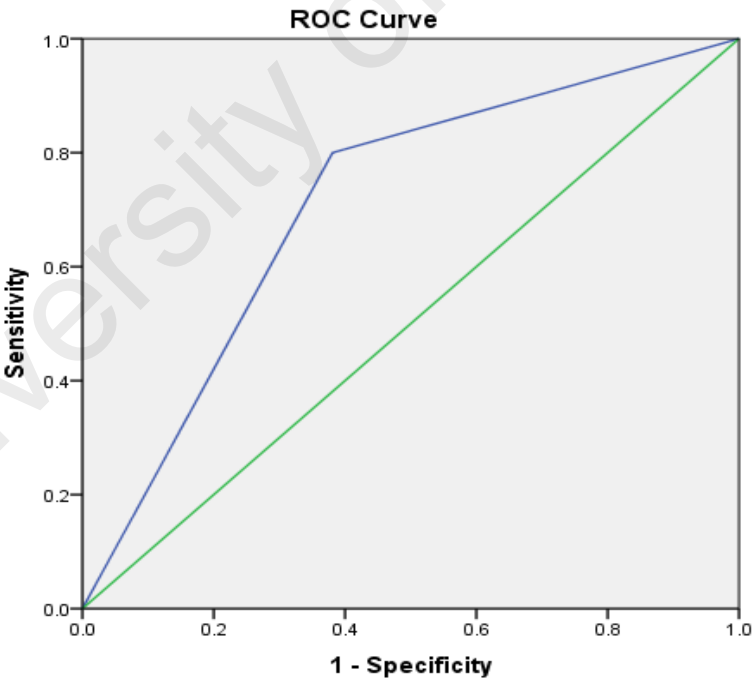

Figure 4.10: ROC curve for OCT differentiation of stages of NCFC at groove-fossa system using AUC_T.

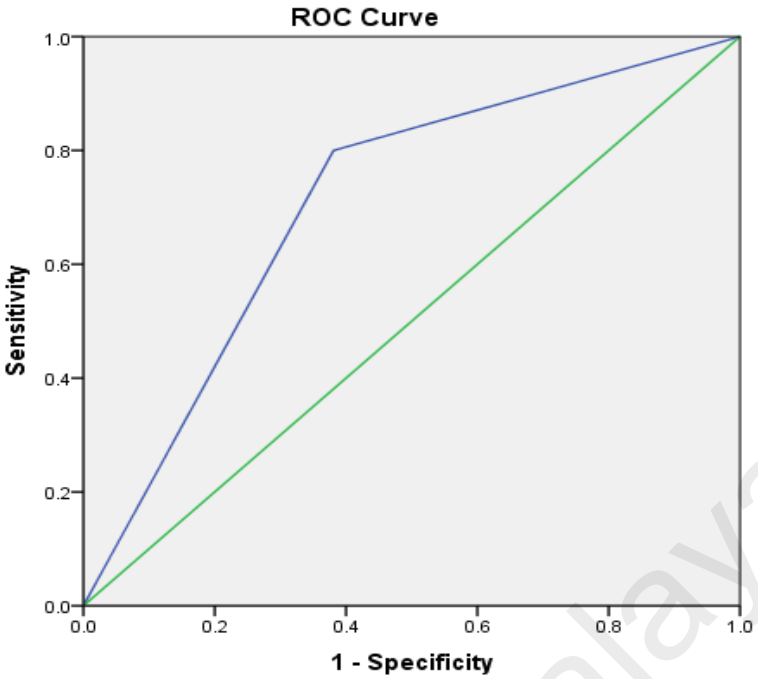

Figure 4.11: ROC curve for OCT differentiation of stages of NCFC at occlusal fissure using AUC_T.

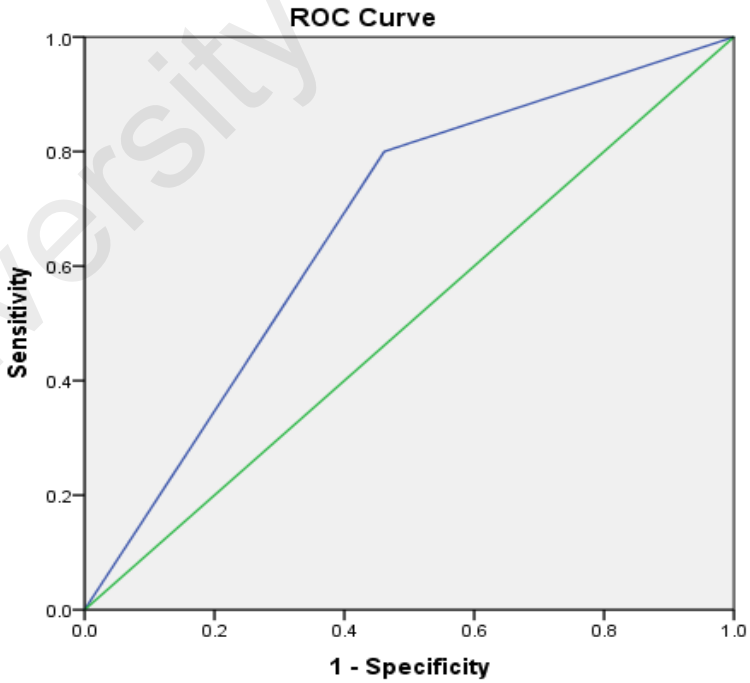

Figure 4.12: ROC curve of OCT differentiation of stages of NCFC at occlusal groove using AUC_T.

Figure 4.10, 4.11 and 4.12 show AUROC curves for the differentiation of stages of NCFC at groove-fossa system, occlusal fissure and occlusal groove using total area under the curve (AUC_T) with AUROC = 0.71, 0.72 and 0.67.

4.4 Research Objective 4: Comparison of the diagnostic accuracy of OCT outcome measures and ICDAS II criteria

4.4.1 Comparison between OCT outcome measure AUC_P and ICDAS II criteria for the detection of sound fissure and NCFC

From 17 occlusal investigation sites analyzed in this study, the ICDAS-R examination revealed that only 2 investigation sites were sound, 8 showed radiolucency in the outer 50% of the enamel and 7 had radiolucency in the inner 50% of the enamel or has reached the DEJ. The disease prevalence was calculated to be 0.88% (95% CI 63.56 – 98.54) for both OCT and ICDAS II cohorts. At sound level threshold detection (ICDAS –R-code 0 versus ICDAS–R-code 1 and 2) all diseased samples (SN > 99%) were correctly detected as NCFC using OCT with highest NPV (> 99 %). On the other hand, 73% of NCFC were correctly identified using ICDAS II. However, both OCT and ICDAS II accurately detected sound occlusal surfaces with excellent SP (> 99 %) and PPV (99 %). The AUROC curve was higher for OCT (> 0.99) (Figure 4.13) as compared to ICDAS II (0.87) (Figure 4.14). Table 4.19 shows the SN, SP, PPV, NPV and AUROC of OCT and ICDAS II for the detection of sound fissure and NCFC corresponding to Micro-CT.

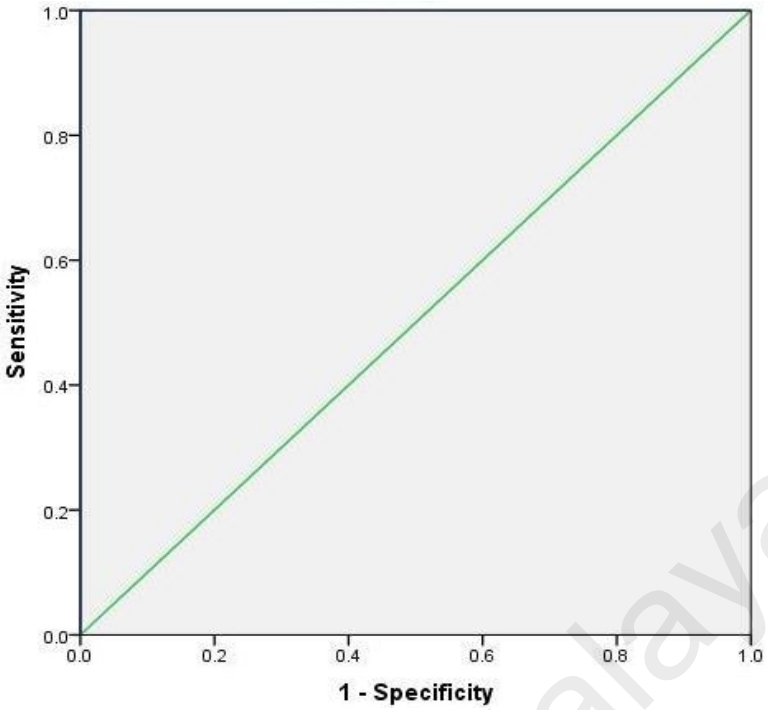

Figure 4.13: ROC curve plot of OCT detection using AUC_P.

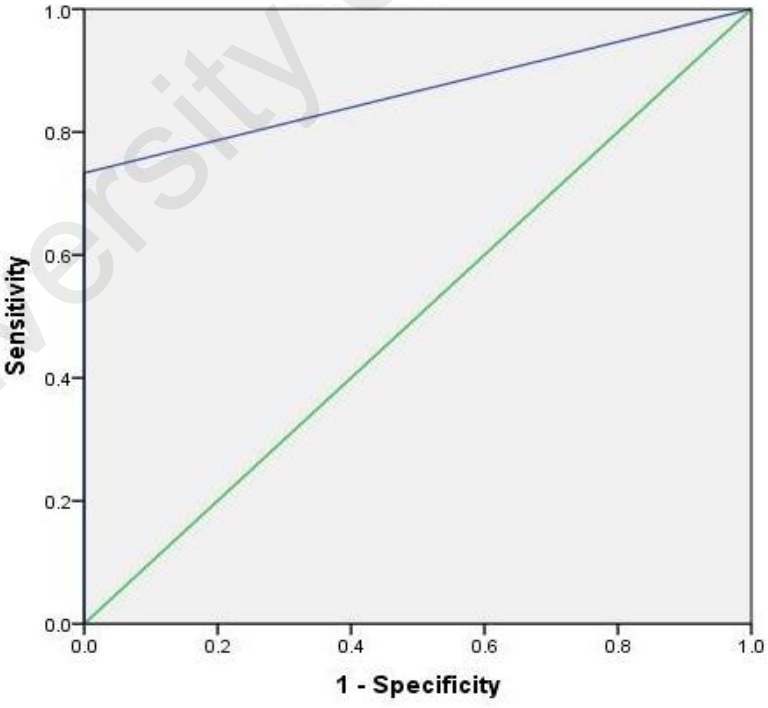

Figure 4.14: ROC curve plot of ICDAS II detection

Figure 4.14 shows AUROC curve of OCT and ICDAS II detection between sound fissure and NCFC with AUROC= > 0.99 and 0.87 respectively using partial area under the curve (AUC_P).

Table 4.19: SN, SP, PPV, NPV and AUROC between OCT and ICDAS II to detect sound fissure and NCFC.

	Cut-off points Sound level threshold detection (ICDAS–R-code 0 versus ICDAS–R-code 1 and 2)				
Detection method	**SN**	**SP**	**PPV (%)**	**NPV (%)**	**AUROC**
OCT (AUC_P)	> 0.99	> 0.99	> 99	> 99	> 0.99
ICDAS II	0.73	> 0.99	> 99	33	0.87

Sensitivity (SN), Specificity (SP), Positive predictive value (PPV), Negative predictive value (NPV), Area under Receiver operating characteristics (AUROC),

4.4.2 Comparison between OCT outcome measure AUC_T and ICDAS II criteria for the differentiation of stages of NCFC

The disease prevalence was calculated at 45%. At non-cavitated level threshold OCT accurately detected ICDAS-R-code 2 with high SN (> 99 %) and NPV (> 99%). However, ICDAS II presented low SN (40%) and NPV (57%). OCT quantitative analysis also presented higher SP (0.83) and PPV (83%) when compared to visual index ICDAS II that showed lower SP (0.67) and PPV (50%). The AUROC curve was significantly higher for OCT (0.92) (Figure 4.15) than ICDAS II (0.53) (Figure 4.16). Table 4.20 shows the SN, SP, PPV, NPV and AUROC curve of OCT and ICDAS II for the differentiation of stages of NCFC corresponding to Micro-CT.

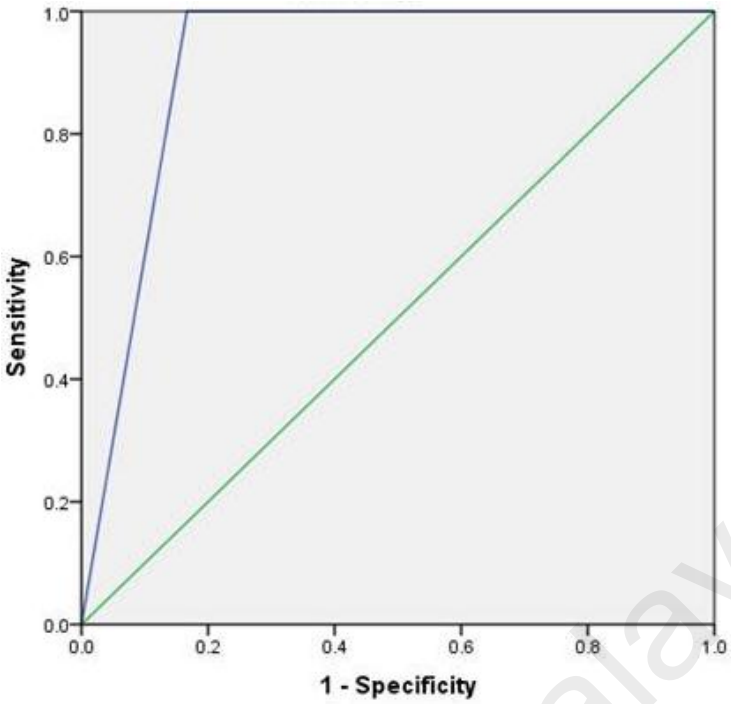

Figure 4.15: ROC curve plot of OCT differentiation using AUC_T.

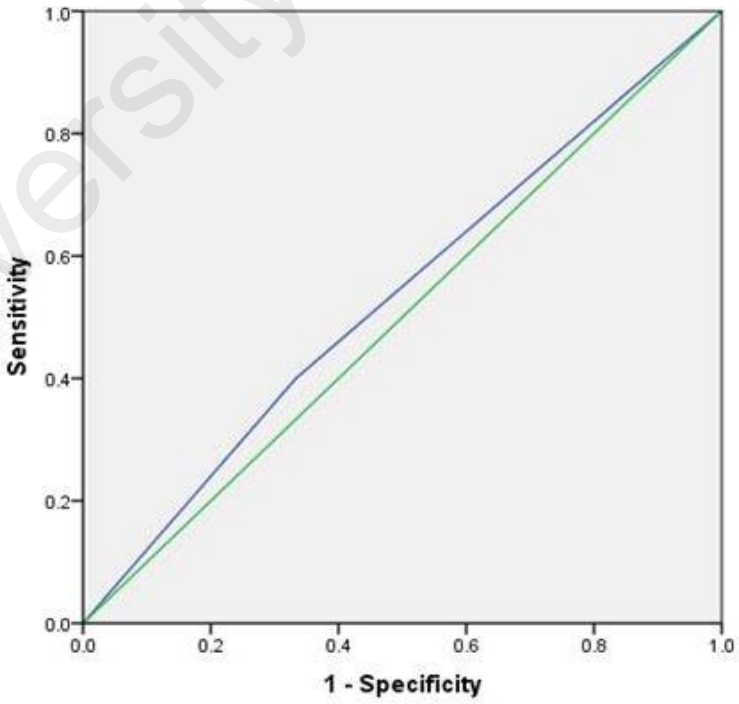

Figure 4.16: ROC curve plot of ICDAS II differentiation.

Figure 4.16 shows AUROC curve of OCT and ICDAS II differentiation between stages of NCFC with AUROC = 0.92 and 0.53 respectively.

Table 4.20: SN, SP, PPV, NPV and AUROC between OCT and ICDAS II for the differentiation of stages of NCFC.

	Cut-off points Non-cavitated level threshold detection (ICDAS –R-code 1 versus ICDAS –R-code 2)				
Detection method	**SN**	**SP**	**PPV (%)**	**NPV (%)**	**AUROC**
OCT (AUC_T)	> 0.99	0.83	83	> 99	0.92
ICDAS II	0.40	0.67	50	57	0.45

Sensitivity (SN), Specificity (SP), Positive predictive value (PPV), Negative predictive value (NPV), Area under Receiver operating characteristics (AUROC)

Table 4.21: Summary of the main results of Research Objective 1, 2, 3 and 4

Research Objective 1:

Unanimous high sensitivity and specificity observed in this study indicates that visual assessment of OCT B-scans is useful to rule out NCFC. This indicates that the reliability of visual assessment of OCT B-scans to confirm the presence of NCFC may be enhanced by the use of interpretation criteria that differentiate increased backscattered intensity due to specular reflection from that due to demineralisation. It could also be increased by the use of a color scale that increased the contrast of the range of backscattered intensity of demineralisation. Detection sensitivity and

Table 4.21: Continued

specificity were not affected whether NCFC were assessed in totality or by wall or slope loci separately. For the monitoring of NCFC dimensions with OCT, measurements should be confined to the *width* measurements of wall and/or slope loci whilst the *depth* measurements of wall loci, or lesion depth, should be avoided.

Research Objective 2:

Difference in rate of light attenuation of OCT signals at 1310 nm could be an indicator of early caries detection. The findings from this research objective indicates that outcome measures AUC_P *and* AUC_T can be used as a marker to objectively detect NCFC and differentiate Ek codes 1 from Ek code 2. Severity assessment is paramount clinical significance especially when the distance between the base of a fissure to the enamel-dentinal junction is most of the time less than 1 mm. This could result in grave clinical consequence under management of a NCFC if not detected early in its course.

Research Objective 3:

High sensitivity and good specificity observed in this study indicates that OCT outcome measures AUC_P identified in research objective 2 can rule out NCFC when the groove-fossa system is assessed in totality or within occlusal groove separately. However, differentiating NCFC using OCT outcome measure AUC_T should be dealt with caution mainly within the occlusal grooves.

Research Objective 4:

OCT can objectively detect and differentiate NCFC with high sensitivity and specificity when compared to universally accepted ICDAS II visual criteria.

CHAPTER 5: DISCUSSION

This chapter addresses the rationale of the methods used in the experiments in achieving the objectives of this study and discusses the key findings from each objective.

5.1 Research Objective 1: Evaluating the accuracy of OCT in detecting sound fissure and naturally occurring NCFC by visual assessment of OCT B-scan

This study takes a closer look at NCFC detection as a whole lesion, at different anatomical sites of the occlusal fissure and reports the agreement between OCT and PLM for measuring the dimensions of NCFC.

5.1.1 Methodological consideration

5.1.1.1 Sampling of specimen

Cavitated lesions were not included in this study because differentiating cavitated lesions from sound surface and NCFC is a straight forward process. The inclusion of cavitated lesions into the sample population of NCFC can result in over estimation of SN, whereas inclusion of a higher number of sound samples can increase the SP (Verdonschot, Wenzel, & Bronkhorst, 1993) during the evaluation of detection performance of NCFC using OCT.

In this study more than one investigation site was selected from one tooth because presence of healthy enamel between the investigation sites indicated the presence of two independent lesions. The severity of caries lesions throughout the groove-fossa system is not uniform. The depth of the lesion within the same tooth

varied from one site to another (Konig, 1963). Hence, it was fair to include more than one investigation site on the same occlusal surface without compromising the independence of samples. This section is common to all research objectives.

5.1.1.2 Polarized light microscopy and Optical coherence tomography

The detection of NCFC as a whole lesion and with respect to its anatomical location (slope or wall of fissure) using OCT and PLM was studied in this research. The identification and standardization of the anatomical locations (slope and wall) between the PLM image and OCT B-scans were carried out by dividing the occlusal fissure. The fissure was divided into two parts, slope and walls of the fissure based on entrance width of 200 µm previously described by Juhl (Juhl, 1983).

The possible reasons to assess the detection performance of OCT at anatomical locations are multi-locus pattern of occurrence of NCFC and the complex anatomy of the occlusal fissure. The pattern of occurrence of NCFC is not specific in an occlusal fissure and the signs of early demineralization does not involve the whole length of the fissure concurrently (Konig, 1963). In fact, it may occur either independently on the slope, wall and then coalesce or at both anatomical sites within the fissure, as multiple foci (Juhl, 1983). The anatomy of occlusal fissure is not uniform and angulation and proximity of the slope and wall of the fissure relative to the incident OCT light is different (Fig 3.15 and Fig 3.16). This anatomical variation could potentially result in better detection ability for the slope lesions than the wall lesions and assist in the early detection of the lesion and its subsequent management plan to preserve the tooth structure as much as possible.

5.1.1.3 Optical coherence tomography

This section discusses the key considerations within the scope of the OCT scanning of sound fissures and NCFC. In this research the occlusal fissure was air dried for 10 seconds prior to OCT scanning being carried out to simulate the clinical scenario. There are numerous techniques reported in the literature to dehydrate the enamel with different degrees depending on the method used (Brodbelt, O'Brien, Fan, Frazer-Dib, & Yu, 1981; Shimamura et al., 2011; Zhang, Mao, Lu, Romberg, & Arola, 2009). Special attention was given for selection of the method for drying the enamel as the level of hydration of the enamel surface affects the OCT signal intensity (Nazari et al., 2013). Shimamura et al examined the effect of dehydration on the sound enamel using air blowing for 10 seconds and 1, 5 and 10 minutes after air blowing for 10 seconds and found that signal intensity was higher for samples that were air-blown for 10 seconds and then left for prolonged drying (Shimamura et al., 2011). In another study, Zhang et al reported the overall shrinkage values of the healthy enamel samples after a 1-hour period of convection was 300 mm/m (0.03%) which can lead to development of micro cracks in the tooth structure (Zhang et al., 2009). Air drying for 10 seconds decreases the relative translucency of the healthy enamel up to 82% compared to wet enamel (Brodbelt et al., 1981). The clinical appearance of non-cavitated caries lesion after air drying of 10 seconds is due to the alteration of the refractive index (Besic & Wiemann, 1972; Kidd & Fejerskov, 2004) and under these conditions light scattering is higher for demineralized enamel compared with hydrated conditions (Theuns, Shellis, Groeneveld, Vandijk, & Poole, 1993).

During OCT scanning, the selection of 1024 single intensity points in x-axis and 104 points in y-axis covering the distance of 3 mm x 3 mm respectively, showed sizable representation of OCT data from sound fissures and NCFC on the occlusal surface. The orientation of OCT laser was kept bucco-lingually perpendicular to the central fissure

leaving the enamel prisms almost parallel to the laser beam while scanning the investigation site. Dental enamel is a highly organized structure of enamel prisms with 4–6 mm transverse dimensions arranged parallel to the long axis of the tooth other than at the edge of the cusp and the cervical area where it runs perpendicular to the surface. The enamel prism consists of densely packed bundles of hydroxyapatite crystals. Evidence suggested that there was no significant difference ($p > 0.05$) between the refractive index of enamel and SS-OCT among long cut prisms and cross-cut prisms (Hariri, Sadr, Shimada, Tagami, & Sumi, 2012).

The OCT B-scans were obtained at a distance of every 30 µm which provided a fair chance of selection of best OCT frame corresponding to its PLM section acquired after 200 µm distance. The selection of the best OCT B-scan from multiple OCT B-scans was carried out in the grey scale by matching the anatomy and the slopes of the occlusal fissure. The selection of the grey scale was done to minimize selection bias due to distinct appearance of the lesion in colored scale. Subsequently, detection and measurement of the lesion was performed using colored scale B-scan to provide higher contrast between demineralized and sound enamel. The method of dehydration of the enamel, orientation of the OCT laser and selection of the best OCT-B scan was common for all objectives.

5.1.1.4 Statistical consideration

We studied the dimension agreement of NCFC between OCT and PLM. The agreement was measured using the Bland Altman test. Currently correlation between OCT and histology has been reported (Gomez, Zakian, et al., 2013). Correlation measures the strength of association between the two methods (Brazdzionyte & Macas, 2007). However, good correlation does not necessarily mean that the two methods are in

agreement according to J.M. Bland and D.G. Altman (Bland & Altman, 1986). A method in poor agreement can have good correlation. Hence, it is important to know if the new method is in agreement with the gold standard (Zaki, Bulgiba, Ismail, & Ismail, 2012). To the best of our knowledge, none of the studies have reported NCFC dimension agreement between OCT and the gold standard at different anatomical locations of the occlusal fissure.

5.1.2 Diagnostic accuracy of qualitative visual assessment of OCT increased back scattered intensity for the detection of sound fissure and NCFC as whole and within different anatomical locations of the fissure

The usability of the criteria developed for the detection of NCFC (Table 3.4) with OCT and PLM was accurate to use as proven with the high inter-observer kappa agreement between 0.85-0.87 and 0.82-0.99 with $p < 0.001$ respectively.

All occlusal fissures had wall lesion n= 50 (100%) while in 37 fissure samples (74%) the lesion was localized to both the slopes (Table 4.3). The finding of wall lesions was similar to that of Juhl et al (Juhl, 1983) who reported 97% of the wall lesions in occlusal fissures. However, only 13% of the specimens had lesions on the slopes. The possible explanation for increased number of slope lesions compared to our findings could be the difference in the sample distribution. In this study the presence of slope lesions in an occlusal fissure was higher for Ek code 2 lesions (n =42%). There may be a possibility that the final cohort of samples in Juhl's study were mostly limited to the outer 50% of the enamel (Ek code 1) which may have under estimated the distribution of slope lesions in an occlusal fissure.

We found that using OCT, the detection of NCFC as whole lesion and at different anatomical locations within the occlusal fissure had excellent SN and SP. However, detection of NCFC on the occlusal fissure as a whole had better SN (0.98) and SP (0.95) than considering the slope or wall lesion separately. Similar to our findings, Gomez and Shimada reported excellent SN (0.98) to fair to good SP (0.52-0.75) in detecting enamel demineralization on the occlusal surface respectively (Gomez, Zakian, et al., 2013; Shimada et al., 2010). The diagnostic thresholds in the above mentioned studies were set in the spectrum of various stages of caries which resulted in high diagnostic performance of OCT on the occlusal surface. However, when Gomez et al changed the diagnostic threshold from sound level detection (enamel and dentin lesions were classified as caries) to enamel level detection (sound and dentin caries were classified as sound), a significant drop in the SP from 0.52 (sound level detection) to 0.39 (enamel level detection) was observed (Gomez, Zakian, et al., 2013). The high SP in this study can be explained by acquiring 3 dimensional (3-D) images across the investigation site which assisted in the best selection of OCT B-scans corresponding to the PLM image. The low SP for OCT visual assessment reported in the in the above mentioned studies could be due to acquiring of single OCT B-scan where the examiner may not be looking at the same OCT frame as the corresponding gold standard which may have contributed in false positive findings (Gomez, Zakian, et al., 2013; Shimada et al., 2010). It is therefore essential to acquire multiple OCT-B scans or 3 dimensional images across the investigation site in order to make reliable conclusions (Douglas, Fried, & Darling, 2010). Another possible reason of high SP was difference in the visual scoring criteria and the use of colored scale B-scans (Large DR3 color map) for detection of NCFC that provided higher contrast between demineralized and sound enamel, unlike the above studies that used grey colored OCT B-scans.

When comparing the detection of wall or slope lesion using OCT, similar SN (0.94, 0.95) was found but higher SP (0.95) and PPV (98%) for the detection of the wall than the slope lesions. This disparity between the detection SP of the wall and slope lesions could be due to the inability of the observers to distinguish specular reflection (Figure 3.16) from the increased backscattered intensity of the slope lesions resulting in increased false positive findings (Jones et al., 2006). The specular reflection is particularly strong for normal incidence and the intensity varies markedly with angle of incidence. The speckle is created due to the coherent addition of waves with a random phase distribution. This can therefore mask or confound any information about scattering at or just below the tooth surface (Fried et al., 2002). The slope lesions were confounded more than wall lesions by this phenomenon due to its angulation to the incident light. The surface intensity increases due to various angles of incidence formed between the incident light and the slope particularly for sound and shiny surfaces (Rakhmatullina et al., 2011). Such high intensity signals at the slope of the fissures may have affected the visual scoring of the OCT B-scans. The high accuracy of detection of wall lesions on the occlusal surface using OCT will be helpful in early diagnosis and tailoring reversible preventive care management for the patient. From a clinical point of view, entrance to the fissure (wall) is a point where the penetration of the dental explorer is seized after coming in contact with the enamel walls (Fejerskov et al., 1973). It is fair to have low SN and SP with the current visual caries detection methods due to difficulty of direct visual examination of these sites (Gomez, Tellez, et al., 2013).

5.1.3 NCFC dimension agreement between OCT and PLM at different anatomical locations of occlusal fissure using qualitative visual assessment of OCT increased back scattered intensity

Inter-observer agreement for lesion dimension measurements of NCFC was moderate to high (0.65-0.98). Dimension measurements of height of slope and width of wall lesions using OCT were in agreement with PLM, although there was slight overestimation observed with the height of slope lesions. This could be due to a calibration offset in the optical properties of the enamel due to refractive index used. Demineralization of enamel results in a change of the refractive index when compared with sound enamel (Besic & Wiemann, 1972). The refractive index is affected by the mineral content of the tooth. Hariri and colleagues reported a change in the refractive index from 1.52 to 1.63 when the mineral content was 50% to 87% in enamel respectively (Hariri et al., 2013). Thus it is an important parameter in light propagation through the teeth and can serve as an indicator of its scattering properties due to local refractive index variation (Knuttel, Bonev, & Knaak, 2004).

There was no agreement for the height of wall lesions between the two methods. An underestimation of height of wall lesions was observed as the laser penetrated deeper in the inner 50% of the enamel. OCT could not quantify the depth of the NCFC on the occlusal surface accurately. This could be explained due to anatomy of the occlusal surface. The penetration depth of OCT varies with the topography of the tooth surface to which the OCT laser is exposed. The complex morphology of the occlusal surface and the variability in the inclination of the occlusal fissure can affect the penetration depth of OCT (Jones et al., 2006). Few studies have designed algorithms for image processing and calculating the depth of the lesion using integrated reflectivity between the sound and demineralized enamel and have shown good correlation with the

mineral loss (Jones et al., 2006; Louie et al., 2010). However, this was not possible with the OCT qualitative visual assessment used in this research objective.

Another possible reason of limited depth penetration is explained by loss of signals due to presence of an early caries lesion that highly scatters the incident light compared to more severe caries. The light scattering and scattering coefficient from a subsurface non-cavitated caries lesion is as high as two orders of magnitude at 1310 nm wave length (Huynh et al., 2004). Darling et al observed a rapid exponential increase in the backscattered intensity during initial lesion development followed by a gradual rise as the lesion severity increased during longitudinal measurement of early artificial demineralization (Darling et al., 2006; Huynh et al., 2004). Our study reported approximately 0.8 mm of physical depth and 1.3 mm of optical depth penetration in enamel with the SS-OCT system. Fried et al stated that shorter wavelengths are more strongly scattered compared with longer wave lengths, later providing maximum depth of 1-2 mm at 1320 nm wavelength (Fried et al., 1995). The intensity of the light reaching a particular depth in the sample is affected by how strongly it reflects or randomly scatters the light (Dunkers et al., 1999). Another probable reason for lesion height disagreement could be presence of debris and organic material in the free fissure space (fissure proper) that may hinder the penetration of the OCT laser to the base of the lesion. An extended depth range with longer optical wavelength would reduce scattering, increase the penetration depth and can improve diagnostic potential of OCT in the future (Cheong, Prahl, & Welch, 1990; Fujimoto & Drexler, 2008).

5.2 Research Objective 2: Identify quantitative OCT outcome measures derived from depth-resolved intensity profile to detect and distinguish stages of NCFC

The objectives of this in-vitro study were to characterize Ek codes 0, 1 and 2 using OCT signals, to explore OCT outcome measures for the differentiation of Ek codes 0, 1 and 2 and to establish a cut-off point between sound (Ek code 0) and NCFC (Ek codes 1 and 2) and stages of NCFC (Ek code 1 and Ek code 2) using OCT outcome measures.

5.2.1 Methodological consideration

5.2.1.1 Sampling of specimen

Premolar teeth with sound fissures and naturally occurring NCFC used for this section were the same cohort as those used in Section 3.2.1. 107 investigation sites with sound fissures and naturally occurring NCFC were selected from 54 human premolar teeth. Special attention was given to carefully remove any possible variable that could confound the OCT findings. The depth of the occlusal fissures varies from one site to another on the same tooth and between teeth. Due to a natural variation between the depth of fissure and difference in scattering properties of enamel and dentin, samples having the base of the fissure more than the inner 2/3 of the enamel and lesions extending in the outer 1/3 of the dentin were excluded from this research. This selection was carried out on the basis that obtained OCT signals from the Ek code 2 having deep fissures and from Ek code 1 that has shallow fissures may be similar. The samples that had lesion in the outer 1/3 of the dentin were removed because the scattering coefficient in dentin is much higher than enamel and is approximately 10–20 dB stronger than the enamel signals which can mask or confound our findings (Fried et al., 2002).

5.2.1.2 Optical coherence tomography

A conventional OCT image showed strong reflection at the tooth–air interface due to Fresnel reflections (Fried et al., 2002; Jones et al., 2006). In this study the surface scattering was managed by excluding superficial depths below the tooth-air interface from the mean depth-resolved intensity profile (A-scans) of sound fissure and NCFC. The difference in the refractive index between the air and the enamel results in these strong reflections at the surface (Fried et al., 2002). Techniques such as digital image processing (Adler, Ko, & Fujimoto, 2004), creating an angle up to 45° to the incidence of light (Rakhmatullina et al., 2011) and systematically excluding combination of depths when samples are more homogeneously demineralized (Amaechi, Higham, Podoleanu, Rogers, & Jackson, 2001) are a few examples commonly used in OCT related research to reduce the specular reflection. Fried et al implemented a threshold level to their data to remove the intensity of specular reflection (Fried et al., 2002). Chew et al, in their attempt to minimize the confounding effect of specular reflection during quantification of initial enamel erosion applied a statistical cut-off depth of 20 μm due to the presence of homogeneous and uniform pattern of in-vitro demineralization (Chew, Zakian, Pretty, & Ellwood, 2014). Evidence has shown the importance of using water (Shimamura et al., 2011) and index matching media (Natsume et al., 2011) to reduce the strong surface Fresnel reflection. Fried et al. immersed the samples in an index matching bath (Fried et al., 1995) whereas Natsume et al. covered the imaging surface with a small amount of 3% hydroxyl ethyl cellulose gel to decrease the strong surface reflection (Natsume et al., 2011). However, these techniques are limited to smooth surfaces with uniform penetration depths and imaging with PS-OCT system where it uses coherent backscattered light and reflected light as opposed to transmitted light which are valuable in removing the confounding influence of intense reflection at the enamel-air interface. These methods are difficult to

implement on the occlusal surfaces due to variation in the topography and difference of system used.

To have sizable representation of OCT data from each Ek code, 50 A-scans were selected using GUI software developed in MATLAB (The Mathworks, USA). The selection of the optimum number of A-scans was based on the maximum depth-resolved intensity (*I*) which can be used to differentiate stages of NCFC (Ek code 1 versus Ek code 2) using OCT outcome measures. This is discussed in detail in Section 3.2.2 under pilot studies. Later, digital image processing was attempted to align the occlusal surface to overcome the difference of reflectivity due to variability of tomography from the occlusal surface using a customized algorithm written in MATLAB software. After OCT data extraction, each intensity point was averaged from 107 samples that resulted in mean quantified values from each sample and was represented as depth-resolved mean A-scan.

5.2.2 Characterization of OCT backscattered intensity through sound (Ek code 0) and NCFC (Ek codes 1 and 2)

To characterize Ek codes 0, 1 and 2, mean depth-resolved A-scans within superficial physical depth of 150 µm were considered. At 130 µm physical depth an overlap between Ek codes 1 and 2 was seen indicating the probability of the NCFC becoming identical.

There was a distinct pattern of behavior of light seen in sound samples compared to NCFC when mean depth-resolved A-scans were examined. The highest I_{max} value and the bimodal pattern of attenuation of light within phase I resulted in an observed difference between sound (Ek code 0) and NCFC (Ek codes 1 and 2). The probability of

highest I_{max} value and presence of bimodal effect of attenuation from Ek code 0 were most likely due to strong specular reflection arising from the surface. This strong specular signal often appears as high intensity columnar artifacts or spikes in the image (Fried et al., 2002). At this interface, the intensity of specular reflection could be around 20 dB higher than the backscattering intensity in other areas and can obscure actual back scatter information about scattering at or just below the tooth surface (Fried, Featherstone, Glena, Bordyn, & Seka, 1993). These strong surface reflections can decrease by 3db at 10 µm below the surface when a high resolution OCT system with an axial depth resolution of less than 10 µm is used. Our findings were similar to Fried et al (Fried et al., 1993) and Nazari et al (Nazari et al., 2013) where sound samples (Ek code 0) demonstrated sharp and distinct peak at the tooth-air interface due to the strong Fresnel reflection (Nazari et al., 2013) with the former being imaged with a layer of oil (R.I=1.63) to optically smoothen the surface, whereas, the width of the specular peak indicated the surface smoothness or residual surface roughness (Fried et al., 1993). In this research the absence of bimodal trend for both Ek codes 1 and 2 was observed. This could have contributed to a change in the refractive index and surface roughening of enamel due to early demineralization resulting in the decreased specular reflection (Rakhmatullina et al., 2011). The change in the refractive index of the enamel can be explained due to enamel demineralization that resulted in increased pore volume contributing to the decrease in the overall tissue density (Boyde, 1984).

The findings of this study showed that the backscattered intensity signals increased with the degree of demineralization, and a higher I_{max} was observed for Ek code 2 (1.11E+09 ± 9.12E+08 a.u) than Ek code 1 (8.19E+08 ± 6.31E+08 a.u) owing to the increased scattering at the numerous micro interfaces created in the deeper layers of enamel due to mineral dissolution. These findings were similar to Nazari et al who observed an increase in the diffused scattering within the lesion under dry demineralized

enamel compared to wet demineralized enamel at different period of demineralization (day 3, 9 and 15 respectively) (Nazari et al., 2013).

For Ek code 0, when compared visually, there was an intense and sharp increase in the signal seen from tooth-air interface at first and the light attenuated rapidly from I_{max} to 30 µm of physical depth derived from mean depth-resolved A-scans. This trend was due to strong surface reflection from the smooth and shiny sound enamel surface and has been explained in detail previously. However, at 40 µm to 150 µm physical depth the specular reflection was minimal and the attenuation rate for Ek code 0 was significantly lower (1.43E+06 a.u./µm) compared to Ek codes 1 and 2 (4.46E+06, 6.40E+06 a.u./µm) respectively signifying slower decay of the signals with the increasing depth within sound enamel. This is because sound enamel is highly transparent in NIR range (750 nm to 1500 nm) and weakly absorbs and scatters light unlike dentin which strongly scatters light (Bühler, Ngaotheppitak, & Fried, 2005; Fried et al., 1995), however, scattering increases with the degree of demineralization (Popescu, Sowa, Hewko, & Choo-Smith, 2008). NCFC show various degrees of mineral loss and different sizes of porosities depending on the severity of lesion that result in the increased backscattered intensity. This can be explained by the research carried out by Popescu et al who reported that there are two types of interactions taking place as the light travels through non-cavitated caries lesion. First interaction is at pore and enamel interface resulting in an increased backscattered intensity due to abrupt alteration in the refractive index. Second is when the light travels virtually without being deviated through the space inside the pores resulting in effective reduction in scattering, allowing the light from the deeper enamel layers to reach the OCT detector (Popescu et al., 2008).

5.2.3 Comparing OCT outcome measures derived from the mean depth-resolved intensity profile (A-scan)

The main objective of this study was to significantly differentiate Ek codes 0, 1 and 2 from each other by identifying OCT outcome measures from mean depth-resolved A-scans. Evidence suggests that various OCT outcome measures can potentially serve as diagnostic markers that can be extracted from mean-depth resolved intensity profiles (A-scans) for distinguishing sound enamel from demineralized lesions. Outcome measures like attenuation coefficient (Mandurah et al., 2013; Popescu et al., 2008; Sowa, Popescu, Friesen, Hewko, & Choo-Smith, 2011), spectral peak ratio analysis (Sowa et al., 2007), area under the curve (Louie et al., 2010) and fractional differences (Chew et al., 2014) are few examples which have been used in OCT linked caries research. After initial exploration of mean depth-resolved A-scans, the outcome measures selected for this research were *AR*, *R*, AUC_P, AUC_T and *FWHM* on the basis that each of the measures was different in respect to its mathematical calculations.

Kruskal Wallis H-test analysis showed that all the above mentioned OCT outcome measures were significantly different from at least one of each Ek code with $p < 0.001$, however, there was an insignificant difference observed for the outcome measure *FWHM* at $p > 0.001$. The post hoc comparison using Dunnet's T3 was than performed for all statistically significant outcome measures to further compare which Ek code was specifically different from the other. The pair-wise comparison revealed that outcome measures *AR* (Table 4.8) and AUC_P (Table 4.10) between Ek code 0 versus Ek codes 1 and 2 were significantly different from one another. Hence, both outcome measures were considered significant measures to differentiate sound fissures from NCFC. While for outcome measure *R*, the difference was only found between Ek code 0 and Ek code 2 (Table 4.9) and could not be suggested as a robust outcome measure.

In this study the chosen superficial physical depths to calculate the AUC_P and *AR* was 40 μm below the tooth-air interface till 150 μm where plateau was reached for all three Ek codes. This selection of depth points 40 μm below the tooth-air interface was carried out to minimize the effect of strong specular reflection from the surface. This combination showed to be the most sensitive in the detection of sound (Ek code 0) versus NCFC (Ek codes 1 and 2) on the occlusal surface. The *AR* of Ek code 0 was significantly different and slower (1.43E+06 a.u./μm) compared to Ek codes 1 and 2 (4.46E+06, 6.40E+06 a.u./μm) respectively. This behavior of sound enamel is similar to transparent dentin (0.61 mm^{-1}) that involves deposition of mineral casts in the dentinal tubules with later displaying higher scattering properties (Mandurah et al., 2015). The lower mean *AR* and AUC_P for Ek code 0 can be attributed to the relatively homogeneous structure of sound enamel containing approximately 87% of mineral content where the hydroxy apatite crystals are packed together in the form of prisms resulting in weak scattering of the light at 1310 nm (Fried et al., 1995; Huynh et al., 2004). Jones et al observed that the magnitude of scattering in healthy enamel at 1310 nm was 30 times lower than the visible range (Jones et al., 2003).

When the light passed through Ek code 1 and 2, the signals attenuated faster, *AR* and AUC_P increased as light penetrated deeper into the NCFC. The possible explanation is during early demineralization there is preferential dissolution of enamel resulting in loss of minerals. The porous structure with decreased mineral content and increased water content possesses smaller refractive index (Nazari et al., 2013). When water evaporates from demineralized enamel after air drying, light scattering occurs in air (R.I=1.0) instead of water (R.I=1.33) and since the refractive index of air is less than that of water, more scattering occurs and the lesion is obvious (Meng et al., 2009; Theuns et al., 1993). Darling et al observed 1 to 2 orders increase in the magnitude of scattering coefficient at 1310 nm due to partial porosities formed at the lesion surface

compared to sound enamel (Darling et al., 2006). The findings of this study were similar to Darling et al who reported higher attenuation of demineralized enamel (100 to 200 cm^{-1}) compared with sound enamel (2 to 3 cm^{-1}) (Darling et al., 2006). Another explanation for increased attenuation and higher AUC_P observed in NCFC in this research is explained by Darling et al who examined sound and demineralized enamel at 1310 nm and concluded that there was the presence of two types of scatterers in dental enamel. The large prisms, 3-6 μm in diameter produce Mie-like scattering effects and the small hydroxy apatite crystals, less than 50 nm in diameter are responsible for a large fraction of Rayleigh-like isotropic scattering. They further observed that demineralization increases the Rayleigh-like isotropic scatterers (Darling et al., 2006). Although the depth and sample used in above studies were not comparable an overall relationship of attenuation between sound and early demineralized enamel was similar.

Dunnet T3 analysis further showed that AUC_T was the only OCT outcome measure that was able to statistically differentiate between Ek code 1 and Ek code 2 with $p < 0.05$ (Table 4.11). This established that out of all OCT outcome measures, AUC_T can be used as a significant indicator for differentiation between stages of NCFC. In the attempt to differentiate Ek code 1 from Ek code 2, the physical depth of 0 μm until 150 μm suited best using the OCT outcome measure $AUC_{T.}$ The inclusion of the superficial depth did not confound the early demineralized samples because the specular reflection decreases with the increased micro roughness (Rakhmatullina et al., 2011). As shown in Figure 4.4, the surface reflections from sound fissures and NCFC (Ek codes 1 and 2) were different from each other carrying potential diagnostic information that was valuable to differentiate NCFC. The higher AUC_T for Ek code 2 compared with Ek code 1 can be explained by Darling et al who observed that demineralization increases the fraction of isotropic scattering (Rayleigh-like) along with the amount of large angle scattering from the lesion (Darling et al., 2006). Findings of this study were similar to

Mandurah et al who artificially induced caries on fresh bovine incisors for 4, 7 and 14 days and showed a higher attenuation coefficient for early demineralized enamel (range 1.34 and 1.47 mm^{-1}) which increased with the degree of demineralization compared to healthy enamel (range 0.08 to 0.29 mm^{-1}) (Mandurah et al., 2013). It is equitable to infer from the results of this study that a higher attenuation rate of Ek code 2 compared with Ek code 1 creates the significant difference in mean AUC_T. Therefore, it is appropriate to state that AUC_T of mean depth-resolved intensity profile increases with severity of demineralization with Ek code 2 having higher mean AUC_T of 7.92E+10 compared to Ek code 1, 6.35E+10.

It has been established from this research that *AR* and AUC_P both outcome measures were significantly differentiated and were able to quantify detection of sound (Ek code 0) and naturally occurring NCFC (Ek codes 1 and 2) on the occlusal surface. To identify the best outcome measure among *AR* and AUC_P, ROC analysis was carried out. Excellent AUROC, 0.95 (95% CI 0.916-0.99) with p value <0.001 for outcome measure AUC_P was calculated whereas good AUROC, 0.88 (95% CI 0.81-0.94) with p value <0.001 was seen for *AR*. Based on the highest AUROC, AUC_P was identified as the robust outcome measure to quantify the detection of sound fissures and NCFC, whereas, AUC_T was the only outcome measure identified for the differentiation of stages between NCFC. ROC analysis further showed a cut off value at 3.038E+10 (a.u.) with 0.86 SN and > 0.99 SP in differentiating sound fissures from NCFC with ROC value of 0.95. Whereas, AUC_T at a cut-off value of 7.031E+10 (a.u.) was limited to low SN 0.61 and moderate SP 0.73 with ROC value of 0.66 for differentiation between Ek code 1 and Ek code 2.

In OCT research, cut-off points have been used to demarcate between sound fissures and demineralized tissues in function of lesion depth and mineral loss (dB

values integrated over depth) (Le, Darling, & Fried, 2010). Le et al also explored an edge finding algorithm to determine the lesion depth in enamel (Le et al., 2010). They defined the depth as a location where the intensity decreased to a dB value of (1/e2) from the peak intensity (Can, Darling, Ho, & Fried, 2008), although such calculation of lesion depth posed challenges due to high dynamic range of the images and was not always effective. In this study the cut-offs value was based on the highest Youden's index (sensitivity + specificity)-1. However, it should be noted that these cut-off are observed within the limitations of this current study and it is recommended to apply these results on larger sample sizes to infer these findings.

5.3 Research Objective 3: Validation of quantitative OCT outcome measures identified in Research Objective 2

The aim of this in-vitro study was to validate the quantitative OCT outcome measures that have been identified in Research Objective 2, Section 4.2.9 and 4.2.10. The OCT outcome measures AUC_P were used to detect sound (ICDAS-R code 0) and naturally occurring NCFC (ICDAS-R code 1 and 2) and AUC_T to differentiate between stages of NCFC (ICDAS-R code 1 and 2) using ICDAS radiological classification.

The new cohort of premolar teeth with sound enamel and naturally occurring NCFC and the gold standard used (Micro-CT) are same for this study and research objective 4. The methodological considerations, OCT scanning and data processing and Micro-CT scanning for research objective 3 and 4 will be discussed together under section 5.3.1.

5.3.1 Methodological consideration

The teeth samples for this study (Research Objective 3) were scored by the examiner of this research. However, for research objective 4, the cohort of tooth samples were scored by the bench mark which was later used for training and calibration purposes in Department of Restorative Dentistry, University of Malaya. Visual assessment is the most common diagnostic method used for caries detection in everyday clinical practice. ICDAS II is an integrated, novel caries detection system that serves as benchmark for clinical practice, epidemiology, research and teaching under graduates and post graduates in the field of cariology (Ismail et al., 2007). It is imperative for a new diagnostic method to be compared with existing established methods to compare its diagnostic accuracy in caries related research (Ricketts, Watson, Liepins, & Kidd, 1998).

5.3.1.1 Micro-CT scanning

In this research Micro-CT was selected as the reference standard to assess lesion severity of NCFC. The new cohort was scored by benchmarking to train and calibrate representatives from 13 universities throughout Malaysia in National Benchmark group calibration workshop in 2014. The calibration was based on lectures, training exercises with photos and hands-on sessions. Since, the calibrated set of teeth were later used as benchmarks for internal training and calibration purposes for staff and under graduate students in the Department of Restorative Dentistry, University Malaya, the histology, was the most preferred method for validation of caries severity could not be used as gold standard. Instead, Micro-CT scanning was used as a reference standard. Micro-CT allows 3-D assessment of the teeth without destroying the integrity of the tooth, accessing the actual carious site, its extension and allowing re-evaluation of the lesion at

multiple time points if needed (Kamburoglu et al., 2011; Mitropoulos, Rahiotis, Stamatakis, & Kakaboura, 2010; Taylor, Satterthwaite, Ellwood, & Pretty, 2010). This technique cannot be adapted into clinical practice due to high radiation dose (Willekens et al., 2010), prolong scanning time, increased reconstruction times, high cost, need for specialized software and high degree of expertise for data extraction and image analysis (Rhodes, Ford, Lynch, Liepins, & Curtis, 1999). However, it can still be used as a reference standard to investigate lesion depth under laboratory conditions (Domark, Hatton, Benison, & Hildebolt, 2013; Kamburoglu et al., 2011; Ozkan, Kanli, Baseren, Arslan, & Tatar, 2015).

Polychromatic X-rays compared to synchrotron radiation uses a broad continuous spectrum in conventional bench-top Micro-CT systems, which tend to shift towards higher energy (beam hardening) as the attenuation through samples rises, since low-energy photons are commonly more attenuated than high-energy photons (Chappard et al., 2006). The unwanted beam hardening which renders inaccuracies in detecting non-cavitated caries lesion and mineral densities often appears as dark bands, cupping, flares or streak artifacts (Duerinckx & Macovski, 1978; Joseph & Spital, 1978). There are several techniques mentioned in the literature to correct the beam hardening effect by using beam filtration (Meganck, Kozloff, Thornton, Broski, & Goldstein, 2009), correction during reconstruction (Schuller et al., 2015) and mineral density calibration (Chen & Fok, 2014; Huang, Jones, He, Darendeliler, & Swain, 2007; Schweizer et al., 2007). In this study after conducting a few pilot studies it was shown that beam voltage set at 90 kv, tube current 90 μA as the Micro-CT scanning settings with a total of 720 projections with four frames per projection significantly minimized the shadows, artifacts and overlap of images. Managing the beam voltage and tube current follows the energy based beam hardening correction principle altering the polychromatic nature of X-rays into singular data (Van de Casteele, Van Dyck, Sijbers,

& Raman, 2004) and averaging method was used to reduce the noise of each projection frame, enhancing the signal-to-noise ratio (Schwass, Swain, Purton, & Leichter, 2009).

To create standardized calibration systems for micro-CT, many researchers have used aluminium, copper or customized phantoms that relate to tissues under examination. Although it is difficult to create phantoms which can mimic complex enamel structures, pure hydroxyapatite (HAP) sintered homogeneously with precise densities can commonly be used for calcified dental tissues (Huang, He, Darendeliler, & Swain, 2010; Schweizer et al., 2007). HAP customized phantoms have shown minimal polychromatic dishing effects when fabricated across a complete range of dimensions (Schwass et al., 2009). The preparation of HAP phantoms used in this study is detailed in Chen et al (Chen & Fok, 2014). The phantoms provide internal standardization that can vary due to instrument fluctuation between the samples (Huang et al., 2007).

Demarcation of the tooth-air interface within the region of interest was an important and crucial step in the determination of presence or absence of early caries. Special care was taken during surface determination of the teeth by setting the cut-off between background and enamel manually as shown in Figure 3.24. Visual detection of NCFC on Micro-CT volume data can be challenging and may affect the inter-examiner and intra-examiner reliability due to variations in scoring sound enamel and early demineralized enamel. In caries-related studies some researchers have used visual criteria for caries diagnosis (Mitropoulos et al., 2010; Ozkan et al., 2015) while others have used automated analysis based on radio opacity threshold to detect and quantify sound versus demineralized enamel (Taylor et al., 2010). Taylor et al used a 90% mineralization state to threshold and highlighted the occlusal demineralization by using median grey values from the air, enamel and dentin (Taylor et al., 2010). Keeping in mind the subjectivity of the visual criteria and its consequences, image thresholding was

carried out on the entire volume data due to the nature of data obtained from Micro-CT scanning and availability of the sophisticated software like VG Studio Max (Version 2.1, 64 bit, Volume Graphics, Charlotte, NC, USA). The thresholding protocol was further standardized by selecting three frames systematically from every one third of the total distance of the investigation site to calculate mean range of grey values for sound enamel and air. The mean maximum of air and mean minimum of sound enamel was used to threshold the entire volume data. This procedure resulted in automated highlighting of the mean range of grey values for demineralized enamel in amber and outlined in green color with a distinct contrast between the sound and demineralized enamel (Figure 3.27). The scoring of ICDAS-R-code 1 and ICDAS-R-code 2 was carried out by setting a vigilant protocol by dividing the full thickness enamel from the base of the fissure up to DEJ into outer 50% and inner 50%. The base of the fissure was identified using surface determination demarcating the enamel-air interface distinctly.

In this study we further aimed to determine the potential of OCT at the fissure, when the structural angle was $\leq 25^0$ and at the groove, when the structural angle was $\geq 25^0$ (Ekstrand et al., 1991). The division of groove-fossa system was carried out for research objective 3. Currently there is no literature available stating the prospective of OCT for the detection and differentiation of NCFC in respect to fissure and groove.

5.3.1.2 OCT scanning

The teeth were scanned with Micro-CT X-ray imaging prior to OCT scanning. The live 3D rendering tool on the tripod coordinate system of Micro-CT helped in identifying and transferring the investigation sites on the stereomicroscope image which was then used as reference for OCT scanning (Figure 3.37). This approach aided in quick and accurate selection of best OCT B-scan based on landmarks and anatomy of

cuspal slopes with the corresponding Micro-CT image. The selection of 1712 single intensity points in x-axis and 504 points in y-axis covering the distance of 5mm x 1.5 mm respectively, showed sizable representation of OCT data from sound enamel and NCFC on the occlusal surface.

5.3.1.3 Statistical consideration

The accuracy of the test was calculated at sound level threshold detection (ICDAS-R code 0 versus ICDAS-R code 1 and 2, and non-cavitated level threshold detection (ICDAS-R code 1 versus ICDAS-R code 2). The first diagnostic threshold (sound level) is relevant to the clinical task which allows detection of sound and non-cavitated lesions which are early in the course of progression. The sound level diagnostic threshold will allow clinicians to implement preventive strategies in time that will promote remineralization or arrest the existing lesion, limiting permanent damage to the tooth structure which will decrease patient's suffering and overall cost of treatment and increase the longevity of the tooth in the dental arch. Detection of NCFC is the first step of the diagnostic process, hence, the second diagnostic threshold (non-cavitated level) is important in determining the severity of the lesion. Under management prospective, both the detection thresholds will assist the clinician in tailoring the comprehensive patient management plan.

5.3.2 Diagnostic accuracy of OCT outcome measures

At sound level detection threshold, we found that AUC_P was able to detect sound enamel from the NCFC with high SN and good SP. There was no difference found in detecting sound enamel and NCFC at overall groove-fossa system and within the

occlusal groove yielding similar SN (> 0.99) and SP (0.79). Although, the probability of detecting an early lesion was higher for the groove-fossa system compared to occlusal groove with highest PPV of 90%. None of the NCFC was falsely detected as diseased within an occlusal fissure. However, the diagnostic potential of OCT could not be calculated for occlusal fissure because all the fissures were diagnosed with early lesions. The high SN reported in this study can be attributed to OCT being a highly sensitive tool to discriminate between sound enamel and NCFC, as mineral loss as little as 10-15% can increase the light scatter by 50 times (Louie et al., 2010). During the caries process, micro porosities are formed as the lesion progresses due to partial dissolution of the individual hydroxyapatite crystals. Huynh et al concluded in their research that these micropores provide scattering centres in near-IR light and its magnitude is dependent on the size of principle scatters present in the enamel (Huynh et al., 2004). Healthy enamel when compared with dentin shows higher birefringence, yet lower scattering anisotropy and weak absorption (Fried et al., 1995). Unlike dentin, where OCT signal patterns vary with the orientation of the dentinal tubules that are surrounded by mineralized structures, OCT signals in enamel are not affected by the structural orientation of the prism. However, when sound enamel is exposed to higher wave length (1310 nm) compared to a shorter wave length (850 nm), absorption and scattering coefficient increases with the decrease in the wave length (Sowa et al., 2011). Holtzman et al reported detection of sound enamel and early caries on the occlusal surface with OCT using simple algorithm and showed higher SN (0.94) and good SP (0.85) (Holtzman et al., 2014). In another study, Holtzman et al observed excellent SN (0.95) and good SP (0.86) while detecting early caries in older adults using the same algorithm (Holtzman et al., 2015). The former study was conducted in the range of various carious lesions from ICDAS II code 0-4, the later used ICDAS II as gold standard which may have exaggerated the true negative findings when compared to our study. The possible

reason of lower SP (0.79) in this study could be explained probably due to inability of the reference standard Micro-CT to detect very early and minimal changes during the course of early demineralization (Figure 5.1). Taylor et al concluded that Micro-CT underestimates enamel caries compared to histological examination (n=3) where manual Micro-CT assessment falsely diagnosed 12 samples as healthy (Taylor et al., 2010). However, Louie et al reported OCT being very sensitive to mineral loss as low as 5% yielding a 20 fold increase in the light scattering (Louie et al., 2010). This disparity between the reference standard and the index test may have contributed in increase false positive findings. Another reason could be probability of an early lesion being included as surface outline during manual surface determination procedure due to difficulty in distinguishing between fissure space and early demineralized enamel. The transition of the range of grey values between the air and enamel was blurred and had smooth edges mainly at the fissure space which may have resulted in the inclusion of early lesion as part of the surface (Figure 5.1).

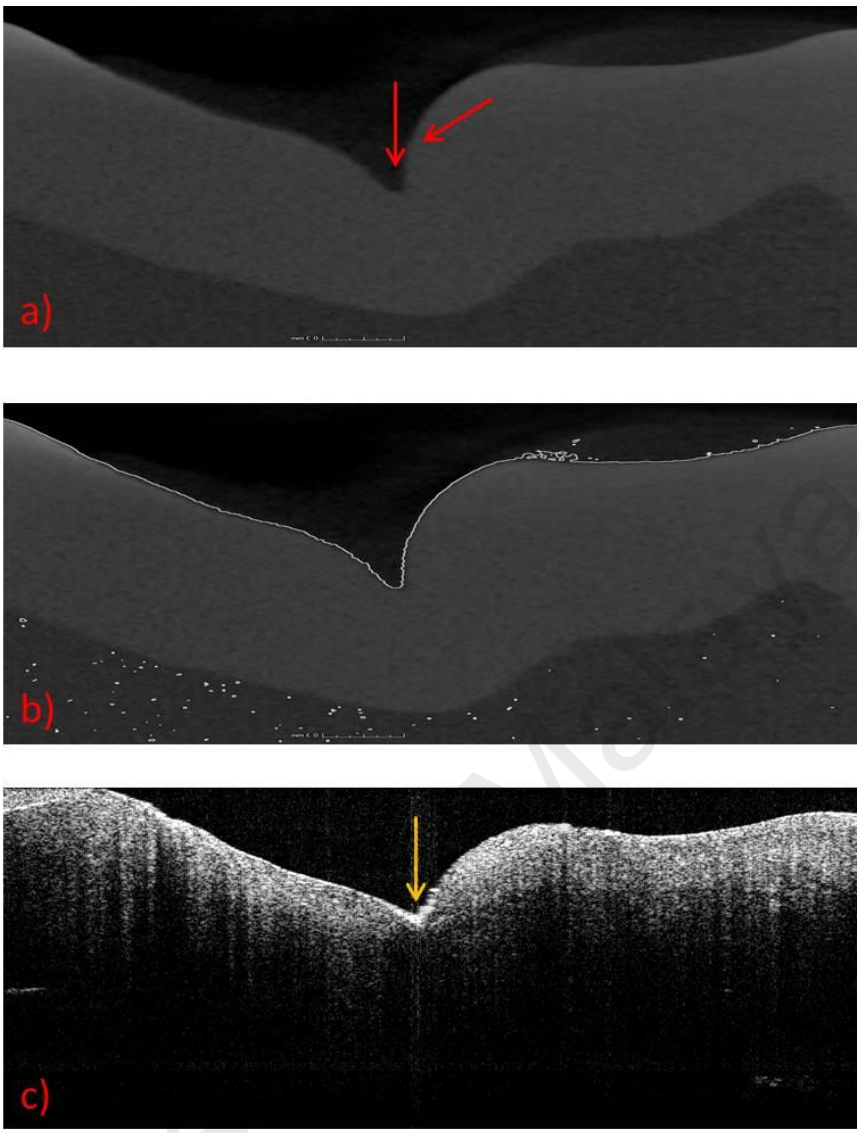

Figure 5.1: Micro-CT image of an occlusal groove. (a) an occlusal groove without surface determination showing blended transition between air and the enamel surface shown by red arrows, (b) inclusion of the blended area after surface determination shown by white line (c) OCT image from the same region of interest with increase in the backscattered intensity (yellow arrow) within an occlusal groove indicating presence of early caries.

Numerous studies have quantified severity of caries lesions and the progression on the occlusal surface (Jones et al., 2006; Jones et al., 2004; Louie et al., 2010; Ngaotheppitak et al., 2006). Various researchers have established relationships between OCT integrated reflectivity and integrated mineral loss for enamel by integrating the reflectivity of the orthogonal polarization (perpendicular-axis) or cross polarization of PS-OCT image (Jones et al., 2006; Jones et al., 2004; Louie et al., 2010; Ngaotheppitak et al., 2006). Louie et al demonstrated a strong correlation between integrated mineral loss and increase integrated light reflectivity on occlusal surfaces of early naturally demineralized enamel (Darling et al., 2006; Jones et al., 2006). Similarly, Jones et al. measured integrated reflectivity to quantify lesion severity of the artificially induced early demineralization on the occlusal surface and showed good correlation with the mineral loss from high resolution digital microradiograph (Jones et al., 2006). To the best of my knowledge, no study has looked into quantifying and validating the differentiation of naturally occurring NCFC that is ICDAS-R-code 1 versus ICDAS-R-code 2 on the occlusal surface using OCT light behavior.

At non-cavitated level detection threshold AUC_T showed similar SN (0.80) and NPV (86-88) when differentiating between ICDAS-R-code 1 and ICDAS-R-code 2 on the occlusal surface independent of the morphological classification of the interlobal grooves. High SN translates to the true detection of ICDAS-R- code 2 on the occlusal surface. This can be explained by Angmar-Mansson and Ten Bosch who concluded that increase porosities results in increase back scattered light at the mineral rich surface (Angmar-Mansson & ten Bosch, 1987). The highest scattering was observed from the body of lesion, which is the zone of demineralization characterized by fully grown large spaces (Darling, 1956). Histologically Ek code 2 lesions are more severe and deep in relation to the DEJ as compared to Ek code 1 (Ekstrand et al., 1998). This increase in the demineralization increases scattering and infer to higher attenuation rate and greater

AUC_T when compare to Ek code 1 lesion as previously described in Section 5.2.3. Darling et al postulated that demineralization substantially increases the proportion of the isotropic scatterers. Hence, when light travels through demineralized enamel, not only it is scattered by the enamel rods, it is also scattered by the multitude of pores resulting from demineralization, resulting in greater intensity of the backscattered light and alteration in the optical refractive index. This increase in scattering is highly forward directed (Darling et al., 2006). Huynh et al observed changes in the scattering anisotropy of dental enamel at 1310nm after artificial demineralization and concluded that demineralization progresses along the core of the enamel rods and produces large scattering centres in the micron range (Huynh et al., 2004).

In this study, when the diagnostic threshold was changed from sound level detection to non-cavitated level detection, lower SP (0.54-075) was observed. The SP varied with the morphology of the groove-fossa system, occlusal fissure showing highest SP (0.75) and PPV (67%) than considering the entire groove-fossa system (0.62) or occlusal groove (0.54) separately. It means that samples with ICDAS-R-code 1 were incorrectly detected as ICDAS-R-code 2 using OCT. The overall low SP observed in this study could be either due to underestimation of the reference standard to identify very early demineralization which has been previously described. Another possibility could be presence of debris and organic material in the empty fissure space which may have confounded the findings of current study. This space can vary from 50–200 μm and consist of colonies of microorganisms, organic deposits and debris when the teeth are fully erupted (Galil & Gwinnett, 1975; Sutalo et al., 1989; Taylor & Gwinnett, 1973). There may also be presence of residual material from the prophylactic paste forced into the fissure/groove during the time of cleaning. It is difficult to remove the entrapped material from these spaces due to anatomical variations and fissure constrictions using conventional methods (Sutalo et al., 1989). It can also impose

difficulties in maintaining the proper oral hygiene resulting in plaque stagnation areas at the entrance of the fissure (Gwinnett & Buonocore, 1972). Taylor and John in their research investigated the penetration of different fissure sealant using different prophylactic measures and concluded that prophylaxis procedures only cleaned and removed debris and other material from the cuspal inclined planes, however, the pits and fissure of the occlusal surface were often filled with debris (Taylor & Gwinnett, 1973). Depending on the size of the orifice and the cuspal inclined planes, the quantity of the organic deposit varies which may predispose the grooves as compared to fissure with higher scattering from these sites due to presence of organic material and contribute in the overall increase in scattering and higher AUC_T resulting in increased false positive findings. Although in this study, we have not calculated the scattering coefficient of back scattered light, AUC_T obtained from the mean depth-resolved intensity profile of Ek code 2 from the previous research objective 2 (Table 4.7) showed higher AUC_T (7.92E+10) when compared to Ek code 1 (6.35E+10) which were statistically different from each other with the p value < 0.05. In this study the occlusal grooves mainly with structural angle between 31 degrees to 76 degrees showed higher false positive findings compared to wider grooves, possibly due to the ability of retaining organic particles and debris and inability to completely clean these grooves due to the anatomy. Therefore, cleaning the fissure space is an important concept that has implication for accurate early diagnosis and management of occlusal lesions (Ekstrand & Bjorndal, 1997; Ekstrand et al., 2001). Lastly, we are validating AUC_T of depth-resolved backscattered intensity with respect to full depth of the lesion. Since the AUC_T is calculated from the superficial depth of 150 µm, there may be chances that within the selected depth the number of pores present in Ek code 1 lesions histologically may be equal when compared to Ek code 2 lesions, or the overall presence of number of pores in Ek code 1 is higher than Ek code 2 where there may be increase in total pore

volume histologically. These disparities may have contributed in higher false positive findings and decrease SP in this study. Thus, further studies are needed to prove the above hypothesis.

5.4 Research Objective 4: Comparison of quantitative OCT outcome measures and ICDAS II criteria

The aim of this study was to compare OCT outcome measures with ICDAS II visual criteria for the detection of sound (ICDAS-R code 0) and NCFC (ICDAS-R codes 1 and 2) and differentiation of stages of NCFC (ICDAS-R code 1 and code 2) using Micro-CT. The cohort of samples was same as Research Objective 3, therefore, the methodological considerations, OCT scanning, data processing, Micro-CT scanning and scoring is same as Section 5.3.1.

We found that using OCT, the detection of sound fissure and NCFC on the occlusal surface had accurate SN (> 0.99), SP (> 0.99) and AUROC (> 0.99) at sound level threshold detection. When comparing ICDAS II with OCT, similar SP (> 0.99) but lower SN (0.73), NPV (33%) and AUROC (0.87) were observed. Detection of early caries lesions were underestimated using visual criteria ICDAS II and most of the NCFC were falsely detected as healthy. When the diagnostic threshold was changed from sound level detection to non-cavitated level detection, there was rapid drop observed in the SN (0.40), NPV (57%) and AUROC (0.45) for ICDAS II whereas OCT consistently showed accurate SN (> 0.99), and excellent AUROC (0.92) in differentiating ICDAS-R-code 1 from ICDAS-R-code 2 with higher NPV. On the other hand, OCT had higher SP (0.83) and PPV (83%) than ICDAS II which showed lower SP (0.67) and PPV (50%) respectively.

Internationally accepted visual detection system ICDAS II, has been proven to have good accuracy and reproducibility (Diniz et al., 2009; Jablonski-Momeni et al., 2008). However, the clinical visual index is subjective and diagnosis is based on the alteration of surface characteristics due to subtle changes occurring sub-surface of teeth as a result of alteration in the refractive index of the enamel during early demineralization (Banting et al., 2005). Precise diagnosis using ICDAS visual index with both high SN and SP may only be achievable by highly trained ICDAS specialist (Jablonski-Momeni et al., 2008; Nelson et al., 2011). However, such systems require training and calibration with a reference examiner to achieve good diagnostic accuracy (Diniz et al., 2009; Jablonski-Momeni et al., 2008; Nelson et al., 2011). In fact, without this expertise, implementation of ICDAS index can be time consuming, laborious and less accurate (Braga, Oliveira, et al., 2009; Diniz et al., 2009). In this study the samples were scored by bench mark examiner and yet suffered from low SN in differentiating ICDAS-R-code 1 from ICDAS-R-code 2 mainly due to difficulty in differentiating the white spot lesion on the basis of color, texture and roughness.

The findings from this study are similar to Jablonski et al who reported similar value of mean SN (0.69) to the present study but slightly lower mean SP (0.82) at D1 threshold where enamel and dentin lesions were scored as diseased when occlusal caries was examined visually on the extracted teeth (Jablonski-Momeni et al., 2008). Unlike our study, Jablonski et al in another study calculated the diagnostic potential of ICDAS II on the occlusal surface of permanent posterior teeth at D1 threshold detection where all histological scores 1-4 were classified as caries, the optimum SN and SP was 0.95 and 0.85 respectively with AUROC of 0.94. According to Diniz et al, ICDAS II presented excellent SN (0.99) and accurate SP (1.0) at D2 threshold where Ek code 0-1 was scored sound fissure and Ek codes 2-6 were considered as caries. In the same study, 4 out of 7 healthy samples were detected correctly by ICDAS II, whereas 11 samples

had caries extending up to halfway through the enamel on histology, only one was detected correctly and 107 had caries extending in the inner half of enamel, out of which 42 samples were detected correctly (Diniz et al., 2009). It is important to note that the diagnostic accuracy of ICDAS II in literature has been explored with range of frank cavitated lesions, a stage in the caries process more pronounced than samples included in the present study. Hence it is clear that inclusion of range of cavitated samples have exaggerated the potential of ICDAS II on the occlusal surface in the above research. Possibly overestimating the diagnostic performance of ICDAS II criteria on the occlusal surface.

In scientific literature, the accuracy of a diagnostic test is based upon the assessment between the reference standard and the index test. Presence of variance, inconsistency and disagreement between the two tests is expected to occur from the index test. Hence, selection of the reference standard and setting its diagnostic threshold forms an integral part in validating the accuracy of a test (Leeflang, Deeks, Takwoingi, & Macaskill, 2013). (Macaskill P, Gatsonis C, Deeks JJ, Harbord RM, & Y., 2010). A Cochrane diagnostic test accuracy review highlighted that the accuracy of a diagnostic test is dependent upon the diagnostic threshold, which is a measure used to define a positive test result in that study. It further stated that the estimates of SN and SP vary dramatically if the diagnostic threshold is changed (Leeflang et al., 2013; Pai, McCulloch, Enanoria, & Colford, 2004). In clinical caries data for a low prevalence group, a decline was observed approximately to one-quarter in the sound surfaces with doubled DMF when the threshold was shifted from sound level detection (Sound versus non-cavitated caries and cavitated caries) to non-cavitated level detection (sound versus non-cavitated caries) (Pitts & Fyffe, 1988). The inclusion of cavitated lesions in the study population can certainly increase the SN of the diagnostic test due to ease and accuracy of identifying frank cavitated lesions, which can increase the diagnostic

accuracy of certain test. Therefore, in our study the diagnostic threshold was calculated at sound level and non-cavitated level threshold.

The sample used in this study were human premolars, however, the outcomes from this study can be extrapolated on the human molar teeth. Although the size and the anatomy of premolar teeth and molar teeth is different the visual interpretation criteria on cross sectional OCT B scan established in this study could potentially be used in molar cohort of teeth for detection of early demineralization. The cuspal slopes of the premolar teeth are steeper than those of molar teeth. The structural angle of the molar teeth vary from 2 degrees to 170 degrees (Ekstrand et al., 1991)whereas premolars teeth ranges from 2 degrees up to 130 degrees (result from this study), hence premolar teeth are more confounded by the specular reflection on slopes. There is higher likelihood of false slope lesions identified in premolar teeth compared to molar teeth. Moreover, OCT outcome measures established in this research could potentially be used to quantify detection and differentiation of NCFC in the molar groove-fossa system. This is mainly because quantitative OCT analysis performed on premolar teeth, the investigation sites were confined to approximately < 150 μm from the center of the fissure and mean depth-resolved backscattered intensity (*I*) were acquired from superficial physical depth of 150 μm and not up to the DEJ, which makes it non-specific and can be used in molar samples too. However, care must be taken when these findings are extrapolated in molar teeth having deep fissures where base of the fissure is less than 1mm from the dentin-enamel junction or when the occlusal fissure is blocked with organic material and debris. Also, the time duration for scanning a molar tooth can be increased when compared to premolars depending on the size of investigation site being scanned. Further studies are required on molar teeth to validate the above findings.

CHAPTER 6: CONCLUSION

The goal of management of dental caries are achieving optimum oral health, prevent the progression of existing non-cavitated caries lesion and restoration of severe lesions by risk-adjusted clinical decision making (Ismail et al., 2013). There is emphasis in the literature to develop an accurate and reliable diagnostic method that can detect caries at the non-cavitated stage, assess severity and monitor progression or regression over time to benefit from the preventive and non-invasive strategies (Ismail et al., 2015; Lam & Chu, 2012).

The potential of OCT was explored and it was concluded that OCT outcome measure AUC_P can quantify and detect sound fissure from the NCFC on the occlusal surface of premolars with high accuracy. Furthermore, OCT outcome measure AUC_T has great potential to differentiate stages of NCFC on the occlusal surface and such quantitative measurements can likely aid in assessing lesion activity and designing comprehensive patient management care. The sequential staging of early lesions can help to motivate and encourage patients to improve and maintain the oral hygiene with the quantitative evidence of detection of NCFC.

The main findings of this research are as follows:

i) The OCT qualitative visual assessment can detect NCFC, as a whole lesion within an occlusal fissure with high SN (0.98) and SP (0.95) and corresponded significantly with PLM.

ii) The detection of NCFC at walls and slopes of the occlusal fissure had similar SN (0.94, 0.95) respectively, however, the SP of detecting sound fissure walls was higher (0.95) than fissure slopes (0.90).

iii) Bland Altman plots showed agreement between OCT and PLM for wWL and hSL within an occlusal fissure with non-significant slope ($p > 0.05$).

iv) Difference in rate of light attenuation between the Ek codes 0, 1 and 2 were observed reviling unique characteristics of each code.

v) AUC_P and AUC_T were the two OCT outcome measures identified in this research that can significantly detect sound (Ek code 0) from NCFC (Ek codes 1 and 2) and differentiate between stages of NCFC (Ek code 1 versus 2) respectively.

vi) AUC_P at cut-off 3.038E+10 (a.u.) showed 0.86 SN and > 0.99 SP with 0.95 AUROC in detecting sound (Ek code 0) from NCFC (Ek codes 1 and 2).

vii) AUC_T at a cut-off value of 7.031E+10 (a.u.) was limited to low SN (0.61) and moderate SP (0.73) with 0.66 AUROC curve in delineating Ek code 1 and Ek code 2.

viii) The OCT outcome measure AUC_P significantly detected sound (ICDAS-R-code 0) from NCFC (ICDAS-R-code 1 and 2) at groove-fossa system and within occlusal groove with excellent SN (> 0.99) and good SP (0.79) with 0.89 AUROC curve.

ix) The OCT outcome measure AUC_T was able to discriminate ICDAS-R-code 1 and ICDAS-R-code 2 with good SN (0.80) at groove fossa system, within occlusal fissure and groove, however, the SP (0.75) was highest at the occlusal fissure with AUROC curve of 0.72.

x) OCT outcome measure AUC_P and ICDAS II criteria both were able to detect sound fissure and NCFC with accurate SP (> 0.99), however, SN (> 0.99) was higher for OCT when compared to ICDAS II visual criteria (0.73). The AUROC curve for OCT was > 0.99.

xi) OCT outcome measure AUC_T was able to quantify and delineate ICDAS-R-code 1 and ICDAS-R-code 2 with excellent SN (> 0.99) and good SP (0.83) as compared to ICDAS II visual criteria that showed poor SN (0.40) and low SP (0.67). The AUROC curve for OCT was 0.92.

6.1 Study limitations

To our knowledge, this is the first study which optically characterized Ekstrand histological codes 0, 1 and 2 lesions. The aim of this study was to develop quantitative OCT outcome measures to assist in high accuracy of quantifying detection and differentiation of sound fissure and NCFC. The limitations of the study are as follows:

i. An underestimation within the depth of the lesion measurement was seen when the NCFC was assessed visually. This was due to limitation of physical depth range of SS-OCT system. In this research it was unable to image the full thickness of enamel and DEJ for most of the teeth samples which may have affected the qualitative assessment of lesion depth.
ii. There has been no study done identifying the difference in OCT signals with and without debris and organic particles within the fissure space. Therefore, this factor was difficult to control in the current study.

6.2 Clinical significance

The International Caries Classification and Management System (ICCMS) is based on the promotion of oral health and preservation of the tooth structure (Ismail et al., 2015). This mission is primarily possible by early detection of non-cavitated caries lesion (Ismail, 1997). Clinically the detection of NCFC and its severity (Ismail, 2004;

Ismail et al., 2007) assessment are performed visually that are based on the surface characteristic of color, reflection and texture (Ekstrand, Martignon, Ricketts, & Qvist, 2007; Nyvad et al., 1999). These parameters are weak indicators and suffer from subjectivity between and within the examiners. Considering these uncertainties, OCT could be a potential diagnostic tool to assist dentists clinically with value-based management plan.

OCT can reliably and accurately detect and quantify sound fissures from naturally occurring NCFC on the occlusal surface. This will assist clinicians in their vital quest to preserve the dental tissue and assist in designing best patient-centered management. Early detection will decrease caries burden and patient suffering caused due to pain, severe caries, occlusal and masticatory impairment and will enhance patient's quality of life (Momoi et al., 2012).

Characterization of NCFC (Ek code 1 and 2) will aid in staging the severity of NCFC objectively on the occlusal surface. To the best of our knowledge, currently there is no accepted "gold standard" to validate an active lesion from an arrested lesion in single examination. In such cases, according to Nyvad and other researchers the known theoretical condition (example remineralizing effect of fluoride) associated with the caries activity can be used as construct validity (Ten Cate, 2004), an accepted gold standard (Ekstrand et al., 2007; Nyvad et al., 2003). Findings from this research can be used to assist the clinical decision making of lesion assessment by quantitatively monitoring the progression of the NCFC. This method will help to establish construct validity and can be used as an objective surrogate for gold standard in future.

Optical characterization will aid in discriminating Ek code 0, 1 and 2 from each other and can be beneficial as training tool for early caries detection in clinical settings. ICDAS II is widely being used across the globe. However, the training of ICDAS II

currently is either validated against extracted teeth in the laboratory or benchmarked against an expert who suffers from subjectivity to a certain degree. OCT can serve as benchmark or validation tool to train ICDAS in clinics where extraction of the tooth for validation is not an option.

The potential of OCT can be extended to clinical practice to empower patients with the knowledge that NCFC are reversible and can be managed by improved oral hygiene, risk management and preventive regimes.

6.3 Future studies

The use of OCT has been assessed in quantifying the detection and differentiation of sound fissure and NCFC without including the cavitated lesions. However, there are also other novel ideas and methods listed below:

i. Determine the potential of OCT to quantify and differentiate Ek codes 0, 1 and 2 at different anatomical locations within an occlusal fissure. This study has looked into qualitative analysis to detect sound fissure from NCFC on various anatomical locations.
ii. Determine the potential of OCT outcome measures in an in-vivo set up to differentiate between Ek code 0, 1 and 2 on the occlusal surface.
iii. Comparison of OCT backscattered intensity to quantify and discriminate between stages of NCFC before and after removal of debris and organic material from the free fissure space.
iv. The proposal of an automated algorithm to analyze the AUC_P and AUC_T OCT outcome measures on the occlusal surface for detection and differentiation of sound fissure and NCFC.

v. Validate the OCT outcome measure AUC_T to monitor remineralization on the occlusal surface.

REFERENCES

Aas, J. A., Paster, B. J., Stokes, L. N., Olsen, I., & Dewhirst, F. E. (2005). Defining the normal bacterial flora of the oral cavity. *Journal of Clinical Microbiology, 43*(11), 5721-5732.

Achilleos, E. E., Rahiotis, C., Kakaboura, A., & Vougiouklakis, G. (2013). Evaluation of a new fluorescence-based device in the detection of incipient occlusal caries lesions. *Lasers in Medical Science, 28*(1), 193-201.

Adler, D. C., Ko, T. H., & Fujimoto, J. G. (2004). Speckle reduction in optical coherence tomography images by use of a spatially adaptive wavelet filter. *Optics Letters, 29*(24), 2878-2880.

Amaechi, B. T., Higham, S. M., Podoleanu, A. G., Rogers, J. A., & Jackson, D. A. (2001). Use of optical coherence tomography for assessment of dental caries: quantitative procedure. *Journal of Oral Rehabilitation, 28*(12), 1092-1093.

Anderson, M. H., Bales, D. J., & Omnell, K. A. (1993). Modern management of dental caries: the cutting edge is not the dental bur. *The Journal of the American Dental Association, 124*(6), 36-44.

Angmar-Mansson, B., & ten Bosch, J. J. (1987). Optical methods for the detection and quantification of caries. *Advances in Dental Research, 1*(1), 14-20.

Angmar-Mansson, B., & ten Bosch, J. J. (2001). Quantitative light-induced fluorescence (QLF): a method for assessment of incipient caries lesions. *Dentomaxillofacial Radiology, 30*(6), 298-307.

Aoba, T., & Fejerskov, O. (2002). Dental fluorosis: chemistry and biology. *Critical Reviews in Oral Biology and Medicine 13*(2), 155-170.

Arends, J., & Tencate, J. M. (1981). Tooth Enamel Remineralization. *Journal of Crystal Growth, 53*(1), 135-147.

Bader, J. D., & Shugars, D. A. (2004). A systematic review of the performance of a laser fluorescence device for detecting caries. *The Journal of the American Dental Association, 135*(10), 1413-1426.

Bader, J. D., Shugars, D. A., & Bonito, A. J. (2001). Systematic reviews of selected dental caries diagnostic and management methods. *Journal of Dental Education, 65*(10), 960-968.

Bader, J. D., Shugars, D. A., & Bonito, A. J. (2002). A systematic review of the performance of methods for identifying carious lesions. *Journal of Public Health Dentistry, 62*(4), 201-213.

Bader, J. D., Shugars, D. A., Rozier, G., Lohr, K. N., Bonito, A. J., Nelson, J. P., et al. (2001). Diagnosis and management of dental caries. *Evidence Report/Technology Assessment*(36), 1-4.

Baelum V, F. O. (2003). Caries diagnosis: A mental resting place on the way to intervention? In Fejerskov O & K. E (Eds.), *Dental Caries: The Disease and Its Clinical Management* (pp. 101-110). Oxford, UK: Blackwell Munksgaard.

Baelum, V., Heidmann, J., & Nyvad, B. (2006). Dental caries paradigms in diagnosis and diagnostic research. *European Journal of Oral Sciences, 114*(4), 263-277.

Baelum, V., Machiulskiene, V., Nyvad, B., Richards, A., & Vaeth, M. (2003). Application of survival analysis to carious lesion transitions in intervention trials. *Community Dentistry and Oral Epidemiology, 31*(4), 252-260.

Bagramian, R. A., Garcia-Godoy, F., & Volpe, A. R. (2009). The global increase in dental caries. A pending public health crisis. *American Journal of Dentistry, 22*(1), 3-8.

Banting, D., Eggertsson, H., Ekstrand, K. R., Ferreira Zandoná, A., Ismail, A. I., Longbottom, C., et al. (2005, September). *Rationale and evidence for the international caries detection and assessment system (ICDAS II).* Paper presented at the Clinical Models Workshop: Remin-Demin, Precavitation, Caries. Proceedings of the 7th Indiana Conference, Indianapolis, IN.

Baumgartner, A., Dichtl, S., Hitzenberger, C. K., Sattmann, H., Robl, B., Moritz, A., et al. (2000). Polarization-sensitive optical coherence tomography of dental structures. *Caries Research, 34*(1), 59-69.

Berg, J. H., & Swift, E. J., Jr. (2010). Critical appraisal. Current caries detection devices. *Journal of Esthetic and Restorative Dentistry, 22*(5), 464-470.

Besic, F. C., & Wiemann, M. R., Jr. (1972). Dispersion staining, dispersion, refractive indices in early enamel caries. *Journal of Dental Research 51*(4), 973-985.

Bjorndal, L., & Thylstrup, A. (1995). A structural analysis of approximal enamel caries lesions and subjacent dentin reactions. *European Journal of Oral Sciences, 103*(1), 25-31.

Black, G. V. (1880). Some points in the natural history of caries of the teeth, and the value of fillings for its arrest. *American Journal of Dentistry 14*, 289-308.

Black, G. V. (1908). *The pathology of the hard tissues of the teeth* (Vol. 1). Chicago, IL: Medico-Dental Publishing Company.

Black, G. V. (1910). A plea for greater earnestness in the study of caries of the enamel in its relation to the practice of dentistry. *Dental Brief, 15*, 161-178.

Black, G. V., & Black, A. D. (1924). *A Work on Operative Dentistry: The Pathology of the Hard Tissues of the Teeth* (Vol. 1). Chicago, IL: Medico-Dental Publishing Company.

Bland, J. M., & Altman, D. G. (1986). Statistical methods for assessing agreement between two methods of clinical measurement. *Lancet, 1*(8476), 307-310.

Borisova, E., Uzunov, T., & Avramov, L. (2006). Laser-induced autofluorescence study of caries model in vitro. *Lasers in Medical Science, 21*(1), 34-41.

Boyar, R. M., Thylstrup, A., Holmen, L., & Bowden, G. H. (1989). The microflora associated with the development of initial enamel decalcification below orthodontic bands in vivo in children living in a fluoridated-water area. *Journal of Dental Research 68*(12), 1734-1738.

Boyde, A. (1984). Dependence of rate of physical erosion on orientation and density in mineralised tissues. *Anatomy and Embryology, 170*(1), 57-62.

Boyde, A. (1989). Enamel. In A. Oksche & L. Vollrath (Eds.), *Handbook of Microscopic Anatomy* (pp. 309-473). Berlin, Germany: Springer Verlag.

Bradshaw, D. J., & Lynch, R. J. (2013). Diet and the microbial aetiology of dental caries: new paradigms. *International Dental Journal, 63 Suppl 2*, 64-72.

Braga, M. M., Mendes, F. M., Martignon, S., Ricketts, D. N., & Ekstrand, K. R. (2009). In vitro comparison of Nyvad's system and ICDAS-II with Lesion Activity Assessment for evaluation of severity and activity of occlusal caries lesions in primary teeth. *Caries Research, 43*(5), 405-412.

Braga, M. M., Oliveira, L. B., Bonini, G. A., Bonecker, M., & Mendes, F. M. (2009). Feasibility of the International Caries Detection and Assessment System (ICDAS-II) in epidemiological surveys and comparability with standard World Health Organization criteria. *Caries Research, 43*(4), 245-249.

Brazdzionyte, J., & Macas, A. (2007). Bland-Altman analysis as an alternative approach for statistical evaluation of agreement between two methods for measuring hemodynamics during acute myocardial infarction. *Medicina, 43*(3), 208-214.

Brodbelt, R. H., O'Brien, W. J., Fan, P. L., Frazer-Dib, J. G., & Yu, R. (1981). Translucency of human dental enamel. *Journal of Dental Research 60*(10), 1749-1753.

Brunelle, J. A. (1989). Oral Health of United States Children. The National Survey of Dental Caries in US Schoolchildren: 1986-87 findings. NIH pub no 89-2247. Washington, DC: US Department of Health and Human Services.

Bühler, C., Ngaotheppitak, P., & Fried, D. (2005). Imaging of occlusal dental caries (decay) with near-IR light at 1310-nm. *Optics Express, 13*(2), 573-582.

Can, A. M., Darling, C. L., Ho, C., & Fried, D. (2008). Non-destructive assessment of inhibition of demineralization in dental enamel irradiated by a lambda=9.3-microm CO2 laser at ablative irradiation intensities with PS-OCT. *Lasers in Surgery and Medicine, 40*(5), 342-349.

Carvalho, J. C. (2014). Caries process on occlusal surfaces: evolving evidence and understanding. *Caries Research, 48*(4), 339-346.

Carvalho, J. C., Ekstrand, K. R., & Thylstrup, A. (1989). Dental plaque and caries on occlusal surfaces of first permanent molars in relation to stage of eruption. *Journal of Dental Research 68*(5), 773-779.

Carvalho, J. C., Figueiredo, M. J., Vieira, E. O., & Mestrinho, H. D. (2009). Caries trends in Brazilian non-privileged preschool children in 1996 and 2006. *Caries Research, 43*(1), 2-9.

Carvalho, J. C., & Mestrinho, H. D. (2014). Diagnosing non-cavitated lesions in epidemiological studies: practical and scientific considerations. *Brazilian Oral Research 28 Spec*(spe), 1-7.

Carvalho, J. C., Silva, E. F., Gomes, R. R., Fonseca, J. A. C., & Mestrinho, H. D. (2011). Impact of Enamel Defects on Early Caries Development in Preschool Children. *Caries Research, 45*(4), 353-360.

Carvalho, J. C., Thylstrup, A., & Ekstrand, K. R. (1992). Results after 3 years of non-operative occlusal caries treatment of erupting permanent first molars. *Community Dentistry and Oral Epidemiology, 20*(4), 187-192.

Carvalho, J. C., Van Nieuwenhuysen, J. P., & D'Hoore, W. (2001). The decline in dental caries among Belgian children between 1983 and 1998. *Community Dentistry and Oral Epidemiology, 29*(1), 55-61.

Ccahuana-Vasquez, R. A., Tabchoury, C. P., Tenuta, L. M., Del Bel Cury, A. A., Vale, G. C., & Cury, J. A. (2007). Effect of frequency of sucrose exposure on dental biofilm composition and enamel demineralization in the presence of fluoride. *Caries Research, 41*(1), 9-15.

Chappard, C., Basillais, A., Benhamou, L., Bonassie, A., Brunet-Imbault, B., Bonnet, N., et al. (2006). Comparison of synchrotron radiation and conventional x-ray microcomputed tomography for assessing trabecular bone microarchitecture of human femoral heads. *Medical Physics, 33*(9), 3568-3577.

Chen, Y., & Fok, A. (2014). Stress distributions in human teeth modeled with a natural graded material distribution. *Dental Materials 30*(12), e337-348.

Cheong, W. F., Prahl, S. A., & Welch, A. J. (1990). A Review of the Optical-Properties of Biological Tissues. *IEEE Journal of Quantum Electronics, 26*(12), 2166-2185.

Chew, H. P., Zakian, C. M., Pretty, I. A., & Ellwood, R. P. (2014). Measuring initial enamel erosion with quantitative light-induced fluorescence and optical coherence tomography: an in vitro validation study. *Caries Research, 48*(3), 254-262.

Choma, M., Sarunic, M., Yang, C., & Izatt, J. (2003). Sensitivity advantage of swept source and Fourier domain optical coherence tomography. *Optics Express, 11*(18), 2183-2189.

Choo-Smith, L. P., Dong, C. C., Cleghorn, B., & Hewko, M. (2009). Shedding new light on early caries detection. *Texas Dental Journal 126*(2), 152-159.

Cortes, D. F., Ekstrand, K. R., Elias-Boneta, A. R., & Ellwood, R. P. (2000). An in vitro comparison of the ability of fibre-optic transillumination, visual inspection and radiographs to detect occlusal caries and evaluate lesion depth. *Caries Research, 34*(6), 443-447.

Cortes, D. F., Ellwood, R. P., & Ekstrand, K. R. (2003). An in vitro comparison of a combined FOTI/visual examination of occlusal caries with other caries diagnostic methods and the effect of stain on their diagnostic performance. *Caries Res, 37*(1), 8-16.

Darling, A. I. (1956). Studies of the early lesion of enamel caries with transmitted light, polarised light and radiography. *British Dental Journal, 101*, 289-297.

Darling, A. I. (1961). The selective attack of caries on the dental enamel. *Annals of the Royal College of Surgeons of England, 29*, 354-369.

Darling, C. L., Huynh, G. D., & Fried, D. (2006). Light scattering properties of natural and artificially demineralized dental enamel at 1310 nm. *Journal of Biomedical Optics, 11*(3), 34023.

Dawes, C. (2004). Factors influencing salivary flow rate and composition. In L. Hunter (Ed.), *Saliva and oral health* (Edgar M, Dawes C, O'Mullane D, eds. ed., pp. 32-49). London, UK: British Dental Journal.

de Josselin de Jong, E., Sundstrom, F., Westerling, H., Tranaeus, S., ten Bosch, J. J., & Angmar-Mansson, B. (1995). A new method for in vivo quantification of changes in initial enamel caries with laser fluorescence. *Caries Research, 29*(1), 2-7.

de Paula, A. B., Campos, J. A., Diniz, M. B., Hebling, J., & Rodrigues, J. A. (2011). In situ and in vitro comparison of laser fluorescence with visual inspection in detecting occlusal caries lesions. *Lasers in Medical Science, 26*(1), 1-5.

Diniz, M. B., Rodrigues, J. A., Hug, I., Cordeiro Rde, C., & Lussi, A. (2009). Reproducibility and accuracy of the ICDAS-II for occlusal caries detection. *Community Dentistry and Oral Epidemiology, 37*(5), 399-404.

Dirks, O. B. (1966). Posteruptive changes in dental enamel. *Journal of Dental Research 45*(3), 503-511.

Domark, J. D., Hatton, J. F., Benison, R. P., & Hildebolt, C. F. (2013). An ex vivo comparison of digital radiography and cone-beam and micro computed tomography in the detection of the number of canals in the mesiobuccal roots of maxillary molars. *Journal of Endodontics 39*(7), 901-905.

Douglas, S. M., Fried, D., & Darling, C. L. (2010). Imaging Natural Occlusal Caries Lesions with Optical Coherence Tomography. *Proceedings of SPIE - The International Society for Optical Engineering, 7549*, 75490N.

Duerinckx, A. J., & Macovski, A. (1978). Polychromatic streak artifacts in computed tomography images. *Journal of Computer Assisted Tomography 2*(4), 481-487.

Dunkers, J. P., Parnas, R. S., Zimba, C. G., Peterson, R. C., Flynn, K. M., Fujimoto, J. G., et al. (1999). Optical coherence tomography of glass reinforced polymer composites. *Composites Part a-Applied Science and Manufacturing, 30*(2), 139-145.

Ekstrand, K., Kuzmina, I., Bjørndal, L., & Thylstrup, A. (1995). Relationship between external and histologic features of progressive stages of caries in the occlusal fossa. *Caries Research, 29*(4), 243-250.

Ekstrand, K., Qvist, V., & Thylstrup, A. (1987). Light microscope study of the effect of probing in occlusal surfaces. *Caries Research, 21*(4), 368-374.

Ekstrand, K. R. (2004). Improving clinical visual detection--potential for caries clinical trials. *Journal of Dental Research 83 Spec No C*, C67-71.

Ekstrand, K. R., & Bjorndal, L. (1997). Structural analyses of plaque and caries in relation to the morphology of the groove-fossa system on erupting mandibular third molars. *Caries Research, 31*(5), 336-348.

Ekstrand, K. R., Carlsen, O., & Thylstrup, A. (1991). Morphometric analysis of occlusal groove-fossa-system in mandibular third molar. *Scandinavian Journal of Dental Research 99*(3), 196-204.

Ekstrand, K. R., Kuzmina, I., Bjorndal, L., & Thylstrup, A. (1995). Relationship between External and Histologic Features of Progressive Stages of Caries in the Occlusal Fossa. *Caries Research, 29*(4), 243-250.

Ekstrand, K. R., Kuzmina, I. N., Kuzmina, E., & Christiansen, M. E. (2000). Two and a half-year outcome of caries-preventive programs offered to groups of children in the Solntsevsky district of Moscow. *Caries Research, 34*(1), 8-19.

Ekstrand, K. R., Martignon, S., Ricketts, D. J., & Qvist, V. (2007). Detection and activity assessment of primary coronal caries lesions: a methodologic study. *Operative Dentistry 32*(3), 225-235.

Ekstrand, K. R., Ricketts, D. N., & Kidd, E. A. (1997). Reproducibility and accuracy of three methods for assessment of demineralization depth of the occlusal surface: an in vitro examination. *Caries Research, 31*(3), 224-231.

Ekstrand, K. R., Ricketts, D. N., & Kidd, E. A. (1998). Do occlusal carious lesions spread laterally at the enamel-dentin junction? A histolopathological study. *Clinical Oral Investigations, 2*(1), 15-20.

Ekstrand, K. R., Ricketts, D. N., & Kidd, E. A. (2001). Occlusal caries: pathology, diagnosis and logical management. *Dental Update, 28*(8), 380-387.

Elfrink, M. E. C., ten Cate, J. M., Jaddoe, V. W. V., Hofman, A., Moll, H. A., & Veerkamp, J. S. J. (2012). Deciduous Molar Hypomineralization and Molar Incisor Hypomineralization. *Journal of Dental Research, 91*(6), 551-555.

Featherstone, J. D. (1999). Prevention and reversal of dental caries: role of low level fluoride. *Community Dentistry and Oral Epidemiology, 27*(1), 31-40.

Featherstone, J. D. (2000). The science and practice of caries prevention. *The Journal of the American Dental Association, 131*(7), 887-899.

Featherstone, J. D. (2004). The continuum of dental caries--evidence for a dynamic disease process. *Journal of Dental Research, 83 Spec No C*, C39-42.

Featherstone, J. D. (2006). Caries prevention and reversal based on the caries balance. *Pediatric Dentistry, 28*(2), 128-132.

Featherstone, J. D., Mayer, I., Driessens, F. C., Verbeeck, R. M., & Heijligers, H. J. (1983). Synthetic apatites containing Na, Mg, and CO3 and their comparison with tooth enamel mineral. *Calcified Tissue International, 35*(2), 169-171.

Featherstone, J. D., & Rodgers, B. E. (1981). Effect of acetic, lactic and other organic acids on the formation of artificial carious lesions. *Caries Research, 15*(5), 377-385.

Federation, F. D. I. W. D. (2013). FDI policy statement on Classification of caries lesions of tooth surfaces and caries management systems: adopted by the FDI General Assembly: 17 September 2011, Mexico City, Mexico. *International Dental Journal, 63*(1), 4-5.

Fejerskov, O., Melsen, B., & Karring, T. (1973). Morphometric analysis of occlusal fissures in human premolars. *Scandinavian Journal of Dental Research 81*(7), 505-509.

Fercher, A. F., Hitzenberger, C. K., Kamp, G., & Elzaiat, S. Y. (1995). Measurement of Intraocular Distances by Backscattering Spectral Interferometry. *Optics Communications, 117*(1-2), 43-48.

Ferreira Zandona, A., Santiago, E., Eckert, G. J., Katz, B. P., Pereira de Oliveira, S., Capin, O. R., et al. (2012). The natural history of dental caries lesions: a 4-year observational study. *Journal of Dental Research 91*(9), 841-846.

Fried, D., Featherstone, J. D., Glena, R. E., Bordyn, B., & Seka, W. D. (1993). Light-scattering properties of dentin and enamel at 543, 632, and 1053 nm. *Proceedings of SPIE 1880, Lasers in Orthopedic, Dental, and Veterinary Medicine, II*, 240-245.

Fried, D., Glena, R. E., Featherstone, J. D., & Seka, W. (1995). Nature of light scattering in dental enamel and dentin at visible and near-infrared wavelengths. *Applied Optics, 34*(7), 1278-1285.

Fried, D., Xie, J., Shafi, S., Featherstone, J. D., Breunig, T. M., & Le, C. (2002). Imaging caries lesions and lesion progression with polarization sensitive optical coherence tomography. *Journal of Biomedical Optics, 7*(4), 618-627.

Fujimoto, J., & Drexler, W. (2008). Introduction to optical coherence tomography. In W. Drexler & J. Fujimoto (Eds.), *Optical Coherence Tomography* (pp. 1-45). Berlin, Germany: Springer.

Fujimoto, J. G., Brezinski, M. E., Tearney, G. J., Boppart, S. A., Bouma, B., Hee, M. R., et al. (1995). Optical biopsy and imaging using optical coherence tomography. *Nature Medicine, 1*(9), 970-972.

Fujimoto, J. G., Pitris, C., Boppart, S. A., & Brezinski, M. E. (2000). Optical coherence tomography: an emerging technology for biomedical imaging and optical biopsy. *Neoplasia, 2*(1-2), 9-25.

Fyffe, H. E., Deery, C., Nugent, Z. J., Nuttall, N. M., & Pitts, N. B. (2000). Effect of diagnostic threshold on the validity and reliability of epidemiological caries diagnosis using the Dundee Selectable Threshold Method for caries diagnosis (DSTM). *Community Dentistry and Oral Epidemiology, 28*(1), 42-51.

Galil, K. A., & Gwinnett, A. J. (1975). Three-dimensional replicas of pits and fissures in human teeth: scanning electron microscopy study. *Archives of Oral Biology, 20*(8), 493-495.

Gao, X. J., Elliott, J. C., & Anderson, P. (1991). Scanning and contact microradiographic study of the effect of degree of saturation on the rate of enamel demineralization. *Journal of Dental Research 70*(10), 1332-1337.

Garcia, A. I. (1989). Caries Incidence and Costs of Prevention Programs. *Journal of Public Health Dentistry, 49*(5), 259-271.

Gomez, J. (2015). Detection and diagnosis of the early caries lesion. *BMC Oral Health, 15 Suppl 1*, S3.

Gomez, J., Tellez, M., Pretty, I. A., Ellwood, R. P., & Ismail, A. I. (2013). Non-cavitated carious lesions detection methods: a systematic review. *Community Dentistry and Oral Epidemiology, 41*(1), 55-66.

Gomez, J., Zakian, C., Salsone, S., Pinto, S. C., Taylor, A., Pretty, I. A., et al. (2013). In vitro performance of different methods in detecting occlusal caries lesions. *Journal of Dentistry 41*(2), 180-186.

Gorelick, L., Geiger, A. M., & Gwinnett, A. J. (1982). Incidence of white spot formation after bonding and banding. *American Journal of Orthodontics, 81*(2), 93-98.

Gostanian, H. V., Shey, Z., Kasinathan, C., Caceda, J., & Janal, M. N. (2006). An in vitro evaluation of the effect of sealant characteristics on laser fluorescence for caries detection. *Pediatric Dentistry, 28*(5), 445-450.

Gwinnett, A. J., & Buonocore, M. G. (1972). A scanning electron microscope study of pit and fissure surfaces conditioned for adhesive sealing. *Archives of Oral Biology, 17*(3), 415-423.

Hall, A., & Girkin, J. M. (2004). A review of potential new diagnostic modalities for caries lesions. *Journal of Dental Research 83 Spec No C*, C89-94.

Hannigan, A., O'Mullane, D. M., Barry, D., Schafer, F., & Roberts, A. J. (2000). A caries susceptibility classification of tooth surfaces by survival time. *Caries Research, 34*(2), 103-108.

Hariri, I., Sadr, A., Nakashima, S., Shimada, Y., Tagami, J., & Sumi, Y. (2013). Estimation of the enamel and dentin mineral content from the refractive index. *Caries Research, 47*(1), 18-26.

Hariri, I., Sadr, A., Shimada, Y., Tagami, J., & Sumi, Y. (2012). Effects of structural orientation of enamel and dentine on light attenuation and local refractive index: An optical coherence tomography study. *Journal of Dentistry, 40*(5), 387-396.

Hayes, A., Azarpazhooh, A., Dempster, L., Ravaghi, V., & Quinonez, C. (2013). Time loss due to dental problems and treatment in the Canadian population: analysis of a nationwide cross-sectional survey. *BMC Oral Health, 13*.

Hellen, A., Mandelis, A., Finer, Y., & Amaechi, B. T. (2011). Quantitative evaluation of the kinetics of human enamel simulated caries using photothermal radiometry and modulated luminescence. *Journal of Biomedical Optics, 16*(7), 071406.

Hicks, J., Garcia-Godoy, F., & Flaitz, C. (2003). Biological factors in dental caries: role of saliva and dental plaque in the dynamic process of demineralization and remineralization (part 1). *Journal of Clinical Pediatric Dentistry, 28*(1), 47-52.

Holmen, L., Thylstrup, A., Ogaard, B., & Kragh, F. (1985). A scanning electron microscopic study of progressive stages of enamel caries in vivo. *Caries Research, 19*(4), 355-367.

Holtzman, J. S., Ballantine, J., Fontana, M., Wang, A., Calantog, A., Benavides, E., et al. (2014). Assessment of early occlusal caries pre- and post-sealant application--an imaging approach. *Lasers in Surgery and Medicine, 46*(6), 499-507.

Holtzman, J. S., Kohanchi, D., Biren-Fetz, J., Fontana, M., Ramchandani, M., Osann, K., et al. (2015). Detection and proportion of very early dental caries in independent living older adults. *Lasers in Surgery and Medicine*.

Holtzman, J. S., Osann, K., Pharar, J., Lee, K., Ahn, Y. C., Tucker, T., et al. (2010). Ability of optical coherence tomography to detect caries beneath commonly used dental sealants. *Lasers in Surgery and Medicine, 42*(8), 752-759.

Hsieh, Y. S., Ho, Y. C., Lee, S. Y., Chuang, C. C., Tsai, J. C., Lin, K. F., et al. (2013). Dental optical coherence tomography. *Sensors, 13*(7), 8928-8949.

Huang, D., Swanson, E. A., Lin, C. P., Schuman, J. S., Stinson, W. G., Chang, W., et al. (1991). Optical coherence tomography. *Science, 254*(5035), 1178-1181.

Huang, T. T., He, L. H., Darendeliler, M. A., & Swain, M. V. (2010). Correlation of mineral density and elastic modulus of natural enamel white spot lesions using X-ray microtomography and nanoindentation. *Acta Biomaterialia, 6*(12), 4553-4559.

Huang, T. T., Jones, A. S., He, L. H., Darendeliler, M. A., & Swain, M. V. (2007). Characterisation of enamel white spot lesions using X-ray micro-tomography. *Journal of Dentistry 35*(9), 737-743.

Huynh, G. D., Darling, C. L., & Fried, D. (2004). Changes in the optical properties of dental enamel at 1310-nm after demineralization. *Proceedings of SPIE 5313, Lasers in Dentistry, X*, 118-124.

Huysmans, M. C., Kuhnisch, J., & ten Bosch, J. J. (2005). Reproducibility of electrical caries measurements: a technical problem? *Caries Research, 39*(5), 403-410.

Ichijo, T., Yamashita, Y., & Terashima, T. (1992). Observations on the structural features and characteristics of biological apatite crystals. 2. Observation on the ultrastructure of human enamel crystals. *The Bulletin of Tokyo Medical and Dental University, 39*(4), 71-80.

Ie, Y. L., & Verdonschot, E. H. (1994). Performance of diagnostic systems in occlusal caries detection compared. *Community Dentistry and Oral Epidemiology, 22*(3), 187-191.

Ismail, A. I. (1997). Clinical diagnosis of precavitated carious lesions. *Community Dentistry and Oral Epidemiology, 25*(1), 13-23.

Ismail, A. I. (2004). Visual and visuo-tactile detection of dental caries. *Journal of Dental Research 83 Spec No C*, C56-66.

Ismail, A. I., Brodeur, J. M., Gagnon, P., Payette, M., Picard, D., Hamalian, T., et al. (1992). Prevalence of Noncavitated and Cavitated Carious Lesions in a Random Sample of 7-9-Year-Old Schoolchildren in Montreal, Quebec. *Community Dentistry and Oral Epidemiology, 20*(5), 250-255.

Ismail, A. I., Pitts, N. B., Tellez, M., Authors of International Caries, C., Management, S., Banerjee, A., et al. (2015). The International Caries Classification and Management System (ICCMS) An Example of a Caries Management Pathway. *BMC Oral Health, 15 Suppl 1*, S9.

Ismail, A. I., Sohn, W., Tellez, M., Amaya, A., Sen, A., Hasson, H., et al. (2007). The International Caries Detection and Assessment System (ICDAS): an integrated system for measuring dental caries. *Community Dentistry and Oral Epidemiology, 35*(3), 170-178.

Ismail, A. I., Tellez, M., Pitts, N. B., Ekstrand, K. R., Ricketts, D., Longbottom, C., et al. (2013). Caries management pathways preserve dental tissues and promote oral health. *Community Dentistry and Oral Epidemiology, 41*(1), e12-40.

Jablonski-Momeni, A., Stachniss, V., Ricketts, D. N., Heinzel-Gutenbrunner, M., & Pieper, K. (2008). Reproducibility and accuracy of the ICDAS-II for detection of occlusal caries in vitro. *Caries Research, 42*(2), 79-87.

Jallad, M., Zero, D., Eckert, G., & Ferreira Zandona, A. (2015). In vitro Detection of Occlusal Caries on Permanent Teeth by a Visual, Light-Induced Fluorescence and Photothermal Radiometry and Modulated Luminescence Methods. *Caries Research, 49*(5), 523-530.

Jenson, L., Budenz, A. W., Featherstone, J. D., Ramos-Gomez, F. J., Spolsky, V. W., & Young, D. A. (2007). Clinical protocols for caries management by risk assessment. *Journal of the California Dental Association, 35*(10), 714-723.

Jeon, R. J., Han, C., Mandelis, A., Sanchez, V., & Abrams, S. H. (2004). Diagnosis of pit and fissure caries using frequency-domain infrared photothermal radiometry and modulated laser luminescence. *Caries Research, 38*(6), 497-513.

Jin, L. J., Lamster, I. B., Greenspan, J. S., Pitts, N. B., Scully, C., & Warnakulasuriya, S. (2016). Global burden of oral diseases: emerging concepts, management and interplay with systemic health. *Oral Diseases, 22*(7), 609-619.

Johansen, E. (1965). Comparison of the ultrastructure and chemical composition of sound and carious enamel from human permanent teeth. In M. Stack & R. Fearnhead (Eds.), *Tooth enamel: Its Composition, Properties, and Fundamental Structure; Report of the Proceedings* (pp. 177-181). Bristol, UK: J Wright and Sons.

Jones, R., Huynh, G., Jones, G., & Fried, D. (2003). Near-infrared transillumination at 1310-nm for the imaging of early dental decay. *Optics Express, 11*(18), 2259-2265.

Jones, R. S., Darling, C. L., Featherstone, J. D., & Fried, D. (2006). Imaging artificial caries on the occlusal surfaces with polarization-sensitive optical coherence tomography. *Caries Research, 40*(2), 81-89.

Jones, R. S., Staninec, M., & Fried, D. (2004). Imaging artificial caries under composite sealants and restorations. *Journal of Biomedical Optics, 9*(6), 1297-1304.

Joseph, P. M., & Spital, R. D. (1978). A method for correcting bone induced artifacts in computed tomography scanners. *Journal of Computer Assisted Tomography 2*(1), 100-108.

Juhl, M. (1983). Localization of carious lesions in occlusal pits and fissures of human premolars. *Scandinavian Journal of Dental Research 91*(4), 251-255.

Kamburoglu, K., Kurt, H., Kolsuz, E., Oztas, B., Tatar, I., & Celik, H. H. (2011). Occlusal Caries Depth Measurements Obtained by Five Different Imaging Modalities. *Journal of Digital Imaging, 24*(5), 804-813.

Karlsson, L. (2010). Caries Detection Methods Based on Changes in Optical Properties between Healthy and Carious Tissue. *International Journal of Dentistry, 2010*, 270729.

Kay, M. I., Young, R. A., & Posner, A. S. (1964). Crystal Structure of Hydroxyapatite. *Nature, 204*, 1050-1052.

Kidd, E. (1996). The carious lesion in enamel. In M. JJ (Ed.), *Prevention of Oral Disease* (3 ed., pp. 95-106). Oxford, UK: Oxford University Press.

Kidd, E. (2005). *Essentials of dental caries: The disease and its management* (3 ed.). New York, NY: Oxford University Press.

Kidd, E. A., Banerjee, A., Ferrier, S., Longbottom, C., & Nugent, Z. (2003). Relationships between a clinical-visual scoring system and two histological techniques: a laboratory study on occlusal and approximal carious lesions. *Caries Research, 37*(2), 125-129.

Kidd, E. A., & Fejerskov, O. (2004). What constitutes dental caries? Histopathology of carious enamel and dentin related to the action of cariogenic biofilms. *Journal of Dental Research, 83 Spec No C*, C35-38.

Knuttel, A., Bonev, S., & Knaak, W. (2004). New method for evaluation of in vivo scattering and refractive index properties obtained with optical coherence tomography. *Journal of Biomedical Optics, 9*(2), 265-273.

Kolenbrander, P. E., Palmer, R. J., Jr., Periasamy, S., & Jakubovics, N. S. (2010). Oral multispecies biofilm development and the key role of cell-cell distance. *Nature Reviews Microbiology, 8*(7), 471-480.

Konig, K., Flemming, G., & Hibst, R. (1998). Laser-induced autofluorescence spectroscopy of dental caries. *Cellular and molecular biology 44*(8), 1293-1300.

Konig, K. G. (1963). Dental morphology in relation to caries resistance with special reference to fissures as susceptible areas. *Journal of Dental Research 2*, 461-476.

Kuhnisch, J., Bucher, K., Henschel, V., Albrecht, A., Garcia-Godoy, F., Mansmann, U., et al. (2011). Diagnostic performance of the universal visual scoring system (UniViSS) on occlusal surfaces. *Clinical Oral Investigations, 15*(2), 215-223.

Kuhnisch, J., Dietz, W., Stosser, L., Hickel, R., & Heinrich-Weltzien, R. (2007). Effects of dental probing on occlusal surfaces--a scanning electron microscopy evaluation. *Caries Research, 41*(1), 43-48.

Kuhnisch, J., Ekstrand, K. R., Pretty, I., Twetman, S., van Loveren, C., Gizani, S., et al. (2016). Best clinical practice guidance for management of early caries lesions in children and young adults: an EAPD policy document. *European Archives of Paediatric Dentistry, 17*(1), 3-12.

Kuhnisch, J., Goddon, I., Berger, S., Senkel, H., Bucher, K., Oehme, T., et al. (2009). Development, methodology and potential of the new Universal Visual Scoring System (UniViSS) for caries detection and diagnosis. *International Journal of Environmental Research and Public Health, 6*(9), 2500-2509.

Kuhnisch J, H.-W. R., Senkel H, Clasen AB, Stober.L. (2001). Dental health and caries topography in 8-year-old German and immigrant children. *European Journal of Paediatric Dentistry 2*(4), 191-196.

Kuhnisch, J., Senkel, H., & Heinrich-Weltzien, R. (2003). Comparative study on the dental health of German and immigrant 8- to 10-years olds in the Westphalian Ennepe-Ruhr district. *Gesundheitswesen, 65*(2), 96-101.

Kuvvetli, S. S., Cildir, S. K., Ergeneli, S., & Sandalli, N. (2008). Prevalence of noncavitated and cavitated carious lesions in a group of 5-year-old Turkish children in Kadikoy, Istanbul. *Journal of Dentistry for Children, 75*(2), 158-163.

Lam, A., & Chu, C. H. (2012). Caries management with fluoride agents. *The New York State Dental Journal 78*(6), 29-36.

Le, M. H., Darling, C. L., & Fried, D. (2010). Automated analysis of lesion depth and integrated reflectivity in PS-OCT scans of tooth demineralization. *Lasers in Surgery and Medicine, 42*(1), 62-68.

Leeflang, M. M., Deeks, J. J., Takwoingi, Y., & Macaskill, P. (2013). Cochrane diagnostic test accuracy reviews. *Systematic Reviews 2*, 82.

LeGeros, R. (1984). Incorporation of magnesium in synthetic and in biological apatites. In S. S. Fearnhead RW (Ed.), *Tooth Enamel* (Vol. IV, pp. 32-36). Amsterdam, The Netherlands: Elsevier.

LeGeros, R. Z. (1991). *Calcium phosphates in oral biology and medicine* (Vol. 15). Basel, Switzerland: Karger AG.

Leitgeb, R., Hitzenberger, C., & Fercher, A. (2003). Performance of fourier domain vs. time domain optical coherence tomography. *Optics Express, 11*(8), 889-894.

Lenander-Lumikari, M., & Loimaranta, V. (2000). Saliva and dental caries. *Advances in Dental Research, 14*, 40-47.

Loe, H. (1995). Changing paradigms in restorative dentistry. *The Journal of the American College of Dentists, 62*(3), 31-36.

Loesche, W. J. (1976). Chemotherapy of dental plaque infections. *Oral Science Reviews 9*, 65-107.

Longbottom, C., & Huysmans, M. C. (2004). Electrical measurements for use in caries clinical trials. *Journal of Dental Research 83 Spec No C*, C76-79.

Longbottom, C. L., Huysmans, M. C., Pitts, N. B., & Fontana, M. (2009). Glossary of key terms. *Monographs in Oral Science 21*, 209-216.

Louie, T., Lee, C., Hsu, D., Hirasuna, K., Manesh, S., Staninec, M., et al. (2010). Clinical assessment of early tooth demineralization using polarization sensitive optical coherence tomography. *Lasers in Surgery and Medicine, 42*(10), 738-745.

Lussi, A. (1991). Validity of diagnostic and treatment decisions of fissure caries. *Caries Research, 25*(4), 296-303.

Lussi, A., & Hellwig, E. (2006). Performance of a new laser fluorescence device for the detection of occlusal caries in vitro. *Journal of Dentistry, 34*(7), 467-471.

Lussi, A., Hibst, R., & Paulus, R. (2004). DIAGNOdent: an optical method for caries detection. *Journal of Dental Research 83 Spec No C*, C80-83.

Lussi, A., Imwinkelried, S., Pitts, N., Longbottom, C., & Reich, E. (1999). Performance and reproducibility of a laser fluorescence system for detection of occlusal caries in vitro. *Caries Research, 33*(4), 261-266.

Lussi, A., Megert, B., Longbottom, C., Reich, E., & Francescut, P. (2001). Clinical performance of a laser fluorescence device for detection of occlusal caries lesions. *European Journal of Oral Sciences, 109*(1), 14-19.

Macaskill P, Gatsonis C, Deeks JJ, Harbord RM, & Y., T. (2010). Analysing and presenting results. In In: Deeks JJ, Bossuyt PM & G. C (Eds.), *Cochrane Handbook for Systematic Reviews of Diagnostic Test Accuracy* (pp. 9-11). Birmingham, UK: Cochrane Diagnostic Test Accuracy Working Group.

Mandel, I. D., & Wotman, S. (1976). The salivary secretions in health and disease. *Oral Science Reviews* (8), 25-47.

Mandurah, M. M., Sadr, A., Bakhsh, T. A., Shimada, Y., Sumi, Y., & Tagami, J. (2015). Characterization of transparent dentin in attrited teeth using optical coherence tomography. *Lasers in Medical Science, 30*(4), 1189-1196.

Mandurah, M. M., Sadr, A., Shimada, Y., Kitasako, Y., Nakashima, S., Bakhsh, T. A., et al. (2013). Monitoring remineralization of enamel subsurface lesions by optical coherence tomography. *Journal of Biomedical Optics, 18*(4), 046006.

Manton, D. J. (2013). Diagnosis of the early carious lesion. *Australian Dental Journal, 58 Suppl 1*, 35-39.

Marcenes, W., Kassebaum, N. J., Bernabe, E., Flaxman, A., Naghavi, M., Lopez, A., et al. (2013). Global burden of oral conditions in 1990-2010: a systematic analysis. *Journal of Dental Research 92*(7), 592-597.

Marsh, P. D. (2003). Are dental diseases examples of ecological catastrophes? *Microbiology, 149*(Pt 2), 279-294.

Maupome, G., & Pretty, I. A. (2004). A closer look at diagnosis in clinical dental practice: part 4. Effectiveness of nonradiographic diagnostic procedures and devices in dental practice. *Journal of the Canadian Dental Association, 70*(7), 470-474.

Meganck, J. A., Kozloff, K. M., Thornton, M. M., Broski, S. M., & Goldstein, S. A. (2009). Beam hardening artifacts in micro-computed tomography scanning can be reduced by X-ray beam filtration and the resulting images can be used to accurately measure BMD. *Bone, 45*(6), 1104-1116.

Mejare, I., Axelsson, S., Dahlen, G., Espelid, I., Norlund, A., Tranaeus, S., et al. (2014). Caries risk assessment. A systematic review. *Acta Odontologica Scandinavica, 72*(2), 81-91.

Mejare, I., Kallestal, C., Stenlund, H., & Johansson, H. (1998). Caries development from 11 to 22 years of age: a prospective radiographic study. Prevalence and distribution. *Caries Research, 32*(1), 10-16.

Mejare, I., Stenlund, H., & Zelezny-Holmlund, C. (2004). Caries incidence and lesion progression from adolescence to young adulthood: a prospective 15-year cohort study in Sweden. *Caries Research, 38*(2), 130-141.

Meng, Z., Yao, X. S., Yao, H., Liang, Y., Liu, T., Li, Y., et al. (2009). Measurement of the refractive index of human teeth by optical coherence tomography. *Journal of Biomedical Optics, 14*(3), 034010.

Mitropoulos, P., Rahiotis, C., Stamatakis, H., & Kakaboura, A. (2010). Diagnostic performance of the visual caries classification system ICDAS II versus radiography and micro-computed tomography for proximal caries detection: an in vitro study. *Journal of Dentistry 38*(11), 859-867.

Momoi, Y., Hayashi, M., Fujitani, M., Fukushima, M., Imazato, S., Kubo, S., et al. (2012). Clinical guidelines for treating caries in adults following a minimal intervention policy--evidence and consensus based report. *J Dent, 40*(2), 95-105.

Mortensen, D., Dannemand, K., Twetman, S., & Keller, M. K. (2014). Detection of non-cavitated occlusal caries with impedance spectroscopy and laser fluorescence: an in vitro study. *The Open Dentistry Journal, 8*, 28-32.

Moynihan, P., & Petersen, P. E. (2004). Diet, nutrition and the prevention of dental diseases. *Public Health Nutrition, 7*(1A), 201-226.

Nagano, T. (1961). Relation between the form of pit and fissure and the primary lesion of caries. *Dental Abstracts, 6,* 426.

Nakajima, Y., Shimada, Y., Miyashin, M., Takagi, Y., Tagami, J., & Sumi, Y. (2012). Noninvasive cross-sectional imaging of incomplete crown fractures (cracks) using swept-source optical coherence tomography. *International Endodontic Journal, 45*(10), 933-941.

Nakajima, Y., Shimada, Y., Sadr, A., Wada, I., Miyashin, M., Takagi, Y., et al. (2014). Detection of occlusal caries in primary teeth using swept source optical coherence tomography. *Journal of Biomedical Optics, 19*(1), 16020.

Natsume, Y., Nakashima, S., Sadr, A., Shimada, Y., Tagami, J., & Sumi, Y. (2011). Estimation of lesion progress in artificial root caries by swept source optical coherence tomography in comparison to transverse microradiography. *Journal of Biomedical Optics, 16*(7), 071408.

Nazari, A., Sadr, A., Campillo-Funollet, M., Nakashima, S., Shimada, Y., Tagami, J., et al. (2013). Effect of hydration on assessment of early enamel lesion using swept-source optical coherence tomography. *Journal of Biophotonics, 6*(2), 171-177.

Nelson, S., Eggertsson, H., Powell, B., Mandelaris, J., Ntragatakis, M., Richardson, T., et al. (2011). Dental examiners consistency in applying the ICDAS criteria for a caries prevention community trial. *Community Dental Health, 28*(3), 238-242.

Neuhaus, K. W., Longbottom, C., Ellwood, R., & Lussi, A. (2009). Novel lesion detection aids. *Monographs in Oral Science 21*, 52-62.

Ngaotheppitak, P., Darling, C., & Fried, D. (2005). Polarization optical coherence tomography for the measuring the severity of caries lesions. *Lasers in Surgery and Medicine, 37*(1), 78-88.

Ngaotheppitak, P., Darling, C. L., Fried, D., Bush, J., & Bell, S. (2006). PS-OCT of Occlusal and Interproximal Caries Lesions viewed from Occlusal Surfaces *Lasers in Dentistry XII, 6137*, L1370-L1370.

Nyvad, B. (2004). Diagnosis versus detection of caries. *Caries Research, 38*(3), 192-198.

Nyvad, B., Crielaard, W., Mira, A., Takahashi, N., & Beighton, D. (2013). Dental caries from a molecular microbiological perspective. *Caries Research, 47*(2), 89-102.

Nyvad, B., Machiulskiene, V., & Baelum, V. (1999). Reliability of a new caries diagnostic system differentiating between active and inactive caries lesions. *Caries Research, 33*(4), 252-260.

Nyvad, B., Machiulskiene, V., & Baelum, V. (2003). Construct and predictive validity of clinical caries diagnostic criteria assessing lesion activity. *Journal of Dental Research 82*(2), 117-122.

Otis, L. L., Colston, B. W., Jr., Everett, M. J., & Nathel, H. (2000). Dental optical coherence tomography: a comparison of two in vitro systems. *Dentomaxillofacial Radiology, 29*(2), 85-89.

Ozawa, N., Sumi, Y., Shimozato, K., Chong, C., & Kurabayashi, T. (2009). In vivo imaging of human labial glands using advanced optical coherence tomography. *Oral Surgery, Oral Medicine, Oral Pathology, Oral Radiology, and Endodontology, 108*(3), 425-429.

Ozkan, G., Kanli, A., Baseren, N. M., Arslan, U., & Tatar, I. (2015). Validation of micro-computed tomography for occlusal caries detection: an in vitro study. *Brazilian Oral Research, 29*(1), S1806-83242015000100309.

Pai, M., McCulloch, M., Enanoria, W., & Colford, J. M., Jr. (2004). Systematic reviews of diagnostic test evaluations: What's behind the scenes? *ACP Journal Club 141*(1), A11-13.

Patel, R. (2012). *The State of Oral Health in Europe*.

Pearce, E. (1998). Plaque minerals and dental caries. *The New Zealand Dental Journal, 94*(415), 12-15.

Petersen, P. E. (2003). The World Oral Health Report 2003: continuous improvement of oral health in the 21st century--the approach of the WHO Global Oral Health Programme. *Community Dentistry and Oral Epidemiology, 31 Suppl 1*, 3-23.

Petersen, P. E. (2005). Priorities for research for oral health in the 21st century--the approach of the WHO Global Oral Health Programme. *Community Dental Health, 22*(2), 71-74.

Petersen, P. E. (2010). Improvement of global oral health - the leadership role of the World Health Organization. *Community Dental Health, 27*(4), 194-198.

Petersen, P. E., Bourgeois, D., Ogawa, H., Estupinan-Day, S., & Ndiaye, C. (2005). The global burden of oral diseases and risks to oral health. *Bulletin of the World Health Organization, 83*(9), 661-669.

Pierce, M. C., Strasswimmer, J., Park, B. H., Cense, B., & de Boer, J. F. (2004). Birefringence measurements in human skin using polarization-sensitive optical coherence tomography. *Lasers in Surgery: Advanced Characterization, Therapeutics, and Systems Xiv, 5312*, 35-40.

Pine, C. M., & ten Bosch, J. J. (1996). Dynamics of and diagnostic methods for detecting small carious lesions. *Caries Research, 30*(6), 381-388.

Pitts, N. (2004). "ICDAS"--an international system for caries detection and assessment being developed to facilitate caries epidemiology, research and appropriate clinical management. *Community Dental Health, 21*(3), 193-198.

Pitts, N., Amaechi, B., Niederman, R., Acevedo, A. M., Vianna, R., Ganss, C., et al. (2011). Global oral health inequalities: dental caries task group--research agenda. *Advances in Dental Research, 23*(2), 211-220.

Pitts, N., & Stamm, J. (2004). International Consensus Workshop on Caries Clinical Trials (ICW-CCT)—final consensus statements: agreeing where the evidence leads. *Journal of Dental Research, 83*(suppl 1), C125-C128.

Pitts, N. B., & Fyffe, H. E. (1988). The effect of varying diagnostic thresholds upon clinical caries data for a low prevalence group. *Journal of Dental Research, 67*(3), 592-596.

Popescu, D. P., Sowa, M. G., Hewko, M. D., & Choo-Smith, L. P. (2008). Assessment of early demineralization in teeth using the signal attenuation in optical coherence tomography images. *Journal of Biomedical Optics, 13*(5), 054053.

Pretty, I. A. (2006). Caries detection and diagnosis: novel technologies. *Journal of Dentistry 34*(10), 727-739.

Rakhmatullina, E., Bossen, A., Hoschele, C., Wang, X., Beyeler, B., Meier, C., et al. (2011). Application of the specular and diffuse reflection analysis for in vitro diagnostics of dental erosion: correlation with enamel softening, roughness, and calcium release. *Journal of Biomedical Optics, 16*(10), 107002.

Rechmann, P., Domejean, S., Rechmann, B. M., Kinsel, R., & Featherstone, J. D. (2016). Approximal and occlusal carious lesions: Restorative treatment decisions by California dentists. *The Journal of the American Dental Association 147*(5), 328-338.

Reich, E., Lussi, A., & Newbrun, E. (1999). Caries-risk assessment. *International Dental Journal, 49*(1), 15-26.

Rhodes, J. S., Ford, T. R., Lynch, J. A., Liepins, P. J., & Curtis, R. V. (1999). Micro-computed tomography: a new tool for experimental endodontology. *International Endodontic Journal, 32*(3), 165-170.

Ricketts, D. N., Kidd, E. A., Smith, B. G., & Wilson, R. F. (1995). Clinical and radiographic diagnosis of occlusal caries: a study in vitro. *Journal of Oral Rehabilitation, 22*(1), 15-20.

Ricketts, D. N., Watson, T. F., Liepins, P. J., & Kidd, E. A. (1998). A comparison of two histological validating techniques for occlusal caries. *Journal of Dentistry, 26*(2), 89-96.

Ricketts, D. N. J., Kidd, E. A. M., & Wilson, R. F. (1997). Electronic diagnosis of occlusal caries in vitro: Adaptation of the technique for epidemiological purposes. *Community Dentistry and Oral Epidemiology, 25*(3), 238-241.

Ripa, L. W. (1973). Occlusal sealing: rationale of the technique and historical review. *The Journal of the American Society for Preventive Dentistry, 3*(1), 32-39.

Robinson, C., Kirkham, J., Brookes, S. J., Bonass, W. A., & Shore, R. C. (1995). The chemistry of enamel development. *The International Journal of Developmental Biology, 39*(1), 145-152.

Robinson, C., Shore, R. C., Brookes, S. J., Strafford, S., Wood, S. R., & Kirkham, J. (2000). The chemistry of enamel caries. *Critical Reviews in Oral Biology and Medicine, 11*(4), 481-495.

Robinson, C., Weatherell, J. A., & Hallsworth, A. S. (1971). Variatoon in composition of dental enamel within thin ground tooth sections. *Caries Research, 5*(1), 44-57.

Robinson, C., Weatherell, J. A., & Hallsworth, A. S. (1981). Distribution of magnesium in mature human enamel. *Caries Research, 15*(1), 70-77.

Robinson, C., Weatherell, J. A., & Hallsworth, A. S. (1983). Alteration in the composition of permenant human enamel during carious attack. In S. Leach & W. M. Edgar (Eds.), *In: Demineralisation and remineralisation of the teeth.* (pp. 209-223). Oxford, UK: IRL press.

Rodrigues, J., Hug, I., Diniz, M., & Lussi, A. (2008). Performance of fluorescence methods, radiographic examination and ICDAS II on occlusal surfaces in vitro. *Caries Research, 42*(4), 297-304.

Sbaraini, A., & Evans, R. W. (2008). Caries risk reduction in patients attending a caries management clinic. *Australian Dental Journal, 53*(4), 340-348.

Schneiderman, A., Elbaum, M., Shultz, T., Keem, S., Greenebaum, M., & Driller, J. (1997). Assessment of dental caries with Digital Imaging Fiber-Optic TransIllumination (DIFOTI): in vitro study. *Caries Research, 31*(2), 103-110.

Schuller, S., Sawall, S., Stannigel, K., Hulsbusch, M., Ulrici, J., Hell, E., et al. (2015). Segmentation-free empirical beam hardening correction for CT. *Medical Physics, 42*(2), 794-803.

Schwass, D. R., Swain, M. V., Purton, D. G., & Leichter, J. W. (2009). A system of calibrating microtomography for use in caries research. *Caries Research, 43*(4), 314-321.

Schweizer, S., Hattendorf, B., Schneider, P., Aeschlimann, B., Gauckler, L., Muller, R., et al. (2007). Preparation and characterization of calibration standards for bone density determination by micro-computed tomography. *The Analyst, 132*(10), 1040-1045.

Scully, C. (1986). Sjogren's syndrome: clinical and laboratory features, immunopathogenesis, and management. *Oral Surgery, Oral Medicine, Oral Pathology, 62*(5), 510-523.

Sheiham, A., & James, W. P. (2015). Diet and Dental Caries: The Pivotal Role of Free Sugars Reemphasized. *Journal of Dental Research 94*(10), 1341-1347.

Shi, X. Q., Welander, U., & Angmar-Mansson, B. (2000). Occlusal caries detection with KaVo DIAGNOdent and radiography: an in vitro comparison. *Caries Research, 34*(2), 151-158.

Shimada, Y., Sadr, A., Burrow, M. F., Tagami, J., Ozawa, N., & Sumi, Y. (2010). Validation of swept-source optical coherence tomography (SS-OCT) for the diagnosis of occlusal caries. *Journal of Dentistry 38*(8), 655-665.

Shimada, Y., Sadr, A., Sumi, Y., & Tagami, J. (2015). Application of Optical Coherence Tomography (OCT) for Diagnosis of Caries, Cracks, and Defects of Restorations. *Current Oral Health Reports, 2*(2), 73-80.

Shimamura, Y., Murayama, R., Kurokawa, H., Miyazaki, M., Mihata, Y., & Kmaguchi, S. (2011). Influence of tooth-surface hydration conditions on optical coherence-tomography imaging. *Journal of Dentistry 39*(8), 572-577.

Silverstone, L. M. (1973). Structure of carious enamel, including the early lesion. *Oral Science Reviews 3*, 100-160.

Simon-Soro, A., Belda-Ferre, P., Cabrera-Rubio, R., Alcaraz, L. D., & Mira, A. (2013). A tissue-dependent hypothesis of dental caries. *Caries Research, 47*(6), 591-600.

Simon-Soro, A., Guillen-Navarro, M., & Mira, A. (2014). Metatranscriptomics reveals overall active bacterial composition in caries lesions. *Journal of Oral Microbiology, 6*, 25443.

Sowa, M. G., Popescu, D. P., Friesen, J. R., Hewko, M. D., & Choo-Smith, L. P. (2011). A comparison of methods using optical coherence tomography to detect demineralized regions in teeth. *Journal of Biophotonics, 4*(11-12), 814-823.

Sowa, M. G., Popescu, D. P., Werner, J., Hewko, M., Ko, A. C., Payette, J., et al. (2007). Precision of Raman depolarization and optical attenuation measurements of sound tooth enamel. *Analytical and Bioanalytical Chemistry, 387*(5), 1613-1619.

Stookey, G. K. (2008). The effect of saliva on dental caries. *The Journal of the American Dental Association 139 Suppl*, 11S-17S.

Sutalo, J., Pupic, V., Velenje, T., Ciglar, I., Skaljac, G., & Tuda, M. (1989). Scanning electron microscopic study of penetrability of sealants in relation to fissure morphology of permanent premolars in humans. *Oral-prophylaxe, 11*(3), 83-88.

Takahashi, N., & Nyvad, B. (2011). The role of bacteria in the caries process: ecological perspectives. *Journal of Dental Research 90*(3), 294-303.

Taylor, A. M., Satterthwaite, J. D., Ellwood, R. P., & Pretty, I. A. (2010). An automated assessment algorithm for micro-CT images of occlusal caries. *Surgeon, 8*(6), 334-340.

Taylor, C. L., & Gwinnett, A. J. (1973). A study of the penetration of sealants into pits and fissures. *The Journal of the American Dental Association 87*(6), 1181-1188.

Ten Cate, J. M. (2004). Fluorides in caries prevention and control: empiricism or science. *Caries Research, 38*(3), 254-257.

ten Cate, J. M. (2013). Contemporary perspective on the use of fluoride products in caries prevention. *British Dental Journal, 214*(4), 161-167.

ten Cate, J. M., & Featherstone, J. D. (1991). Mechanistic aspects of the interactions between fluoride and dental enamel. *Critical Reviews in Oral Biology and Medicine, 2*(3), 283-296.

Terrer, E., Koubi, S., Dionne, A., Weisrock, G., Sarraquigne, C., Mazuir, A., et al. (2009). A new concept in restorative dentistry: light-induced fluorescence evaluator for diagnosis and treatment. Part 1: Diagnosis and treatment of initial occlusal caries. *The Journal of Contemporary Dental Practice, 10*(6), E086-094.

Theilade, E. (1986). The non-specific theory in microbial etiology of inflammatory periodontal diseases. *Journal of Clinical Periodontology, 13*(10), 905-911.

Theuns, H. M., Shellis, R. P., Groeneveld, A., Vandijk, J. W. E., & Poole, D. F. G. (1993). Relationships between Birefringence and Mineral-Content in Artificial Caries Lesions of Enamel. *Caries Research, 27*(1), 9-14.

Thomas, J. G., & Nakaishi, L. A. (2006). Managing the complexity of a dynamic biofilm. *The Journal of the American Dental Association 137 Suppl*, 10S-15S.

Thylstrup, A., & Fejerskov, O. (1994). Clinical and pathological features of dental caries In Thylstrup A & F. O (Eds.), *Textbook of Clinical Cariology* (pp. 111-157). Copenhagen, Denmark: Munksgaard.

Thylstrup, A., & Qvist, V. (1987). Principal enamel and dentin reactions during caries progression. In A. Thylstrup, Leach SA,Qvist,V. (Ed.), *Dentine and Dentine Reactions in Oral Cavity* (Oxford:IRL Press ed., pp. 3-16). Oxford, UK: IRL Press.

Touger-Decker, R., & van Loveren, C. (2003). Sugars and dental caries. *The American Journal of Clinical Nutrition, 78*(4), 881S-892S.

Van de Casteele, E., Van Dyck, D., Sijbers, J., & Raman, E. (2004). A model-based correction method for beam hardening artefacts in X-ray microtomography. *Journal of X-Ray Science and Technology, 12*(1), 43-57.

van der Veen, M. H., & de Josselin de Jong, E. (2000). Application of quantitative light-induced fluorescence for assessing early caries lesions. *Monographs in Oral Science 17*, 144-162.

van Ruyven, F. O., Lingstrom, P., van Houte, J., & Kent, R. (2000). Relationship among mutans streptococci, "low-pH" bacteria, and lodophilic polysaccharide-producing bacteria in dental plaque and early enamel caries in humans. *Journal of Dental Research 79*(2), 778-784.

Verdonschot, E. H., Wenzel, A., & Bronkhorst, E. M. (1993). Assessment of diagnostic accuracy in caries detection: an analysis of two methods. *Community Dentistry and Oral Epidemiology, 21*(4), 203-208.

Walsh, L. J., & Brostek, A. M. (2013). Minimum intervention dentistry principles and objectives. *Australian Dental Journal, 58 Suppl 1*, 3-16.

Weathereel JA, Robinson C, & Haeesworth AS. (1983). Formation of lesions in enamel using moist acid vapour. In Leach SA & Edgar WM (Eds.), *Demineralisation and Reminerlisation of the Teeth* (pp. 225-241). Oxford: IRL Press.

Weatherell, J. A., Robinson, C., & Hallsworth, A. S. (1972). Changes in the fluoride concentration of the labial enamel surface with age. *Caries Research, 6*(4), 312-324.

Weatherell, J. A., Robinson, C., & Hiller, C. R. (1968). Distribution of carbonate in thin sections of dental enamel. *Caries Research, 2*(1), 1-9.

Weatherell, J. A., Weidmann, S. M., & Eyre, D. R. (1968). Histological appearance and chemical composition of enamel proteins from mature human molars. *Caries Research, 2*(4), 281-293.

Weintraub, J. A., & Burt, B. A. (1987). Prevention of dental caries by the use of pit-and-fissure sealants. *Journal of Public Health Policy, 8*(4), 542-560.

Wenzel, A., Larsen, M. J., & Fejerskov, O. (1991). Detection of Occlusal Caries without Cavitation by Visual Inspection, Film Radiographs, Xeroradiographs, and Digitized Radiographs. *Caries Research, 25*(5), 365-371.

Willekens, I., Buls, N., Lahoutte, T., Baeyens, L., Vanhove, C., Caveliers, V., et al. (2010). Evaluation of the radiation dose in micro-CT with optimization of the scan protocol. *Contrast Media and Molecular Imaging, 5*(4), 201-207.

Wright, J. T. (2010). Defining the contribution of genetics in the etiology of dental caries. *Journal of Dental Research, 89*(11), 1173-1174.

Wulff HR, & PC, G. (2000). *Rational Diagnosis and Treatment: Evidence-Based Clinical Decision Making* (3 ed.). Oxford, UK: Blackwell Science.

Young, D. A., Fontana, M., & Wolff, M. S. (2010). Current concepts in cariology. In D. A. Young, M. Fontana & M. S. Wolff (Eds.), *Dental Clinics of North America* (1 ed., Vol. 54). Amsterdam, The Netherlands: Saunders.

Young, D. A., Kutsch, V. K., & Whitehouse, J. (2009). A clinician's guide to CAMBRA: a simple approach. *Compendium of Continuing Education in Dentistry, 30*(2), 92-94, 96, 98, passim.

Young, R. A. (1975). Biological apatite vs hydroxyapatite at the atomic level. *Clinical Orthopaedics and Related Research*(113), 249-262.

Zaki, R., Bulgiba, A., Ismail, R., & Ismail, N. A. (2012). Statistical Methods Used to Test for Agreement of Medical Instruments Measuring Continuous Variables in Method Comparison Studies: A Systematic Review. *PLOS ONE, 7*(5).

Zelander, T. (1973). The enamel. In Mjor IA & P. JJ (Eds.), *Histology of the Human Tooth*. Copenhagen, Denmark: Munksgaard.

Zero, D. T., van Houte, J., & Russo, J. (1986). The intra-oral effect on enamel demineralization of extracellular matrix material synthesized from sucrose by Streptococcus mutans. *Journal of Dental Research, 65*(6), 918-923.

Zhang, D., Mao, S., Lu, C., Romberg, E., & Arola, D. (2009). Dehydration and the dynamic dimensional changes within dentin and enamel. *Dental Materials, 25*(7), 937-945.

LIST OF PUBLICATIONS AND PAPERS

Poster and oral presentation at 61st ORCA Annual Congress 2014 in Greifswald, Germany. Correlation between Optical Coherence Tomography and Polarized Light Microscopy for detection of Early Fissure Caries.